Opto-Electronic Properties of Charged

Conjugated Molecules

Opto-Electronic Properties of Charged Conjugated Molecules

Proefschrift

ter verkrijging van de graad van doctor
aan de Technische Universiteit Delft,
op gezag van de Rector Magnificus prof. dr. ir. J. T. Fokkema,
voorzitter van het College voor Promoties,
in het openbaar te verdedigen op maandag 23 april 2007 om 12:30 uur

door

Silvia FRĂȚILOIU

Licențiat in fizică-chimie, Universitatea Transilvania Brașov,
geboren te Brașov, Roemenië

Dit proefschrift is goedgekeurd door de promotor:
Prof. dr. L. D. A. Siebbeles

Samenstelling promotiecommisie:

Rector Magnificus,	voorzitter
Prof. dr. L. D. A. Siebbeles,	Technische Universiteit Delft, promotor
Prof. dr. E. J. R. Sudhölter,	Technische Universiteit Delft
Prof. dr. S. J. Picken,	Technische Universiteit Delft
Prof. dr. J. Schoonman,	Technische Universiteit Delft
Prof. dr. L. W. Jenneskens,	Universiteit Utrecht
Dr. F. C. Grozema,	Technische Universiteit Delft
Dr. J. Cornil,	University of Mons-Hainaut

Dr. Ferdinand Grozema heeft als begeleider in belangrijke mate aan de totstandkomming van het proefschrift bijgedragen.

Părinților mei, cu dragoste

Contents

3   Methods for Electronic Structure Calculations

4   Opto-Electronic Properties of Positively Charged Phenylenevinylene Oligomers
Time-resolved VIS/NIR Spectroscopy versus Time-Dependent DFT

5   Optical Properties and Delocalization of Excess Negative Charges on Oligo(Phenylenevinylene)s
A Quantum Chemical Study

Chapter 1

Introduction

1.1 Conjugated polymers

Conjugated polymers are polyunsaturated compounds, in which the backbone carbon atoms are *sp* or *sp²* hybridized. Before 1977, conjugated polymers received little attention, due to their "inferior" properties compared with the already studied polymers. In their pure state conjugated polymers are insulators or wide bandgap semiconductors. In 1977 Heeger, MacDiarmid and Shirakawa demonstrated that poly(acetylene), the simplest polyconjugated system, becomes conductive after reaction with bromine or iodine vapors.[1] Spectroscopic studies showed the redox chemical nature of this reaction and explained the reaction mechanism; the neutral poly(acetylene) chains are transformed into polycarbocations with simultaneous insertion of the corresponding numbers of Br_3^- or I_3^- anions in order to neutralize the positive charges.[2] Since this important discovery intensive research has been performed, concerning the chemistry and physics of conjugated polymers, both in their neutral (undoped) and charged (doped) states. The application of conjugated polymers as semiconducting materials in "plastic electronic" devices has been a principal focus of the 1990s. In 2000 Heeger, MacDiarmid and Shirakawa were granted the Nobel Prize in chemistry for their work on conjugated and conductive polymers.[3-5]

The second major development in the field of conjugated polymers was the discovery of electroluminescence in poly(p-phenylenevinylene) by Burroughes et al.[6] Electroluminescent conjugated polymers are fluorescent polymers that emit light when excited by flow of an electric current. This discovery challenged the domination of inorganic materials in light-emitting diodes.

In the last few years, review papers on various aspects of conjugated polymers have been published.[7-12] In the following paragraphs an overview of the conductive and optical properties of conjugated polymers is given and the most important applications in opto-electronic devices and molecular electronics are discussed. The most intensively studied conjugated polymers are shown schematically in Figure 1.1. As obvious from this figure, conjugated polymers contain an alternating sequence of single and double (or triple) bonds between the carbon atoms.
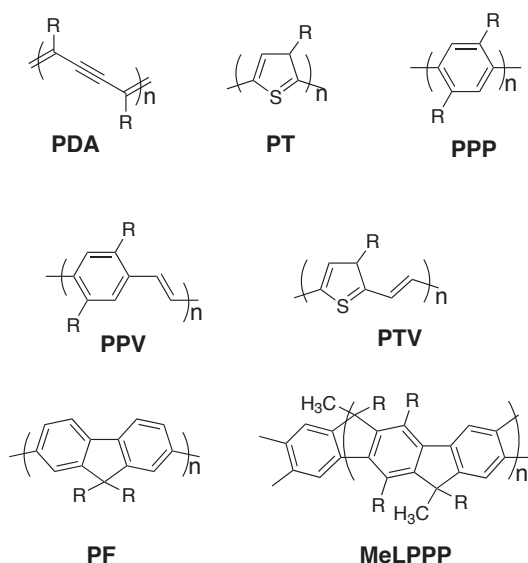
Figure 1.1: Chemical structures of some of the most important conjugated polymers. (n is the number of repeat units.) PDA-polydiacetylene, PT-polythiophene, PPP-polyparaphenylene, PPV-polyphenylenevinylene, PTV-polythienylenevinylene, PF-polyfluorene, MeLPPP-methyl-substituted ladder-type polyparaphenylene, R-solubilizing side chains.

Unsubstituted conjugated polymers that were used initially are insoluble. Introduction of alkyl or alkoxy substituents on the backbone makes the polymer soluble, so that processing from solution becomes possible. The introduction of substituents can also modify the electronic properties of the polymers, leading to changes in the optical absorption and emission spectra.[13,14] Additionally, the presence of substituents has been shown to increase the luminescence yield.[15] The addition of side chains in a regular way can lead to improved charge transport properties in solid materials, due to the self-organization of the polymer. This has been found for example for alkyl substituted polythiophenes, which self-organize into a lamellar structure.[16] Apart from the advantages mentioned above, conjugated polymers are flexible, they have a low weight and a relatively low processing cost. All these advantages make conjugated polymers suitable competitors of the traditional inorganic materials for specific applications in opto-electronic devices and molecular electronics.

1.2 Conductive properties of conjugated polymers

As mentioned in section 1.1, conjugated polymers consist of *sp* and *sp^2* hybridized backbone carbon atoms. In the simplest conjugated polymer, polyacetylene, the *sp^2* orbitals determine the σ-bonding. The *2p$_z$* orbitals are singly occupied with electrons and they are oriented perpendicular to the molecular plane (see Figure 1.2). The *2p$_z$* orbitals of the carbon atoms form π molecular orbitals, which are delocalized over the polymer chain. This delocalized π-system provides a pathway for charge transport along the backbone of the polymer. The π orbitals are half-filled with electrons since two electrons of opposite spin per carbon atom can be accommodated. This leads to a half-filled band, from which metallic behavior can be expected. However, this was not observed. Due to the Peierls distortion[17] the bonds between

neighboring carbon atoms are unequal, leading to an alternation of the length of single and double bonds. As a consequence, the band is split in a valence band (which is fully occupied) and a conduction band (which is empty) with a bandgap of 1.4 eV. Conjugated polymers have a bandgap of typically 1-3 eV, similar to the bandgap in conventional inorganic semiconductors.[18]
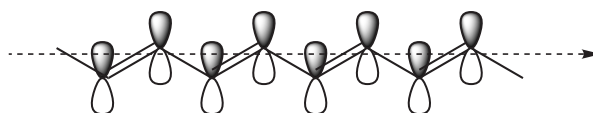
Figure 1.2: Scheme of the singly occupied p_z orbitals in polyacetylene, which provides the pathway for charge transport along the π-conjugated backbone.

When bands are completely filled or empty, there is no conduction. Thermal excitation of electrons from the valence band to the conduction band does not occur to a significant extent since conjugated polymers are wide bandgap semiconductors. Charges can be introduced in conjugated polymer bands by doping. Doping can be done chemically, electrochemically and photochemically. Further information about doping mechanisms and applications can be found in literature.[8] The charge carriers introduced in conjugated polymers are able to move along the delocalized π-system giving rise to electrical conductivity. For highly ordered (crystalline) materials charge transport can be described by the band structure model.[19] Band theory is not adequate to describe charge transport in disordered solid materials, such as polymer films.[20] In these materials the charge carriers are localized to some extent. For this reason, charge transport in disordered materials is often described by a thermally activated hopping mechanism.[21,22] According to this mechanism, the charge performs thermally activated hops between different localization sites.

The two charge transport models are characterized by the magnitude and temperature dependence of the charge carrier mobility. In band transport the charge carrier mobilities are usually high ($>> 1$ cm^{2}V^{-1}s^{-1}) and decrease with increasing temperature. In the hopping model much lower mobilities are found ($<< 1$ cm^{2}V^{-1}s^{-1}) and the mobilities increase with increasing temperature.

1.3 Optical properties of conjugated polymers

All polymers shown schematically in Figure 1.1 are colored. This is caused by a strong absorption in the visible range of the spectrum, usually due to a π-π^* optical transition (see Figure 1.3a). In principle, the size of the optical gap can be varied by appropriate functionalization of the conjugated backbone (introduction of side chains). In addition, changes in the backbone (specifically the combination of electron donating and electron withdrawing moieties in copolymers) lead to a decrease of the bond length alternation in conjugated polymers, which reduces the bandgap. The first low bandgap conjugated polymer obtained in this way was poly(isothianaphtene) with a bandgap of 1.1 eV, which is almost 1 eV lower than the bandgap of polythiophene.[23] This is beneficial for application in photovoltaic devices (see section 1.5.1) Therefore, many attempts have been made to

synthesize conjugated polymers with a bandgap as low as possible.[24] The optical properties of the polymer can also be tuned by introducing conjugation breaks into the polymer structure.[25]

When charges are introduced into the polymer, the optical properties change. In order to describe the optical absorption properties for polymer anions and cations a one-electron band structure model[19,26] has been used. This model (illustrated in Figure 1.3) predicts that upon oxidative or reductive doping, spatially localized geometric defects are formed. These charges, coupled to geometric defects of the backbone, are known as polarons or bipolarons for singly and doubly charged chains, respectively. The formation of polarons (bipolarons) is accompanied by the formation of two new localized levels in the gap between the valence band and the conduction band. These levels are denoted P1 and P2 for polarons and BIP1 and BIP2 for bipolarons (see Figures 1.3(b) and (c)).
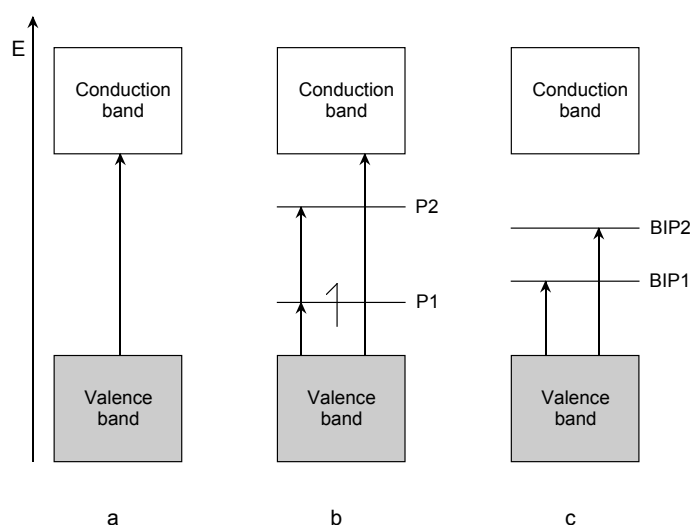
Figure 1.3: One-electron band structure model for (a) the neutral state; (b) in the presence of a positively charged polaron; and (c) in the presence of a positively charged bipolaron. The sub-gap optical transitions induced upon doping are also represented.

In case of cations the lowest polaronic level P1 is singly occupied, while the highest polaronic level P2 is empty. The bipolaron levels BIP1 and BIP2 are empty. Fesser et al.[27] predicted three sub-gap optical transitions for positive polarons and only two for bipolarons. These transitions are illustrated by arrows in Figures 1.3 (b) and (c).

In the case of short conjugated chains (oligomers), the band structure model does not apply. Oligomers have discrete energy levels instead of bands, and the cation and anion spectra have to be described in term of the molecular orbitals. As an example, Figure 1.4 shows the representation of molecular orbitals for phenylenevinylene oligomers, which belong to C_{2h} symmetry group (the order of irreducible representation is a_u, b_g, a_u, b_g, *etc.*). Theoretical and experimental results on conjugated oligomers have shown that only two sub-gap optical transitions occur for cations: one transition (RC1) originating from excitation from the doubly occupied molecular orbital (H) to the lower polaronic level (P1) and the other sub-gap transition (RC2) takes place between the two polaronic levels (P1→P2). The absence of any transition between the doubly occupied molecular orbital (H) and the higher polaronic

level (P2) is related to the selection rules imposed by the symmetry. Both levels belong to the same irreducible representation a_u and transitions between states of identical irreducible representations are forbidden. The RC1 electron transition from an a_u level to the next b_g level and the RC2 transition from the b_g level to the next a_u level are due to excitations with a transition dipole moment along the chain axis and therefore have significant intensities. Additional symmetry-allowed transitions can be found (e.g. P1→L+1), but they are weak because the excitation is not polarized along the chain axis.
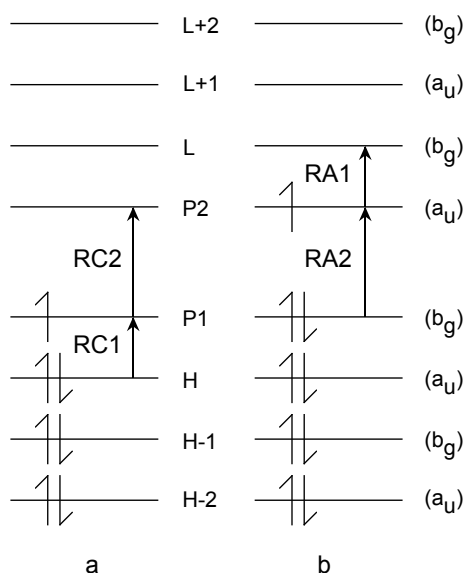
Figure 1.4: Scheme of the molecular orbitals for (a) singly positively charged polaron (cation); and (b) singly negatively charged polaron of phenylenevinylene oligomers. The sub-gap optical transitions induced upon doping and the irreducible representation are also represented.

In case of anions the occupation of the energy levels is different from that for cations (see Figure 1.4(b)). P1 is doubly occupied and P2 is singly occupied. Two sub-gap optical transitions are found also in case of anions. One transition (RA1) is due to excitation from the singly occupied molecular orbital (P2) to the lowest unoccupied molecular orbital (L). The second transition (RA2) corresponds to excitation from the highest doubly occupied molecular orbital (P1) to the singly occupied molecular orbital (P2).

The scheme discussed here is used in chapters 5, 6, 7 and 8 to describe the optical absorption spectra of phenylenevinylene and fluorene oligomers.

1.4 Conjugated oligomers as model systems for conjugated polymers

Conjugated oligomers have several advantages over polymers, such as well-defined chain length, absence of chain defects, and ease of purification and characterization. In addition, oligomers have more predictable and reproducible properties, facilitating the investigation of structure-property relations. Therefore, conjugated oligomers are considered as model systems for conjugated polymers.[28,29] One general strategy adopted in the research of fully conjugated polymers is to investigate the properties of a series of the corresponding oligomers

with increasing the chain length. The extrapolation of oligomer data provides the properties of the corresponding polymer. This strategy was successfully applied to describe electronic structures and photophysical properties of different systems.[30-32] However, for charge transport properties the extrapolation of oligomer properties to polymer requires special attention, because linear conjugated oligomers in films have a strong tendency to crystallize. There are some reports about the charge transport properties of a few series of oligomers as a function of oligomer length,[33,34] but they are not relevant for films of the corresponding polymers, since these are disordered. The extrapolation of optical properties is addressed in chapter 9 for fluorene copolymers.

1.5 Applications of conjugated oligomers and polymers

1.5.1 Opto-electronic devices

Light-emitting diodes (LEDs)

Electroluminescence (the generation of light by electrical excitation) from conjugated polymers was reported for the first time in 1990, using poly(p-phenylenevinylene) (PPV).[6] In a light-emitting diode, the conjugated polymer acts as a semiconducting layer between metallic electrodes. A schematic picture of a light-emitting diode based on conjugated polymer is shown in Figure 1.5. In this structure the indium-tin oxide (ITO) layer functions as a transparent electrode, and allows the light generated within the diode to leave the device. The cathode is formed by thermal evaporation of a metal.
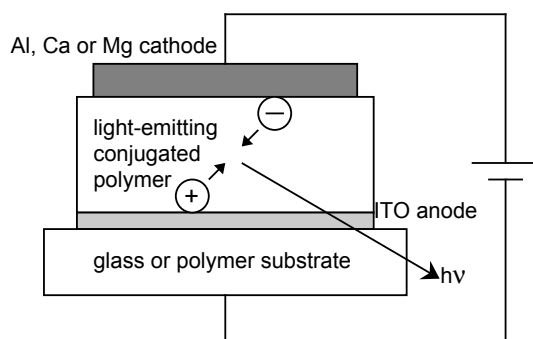
Figure 1.5: Scheme of a single-layer light-emitting diode.

LED operation is achieved by injection of electrons and holes from the opposite electrodes. In this way electrons are injected into the LUMO to form radical anions, while the holes are injected into the HOMO to form radical cations of the electroluminescent PPV. The resulting charges can migrate through the PPV layer under the influence of an applied electric field. Combination of the electron with the hole leads to the formation of an exciton (singlet and triplet excited states). The singlet state can decay to the ground state by emitting a photon, as illustrated in Figure 1.6.
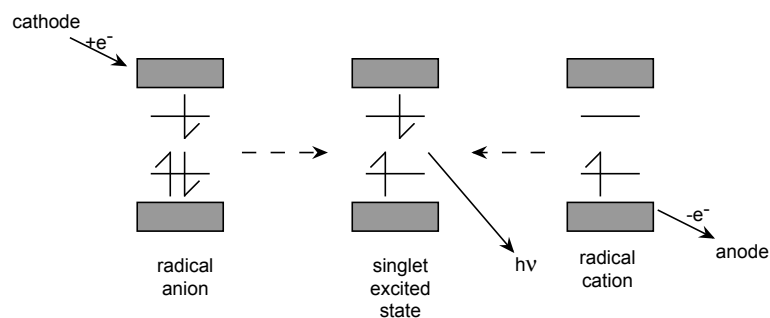
Figure 1.6: Schematic representation of light-emitting diode operation.

The color of the light emitted by a LED strongly depends on the polymer used as the semiconducting layer. Polythiophenes show emission in the red wavelength region,[35] poly(phenylenevinylene)s emit in the yellow-green region of the spectrum,[6,11] poly(p-phenylene) and polyfluorenes are blue light-emitting polymers.[36,37] As mentioned in section 1.3, the substitution of conjugated polymers with electron donating or withdrawing groups influences the magnitude of the bandgap. In this way the emission color of the polymer can be tuned.[38]

Field-effect transistors (FETs)

Since the report of the first organic field-effect transistor in 1986,[39] a lot of work has been done in order to improve the performance of materials and the design and fabrication of these devices. A schematic representation of a FET is shown in Figure 1.7. In such devices, the current that flows between two electrodes, the source and drain, is modulated by applying a voltage to a third electrode, called the gate. The parameters that characterize the performance of a FET are the charge carrier mobility and the current modulation (or on/off ratio). The charge carrier mobility, μ describes how easily charge carriers can move within the active layer under the influence of an electric field. Typical values for the charge carrier mobility in a FET based on conjugated polymer range from 10^{-5}-10^{-2} $cm^2V^{-1}s^{-1}$.[40] Molecular crystal organic FETs exhibit higher mobilities due to their molecular packing, which determines the electronic behavior. A value of 35 $cm^2V^{-1}s^{-1}$ has been reported for the hole mobility of single crystal pentacene at room temperature.[41] The second parameter, the current modulation (or the on/off ratio) is an indicator of the switching performance and represents the ratio of the current in "on" and "off" states. Ratios as high as 10^6 can be reached in organic FETs.[42]
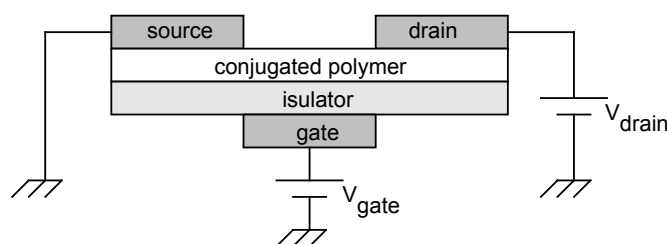
Figure 1.7: Scheme of a conjugated polymer based field-effect transistor.

In an organic field-effect transistor the active layer is a thin film of a conjugated polymer or oligomer, which can function either as a p-type material or n-type. In p-type semiconductors (pentacene,[43] α-sexithiophene[44] and poly-3-hexylthiophene[16,45]) the majority carriers are holes, while in n-type (perylene single crystal,[46] liquid crystalline perylene diimides[47]) the majority carriers are electrons. In order to improve the performance criteria mentioned above (mobility and on/off ratio), intensive research has been performed in optimizing the structure of the active layer. Solubility of the conjugated polymers and oligomers used as the active layer in a FET is assured by introducing substituents in the chemical structure. The type, size and regioregularity (position)[16] of the substituents affect the charge carrier mobility. Other factors such as: molecular weight[48] and type of solvent[45] used for deposition have large effects on the morphology of the thin film, influencing supramolecular order (single crystals have close to ideal ordering) and consequently the charge carrier mobility. For recent reviews the reader is referred to literature.[49-51]

Photovoltaic cells

Conjugated polymers can also be used as the absorbing layer in photovoltaic cells. Reviews on polymeric photovoltaic materials can be found in recent literature.[52-54]
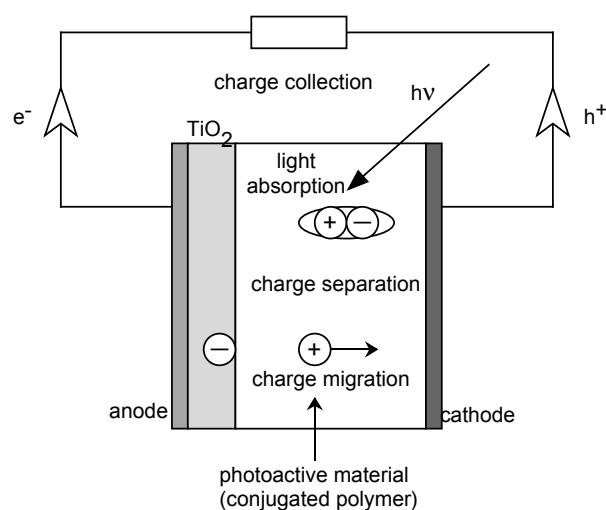
Figure 1.8: Scheme of the working principle of a polymer solar cell.

Figure 1.8 schematically shows the design and working principle of a basic solar cell. This simplified polymer solar cell consists of a conjugated polymer layer placed on an inorganic semiconductor (e.g. TiO_2). These layers are sandwiched between two electrodes. In general, the working principle of a solar cell is the reversed LED working principle. In the simplified solar cell shown in Figure 1.8 the photoactive material is illuminated through an optically transparent anode. The absorption of light by the conjugated polymer results in the excitation of an electron from the HOMO to the LUMO. In this way an exciton (electron-hole pair) is formed. The exciton (in the singlet excited state) migrates through the conjugated polymer until it reaches the interface with the TiO_2, where electron transfer takes place. The electron is transported to the anode via TiO_2. The positive charge in the conjugated polymer

must migrate to the cathode. The exciton must, during its lifetime, diffuse to the interface. Therefore, the exciton should have an appreciable lifetime and/or a relatively high diffusion constant. To avoid tiny diffusion distances the conjugated polymer layer is replaced by a bulk heterojunction, which consists of an interpenetrating network of electron donor and acceptor materials.[55,56] In these bulk heterojunctions the distance that excitons have to travel to reach the interface is reduced. Recently, a power-conversion efficiency of 4.4% has been reported for solar cells containing blends of poly(3-hexylthiophene) (P3HT) and a fullerene derivative [1-(3-methoxycarbonyl)-propyl-1-phenyl-(6,6) C_{61}] (PCBM).[57]

Another limiting parameter of polymer photovoltaics is the mismatch between the absorption spectrum of the conjugated polymer and the terrestrial solar spectrum. The use of low-bandgap conjugated polymers is a viable method to expand the absorption spectrum of solar cells and to increase their efficiency.[58-61] The conjugated polymer layer should be sufficiently thick to absorb all incident light. However, an increase of the layer thickness also affects charge and exciton transport.

Solid-state lasers

Recent reports highlighted conjugated polymers as a new class of solid-state laser materials.[62-64] In 1992 Moses observed for the first time lasing from conjugated polymers by photopumping a solution of poly(2-methoxy-5-(2'-ethylhexyloxy)-1,4-phenylenevinylene) (MEH-PPV).[65] After this moment intensive work has been performed to demonstrate the lasing from polymers in the solid state. Conjugated polymers have the electronic structure of a four-level system because structural and vibronic relaxation in the excited state shifts the energy levels. The main advantage of a four-level system is that the stimulated emission spectrum does not overlap with the ground state absorption spectrum. An advantage of using conjugated polymers as lasing materials is that the conjugation length varies in polymer films since these are disordered. This means that there are variations in the bandgap energy. Consequently, the energy can be absorbed in one region and then transferred to another region where the bandgap is smaller. Additionally, conjugated polymers have high luminescence efficiency and high chromophore density, making them suitable for applications as laser materials. A schematic diagram of the four-level system is illustrated in Figure 1.9 for a PPV derivative polymer (DP6-PPV). When the ground state (GS) is photopumped, ground-state absorption (GSA) occurs and excited-state vibrational levels are generated. Within 100 fs, excited electrons cascade into the lowest energy vibrational state and induce a structural relaxation, which shifts the energy of the excited state (ES). From there several processes can occur. At low photon densities, photoluminescence (PL) and non-radiative (NR) recombination are the dominant processes and the excited-state lifetime is less than 1 ns. If the photon density is high, stimulated emission (SE) can become the dominant process and the excited-state lifetime can be shortened. For this particular polymer excited-state absorption (ESA) does not compete with SE because it occurs at longer wavelengths. Once an electron decays from the excited state, structural relaxation to the ground state (GS) occurs rapidly. Consequently, the population inversion needed for lasing to occur can be obtained at low excitation densities.
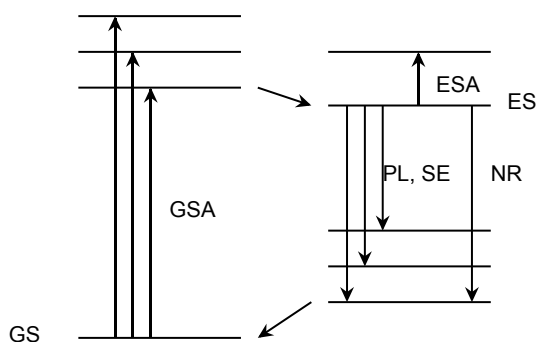
Figure 1.9: Schematic diagram of the four-level energy system and important transitions for a conjugated polymer such as DP6-PPV.

1.5.2 Molecular electronics

Molecular electronics is defined as the technology that deals with the use of single molecules, small groups of molecules, carbon nanotubes, or nanoscale metallic or semiconductor wires, which perform electronic functions. The electronic and optical properties of conjugated polymers make them suitable candidates for application as wires in molecular electronics.[66-68]

The first concrete idea of a device consisting of a single molecule belonged to Aviram and Ratner.[69] They predicted that a molecular analogue of a p-n junction, in which an electron donor species is in contact with an electron acceptor species, should act as a molecular rectifier. Since this moment, a lot of work has been performed to prove that a suitably designed organic molecule deposited in a layer between two electrodes would give current-voltage characteristics, similar to the behavior of a p-n junction.[70,71]

The gap between molecular structure and macroscopic electronic device behavior can be bridged by wiring up the molecular electronic components. In order to connect molecular electronic components, molecular wires are needed. Molecular wires can be realized using metallic carbon nanotubes or conjugated oligomers or polymers. An advantage of using conjugated systems instead of carbon nanotubes is the possibility to chemically control the properties of the molecular wire. One example is supramolecular ordering in the conjugated systems, which can be achieved by exploiting their self-assembly properties. In this way it is possible to build self-organizing circuits.[72] The most important characteristic of a molecular wire is the conductivity of the wire. In an ideal molecular wire the charge can be transferred over long distances at very fast rates.

Molecular switches are molecules capable of reversible change via external stimuli used in molecular devices and as molecular memory materials. One example of a molecular switch is the photochromic switch consisting of dithienylcyclopentenes.[73,74] In the open form the thienyl rings are not connected, which means that the conjugation is broken. By illumination with ultra-violet light the closed form is obtained, in which the conjugation is maintained. This molecule can be switched back to the open form by irradiation with visible light.

Over the past decade, considerable progress has been made towards applications of conjugated polymers to opto-electronics and molecular electronics, some of them have already attained commercial viability.[75]

1.6 Thesis aim and outline

The aim of this thesis is to provide fundamental insight into the nature and opto-electronic properties of charge carriers on conjugated oligomers and polymers. Electronic structure, optical absorption properties and distribution of charge carriers along the chains of different conjugated materials are central issues of this thesis. In order to achieve this, both experimental and theoretical studies have been performed. Quantum chemical calculations can give valuable information about the electronic structure and charge distribution, useful for explaining and interpreting the experimental results.

The first three chapters of this thesis are introductory and give a general description of the methods used. The next six chapters present in detail the scientific research performed on different conjugated materials. After a general introduction, where the reader is familiarized with conjugated polymers, their properties and applications, chapter 2 describes the experimental techniques used. The theoretical background of the quantum chemical methods applied to different conjugated molecules is discussed in chapter 3.

In chapter 4 a combined experimental and theoretical study of the optical properties of positively charged unsubstituted and dialkoxy-substituted phenylenevinylene oligomers is presented. The distribution of the excess positive charge gives insight into the effect of chain length and alkoxy substitution.

The excess negative charges on the same series of phenylenevinylene oligomers were investigated in chapter 5, using two different theoretical methods. The similarities and differences between the results of these two methods are discussed.

Until now, the work has been focused on linear one-dimensional conjugated oligomers. In chapter 6 optical absorption, charge distribution and charge transport are presented for five different two-dimensional phenylenevinylene oligomers. The results from chapter 6 are compared with those from previous chapters for the linear counterparts.

Chapters 7 and 8 deal with another class of conjugated oligomers and polymers: fluorenes. Chapter 7 presents experimental and theoretical studies on cations and anions of non-functionalized fluorenes. The optical absorption spectra, geometry deformations and charge distributions are discussed.

Chapter 8 presents a study of charges on fluorene co-oligomers. The possibility of tuning the optical properties of fluorenes by different functionalization is investigated.

Since in chapters 4-6 different results have been obtained for phenylenevinylene anions and cations using two distinct quantum chemical methods, the idea of finding the method that describes as accurate as possible the opto-electronic properties became challenging. The different results obtained using Density Functional Theory (DFT) and Intermediate Neglect of Differential Overlap combined with Single Interaction Configuration (INDO/s-CIS) is due to

the way in which electron correlation is taken into account in the two methods. Second-order Moller-Plesset perturbation theory (MP2) has been used in chapter 9, to investigate the effects of geometry (optimized using DFT and HF) and electron correlation, basis set, methoxy subtitution and spin contamination on the charge distribution for phenylenevinylene and thiophene oligomers.

1.7 References

(1)   Shirakawa, H.; Louis, E. J.; MacDiarmid, A. G.; Chiang, C. K.; Heeger, A. J. *Chem. Commun.* **1977**, 578.

(2)   Lefrant, S.; Lichtman, L. S.; Temkin, M.; Fichten, D. C.; Miller, D. C.; E., W. G.; Burlich, J. M. *Solid State Commun.* **1979**, *29*, 191.

(3)   Shirakawa, H. *Angew. Chem. Int. Ed. Engl.* **2001**, *40*, 2574.

(4)   MacDiarmid, A. G. *Angew. Chem. Int. Ed. Engl.* **2001**, *40*, 2581.

(5)   Heeger, A. *Angew. Chem. Int. Ed. Engl.* **2001**, *40*, 2591.

(6)   Burroughes, J. H.; Bradley, D. D. C.; Brown, A. R.; Marks, R. N.; Mackay, K.; Friend, R. H.; Burns, P. L.; Holmes, A. B. *Nature* **1990**, *347*, 539.

(7)   Reddinger, J. L.; Reynolds, J. R. Molecular Engineering of π-Conjugated Plymers; in *Advances in Polymer Science*; Springer-Verlag, Ed. Berlin Heidelberg, 1999.

(8)   Pron, A.; Rannou, P. *Prog. Polym. Sci.* **2002**, *27*, 135.

(9)   Bredas, J.-L.; Beljonne, D.; Coropceanu, V.; Cornil, J. *Chem. Rev.* **2004**, *104*, 4971.

(10)   Moliton, A.; Hiorns, R. C. *Polym. Int.* **2004**, *53*, 1397.

(11)   Kraft, A.; Grimsdale, A. C.; Holmes, A. B. *Angew. Chem. Int. Ed.* **1998**, *37*, 402.

(12)   Friend, R. H.; Gymer, R. W.; Holmes, A. B.; Burroughes, J. H.; Marks, R. N.; Taliani, C.; Bradley, D. D. C.; Dos Santos, D. A.; Bredas, J. L.; Logdlund, M.; Salaneck, W. R. *Nature* **1999**, *397*, 121.

(13)   Burn, P. L.; Holmes, A. B.; Kraft, A.; Bradley, D. D. C.; Brown, A. R.; Friend, R. H.; Gymer, R. W. *Nature* **1992**, *356*, 47.

(14)   Hilberer, A.; Brouwer, H. J.; Van der Scheer, B. J.; J. Wildeman, J.; Hadziioannou, G. *Macromolecules* **1995**, *28*, 4525.

(15)   Samuel, I. D. W.; Rumbles, G.; Collison, C. J. *Phys. Rev. B* **1995**, *52*, 11573.

(16)   Sirringhaus, H.; Brown, P. J.; Friend, R. H.; Nielsen, M. M.; Bechgaard, K.; Langeveld-Voss, B. M. W.; Spiering, A. J. H.; Janssen, R. A. J.; Meijer, E. W.; Herwig, P. T.; de Leeuw, D. M. *Nature* **1999**, *401*, 685.

(17)   Peierls, R. E. *Quantum Theory of Solids*; Oxford University Press: London, 1955.

(18)   Heeger, A. J.; Kivelson, S.; Schrieffer, J. R.; Su, W. P. *Rev. Mod. Phys.* **1988**, *60*, 781.

(19)   Kittel, C. *Introduction to Solid State Physiscs*, 8th ed.; John Wiley & Sons, Inc.: New York, 1995.

(20)   Pope, M.; Swenberg, C. E. *Electronic Processes in Organic Crystals and Polymers*; Oxford university Press: Oxford, 1999.

(21)   Bassler, H. *Phys. Stat. Sol. B* **1993**, *175*, 15.

(22)   Van de Craats, A. M.; Siebbeles, L. D. A.; Bleyl, I.; Haarer, D.; Berlin, Y. A.; Zharikov, A. A.; Warman, J. M. *J. Phys. Chem. B* **1998**, *102*, 9625.

(23)   Wudl, F.; Kobayashi, M.; Heeger, A. J. *J. Org. Chem.* **1984**, *49*, 3382.

(24) Pomerantz, M. Low Band Gap Conducting Polymers; in *Handbook of Conducting Polymers*; 2nd ed.; Skotheim, T. A., Elsenbaumer, R. L., Reynolds, J. R., Eds.; Marcel Dekker Inc.: New York, 1998.

(25) Padmanaban, G.; Ramakrishnan, S. *J. Am. Chem. Soc.* **2000**, *122*, 2244.

(26) Furukawa, Y. *Synth. Met.* **1995**, *69*, 629.

(27) Fesser, K.; Bishop, A. R.; Campbell, D. K. *Phys. Rev. B* **1983**, *27*, 4804.

(28) Mullen, K.; Wegner, G. *Electronic Materials: The Oligomer Approach*; Wiley-VCH: Weinheim, 1998.

(29) Van Hutten, P. F.; Hadziiannou, G. A Model Oligomer Approach to Semiconducting Polymers; in *Semiconducting Polymers: Chemistry, Physics and Engineering*; Hadziiannou, G., van Hutten, P. F., Eds.; Wiley-VCH: Weinheim, 2000.

(30) Woo, H. S.; Lhost, O.; Graham, S. C.; Bradley, D. D. C.; Friend, R. H.; Quattrocchi, C.; Bredas, J. L.; Schenk, R.; Mullen, K. *Synth. Met.* **1993**, *59*, 13.

(31) Schmidt, A.; Anderson, M. L.; Dunphy, D.; Wehrmeister, T.; Mullen, K.; Armstrong, N. R. *Adv. Mater.* **1995**, *7*, 722.

(32) Klaerner, G.; Miller, R. D. *Macromolecules* **1998**, *31*, 2007.

(33) Gundlach, D. J.; Lin, Y.-Y.; Jackson, T. N.; Schlom, D. G. *Appl. Phys. Lett.* **1997**, *71*, 3853.

(34) Halik, M.; Klauk, H.; Zschieschang, U.; Schmid, G.; Ponomarenko, S.; Kirchmeyer, S.; Weber, W. *Adv. Mater.* **2003**, *15*, 917.

(35) Perepichka, I. F.; Perepichka, D. F.; Meng, H.; Wudl, F. *Adv. Mater.* **2005**, *17*, 2281.

(36) Kim, D. Y.; Cho, H. N.; Kim, C. Y. *Progr. Polym. Science* **2000**, *25*, 1089.

(37) Scherf, U.; List, E. J. W. *Adv. Mater.* **2002**, *14*, 477.

(38) Somanathan, N.; Radhakrishnan, S. *Int. J. Mod. Phys. B* **2005**, *19*, 4645.

(39) Tsumura, A.; Koezuka, H.; Ando, T. *Appl. Phys. Lett.* **1986**, *49*, 1210.

(40) Chua, L.-L.; Zaumseil, J.; Chang, J.-F.; Ou, E. C.-W.; Ho, P. K.-H.; Sirringhaus, H.; Friend, R. H. *Nature* **2005**, *434*, 194.

(41) Jurchescu, O. D.; Baas, J.; Palstra, T. T. M. *Appl. Phys. Lett.* **2004**, *84*, 3061.

(42) Dodabalapur, A.; Torsi, L.; Katz, H. E. *Science* **1995**, *268*, 270.

(43) Lin, Y.-Y.; Gundlach, D. J.; Nelson, S. F.; Jackson, T. N. *IEEE Trans. Electron Dev.* **1997**, *44*, 1325.

(44) Katz, H. E. *J. Mater. Chem.* **1997**, *7*, 369.

(45) Bao, Z.; Dodabalapur, A.; Lovinger, A. J. *Appl. Phys. Lett.* **1996**, *69*, 4108.

(46) Schon, J. H.; Kloc, C.; Batlogg, B. *Appl. Phys. Lett.* **2000**, *77*, 3776.

(47) Struijk, C. W.; Sieval, A. B.; Dakhorst, J. E. J.; van Dijk, M.; Kimkes, P.; Koehorst, R. B. M.; Donker, H.; Schaafsma, T. J.; Picken, S. J.; van de Craats, A. M.; Warman, J. M.; Zuilhof, H.; Sudholter, E. J. R. *J. Am. Chem. Soc.* **2000**, *122*, 11057.

(48) Kline, R. J.; McGehee, M. D.; Kadnikova, E. N.; Liu, Y.; Frechet, M. J. *Adv. Mater.* **2003**, *15*, 1519.

(49) Reese, C.; Roberts, M.; Ling, M.; Bao, Z. *Mater. Today* **2004**, *7*, 20.

(50) Dimitrakopoulos, C. D.; Mascaro, D. J. *IBM J. Res. & Dev.* **2001**, *45*, 11.

(51) Veres, J.; Ogier, S.; Lloyd, G. *Chem. Mater.* **2004**, *16*, 4543.

(52) Gratzel, M. *Nature* **2001**, *414*, 338.

(53) Brabec, C. J.; Sariciftci, N. S.; Hummelen, J. C. *Adv. Funct. Mater.* **2001**, *11*, 15.

(54) Brabec, C.; Dyakonov, V.; Parisi, J.; Sariciftci, N. S. *Organic Photovoltaics*; Springer: Berlin, 2003.

(55) Halls, J. J. M.; Walsh, C. A.; Greenham, N. C.; Marseglla, E. A.; Friend, R. H.; Moratti, S. C.; Holmes, A. B. *Nature* **1995**, *376*, 498.

(56) Roncali, J. *Chem. Soc. Rev.* **2005**, *34*, 483.

(57) Kim, Y.; Cook, S.; Tuladhar, S. M.; Choulis, S. A.; Nelson, J.; Durrant, J. R.; Bradley, D. D. C.; Giles, M.; McCulloch, I.; Ha, C.-S.; Ree, M. *Nature Mater.* **2006**, *5*, 197.

(58) Shaheen, S. E.; Vangeneugden, D.; Kiebooms, R.; Vanderzande, D.; Fromherz, T.; Padinger, F.; Brabec, C. J.; Sariciftci, N. S. *Synth. Met.* **2001**, *121*, 1583.

(59) Vangeneugden, D. L.; Vanderzande, D. J. M.; Salbeck, J.; van Hal, P. A.; Janssen, R. A. J.; Hummelen, J. C.; Brabec, C. J.; Shaheen, S. E.; Sariciftci, N. S. *J. Phys. Chem. B* **2001**, *105*, 11106.

(60) Winder, C.; Sariciftci, N. S. *J. Mater. Chem.* **2004**, *14*, 1077.

(61) Dhanabalan, A.; van Duren, J. K. J.; van Hal, P. A.; van Dongen, J. L. J.; Janssen, R. A. J. *Adv. Funct. Mater.* **2001**, *11*, 255.

(62) Hide, F.; Schwartz, B. J.; Diaz-Garcia, M. A.; Heeger, A. *Synth. Met.* **1997**, *91*, 35.

(63) Kranzelbionder, G.; Leising, G. *Rep. Prog. Phys.* **2000**, *63*, 729.

(64) McGehee, M. D.; Heeger, A. J. *Adv. Mater.* **2000**, *12*, 1655.

(65) Moses, D. *Appl. Phys. Lett.* **1992**, *60*, 3215.

(66) Joachim, C.; Gimzewski, J. K.; Aviram, A. *Nature* **2000**, *408*, 541.

(67) Carroll, R. L.; Gorman, C. B. *Angew. Chem. Int. Ed.* **2002**, *41*, 4378.

(68) Saxena, V.; Malhotra, B. D. *Curr. Appl. Phys.* **2003**, *3*, 293.

(69) Aviram, A.; Ratner, M. A. *Chem. Phys. Lett.* **1974**, *29*, 277.

(70) Geddes, N. J.; Sambles, J. R.; Jarvis, D. J.; Parker, W. G.; Sandman, D. J. *Appl. Phys. Lett.* **1990**, *56*, 1916.

(71) Martin, A. S.; Sambles, J. R.; Ashwell, G. J. *Phys. Rev. Lett.* **1993**, *70*, 218.

(72) Hoeben, F. J. M.; Jonkheijm, P.; Meijer, E. W.; Schenning, A. P. H. J. *Chem. Rev.* **2005**, *105*, 1491.

(73) Browne, W. R.; de Jong, J. J. D.; Kudernac, T.; Walko, M.; Lucas, L. N.; Uchida, K.; van Esch, J. H.; Feringa, B. L. *Chem. Eur. J.* **2005**, *11*, 6414.

(74) Browne, W. R.; de Jong, J. J. D.; Kudernac, T.; Walko, M.; Lucas, L. N.; Uchida, K.; van Esch, J. H.; Feringa, B. L. *Chem. Eur. J.* **2005**, *11*, 6430.

(75) Forrest, S. R. *Nature* **2004**, *428*, 911.

Chapter 2

Experimental Methodology

2.1 Introduction

Experimental methods to produce radical cations and anions in solution include: chemical oxidation or reduction, electrochemical redox reactions, photoionization and radiation-chemical processes. The formation of side products in chemical oxidations or reductions and in electrochemical redox reactions is often inevitable, which makes it difficult to distinguish between the absorption band of the radical ion and that of the side product. Photoionization or ionization with high-energy electrons, together with time-resolved detection, allows a direct observation of the radical cations and anions, while avoiding complications due to side products.

The optical properties of a medium change when radical ions are introduced. Transient changes in the optical absorption spectrum of a sample upon irradiation with a short electron pulse can be measured using the time-resolved optical absorption technique. In the experiments described in the present thesis this technique is used to measure the optical absorption spectra of radical cations and anions of different oligomers or polymers and to follow the formation and decay kinetics of these charged species.

Figure 2.1 shows photographs of the equipment used to perform the experiments. The charges were generated by irradiation with electron pulses from a Van de Graaff accelerator, shown in Figure 2.1(a). The detection of the charges was performed using a home-built optical absorption setup, illustrated in Figure 2.1(b). The oligomer or polymer solution was placed in a quartz cell shown in Figure 2.1(c). In order to understand the results presented in this thesis, a brief description of the concepts, equipment, and data processing methods used is given in the following sections.

2.2 Pulse radiolysis: generation of charge carriers

Pulse radiolysis is a powerful technique, in which short lived species (excited states, ions, electrons and free radicals) are generated by high-energy electron or ion pulses and measured by a time-resolved detection method.[1,2] It has been applied to many fields such as radical reactions in chemistry,[3] biology,[4] medicine[4] and atmospheric chemistry.[5] Radiation effects in

nuclear technology,[6] water chemistry in nuclear reactors and groundwater chemistry relevant to radioactive waste repositories have also been investigated by pulse radiolysis.[5]

The pulse radiolysis technique was developed in the early 1960s. In 1963, Hart and Boag,[7] and Keene[8] independently discovered that hydrated electrons can be generated by pulse radiolysis and detected with a time resolution of microseconds. Since then, large efforts have been made to reach a better time resolution for studying radiation-induced elementary processes. Recently, electron pulses with a duration of 98 fs have been produced.[9] Moreover, attempts are being made to reduce the pulse duration to the attosecond time region.[10]

(a)

(b)

(c)
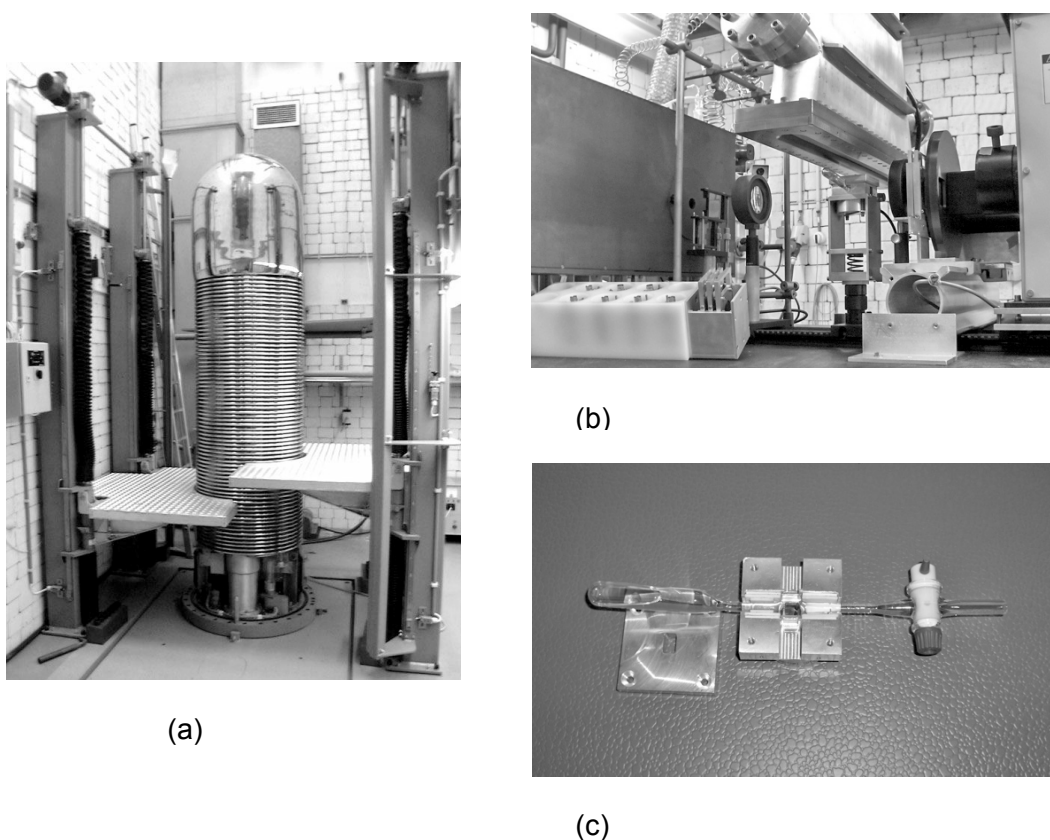
Figure 2.1: (a) Van de Graaff accelerator (b) optical absorption detection setup (c) quartz cell containing oligomer or polymer solution.

Different kinds of radiation sources are used in pulse radiolysis experiments.[11] Most commonly, electrons with energies in the MeV range are used. The high-energy electrons have a high penetrating power, which leads to ionizations and excitations throughout the entire material. The penetration depth of a 3 MeV electron in materials with a density of 1 g/cm^3 (a typical density for organic materials as studied in this thesis) is 1.5 cm.[12]

In the pulse radiolysis experiments described in this thesis the sample of interest is irradiated with short pulses of high-energy electrons from a Van de Graaff accelerator. When high-energy electrons (primary electrons) pass through a material the bound electrons in the material experience a rapidly changing electric field. Through this Coulombic interaction the primary electrons lose their energy in sequences of consecutive ionizations and excitations of

the molecules in the material.[13,14] The average energy that is transferred in one ionization or excitation is approximately 40 eV for hydrocarbon liquids and solids. The average distance between ionization or excitation events along the path or track of a primary 3 MeV electron is approximately 200 nm.[13,15] Most secondary electrons (formed in the ionization events) do not have sufficient energy to cause further ionizations and become thermalized (they reach an energy on the order of $k_B T$) at a distance of 5-10 nm from their parent cations.[12] Secondary electrons with a sufficiently high energy can cause further ionizations leading to formation of tertiary, etc. electrons.

Studies of the ionization of hydrocarbon media by high energy radiation have shown that a small fraction (few percent) of the electron-hole pairs undergo escape from their mutual Coulombic attraction and become "free ions".[16,17] The charges that do not escape undergo geminate recombination typically on a subnanosecond timescale. The yield of free ions (G) is usually expressed as the number of free ions produced per 100 eV energy deposited in the material.[2,14,18] The yield of free ions has been determined for a variety of organic solvents.[2] If a solute is added to the solvent, the free ions can react with the solute, generating positively or negatively charged species of the solute. In this way, positive and negative charges on conjugated oligomers were created and their properties were studied in the work described in this thesis.

2.2.1 Van de Graaff accelerator

In the present pulse radiolysis experiments a Van de Graaff accelerator (shown schematically in Figure 2.2) was used to produce short pulses of 3 MeV electrons.
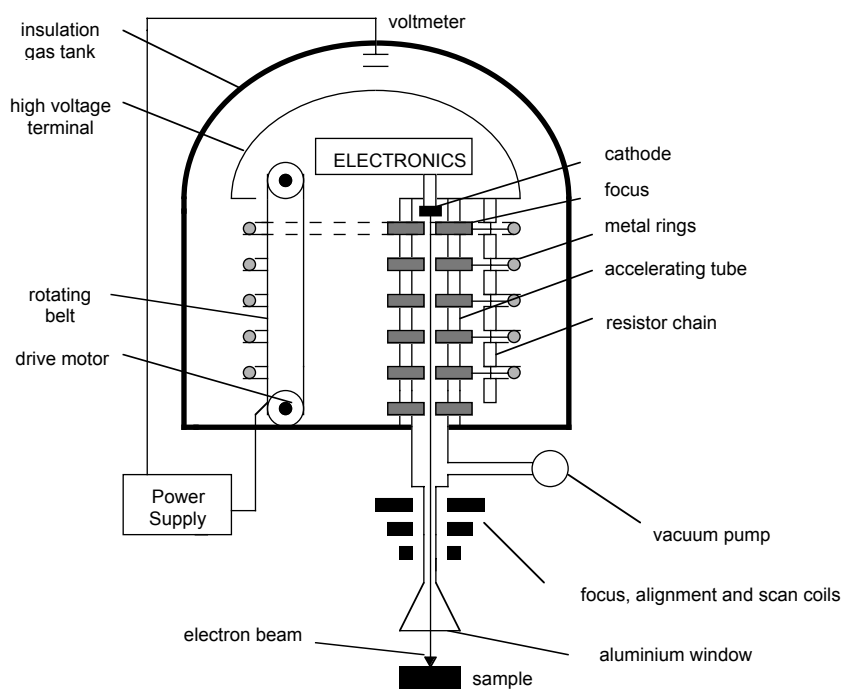
Figure 2.2: Scheme of the Van de Graaff accelerator.

The electrons are generated by an electron gun (hot cathode) and they are accelerated by a high voltage dc electric field (3 MV). At the exit of the accelerating tube the electrons have a kinetic energy of 3 MeV and a velocity close to the speed of light. The electron beam can be focused and aligned by electromagnetic coils and it can also be deflected onto a coaxial target. The amount of charge per pulse can be measured by an electrometer connected to this target. The maximum current in the pulse is 4 A. Pulses of 2, 5, 10, 20, 50 and 250 ns duration are obtained using a linear pulser in which the length of the pulse-forming coaxial cable determines the pulse duration. Detailed information about the Van de Graaff accelerator used in the experiments described in this thesis can be found elsewhere.[19-22]

2.2.2 Dosimetry

The initial concentration of charge carriers is determined by the amount of energy that is transferred from the incident 3 MeV electrons to the solution of the oligomer or polymer. The radiation dose (expressed in Gy) is often taken as the amount of energy transferred per unit mass (1Gy = 1 J/kg).[2] For analysis of the optical absorption data in solution it is more convenient to express the dose as energy per unit volume. Therefore, in this thesis the absorbed dose per unit volume, D_V (in J/m^3), is used. The dosimetry was performed using a KSCN solution (10 mM) in N_2O-saturated water. For this solution the yield of free ions (G) and the molar extinction coefficient (ε) are accurately known ($G\varepsilon(SCN)_2^- = 5.18 \times 10^{-4}$ m^2/J at 475 nm).[23] Such a solution was irradiated with 2, 5, 10, 20 and 50 ns pulses of 3 MeV electrons from the Van de Graaff accelerator. Optical absorption transients monitoring the change in absorbance upon irradiation as a function of time were recorded for different pulse durations. The beam charge per pulse was measured for each pulse duration. In Figure 2.3 the radiation dose is given as a function of the amount of charge per pulse. From the slope of the linear fit to the experimental data, the average radiation dose per unit volume in water is found to be D_{water}=1.56 J/m^3 per nC beam charge.

For a solvent, *S*, other than water, the radiation dose is to a good approximation equal to the radiation dose determined in water multiplied by the ratio of the number of electrons per kilogram for *S* divided by the number of electrons per kilogram for water. The factor relating the dose in the two media is $F_e(S)$, given by:

$$F_e(S) = \frac{18 \times N_S}{10 \times W_S} \tag{2.1}$$

with N_S the number of electrons per molecule and W_S the molecular weight. For example for benzene $N_S = 42$ and $W_S = 78$, which gives a value for $F_e(S)$ of 0.969.

The total dose in a pulse for solvent S is given by:

$$D(S) = F_e(S) \times D_{water} \quad \text{in J/kg} \tag{2.2}$$

The total dose absorbed in a pulse per unit volume is

$$D_V(S) = d_S \times F_e(S) \times D_{water} \quad \text{in J/m}^3 \qquad (2.3)$$

with d_S the density of the solvent (880 kg/m^3 for benzene).[24]
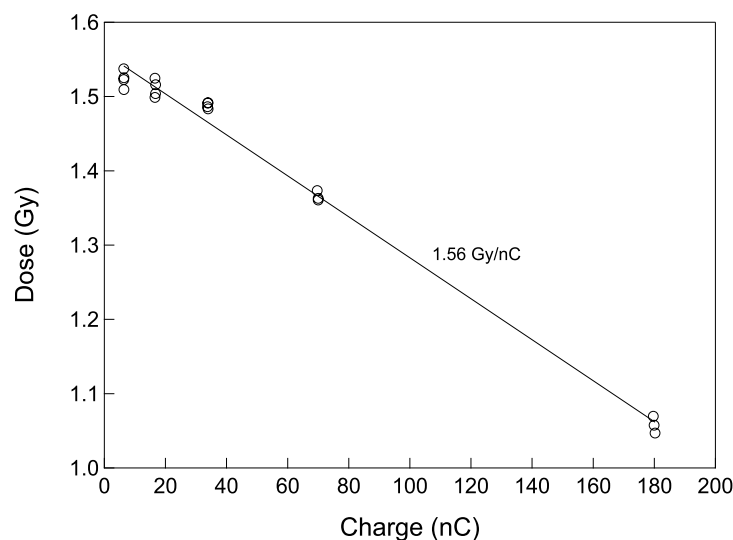
Figure 2.3: Radiation dose per pulse for KSCN in N$_2$O-saturated water measured at 2, 5, 10, 20 and 50 ns pulses. The slope of the linear fit expresses the average dose deposed in the solution.

The optical absorption spectra described in this thesis are presented as the change in absorbance upon irradiation normalized to the absorbed radiation dose and to the optical path length.

2.3 Time-resolved absorption spectroscopy: detection of charge carriers

Different methods can be used to detect the charges generated by pulse radiolysis: optical absorption and emission, magnetic resonance, microwave absorption and conductivity.[1] Time-resolved detection techniques can provide information about the nature of short-lived intermediates and about the kinetics of their formation and decay, which would not always be detectable in steady-state measurements. The most common technique used for monitoring transient behavior in pulse radiolysis is optical absorption spectroscopy. Time-resolved optical absorption spectroscopy has been applied to measure the spectrum of radical ions in rigid matrices[25] or in solution.[26] In this thesis we will discuss the time-resolved optical absorption spectra of positive and negative charges on different chains of conjugated oligomers and polymers in solution.

2.3.1 The optical absorption detection apparatus

The time-resolved VIS/NIR optical absorption setup, used to detect positively and negatively charged species is shown schematically in Figure 2.4. It consists of two parts: the optics and

the electronics. The optical absorption setup detects and records the change in analyzing light after passing the sample and the monochromator.[27]
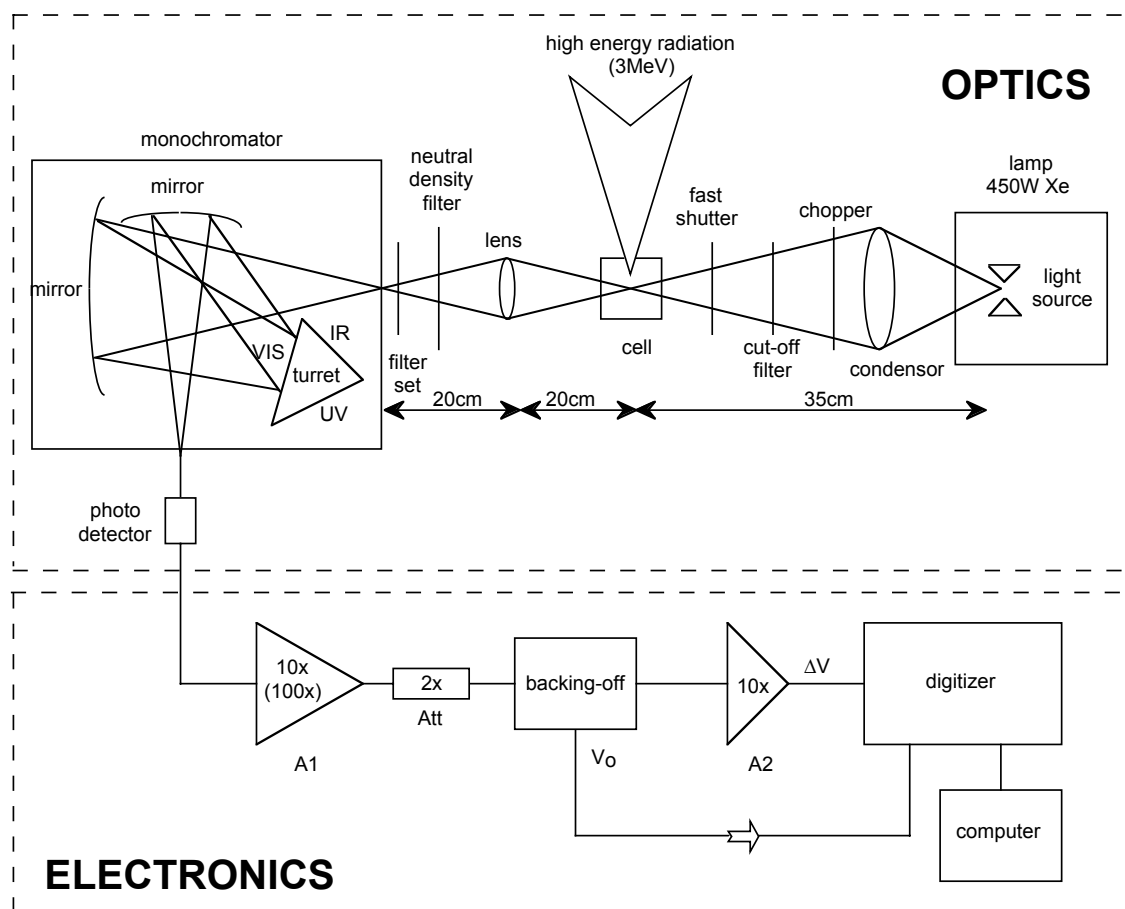
Figure 2.4: Scheme of the optical absorption detection apparatus.

The main components of the optical part are: a light source, a monochromator and a photodetector. The detection light source is an Osram XBO high-pressure Xe-lamp (450 W) containing a condensor, which focuses the light beam into the sample. Continuous illumination can cause damage to the sample. In order to avoid this a fast shutter has been placed between the light source and the cell containing the sample. The fast shutter opens during and after the electron pulse, allowing the light to pass through the sample. To avoid photolysis of the sample by the analyzing light, short-wavelength cut-off filters have been placed between the light source and the fast shutter. A chopper, located in front of the condensor protects the cut-off filters and the fast shutter. The solution under investigation is placed in a quartz cell with optical path length of 12.5 mm and height of 6 mm. After passing the sample, the light is focused by a lens into the entrance slit of the monochromator (Jobin Yvon HL 300). The monochromator selects a given output wavelength at the exit by rotating a turret. The turret is made of three gratings for the ultraviolet, visible and infrared region, respectivelly. A neutral density filter, placed between the lens and monochromator controls the intensity of the light beam entering the monochromator. A filter set situated at the monochromator entrance cuts higher order wavelengths from the Xe lamp which are implicitly selected. For detection up to 1000 nm, a silicon photodiode is used. Between 1000

nm and 1600 nm, a short-wavelength enhanced InGaAs PIN photodiode G5125-10 (Hamamatsu, Japan) is used, while for wavelengths higher than 1600 nm this is replaced by a long-wavelength enhanced InGaAs PIN photodiode G5853-01 (Hamamatsu, Japan) .

The time-resolved signal from the photodetector is amplified 10 or 100 times in an amplifier (A1) in the electronic part. In time-resolved optical absorption measurements the main interest is the change of the light absorption upon irradiation. The signal due to this absorption is usually small compared with the signal obtained from the photodetector without irradiation. In order to compensate the latter signal at each wavelength, the electronic part incorporates a backing-off system. The maximum limit of the backing-off system is 500 mV. The backing-off system has two exits. One exit gives the voltage corresponding to the change in photodetector signal after passing the sample (ΔV). This voltage can be further amplified in a second amplifier (A2 in Figure 2.4) before being recorded by the digitizer. The second exit of the backing-off system gives the voltage corresponding to the signal from the photodetector without irradiation and is also recorded by the digitizer (V_0). The time-resolved change in photodetector signal is monitored either with a Tektronic TDS 680B or with a LeCroy LT374L digitizer. A logarithmic time scale can be obtained when the LeCroy LT374L digitizer is used. The opening and the closing of the fast shutter, the triggering of both the backing-off circuit and the the digitizer are regulated by a synchronization system including delay units and phase shifters. All the active components from the electronic part are enclosed in a Faraday cage in order to reduce the electromagnetically induced noise, emanating from the accelerator pulse.

2.3.2 Time-resolved VIS/NIR spectroscopy measurements

Figure 2.5 schematically shows an optical absorption transient displayed on the digitizer when at a time t an electron pulse induces a change in absorbance, initially leading to a decrease in the voltage by ΔV.
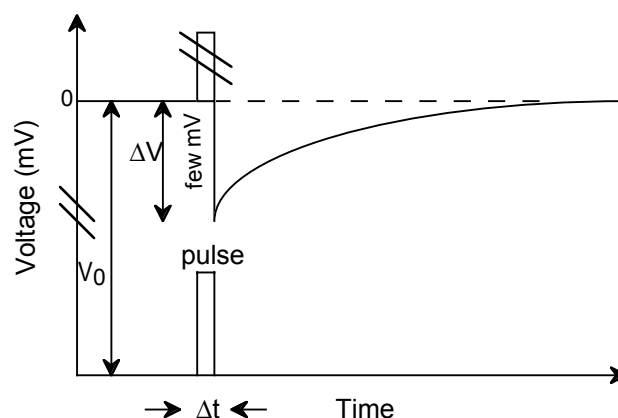
Figure 2.5: Schematic drawing of the voltage corresponding to the change in absorbance of the charge carriers induced by an electron pulse of duration Δt as a function of time.

In practice, two voltages are measured on the digitizer: the amplified voltage corresponding to the change in photodetector signal (ΔV) and the amplified voltage corresponding to the initial photodetector signal (V_0). The LeCroy LT374L digitizer records optical absorption transients, in which the amplified voltage corresponding to the change in photodetector signal (ΔV) is given over an extended time-domain from nanoseconds to milliseconds.

2.3.3 Data analysis

The voltage signal measured on the detector (in mV) is scaled to the change in absorbance (ΔA) as follows. The intensity of the absorption by a sample varies with the length l of the sample in accord with the Beer-Lambert law:[27]

$$\log \frac{I_{out}}{I_{in}} = -\varepsilon[P]l \tag{2.4}$$

where I_{in} is the incident light intensity, I_{out} is the intensity after passage through a sample of length l, and $[P]$ is the molar concentration of the absorbing species. The quantity ε is the molar absorption coefficient or the extinction coefficient. The dimensionless product

$$A = \varepsilon[P]l \tag{2.5}$$

is the absorbance of the sample.

In our experiments the quantity of interest is the change in absorbance upon irradiation, ΔA. ΔA is defined as the difference between the absorbance after the electron pulse and the absorbance before the pulse. The absorbance before the electron pulse, A_0 is given by

$$A_0 = -\log \frac{I_{out}}{I_{in}} \tag{2.6}$$

The absorbance after the electron pulse (A) is equal to:

$$A = -\log \frac{I_{out} - \Delta I_{out}}{I_{in}} \tag{2.7}$$

with ΔI_{out} the change in photodetector signal. The change in absorbance is equal to:

$$\Delta A = A - A_0 = -\log \left(1 - \frac{\Delta I_{out}}{I_{out}} \right) \tag{2.8}$$

The photodetector is a current source and the current measured by the photodetector is proportional to the light intensity. The current measured by the photodetector is transformed

into a voltage by 50 Ω resistors. All amplifiers are 50 Ω impedances. The amplified voltage corresponding to the initial photodetector signal (V_0) is a measure of I_{out}:

$$V_0 = C \times I_{out} \times A1 \times 50\Omega \qquad (2.9)$$

where C is a constant. The amplified voltage corresponding to the change in photodetector signal (ΔV) is proportional to ΔI_{out}:

$$\Delta V = C \times \Delta I_{out} \times A1 \times \frac{1}{Att} \times A2 \times 50\Omega \qquad (2.10)$$

Att is the attenuation factor of the first amplifier $(A1)$ when the backing-off is active during the time window of the measurement $(Att = 2)$. The fraction $\frac{\Delta I_{out}}{I_{out}}$ is calculated using eqs. 2.9 and 2.10.

$$\frac{\Delta I_{out}}{I_{out}} = \frac{\Delta V}{V_0} \cdot \frac{Att}{A2} = \frac{\Delta V}{V_0} \cdot \frac{1}{F_A} \qquad (2.11)$$

The ratio $\frac{A2}{Att}$ indicated as F_A, varies depending on the amplification used. In Table 2.1 the values of F_A for different amplification are presented.

Table 2.1: F_A values as function of the amplification used in the experiments.

Amplification before the backing-off	Amplification after the backing-off	F_A
10	10	5
100	10	5

2.3.4 Formation and recombination kinetics of charged species in solutions

As mentioned in the beginning of paragraph 2.3, time-resolved absorption spectroscopy gives information about the kinetics of formation and decay of a transient species. In time-resolved optical absorption measurements it is possible to follow the kinetics of charged (cations and anions) or uncharged (triplet excited states) species. The main advantage that time-resolved optical absorption measurements have in comparison with other time-resolved detection techniques (e.g. in time-resolved microwave conductivity measurements) is the possibility to follow the kinetics of both mobile and immobile charged species. In time-resolved microwave conductivity measurements, for example, only the kinetics of mobile species can be followed. In Figure 2.6 the optical absorption transient of a fluorene trimer is presented, showing the change in absorbance recorded on a logarithmic time scale.
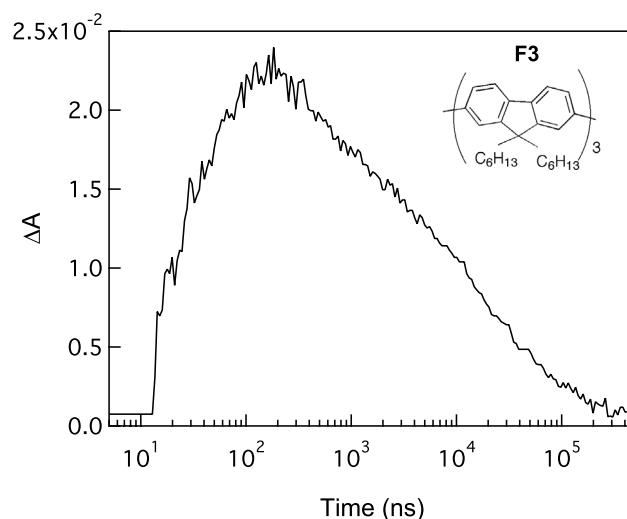
Figure 2.6: Optical absorption transient of a fluorene trimer in O_2-saturated benzene at the maximum of absorption (1920 nm). The chemical structure of the fluorene trimer (F3) is inserted in the graph. The formation and recombination of the fluorene radical cation is shown as *ΔA vs.* time.

The data during and directly after the electron pulse could not be measured due to Cerenkov radiation. Cerenkov radiation is the blue light emitted when charged particles enter a medium at a velocity exceeding the speed of light in that medium.[28] The amount of Cerenkov radiation is higher at shorter wavelengths because the number of photons emitted by the charged particles decreases with increasing the wavelength. In the optical absorption transient in Figure 2.6 the Cerenkov radiation cuts the data during the pulse (5 ns duration) and directly after the pulse (up to 13 ns). The change in absorbance increases initially after the electron pulse on a time scale of about 50 ns, corresponding to the formation of fluorene radical cations. The decay of the transient absorption in Figure 2.6 on a time scale of hundreds to thousands of nanoseconds is attributed to second-order charge recombination. A detailed discussion of the formation and recombination kinetics of positively and/or negatively charged oligomers/polymers in solution is discussed in chapters 6, 7 and 8 for X-shaped phenylenevinylenes, oligofluorenes and fluorene copolymers, respectively.

2.3.5 Optical absorption spectra

Time-resolved optical absorption transients can be used to construct the optical absorption spectra of charged species. Optical absorption spectra of charged species are obtained by recording the transient changes in absorbance of the solutions at different wavelengths in the same time interval. An example of such an absorption spectrum is shown in Figure 2.7.

Two absorption bands are observed in Figure 2.7 for the PV2(1 da) radical cation in benzene. A low energy band appears at 1.27 eV. A high-energy band has a maximum at 2.08 eV and exhibits two vibrational transitions. Such optical absorption spectra will be discussed in detail in the following chapters of the thesis.
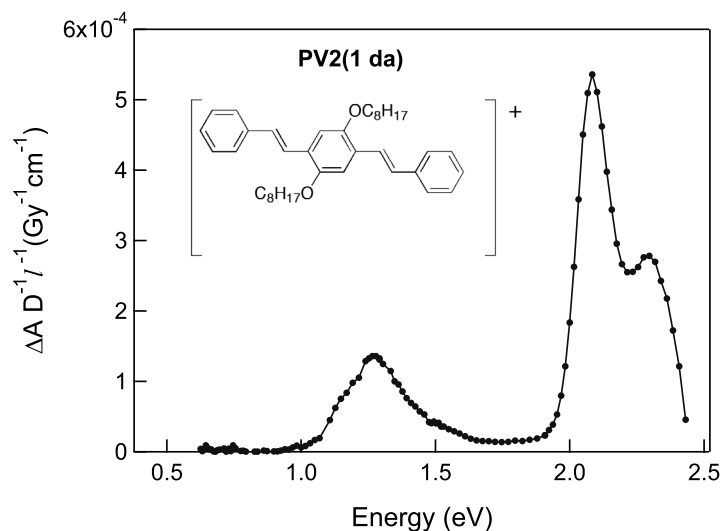
Figure 2.7: Optical absorption spectrum of a dialkoxy substituted phenylenevinylene PV2(1 da) radical cation in benzene. (The chemical structure is inserted in the graph.) The absorbance changes upon irradiation are normalized to the radiation dose and optical path length.

2.3.6 Estimation of extinction coefficients

From dosimetry measurements and pulse radiolysis data an estimation of the lower limit of the experimental extinction coefficients (ε) can be made, if it is assumed that all the charges generated during pulse radiolysis experiments react with the oligomers present in solution. The change in optical absorbance is related to the radiation dose, the yield of free charge carriers per unit dose (G), and the molar extinction coefficient (ε). As described in section 2.2.2, the radiation dose per pulse was determined using KSCN solution (10 mM) in N_2O-saturated water[23] and it was determined to be 1.56 Gy per nC of beam charge. For the optical experiments described in this thesis, the yield of free charge carriers in benzene was taken from literature $0.053(100eV)^{-1}$.[29] For experiments performed in THF the yield of free ions is $0.3(100\ eV)^{-1}$.[30]

The change in absorbance is related to the extinction coefficient, as given by eq. 2.5. The concentration [P] formed in a pulse is given by:

$$[P] = G \times D_V(S) \tag{2.12}$$

Hence, the change in absorbance is given by:

$$\Delta A = \varepsilon \times l \times G \times D_V(S) \tag{2.13}$$

From eq. 2.13, the lower limit of the molar extinction coefficient can be estimated. Note, that in literature G is expressed as number of molecules formed per 100 eV absorbed. In eq. 2.13 G has to be converted in number of moles formed per joule of absorbed energy. In the case of benzene, G=0.053 molecules per 100 eV, which corresponds to $0.053/9.63 \times 10^6$ mol/J.

This procedure is applied in chapter 7 to estimate the molar extinction coefficients for cations and anions of fluorene oligomers. A precise determination of the molar extinction coefficients can be realized by kinetic fitting of the time-resolved optical absorption transients. However, this is not the aim of the present thesis and therefore it will be discussed elsewhere.

2.4 References

(1)   Tabata, Y. *Pulse Radiolysis*; CRC Press, Inc.: Boca Raton, 1991.

(2)   Tabata, Y.; Ito, Y.; Tagawa, S. *Handbook of Radiation Chemistry*; CRC Press, Inc.: Boca Raton, 1991.

(3)   Farhataziz, I.; Rodgers, M. A. J. *Radiation Chemistry: Principles and Applications*; VCH Publishers, Inc.: New York, 1987.

(4)   Bensasson, R. V.; Land, E. J.; Truscott, T. G. *Excited States and Free Radicals in Biology and Medicine. Contributions from Flash Photolysis and Pulse Radiolysis*; Oxford University Press: Oxford, New York, Tokyo, 1993.

(5)   Cooper, W. J.; Curry, R. D.; O'Shea, K. E. *Environmental Applications of Ionizing Radiation* John Wiley & Sons, Inc. New York, 1998.

(6)   Katsumura, Y. in *Charged-Particle and Photon Interactions with Matters, Chemical, Physicochemical, and Biological Consequences with Applications*; Mozumder, A., Hatano, Y., Eds.; Marcel Dekker, Inc.: New York, 2004; pp 697.

(7)   Boag, J. W.; Hart, E. J. *Nature* **1963**, *197*, 45.

(8)   Keene, J. P. *Nature* **1963**, *197*, 47.

(9)   Yang, J.; Kondoh, T.; Kozawa, T.; Yoshida, Y.; Tagawa, S. *Radiat. Phys. Chem.* **2006**, *75*, 1034.

(10)   Yoshida, Y.; Yang, J.; Kondo, T. *Proceedings of 2005 Particle Accelerator Conference, Knoxville, Tennessee* **2005**.

(11)   Sauer Jr., M. C. Sources of Pulsed Radiation; in *The Study of Fast Processes and Transient Species by Electron Pulse Radiolysis*; Baxendale, J. H., Busi, F., Eds.; D. Reidel Publishing Company: Dordrecht, Boston, London, 1982.

(12)   Freeman, G. R. *Kinetics of Nonhomogeneous Processes*; John Wiley & Sons: New York, 1987.

(13)   Hummel, A. *Radiation Chemistry: The Chemical Effects of Ionizing Radiation and Their Applications* Delft, 1995.

(14)   Turner, J. E. *Atoms, Radiation, and Radiation Protection* New York, 1995.

(15)   Hummel, A. in *The Chemistry of Alkanes and Cycloalkanes*; Patai, S., Rappoport, Z., Eds.; John Wiley & Sons, Inc.: New York, 1992.

(16)   Warman, J. M. In *The Study of Fast Processes and Transient Species by Electron Pulse Radiolysis*; Baxendale, J. H., Busi, F., Eds.; D. Reidel Publishing Company: Dordrecht, 1982.

(17)   Siebbeles, L. D. A.; Bartczak, W. M.; Terrisol, M.; Hummel, A. *J. Phys. Chem. A* **1997**, *101*, 1619.

(18)   Mozumder, A. *Fundamentals of Radiation Chemistry*; Academic Press: San Diego, 1999.

(19) Luthjens, L. H.; Hom, M. L.; Vermeulen, M. J. W. *Rev. Sci. Instr.* **1978**, *49*, 230.

(20) Luthjens, L. H.; Hom, M. L.; Vermeulen, M. J. W. *Rev. Sci. Instr.* **1980**, *51*, 1183.

(21) Luthjens, L. H.; Vermeulen, M. J. W.; Hom, M. L. *Rev. Sci. Instr.* **1982**, *53*, 476.

(22) Luthjens, L. H.; Hom, M. L.; Vermeulen, M. J. W. *Rev. Sci. Instr.* **1986**, *57*, 2230.

(23) Buxton, G. V.; Stuart, C. R. *J. Chem. Soc. Faraday Trans.* **1995**, *91*, 279.

(24) Lide, D. R. *CRC Handbook of Chemistry and Physics*; CRC Press: Boca Raton, 1994.

(25) Shida, T.; Haselbach, E.; Bally, T. *Acc. Chem. Res.* **1984**, *17*, 180.

(26) Fox, M. A. *Chem. Rev.* **1978**, *79*, 253.

(27) Atkins, P. W. *Physical Chemistry*; Oxford University Press: New York, 1994.

(28) Jelley, J. V. *Cerenkov Radiation, and its Applications*; Pergamon Press: New York, 1958.

(29) Schmidt, W. F.; Allen, A. O. *J. Chem. Phys.* **1970**, *52*, 2345.

(30) Shaede, E. A.; Kurihara, H.; Dorfman, L. M. *Int. J. Radiat. Phys. Chem.* **1974**, *6*, 47.

Chapter 3

Methods for Electronic Structure Calculations

3.1 Introduction

In the early 20th century physicists found that classical mechanics does not correctly describe the behavior of small particles, such as the electrons and nuclei of atoms and molecules. This led to the development of quantum mechanics. The approach used in quantum mechanics is to postulate some basic principles and then to use these postulates to deduce experimentally testable consequences, such as the energy levels of the atoms.[1] One of the postulates of quantum mechanics is that the motion of electrons and nuclei in atoms and molecules can be described by a *wave function Ψ*, which is a function of the particle coordinates. Since the state will, in general, change with time, Ψ is also a function of time $\Psi(x, t)$. The wave function $\Psi(x, t)$ evolves in time according to the *time dependent Schrödinger equation:*[2]

$$i\hbar \frac{\partial \Psi}{\partial t} = \hat{H}\Psi \tag{3.1}$$

$\hat{H}$ is the Hamiltonian operator, which describes the total energy of the system as a function of coordinates (x, y, z) and momenta (p_x, p_y, p_z). For a one-particle, three-dimensional system, the classical Hamiltonian is:

$$H = T + V = \frac{1}{2m}\left(p_x^2 + p_y^2 + p_z^2\right) + V(x, y, z) \tag{3.2}$$

with T defining the kinetic energy and V the potential energy.

The *time-independent Schrödinger equation* is used for describing steady state properties. This is obtained by considering the potential energy as independent of time and applying the separation-of-variable procedure $\left[\Psi(x,t) = \psi(x)\theta(t)\right]$. The expression of the time-independent Schrödinger equation is:

$$\hat{H}\psi = E\psi \tag{3.3}$$

where E is the total energy of the system. The Hamiltonian operator $\hat{H}$ of a one-particle, three-dimensional system is written as :

$$\hat{H} = -\frac{\hbar^2}{2m}\left(\frac{\partial^2}{\partial x^2} + \frac{\partial^2}{\partial y^2} + \frac{\partial^2}{\partial z^2}\right) + V(x,y,z) \tag{3.4}$$

For a three-dimensional system with n particles the time-independent Schrödinger equation is:

$$\left[\sum_{i=1}^{n}\frac{\hbar^2}{2m_i}\nabla_i^2 + V(x_1,...,z_n)\right]\psi = E\psi \tag{3.5}$$

where the time-independent wave function is a function of the *3n* coordinates of the *n* particles:

$$\psi = \psi(x_1,y_1,z_1,...,x_n,y_n,z_n) \tag{3.6}$$

and ∇_i^2 is the laplacian operator corresponding to the particle *i*:

$$\nabla_i^2 = \left(\frac{\partial^2}{\partial x_i^2} + \frac{\partial^2}{\partial y_i^2} + \frac{\partial^2}{\partial z_i^2}\right) \tag{3.7}$$

Unfortunately, the Schrödinger equation cannot be solved analytically even for the simplest molecule, H_2^+, which consists of only three particles. The first approximation that is usually made is the *Born-Oppenheimer approximation*. In this approximation the motion of the electrons in a molecule is treated independent from the motion of nuclei, since the latter are much heavier. Because of the large difference in mass, the electrons can respond instantaneously to a displacement of the nuclei. This means that it is possible to solve the Schrödinger equation for the electrons in the static electric potential arising from nuclei, considering the latter fixed. The Hamiltonian includes in the Born-Oppenheimer approximation the kinetic energy terms for electrons (indexed by *i*), the electron-nucleus potential (with a distance of separation r_{Ai}), the nuclear-nuclear potential (with a distance of separation R_{AB}) and the electron-electron repulsion (with a distance of separation r_{ij}).[3]

$$\hat{H} = -\frac{1}{2}\sum_i^{electrons}\nabla_i^2 - \sum_A^{nuclei}\sum_i^{electrons}\frac{Z_A}{r_{Ai}} + \sum_{A>B}^{nuclei}\sum_B^{nuclei}\frac{Z_A Z_B}{R_{AB}} + \sum_{i>j}^{electrons}\sum_j^{electrons}\frac{1}{r_{ij}} \tag{3.8}$$

In eq. 3.8 and the rest of this chapter atomic units are assumed, so that $m_i = 1$, $\hbar = 1$ and $4\pi\varepsilon_0 = 1$. The nuclear-nuclear potential is independent on the electron coordinates and does not influence the electronic wave function. An exact solution to this equation is possible only for one-electron systems, e.g. H_2^+, due to the presence of the last term in eq. 3.8, which describes the mutual electrostatic repulsion between electrons. In order to calculate the repulsion of one electron with the other electrons in the system, the wave function for the other electrons must be known and vice versa. This means, that for multi-electron systems

only an approximate solution of the Schrödinger equation can be obtained. A large variety of methods to obtain approximate solutions for ψ have been developed with attempts to describe the electronic properties as accurately as possible. In the following paragraphs some of these methods are briefly described. These methods have been used in the electronic structure calculations discussed in the chapters of this thesis. For a complete and detailed description of the available methods the reader is referred to literature.[1,4-7]

3.2 The Hartree-Fock self-consistent field approximation

The *Hartree-Fock self-consistent field* approach assumes that one electron moves in a potential that is an average of the other electrons and the nuclei. The *N*-electron wave function that is used in Hartree-Fock (HF) calculations is a single Slater determinant and it is approximated by a product of *N* one-electron wave functions. To take into account the electron spin, the one-electron wave functions or the one-electron spin-orbitals (denoted $\chi_i(\vec{x})$) are written as products of spatial orbitals, $\phi_i(\vec{x})$, and spin functions, α or β.

$$\psi = \frac{1}{\sqrt{N!}} \begin{vmatrix} \phi_1(x_1)\alpha(1) & \phi_1(x_1)\beta(1) & ... & \phi_{\frac{N}{2}}(x_1)\alpha(1) & \phi_{\frac{N}{2}}(x_1)\beta(1) \\ \phi_1(x_2)\alpha(2) & \phi_1(x_2)\beta(2) & ... & \phi_{\frac{N}{2}}(x_2)\alpha(2) & \phi_{\frac{N}{2}}(x_2)\beta(2) \\ \vdots & \vdots & \vdots & \vdots & \vdots \\ \phi_1(x_N)\alpha(N) & \phi_1(x_N)\beta(N) & ... & \phi_{\frac{N}{2}}(x_N)\alpha(N) & \phi_{\frac{N}{2}}(x_N)\beta(N) \end{vmatrix} \qquad (3.9)$$

Such a determinant satisfies the *antisymmetry principle*, which states that a wave function describing fermions (particles with half-integer spin) should be antisymmetric with respect to the interchange of any set of space-spin coordinates.

To simplify the expression of the Hamiltonian in eq. 3.8, the following notations are used for the one-electron operator

$$h(i) = -\frac{1}{2}\nabla_i^2 - \sum_A^{nuclei} \frac{Z_A}{r_{Ai}} \qquad (3.10)$$

and the two-electron operator

$$v(i,j) = \sum_j^{electrons} \frac{1}{r_{ij}} \qquad (3.11)$$

Eq. 3.8 becomes

$$\hat{H}_{el} = \sum_i^{electrons} h(i) + \sum_{i<j}^{electrons} v(i,j) \qquad (3.12)$$

if we ignore the nuclear-nuclear potential, which is a constant and does not change the eigen functions.

Given the wave function ψ as a single Slater determinant (eq. 3.9), the expectation value of the total electron energy E_{el} is obtained by:

$$E_{el} = \left\langle \psi \left| \hat{H}_{el} \right| \psi \right\rangle \tag{3.13}$$

and can be evaluated by inserting the Hamiltonian (eq. 3.12) into eq. 3.13. The central problem in a Hartree-Fock calculation is to find the best possible wave functions within the approximation of HF theory. The solution to this problem is based on the *variational principle*, which states that the best spin orbitals are those that minimize the electronic energy E_{el}. It means that the correct wave function will be the function that has the lowest energy (ground state energy) and any approximate wave function will have an energy above the ground state. Basically the Hartree-Fock method determines the set of spin orbitals, which minimize the energy and give "the best single determinant" wave function. The energy corresponding to a single determinant wave function can be written in terms of integrals of the one- and two-electron operators:

$$E_{el} = \sum_i^N \left\langle i|h|i \right\rangle + \sum_i^N \sum_{j>i}^N \left(\left\langle ij|ij \right\rangle - \left\langle ij|ji \right\rangle \right) \tag{3.14}$$

The one electron-integral is

$$\left\langle i|h|i \right\rangle = \left\langle \chi_i |h| \chi_i \right\rangle = \int dx_1 \chi_i^*(x_1) h(r_1) \chi_i(x_1) \tag{3.15}$$

and two-electron integrals are:

$$\left\langle ij|ij \right\rangle = \int dx_1 dx_2 \chi_i^*(x_1) \chi_j^*(x_2) r_{12}^{-1} \chi_i(x_1) \chi_j(x_2) \tag{3.16}$$

$$\left\langle ij|ji \right\rangle = \int dx_1 dx_2 \chi_i^*(x_1) \chi_j^*(x_2) r_{12}^{-1} \chi_j(x_1) \chi_i(x_2) \tag{3.17}$$

where $r_{12} = |r_1 - r_2|$. Note that in eq. 3.14 the Bracket notation is used for a concise and simple expression of the electronic energy. By using Lagrange's method of undetermined multipliers[5] to minimize the electronic energy with the constraint that the spin orbitals remain orthonormal, the Hartree-Fock equations defining the orbitals are obtained.

$$h(x_1)\chi_i(x_1) + \sum_{j\neq i} \left[\int dx_2 \left| \chi_j(x_2) \right|^2 r_{12}^{-1} \right] \chi_i(x_1) - \sum_{j\neq i} \left[\int dx_2 \chi_j^*(x_2) \chi_i(x_2) r_{12}^{-1} \right] \chi_j(x_1) = \varepsilon_i \chi_i(x_1) \tag{3.18}$$

where ε_i is the energy eigenvalue associated with the orbital χ_i and $h(x_1)$ is the one-electron operator (expressed as in eq. 3.10).

The solutions of Hartree-Fock equations depend on the orbitals. Hence, the Hartree-Fock equations have to be solved iteratively, starting with some initial guess of the wave function. For this reason, Hartree-Fock is called a self-consistent-field (SCF) approach.

The first term in square brackets in eq. 3.18 gives the Coulomb term and describes the Coulomb interaction of an electron in the spin orbital χ_i with the average charge distribution of all other electrons. The other term in square brackets in eq. 3.18 arises from the antisymmetry requirement of the wave function. It is similar to the Coulomb term, except that the spin orbitals χ_i and χ_j have been exchanged. Therefore it is called the exchange term. Eq. 3.18 can be written in a simplified form as

$$\left[h(x_1) + \sum_{j \neq i} J_j(x_1) - \sum_{j \neq i} K_j(x_1) \right] \chi_i(x_1) = \varepsilon_i \chi_i(x_1) \tag{3.19}$$

or

$$f(x_1) \chi_i(x_1) = \varepsilon_i \chi_i(x_1) \tag{3.20}$$

with $f(x_1)$ the Fock operator. The Coulomb operator $J_j(x_1)$ and the exchange operator $K_j(x_1)$ are defined according to

$$J_j(x_1) \chi_i(x_1) = \left[\int dx_2 \left| \chi_j(x_2) \right|^2 r_{12}^{-1} \right] \chi_i(x_1) \tag{3.21}$$

$$K_j(x_1) \chi_i(x_1) = \left[\int dx_2 \chi_j^*(x_2) r_{12}^{-1} \chi_i(x_2) \right] \chi_j(x_1) \tag{3.22}$$

Roothaan and Hall (1951) found it convenient to express the one-electron wave functions χ_i as a linear combination of atom-centered functions $\tilde{\chi}$ (which resemble the atomic orbitals), called *basis functions*.

$$\chi_i = \sum_{\mu=1}^{K} C_{\mu i} \tilde{\chi}_\mu \tag{3.23}$$

$C_{\mu i}$ are the molecular orbital expansion coefficients and correspond to the contribution of each atomic orbital to the corresponding molecular orbital. K is the total number of basis functions. Using the Roothaan-Hall notation, eq. 3.20 becomes

$$f(x_1) \sum_\nu C_{\nu i} \tilde{\chi}_\nu(x_1) = \varepsilon_i \sum_\nu C_{\nu i} \tilde{\chi}_\nu(x_1) \tag{3.24}$$

Multiplying from the left by $\tilde{\chi}_\mu(x_1)$ and integrating over all space yields a matrix equation

$$\sum_v C_{vi} \int dx_1 \tilde{\chi}_\mu^*(x_1) f(x_1) \tilde{\chi}_v(x_1) = \varepsilon_i \sum_v C_{vi} \int dx_1 \tilde{\chi}_\mu^*(x_1) \tilde{\chi}_v(x_1) \qquad (3.25)$$

This can be simplified by introducing the matrix element notation

$$S_{\mu v} = \int dx_1 \tilde{\chi}_\mu^*(x_1) \tilde{\chi}_v(x_1) \qquad (3.26)$$

$$F_{\mu v} = \int dx_1 \tilde{\chi}_\mu^*(x_1) f(x_1) \tilde{\chi}_v(x_1) \qquad (3.27)$$

The Hartree-Fock-Roothaan equations can be written in matrix form

$$\sum_v F_{\mu v} C_{vi} = \varepsilon_i \sum_v S_{\mu v} C_{vi} \qquad (3.28)$$

or as matrices $FC = SC\varepsilon$ $\qquad (3.29)$

where ε is a diagonal matrix of the orbital energies ε_i, S is the overlap matrix, F is the Fock matrix and C is a matrix of order K with $C_{\mu i}$ as elements.

In the case of closed-shell molecules (most molecules in their neutral ground state) all the electrons in the occupied molecular orbitals are paired, one with alpha-spin and one with beta-spin. For such molecules a *spin-restricted Hartree-Fock calculation (RHF)* can be applied, with the equations described above. In this case, two electrons, which have the same spatial distribution, share the same wave function and the same eigenvalues. However, most of the calculations presented in this thesis are performed for cations and anions of different conjugated oligomers. Cations and anions are open-shell molecules because they have one unpaired electron. There are two ways to treat open-shell molecules. One is called *spin-restricted open-shell Hartree-Fock (ROHF)* theory. In this theory, a single set of molecular spatial orbitals is used, some being doubly occupied and some being singly occupied. It means that two electrons in the same spatial orbital share the same wave function and the same eigenvalues (as was the case in *RHF*). But, an unpaired electron in a molecular spatial orbital will have a Coulomb interaction with all other electrons from a different molecular spatial orbital and an exchange interaction only with the electrons of the same spin from the other molecular spatial orbitals. The second approach is the *spin-unrestricted open-shell Hartree-Fock (UHF)* theory. In this approach, each electron in a molecular orbital can have a different spatial function. In this way, two distinct sets of spatial orbitals are assigned to alpha and beta electrons, respectively. In this case two electrons (with alpha and beta spin, respectivelly) that would be in the same spatial orbital in a restricted calculation have a different spatial distribution. Hence the spins of these electrons do not cancel. This is called *spin contamination*. The spin contamination of the cations and anions corresponds to the mixing with higher lying quartet and sextet states in the wave function of the doublet state, which describes the cation and anions in their ground state. To avoid the spin contamination problem the calculations of the cations and anions from chapters 4 to 10 were performed using the *ROHF* theory.

3.3 Basis sets

As mentioned in the previous section, the molecular orbitals are expanded as a linear combination of so-called basis functions (eq. 3.23). In order to obtain the exact solution of the Hartree-Fock equation an infinite number of basis functions (a complete basis set) should be used. However, this is impossible to realize in actual calculations. In practice, a finite set of basis functions is used to perform the calculations. A variety of basis sets has been developed[8] and the choice of the basis set should be a compromise of reaching accurate results with a low computational cost. The natural choice is to use *Slater Type Orbitals (STO)* since they are of the form of hydrogen orbitals. The STOs[9] are exponentially decaying functions:

$$\phi_{abc}^{STO}(x,y,z) = Nx^a y^b z^c e^{-\varsigma r} \tag{3.30}$$

where N is a normalization constant, x, y and z are the cartesian coordinates of the atom $(r^2 = x^2 + y^2 + z^2)$, a, b and c are parameters that control the angular momentum $(L = a + b + c)$, ζ is the orbital exponent which controls the spatial extent of the orbital. STOs give the exact solutions for atomic one-electron systems. In practice the evaluation of one- and two-electron integrals using STOs is time-consuming, which has lead to the introduction of the *Gaussian Type Orbitals (GTO)*. GTOs[10] have the following functional form:

$$\phi_{abc}^{GTO}(x,y,z) = Nx^a y^b z^c e^{-\varsigma r^2} \tag{3.31}$$

GTOs are computationally preferred because the evaluation of the multi-center two-electron integrals can be performed analytically. However, a large number of individual GTO functions have to be used to get a reliable description. Because STOs give a better description than GTOs, but the computational cost of using GTOs is lower, the *Contracted Gaussian-Type Orbitals (CGTO)* were introduced. CGTO is a fixed linear combinations of enough GTOs that mimics an STO.

$$\phi_{abc}^{CGTO}(x,y,z) = N\sum_{i=1}^{n} C_i x^a y^b z^c e^{-\varsigma_i r^2} \tag{3.32}$$

The use of CGTOs in calculations leads to similar accuracy as in the case of STOs, but at lower computational cost.

The smallest number of basis functions that can be used to describe the electronic structure of a system is called the *minimal basis set*. This set includes only one basis function per type of occupied atomic orbital in the ground state. It means that for hydrogen, for example, only a single *s*-type function is used, while for carbon two *s*- functions and a *p*-shell (three *p*-functions: p_x, p_y and p_z) are used. Calculations with a minimal basis set are used to get a reasonable first impression. For higher accuracy it is necessary to use *extended basis sets*, in which the number of functions per atom is increased. For example a *Double Zeta (DZ)* basis set employs two *s*-type functions for hydrogen (1*s* and 1*s'*), four s- functions (1*s*, 1*s'*, 2*s* and 2*s'*) and two p-shells (with six functionals: $2p_x$, $2p_y$, $2p_z$, and $2p_x'$, $2p_y'$, $2p_z'$) for carbon,

etc. A *Triple Zeta (TZ)* basis set for a carbon atom contains three times as many functions as the minimum basis set, *i.e.* six *s*- functions and three *p*-shells (nine *p*-functions).

A variation of the extended basis sets is the *split-valence basis set.* A split-valence basis set uses only one basis function for each core (inner) atomic orbital, and a larger number of basis functions for the valence (outer) atomic orbitals. This assignment is reasonably good since the valence orbitals of atoms are more affected by the molecular environment and by forming the bonds than the core orbitals.

The next step in improving the basis set is to add functions of higher angular momentum than that required for the description of the ground state. These are called *polarization functions*. If we consider the simplest case, the hydrogen atom, the exact wave function for the isolated hydrogen atom is a 1*s* orbital. When the hydrogen atom is placed in a uniform electric field, then the electron cloud is polarized along the direction of the electric field and the charge distribution around the nucleus becomes asymmetric. A hydrogen atom in a molecule finds itself in a similar situation, more exactly in a nonuniform electric field arising from the nonspherical environment. By adding *p*-type functions to the hydrogen basis set this effect can be accounted for. In a similar manner *d* functions play the role of polarization for the heavy atoms that have an *sp*-ground state and *f* functions are added to transition metal atoms. Adding a polarization function to a DZ basis function yields a *Double Zeta plus Polarization (DZP)* basis set.

For anions, Rydberg states and molecules with highly diffuse electron densities it is necessary to include *diffuse functions*. They are large-size versions of *s*- and *p*-type functions that allow orbitals to occupy a larger region of space. They have small orbital exponents ζ, which means that the electron is held far away from the nucleus.

John Pople (Nobel laureate in 1998) dedicated a large part of his work to the development of basis sets. *Pople style basis sets* are optimized to get the lowest Hartree-Fock energy. The general notation for describing these basis sets is:[11]

k-nlm(+)G(*)   (3.33)

with *k* indicating how many CGTOs are used to represent the core orbital, and *nlm* indicating both how many functions the valence orbitals are split into, and how many CGTOs are used for their representation. The presence of polarization functions is indicated by symbol "***" placed after the *G*. The presence of diffuse functions is indicated by the symbol "*+*" placed before the G. For example, *6-311G**[12,13] consists of 6GTOs for the core and 3 functions for the valence shell (one containing 3 GTOs and two uncontracted GTOs) plus *d* polarization functions on non-hydrogen atoms.

Thom Dunning has pointed out that the basis sets optimized at the Hartree-Fock level are not ideal for describing the interactions between electrons in electron correlation methods (Configuration Interaction and Møller-Plesset perturbation). For such methods, special basis sets have been developed, for example *correlation consistent basis sets*.[14] Correlation-consistent basis sets are designed to recover the largest part of the correlation energy of the valence electrons. (The correlation energy will be discussed in details in section 3.5.) The

name *correlation consistent* refers also to the fact that the functions that contribute similar amounts to the correlation energy are included at the same stage, independently of the function type. For example, even though the first *d*-function produces a large energy lowering, the contribution of a second *d*-function will be similar with that from the first *f*-function. Therefore addition of the polarization functions should be done in the order *1d, 2d, 1f*. The most simple correlation consistent basis set is *cc-pVDZ (correlation consistent-polarized valence double zeta)*. For the first[14,15] and second row atoms,[16] the *cc-pVDZ* basis set adds *1s*, *1p* and *1d* functions. For example *cc-pVDZ* for the C atom consists of *3s2p1d*. The *cc-pVTZ* set adds another *s*, *p*, *d*, and an *f* function. For the C atom *cc-pVTZ* would be *4s3p2d1f*. Various augmentations to these base sets have been developed. These include the addition of diffuse functions to better describe anions and weakly interacting molecules (*aug-cc-pVnZ*), as well as basis sets designed for describing the effects of correlating the core electrons (*cc-pCVnZ* and *cc-pwCVnZ*). Another advantage of using correlation consistent basis sets is that they are designed to converge smoothly toward the complete (infinite) basis set limit. Since computer time in electronic structure calculations increases with power 4 or higher of the number of basis functions, a compromise has to be reached between basis set dimension and the desired accuracy. Therefore we have chosen a *cc-pVDZ* basis set for performing the correlated calculations in chapters 4 to 9.

3.4 Semi-empirical methods

Hartree-Fock calculations are computationally expensive due to the high number of two-electron integrals necessary to construct the Fock matrix in eq. 3.29. It has been mentioned in the previous paragraph that the cost of performing a HF calculation scales with the fourth power of the number of basis functions. In order to handle large size molecules and inorganic molecules including transition state elements, additional approximations to the HF method have been developed. These approximations were introduced to reduce the number of two-electron integrals and they lead to the formation of so-called *semi-empirical methods*. The first approximation in the semi-emiprical methods is to consider only the valence electrons explicitly. Moreover, only a minimum basis set is used for these valence electrons. The central assumption of semi-empirical methods is the *Zero Differential Overlap* (*ZDO*) approximation, which neglects all integrals involving products of basis functions depending on the same electron coordinates when located on different atoms. The consequence of ZDO is that all three- and four-center two-electron integrals, which are by far the most numerous, are neglected. To compensate for these approximations, the remaining integrals are treated as parameters, whose values are adjusted to fit experimental data or results from *ab initio* calculations.

3.4.1 Intermediate Neglect of Differential Overlap (INDO) approximation

The Intermediate Neglect of Differential Overlap (INDO) approximation was originally proposed by Pople et al.[17] and, independently, by Dixon.[18] In addition to the general approximations specified for semi-empirical methods, the INDO approximation neglects all two-center two-electron integrals, which are not of the Coulomb type. Furthermore, the one-

electron integrals involving two different functions on the same atom with the operator from another atom disappear. A detailed description of all approximations involved in the INDO method is described below. The evaluation of the Fock matrices from eq. 3.29 is simplified as follows:

1) the overlap integrals $S_{\mu\nu}$ defined in eq. 3.26 are neglected unless $\mu=\nu$.

2) the two-, three-, and four-center integrals of the type $\langle\mu\lambda|\nu\sigma\rangle$ are set equal to zero unless $\mu=\lambda$ and $\nu=\sigma$. The remaining integrals are further simplified by the approximation $\langle\mu\mu|\nu\nu\rangle=\gamma_{AB}$ (μ on A, ν on B), where γ_{AB} is approximated as the Coulomb integral $\langle s_A s_A|s_B s_B\rangle$, involving valence s-orbitals of atoms A and B with which μ and ν are associated, respectively .

3) the one-center core-matrix elements $H_{\mu\mu}^{core}$ are given by:

$$H_{\mu\mu}^{core} = \int dr_1 \tilde{\chi}_\mu^*(x_1) h(x_1) \tilde{\chi}_\mu(x_1) = U_{\mu\mu} - \sum_{B(\neq A)} Z_B \gamma_{AB} \tag{3.34}$$

where Z_B is the core charge of atom B and $U_{\mu\mu}$ is the corresponding one-center core integral.

4) the two-center core-matrix elements $H_{\mu\nu}^{core}$ are given by:

$$H_{\mu\nu}^{core} = \int dr_1 \tilde{\chi}_\mu^*(x_1) h(x_1) \tilde{\chi}_\nu(x_1) = \frac{1}{2}(\beta_A^0 + \beta_B^0) S_{\mu\nu} \tag{3.35}$$

where β^0 are called atomic resonance integrals, which are empirical parameters.

Under these approximations, the elements of the Fock matrix, F, for α-spin become:

$$F_{\mu\mu}^\alpha = U_{\mu\mu} + \sum_{\lambda\sigma}\left[P_{\lambda\sigma}\langle\mu\mu|\lambda\sigma\rangle - P_{\lambda\sigma}^\alpha\langle\mu\lambda|\mu\sigma\rangle\right] + \sum_{B\neq A}\left(P_{BB} - Z_B\right)\gamma_{AB} \tag{3.36}$$

$$F_{\mu\nu}^\alpha = U_{\mu\nu} + \sum_{\lambda\sigma}[P_{\lambda\sigma}\langle\mu\nu|\lambda\sigma\rangle - P_{\lambda\sigma}^\alpha\langle\mu\lambda|\nu\sigma\rangle] \tag{3.37}$$

with the Fock elements for β-spin having a similar form. $P_{\lambda\sigma}$ is the density matrix, defined as:

$$P_{\lambda\sigma} = 2\sum_a^{N/2} C_{\lambda a} C_{\sigma a}^* \tag{3.38}$$

The INDO method has been especially parametrized by Zerner and co-workers[19-21] for the calculation of electronic spectra of organic molecules and complexes containing transition metals and it is known as INDO/s. In the INDO/s procedure the one-center core electron integrals $U_{\mu\mu}$ are obtained from the difference between the ionization potential and the electron affinity (taken from atomic spectra) and these integrals are used to calculate the ground state configuration in terms of molecular orbital coefficients and eigenvalues. The second change in parametrization relates to the atomic resonance integrals, β^0. Following an earlier suggestion of Mulliken,[22] Del Bene and Jaffe[23] distinguished between the two-center

core-matrix elements corresponding to σ and π orbitals, by introducing a new parameter k. Thus, eq. 3.35 becomes:

$$H_{\mu v}^{core,\sigma} = \frac{1}{2}(\beta_A^0 + \beta_B^0)S_{\mu v}$$

(3.39)

$$H_{\mu v}^{core,\pi} = \frac{1}{2}k(\beta_A^0 + \beta_B^0)S_{\mu v}$$

(3.40)

They found that a value of 0.585 for k gives the most consistent spectroscopic data. When $k=1$ INDO/s becomes INDO.

3.5 Electron correlation

As discussed in section 3.2, a Hartree-Fock self consistent field wave function takes into account the interactions between electrons only in an average way. In reality the electrons interact instantaneously. A Hartree-Fock wave function partly accounts for instantaneous electron correlation. This is accomplished by the fact that the Hartree–Fock function satisfies the antisymmetry requirement of the Pauli principle. This is known as *exchange correlation*. However, the Hartree-Fock (HF) function does not correlate the motion of electrons with opposite spins, i. e. there is a nonzero probability of two electrons with opposite spins occupying the exact same point in space. This is corrected by taking into account the so-called *Coulomb correlation*. The correlation energy (E_{corr}) is defined as the difference between the exact nonrelativistic energy (E_{exact}) and the Hartree-Fock limit energy (E_{HF}):[5]

$$E_{corr} = E_{exact} - E_{HF}$$

(3.41)

There are many methods to include electron correlation in electronic structure calculations. The most popular approaches use the HF wave function as a starting point (configuration interaction theory, coupled cluster theory and perturbation theory), but also alternative methods have been developed (density functional theory).

3.5.1 Configuration interaction

Configuration interaction (CI) is conceptually (but not computationally) the simplest method for obtaining the correlation energy. The idea behind this method is to represent the exact ground state and excited-state wave functions as a linear combination of all possible *n*-electron Slater determinants arising from a complete set of spin-orbitals. Therefore, the exact electronic wave function Ψ in the limit of a complete basis set for any state of the system can be written as:[2]

$$\Psi = c_0 |\psi_0\rangle + \sum_{ar} c_a^r |\psi_a^r\rangle + \sum_{\substack{a<b \\ r<s}} c_{ab}^{rs} |\psi_{ab}^{rs}\rangle + \sum_{\substack{a<b<c \\ r<s<t}} c_{abc}^{rst} |\psi_{abc}^{rst}\rangle + \cdots$$

(3.42)

In eq. 3.42 ψ_0 is the reference determinant and it is, usually, the HF ground state wave function. ψ_a^r is a singly excited determinant in which an electron is taken from (HF) orbital a and is transferred to orbital r, which was unoccupied in the HF reference wave function. c_a^r is the corresponding expansion coefficient for the single excited determinant. ψ_{ab}^{rs} are doubly excited determinants, in which two electrons are promoted, one from orbital a to orbital r, and the other one from orbital b to orbital s. c_{ab}^{rs} are the corresponding expansion coefficients, etc.

The number of possible electron configurations (such those in eq. 3.42) with the proper symmetry increases very rapidly as the number of electrons and the number of basis functions increases. For n electrons and b basis functions, the number of electron configurations is approximately proportional to b^n. A CI calculation that includes all possible configurations with proper symmetry is called a *full CI calculation*. Because of the huge number of electron configurations, full CI calculations are impossible to perform except for the smallest systems (such as H_2). Therefore, the expansion in eq. 3.42 is usually truncated, *e.g.* by including only the singly and doubly excited determinants. This leads to the truncated CI methods known as: *Configuration Interaction Single* excitations (*CIS*) only, *Configuration Interaction Double* excitations (*CID*) only, and *Configuration Interaction Single and Double* excitations (*CISD*) only. At this point it is important to distinguish between static and dynamic correlation. The dominant configurations and the configurations that are nearly degenerate with the dominant configurations of the CI expansion (*i.e.* the determinants that are absolutely necessary to give a first order description of the excited state) represent the *static correlation*. *Dynamic correlation* consists of configurations generated by all single and all multiple excitations added to the configurations corresponding to the static correlation. A CIS calculation contains mainly static correlation and very little dynamic correlation.

As mentioned in the beginning of this section, the CI method gives solutions not only for the wave functions describing the ground state, but also for the excited state wave functions. Therefore, the CI method can be used to calculate electronic absorption spectra of molecules. In general, CIS gives a good description of the excited state for one-electron excitation and implicitly a good description of the electronic absorption spectra. To construct an excited determinant (such as ψ_a^r or ψ_{ab}^{rs}) the reference wave function (ψ_0) can be either an *ab initio* HF wave function, or a wave function obtained from a semi-empirical calculation (e.g. INDO/s). In the calculations of the electronic absorption spectra described in chapters 4 to 6, the reference determinant was obtained from the INDO/s method and it was used afterwards in a CIS calculation to get the wave function of the excited state. This combination of methods is known to give a very good description of electronic absorption spectra with a relatively small computational cost and therefore it was applied in this thesis.

3.5.2 Møller-Plesset perturbation theory

In the work of this thesis electronic structure calculations were not only used to analyze optical absorption spectra of cations and anions of different oligomers, but also to investigate the effect of the dynamic correlation on the charge distribution along oligomer chains. Although CID is able to give such information, the computational cost is much too high, making it impossible to perform such calculations for the systems considered in this thesis. An alternative approach to incorporate dynamic electron correlation is perturbation theory. In

this method the calculations are not variational in the sense that perturbation theory gives in general energies that are not upper bounds to the exact energy. *The Møller-Plesset (MP) method*[24] is a perturbation theory in which the Hamiltonian is expressed as:

$$H_\lambda = H_0 + \lambda V \tag{3.43}$$

where H_0 is the non-perturbed Hamiltonian and V is the perturbation. The energy and the exact wave function can be written as a Taylor expansion in powers of the perturbation parameter λ:

$$\psi_\lambda = \psi^{(0)} + \lambda \psi^{(1)} + \lambda^2 \psi^{(2)} + \dots \tag{3.44}$$

$$E_\lambda = E^{(0)} + \lambda E^{(1)} + \lambda^2 E^{(2)} + \dots \tag{3.45}$$

The zero order energy and the zero order wave function are respectively:

$$E^{(0)} = \sum_i^{occupied} \varepsilon_i \tag{3.46}$$

$$\psi^{(0)} = \psi_{HF} \tag{3.47}$$

Note, the first order correction to the energy $E^{(1)}$ is zero (*Brillouin theorem*).[5] The first order correction to the wave function is a sum over singly excited determinants:

$$\psi^{(1)} = \sum_{s>0} \frac{V_{s0}}{\varepsilon_0 - \varepsilon_s} \psi_s \tag{3.48}$$

where $V_{s0} = \langle \psi_s | V | \psi_0 \rangle$ and ψ_s is the one-determinant wave function that results from one electron excitation. The second-order correction to the energy, which is the first contribution to the correlation energy, involves a sum over doubly excited determinants (from occupied a and b molecular orbitals to virtual r and s molecular orbitals):

$$E^{(2)} = \sum_{a<b}^{occupied} \sum_{r<s}^{virtual} \frac{\langle \psi^{(0)} | H_\lambda | \psi_{ab}^{rs} \rangle \langle \psi_{ab}^{rs} | H_\lambda | \psi^{(0)} \rangle}{E_0 - E_{ab}^{rs}} \tag{3.49}$$

Eq. 3.49 represents the energy in the second order Møller-Plesset perturbation theory E(MP2). The computational cost of an MP2 calculation increases with the fifth power of the number of basis function, an MP3 calculation scales to the sixth power, etc. This limits the applicability of Møller-Plesset theory only to small systems. In this thesis MP2 has been applied to calculate the distribution of an excess positive charge in phenylenevinylene and thiophene oligomers in chapter 9.

3.6 Density Functional Theory

All approaches to the electron correlation described above are reasonably accurate, but they are time consuming, which excludes the treatment of large molecules. *Density Functional Theory (DFT)* provides an alternative to include correlation effects in an approximate way, while the computational efficiency is at least as good as for HF theory. The basic concept behind DFT is that the central quantity is not a wave function (as was the case of all methods discussed until now), but the *electron density*. A few reviews of DFT have been published,[25,26] including the Nobel lecture of Walter Kohn.[27] Density Functional Theory is based on the *Hohenberg-Kohn theorems*.[28] Pierre Hohenberg and Walter Kohn established in 1964 that there is a one-to-one correspondence between electronic densities, *ρ(r)* of a system in a nondegenerate ground state and the potential due to the nuclei, *υ(r)*. In other words, once the electron density is known, the potential due to the nuclei, and consequently the Hamiltonian of the system are uniquely determined. All physical properties obtainable with *υ(r)* can, hence, be expressed in terms of electronic density. The second Hohenberg-Kohn theorem gives the variational principle of the energy as a functional of the electronic density and states that the exact density is that density which minimizes the energy as a functional of the density.

The electronic energy of the ground state, E_0, is a functional of the electronic density of this state, ρ_0:

$$E_0 = E_0\left(\rho_0\right) \tag{3.50}$$

In the beginning of this chapter (eq. 3.8) the Hamiltonian operator was expressed as a sum of the kinetic energy operator, electron-nucleus attraction operator and electron-electron repulsion operator.

$$\hat{H} = \hat{T} + \hat{V} + \hat{V}_{ee} = \sum_{i=1}^{N}\left(-\frac{1}{2}\nabla_i^2\right) + \sum_{i=1}^{N}\upsilon(r_i) + \sum_{i<j}^{N}\frac{1}{\left|r_i - r_j\right|} \tag{3.51}$$

Taking the expectation value of the ground state energy, gives:

$$\left\langle E\right\rangle = \left\langle T\right\rangle + \left\langle V\right\rangle + \left\langle V_{ee}\right\rangle \tag{3.52}$$

Each of these expectation values are determined by the electron density of the ground state *ρ(r)*. This means that each term of eq. 3.52 is a functional of ρ :

$$E_0\left(\rho\right) = T\left(\rho\right) + V\left(\rho\right) + V_{ee}\left(\rho\right) = T\left(\rho\right) + \int\rho(r)\upsilon(r)dr + V_{ee}\left(\rho\right) \tag{3.53}$$

with

$$V(\rho) = \int\rho(r)\upsilon(r)dr \tag{3.54}$$

The exact form of $T(\rho)$ is not known. However, the kinetic energy functional can be easily calculated once that the wave function is known. Kohn and Sham[29] proposed a method to evaluate the kinetic energy functional from the electron density, $\rho(r)$. The central assumption in the Kohn-Sham theory is that for each interacting electron system with a potential $\upsilon(r)$ due to the nuclei, there is a local potential $\upsilon_s(r)$ (called the Kohn-Sham potential) such that the density $\rho_s(r)$ of the non-interacting system equals the density $\rho(r)$ of the interacting system.

If a reference system with N electrons which do not interact with each other and which are moving in a local potential $\upsilon_s(r)$ is considered, then the energy of such a system is:

$$E_s(\rho) = T_s(\rho) + \int \rho(r)\upsilon_s(r)dr \tag{3.55}$$

$$\text{where } T_s(\rho) = \sum_{i=1}^{N_{occ}} \left\langle \chi_i \left| -\frac{1}{2}\nabla^2 \right| \chi_i \right\rangle \tag{3.56}$$

When a real system is considered (in which the N electrons repel each other), the energy of the system becomes

$$E(\rho) = T(\rho) + V(\rho) + V_{ee}(\rho) = T_s(\rho) + T_c(\rho) + V(\rho) + J(\rho) + W_{XC}(\rho) \tag{3.57}$$

where

$$T(\rho) = T_s(\rho) + T_c(\rho) \tag{3.58}$$

$$V_{ee}(\rho) = J(\rho) + W_{XC}(\rho) \tag{3.59}$$

$T_c(\rho)$ is called correlation kinetic energy and represents the difference between the kinetic energy of the real system, $T(\rho)$ and the kinetic energy of the non-interacting system, $T_s(\rho)$. $J(\rho)$ is the Coulomb repulsion energy:

$$J(\rho) = \frac{1}{2} \int \int \frac{\rho(r_1)\rho(r_2)}{|r_1 - r_2|} dr_1 dr_2 \tag{3.60}$$

$W_{XC}(\rho)$ is the exchange-correlation energy of the electronic part.

The second and the last term in eq. 3.57 are grouped in one term, $E_{XC}(\rho)$, called the total *exchange-correlation energy* functional

$$E_{XC}(\rho) = T_c(\rho) + W_{XC}(\rho) \tag{3.61}$$

which accounts for the self-interaction and all other non-classical effects of the quantum electron-electron interaction, including the correlation kinetic energy. Introducing eqs. 3.54, 3.56 and 3.60 in eq. 3.57, gives:

$$E(\rho) = \sum_{i=1}^{N_{occ}} \left\langle \chi_i \left| -\frac{1}{2}\nabla^2 \right| \chi_i \right\rangle + \int \rho(r)\upsilon(r)dr + \frac{1}{2}\int\int \frac{\rho(r_1)\rho(r_2)}{|r_1 - r_2|} dr_1 dr_2 + E_{XC}(\rho) \tag{3.62}$$

The Kohn-Sham (KS) orbitals are found using the second Hohenberg-Kohn theorem, but instead varying the electron density $\rho(r)$, the KS orbitals, χ_i^{KS}, which determine $\rho(r)$ can be varied. By doing so, the KS orbitals that minimize the molecular ground-state energy $E(\rho)$ satisfy the relation:

$$\left(-\frac{1}{2}\nabla^2 + \upsilon(r) + \int \frac{\rho(r_2)}{|r_1 - r_2|} dr_2 + \upsilon_{XC}(r) \right) \chi_i(r) = \varepsilon_i \chi_i(r) \tag{3.63}$$

In equation 3.63 the sum $\upsilon(r) + \int \dfrac{\rho(r_2)}{|r_1 - r_2|} dr_2 + \upsilon_{XC}(r) = \upsilon_s(r)$ $\tag{3.64}$

is called the Kohn-Sham effective potential. The KS orbitals allows us to calculate the electron density:

$$\rho(r) = \sum_{i=1}^{N_{occ}} |\chi_i(r)|^2 \tag{3.65}$$

Equations 3.62, 3.63 and 3.65 constitute the *ground state Kohn-Sham equations*. These equations reduce the problem of finding the ground state density to finding a good approximation for the exchange-correlation energy, E_{XC}.

3.6.1 The exchange-correlation functional

The central issue of DFT is that the functional that describes the *exchange-correlation energy (E_{XC})* is not known. Different approximations have been proposed and we will present in this section only a few of them.

Local Density Approximation (LDA)

The term $E_{XC}(\rho)$ is split into two contributions:

$$E_{XC}(\rho) = E_X(\rho) + E_C(\rho) \tag{3.66}$$

where $E_X(\rho)$ is the term for the exchange energy and $E_C(\rho)$ is the term for the correlation energy. *The Local Density Approximation (LDA)*[1,6] assumes that the electronic density can be

treated locally as that of a uniform electron gas and hence the local exchange functional is derived from the exact solution of a uniform gas model:

$$E_X^{LDA}(\rho) = -\frac{3}{2}\left(\frac{3}{4\pi}\right)^{1/2} \int \rho^{4/3}(r)dr \qquad (3.67)$$

Vosko, Wilk and Nusair (VWN) obtained a complicated expression for the correlation energy $E_C^{LDA}(\rho)$ of a uniform electron gas using Monte Carlo calculations.[30]

Generalized Gradient Approximation (GGA)

In the Local Density Approximation, the functional used to obtain the exchange-correlation energy only depends on the electron density. An improvement to this method is to consider exchange-correlation functionals that are dependent not only on the electron density, but also on the gradient of the electron density. Such corrections were introduced for the first time by Perdew and Yang and they are known as the *Generalized Gradient Approximation (GGA)*.[31] These functionals were designed as PW86 or PWx86. Other commonly used gradient corrections are:

- exchange Becke's 1988 functional (B88, Bx88, Becke88 or B)[32]
- correlation Lee-Yang-Parr functional (LYP)[33]

Any exchange functional can be combined with any correlation functional. For example, the well-known BLYP method includes the gradient-corrected exchange functional proposed by Becke, and the gradient-corrected functional of Lee, Yang and Parr.

Hybrid functionals:B3LYP

A new class of functionals has been developed by considering the similarities between the methodology of Hartree-Fock theory and Kohn-Sham DFT. These functionals are called *hybrid functionals* and they combine part of the exact Hartree-Fock exchange energy with exchange-correlation energies of a gradient-corrected functional:

$$E_{XC}^{hybrid} = c^{HF} E_X^{HF} + c^{DFT} E_{XC}^{DFT} \qquad (3.68)$$

where c^{HF} and c^{DFT} are constants. The most popular hybrid functional is B3LYP,[34] defined as:

$$E_{XC}^{B3LYP} = (1-a-b)E_X^{LDA} + aE_X^{HF} + bE_X^{B88} + (1-c)E_C^{VWN} + cE_C^{LYP} \qquad (3.69)$$

where $a = 0.20$, $b = 0.72$ and $c = 0.81$ are determined by fitting to experimental data. E_X^{LDA} is given by eq. 3.67. E_X^{HF} is the exact Hartree-Fock energy, E_X^{B88} is Becke's 1988 gradient correction for exchange,[32] E_C^{VWN} is the correlation energy from the Vosko, Wilk and Nusair functional,[30] and E_C^{LYP} is the correlation energy for the Lee-Yang-Parr gradient correction.[33] It has been found that B3LYP provide accurate molecular geometries, atomization and ionization energies and vibrational frequencies.

3.7 Time-Dependent Density Functional Theory

DFT became popular in the last decade due to a rather good quality of results together with a relatively low computational cost. The central quantity in DFT is the ground state charge density and therefore the molecular properties which are functionals of charge density can be calculated. However, in this form DFT does not cover the treatment of time-dependent fields, as encountered in optics and spectroscopy. Even though static response properties (i.e. static polarizabilities) can be calculated using DFT, the calculation of dynamic response properties belongs exclusively to the extension of DFT into time domain. *The Time-Dependent Density Functional Theory (TDDFT)* is a response theory of the ground state charge density to a time-dependent perturbation. It allows the treatment of electric response properties and optical properties, specifically dynamic polarizabilities and excitation spectra. The first steps towards a time-dependent density functional theory were taken by the work of Peuckert,[35] Zangwill and Soven,[36] Deb and Ghosh[37,38] and Bartolotti.[39,40] The theoretical breakthrough came with the work of Runge and Gross, in which a set of single-particle equations for basically all time-dependent external potentials was derived, known as *time-dependent Kohn-Sham equations.*[41] In this paragraph a brief discussion of the time-dependent Kohn-Sham equations is presented. For more details the reader is referred to recent reviews.[42,43]

Just as in case of ground state density functional theory we can consider a system of non-interacting particles with the same density as the fully interacting system. The one-to-one correspondence of time-dependent densities and time-dependent potentials (proven by Runge and Gross)[41] allows us to write the time-dependent Kohn-Sham equations, analog to the time-independent Kohn-Sham equations (eq. 3.63):

$$\left(-\frac{1}{2}\nabla^2 + \upsilon(r,t) + \int \frac{\rho(r_2,t)}{|r_1 - r_2|} dr_2 + \upsilon_{XC}(r,t) \right) \chi_i(r,t) = i\frac{\partial}{\partial t}\chi_i(r,t) \tag{3.70}$$

where the density $\rho(r,t) = \sum_{i=1}^{N} |\chi_i(r,t)|^2$ $\qquad$ (3.71)

is that of the interacting system. The Kohn-Sham effective potential can be written as:

$$\upsilon_s(r,t) = \upsilon(r,t) + \int \frac{\rho(r_2,t)}{|r_1 - r_2|} dr_2 + \upsilon_{XC}(r,t) \tag{3.72}$$

where $\upsilon(r,t)$ is the external time-dependent field which includes the (constant) nuclear potential. Eq. 3.72 formally defines the time-dependent exchange-correlation potential $\upsilon_{XC}(r,t)$. In the limit of a slowly varying external potential $\upsilon(r,t)$ the adiabatic local density approximation (ALDA) is used to calculate the time-dependent exchange-correlation potential $\upsilon_{XC}(r,t)$. $\upsilon_{XC}(r,t)$, which is rigorously defined as the functional derivative of the exchange-correlation action $A_{XC}[\rho]$ with respect to the time-dependent electron density is

approximated in ALDA as the functional derivative of the standard, time-independent E_{XC} with respect to the charge density at a particular time t.[44]

$$\upsilon_{XC}[\rho](r,t) = \frac{\partial A_{XC}[\rho]}{\partial \rho(r,t)} \approx \frac{\partial E_{XC}[\rho]}{\partial \rho_t(r)} = \upsilon_{XC}[\rho_t(r)] \qquad (3.73)$$

3.7.1 Excitation Energies and Oscillator Strengths

Time-dependent response theory concerns the response of a system initially in a stationary state (generally taken to be the ground state) to a perturbation. A linear response implies that only first order perturbation terms of the time-dependent Kohn-Sham equations are taken in consideration, which considerably simplifies the problem. The linear response of a molecule to a frequency-dependent electric perturbation can be described by the frequency-dependent dynamic polarizability. Specifically, the frequency-dependent dynamic polarizability $\alpha(\omega)$ describes the response of the dipole moment to a time-dependent electric field with a frequency $\omega(t)$. The interaction of a molecule with light can be considered as the interaction with an electric field that varies sinusoidally in time, in other words as a time-dependent electric perturbation. This means that there is a direct relation between the frequency-dependent dynamic polarizability and the optical excitation spectrum. $\alpha(\omega)$ is in a first order perturbation theory, related to the electric dipole moment $\vec{\mu}$ according to:[2]

$$\alpha(\omega) = \frac{2}{3} \sum_\lambda \frac{\omega_{\lambda 0} |\mu_{\lambda 0}|^2}{\omega_{\lambda 0}^2 - \omega^2} = \sum_\lambda \frac{f_{\lambda 0}}{\omega_{\lambda 0}^2 - \omega^2} \qquad (3.74)$$

where $\omega_{\lambda 0}$ is the *excitation energy* between the ground state 0 and excited state λ, $|\mu_{\lambda 0}|^2 = \vec{\mu}_{0\lambda} \cdot \vec{\mu}_{\lambda 0}$, and $f_{\lambda 0}$ is the *oscillator strength* of the excitation. From eq. 3.74 it can be seen that the frequency-dependent dynamic polarizability becomes infinite for $\omega_{\lambda 0} = \omega$, which means that it has poles at the electronic excitation energies ω_λ. Therefore the absorption spectrum of a molecule can be obtained by calculating the polarizability as a function of frequency. However, the frequency (which is related to excitation energy) and the strength (which is related to the oscillator strength of an excitation) of the poles can also be obtained directly. It was shown that the excitation energies and oscilator strengths can be obtained from the following eigenvalue equation:[44]

$$\Omega \vec{F} = \omega_\lambda^2 \vec{F} \qquad (3.75)$$

where the F vectors are related to oscillator strengths. Note that the elements of the eigen vectors F are roughly comparable to the configuration interaction coefficients in a CIS calculation (described in paragraph 3.5.1) and are a measure to what extent the corresponding excitation can be interpreted as a pure single-particle excitation or if several such excitations play a crucial role in the transition. The matrix Ω describes the linear response TDDFT equations in a matrix form including the Random Phase Approximation[45]. Further details of the procedure can be found in literature.[44]

The frequency dependent dynamic polarizability can be written in terms of the F vectors and calculated excitation energies

$$\alpha(\omega) = \frac{2}{3} \sum_{\lambda} \sum_{\zeta} \frac{D_{\zeta} S^{-1/2} F_{\lambda} F_{\lambda}^{\dagger} S^{-1/2} D_{\zeta}}{\omega_{\lambda}^2 - \omega^2} \tag{3.76}$$

where D_{ζ} is a matrix of dipole matrix elements (direction $\zeta = x,y,z$) over occupied and virtual molecular orbitals and the elements of the matrix S are:

$$S_{ia\sigma, jb\tau} = \delta_{ab} \delta_{ij} \delta_{\sigma\tau} \frac{1}{\varepsilon_{b\tau} - \varepsilon_{j\tau}} \tag{3.77}$$

Here a and b refer to energies of unoccupied orbitals and i and j to energies of occupied orbitals, while σ and τ are spin indices. From comparison of eqs 3.74 and 3.76 the oscillator strength is given by the following expression:

$$f_{\lambda 0} = \frac{2}{3} \sum_{\zeta} \left(\left| D_{\zeta} S^{-1/2} F_{\lambda} \right|^2 \right) \tag{3.78}$$

The time-dependent density functional response equations shown above have been implemented in different programs,[46,47] giving the possibility to calculate excitation spectra of different molecules. This method was employed in this thesis to calculate the optical absorption spectra of different charged conjugated oligomers.

3.8 Population analysis

A well-known method to analyze SCF wave functions or electron densities (in case of DFT) is *population analysis*. Mulliken proposed a method that partitions the electrons of an *n*-electron molecule into net populations n_{μ} in the basis functions $\tilde{\chi}_{\mu}$ and overlap populations $n_{\mu-s}$. As we have seen in eq. 3.23, a one-electron wave function has the form:

$$\chi_i = \sum_{\mu=1}^{K} C_{\mu i} \tilde{\chi}_{\mu} = C_{1i} \tilde{\chi}_1 + C_{2i} \tilde{\chi}_2 + ... + C_{Ki} \tilde{\chi}_K \tag{3.79}$$

The probability density associated with one electron in χ_i is:

$$|\chi_i|^2 = C_{1i}^2 \tilde{\chi}_1^2 + C_{2i}^2 \tilde{\chi}_2^2 + ... + 2C_{1i}C_{2i}\tilde{\chi}_1\tilde{\chi}_2 + 2C_{1i}C_{3i}\tilde{\chi}_1\tilde{\chi}_3 + 2C_{2i}C_{3i}\tilde{\chi}_2\tilde{\chi}_3 + ... \tag{3.80}$$

Integrating this equation over three-dimensional space and using the fact that χ_i and $\tilde{\chi}_{\mu}$ are normalized, give:

$$1 = C_{1i}^2 + C_{2i}^2 + ... + 2C_{1i}C_{2i}S_{12} + 2C_{1i}C_{3i}S_{13} + 2C_{2i}C_{3i}S_{23} + ... \tag{3.81}$$

where S are overlap integrals of the form: $S = \int \tilde{\chi}_1 \tilde{\chi}_2 dv_1 dv_2$. Mulliken proposed to partition the terms in eq. 3.81 in the following way: one electron from χ_i contributes C_{1i}^2 to the net population in $\tilde{\chi}_1$, C_{2i}^2 to the net population in $\tilde{\chi}_2$, etc., and contributes $2C_{1i}C_{2i}S_{12}$ to the overlap population between $\tilde{\chi}_1$ and $\tilde{\chi}_2$, $2C_{1i}C_{3i}S_{13}$ to the overlap population between $\tilde{\chi}_1$ and $\tilde{\chi}_3$, etc.

Considering n_i electrons in a molecular orbital χ_i ($n_i = 0,1,2$), $n_{\mu,i}$ the contribution of the electrons from χ_i to the net population in $\tilde{\chi}_\mu$, and $n_{\mu-s,i}$ the contribution of the electrons from χ_i to the overlap between $\tilde{\chi}_\mu$ and $\tilde{\chi}_s$, then:

$$n_{\mu,i} = n_i C_{\mu i}^2 \tag{3.82}$$

$$n_{\mu-s,i} = n_i \left(2C_{\mu i} C_{si} S_{\mu s} \right) \tag{3.83}$$

By summing over the occupied molecular orbitals, the Mulliken *net population* n_μ in $\tilde{\chi}_\mu$ and the *overlap population* $n_{\mu-s}$ for the pair $\tilde{\chi}_\mu$ and $\tilde{\chi}_s$ are obtained:

$$n_\mu = \sum_i n_{\mu,i} \tag{3.84}$$

$$n_{\mu-s} = \sum_i n_{\mu-s,i} \tag{3.85}$$

At this point a decision regarding the assignment of the overlap population to different atoms should be taken. The simplest way (the one used in the Mulliken scheme) is to partion the contributions equally between the two atoms. In this way half of the overlap population is assigned to one atom and the other half to the second atom. The sum of all the net and overlap populations equals the total number of electrons in the molecule.

$$\sum_\mu n_\mu + \sum_{\mu>s} \sum_s n_{\mu-s} = n \tag{3.86}$$

It should be noted that population analysis methods are rather arbitrary. Two different population analysis methods give different atomic charges. Unfortunately, there are no unique criteria to determine which method gives the best partitioning and the best results. *Mulliken population analysis* was applied in this thesis to describe the distribution of an excess positive and negative charge along the chain of different conjugated oligomers.

3.9 References

(1)   Levine, I. N. *Quantum Chemistry*; Prentice Hall: Upper Saddle River, New Jersey, 2000.

(2)   Atkins, P. W.; Friedman, R. S. *Molecular Quantum Mechanics*; Oxford University Press: Oxford, 1997.

(3)   Mueller, M. *Fundamentals of Quantum Chemistry*; Kluwer Academic/ Plenum Publishers: New York, 2001.

(4)   Hasanein, A. A.; Evans, M. W. *Computational Methods in Quantum Chemistry*; World Scientific Publishing Co. Pte. Ltd.: Singapore, 1996.

(5)   Szabo, A.; Ostlund, N. S. *Modern Quantum Chemistry: Introduction to Advanced Electronic Structure Theory*; Dover Publications, Inc.: Mineola, New York, 1996.

(6)   Jensen, F. *Introduction to Computational Chemistry*; John Wiley & Sons Ltd.: Chichester, 1999.

(7)   Helgaker, T.; Jorgensen, P.; Olsen, J. *Molecular Electronic-Structure Theory*; John Wiley & Sons, Ltd.: Chichester, 2000.

(8)   Poirier, R.; Kari, R.; Csizmadia, I. G. *Handbook of Gaussian Basis Sets*; Elsevier Science: New York, 1985.

(9)   Slater, J. *Phys. Rev.* **1930**, *36*, 57.

(10)   Boys, S. F. *Proc. R. Soc. (London) A* **1950**, *200*, 542.

(11)   Hehre, W. J.; Radom, L.; Schleyer, P. V.; Pople, J. A. *Ab Initio Molecular Orbital Theory*; John Wiley & Sons Ltd.: New York, 1986.

(12)   Hariharan, P. C.; Pople, J. A. *Theor. Chim. Acta* **1973**, *28*, 213.

(13)   Francl, M. M.; Pietro, W. J.; Hehre, W. J. *J. Chem. Phys.* **1982**, *77*, 3654.

(14)   Dunning, T. H. *J. Chem. Phys.* **1989**, *90*, 1007.

(15)   Peterson, K. A.; Kendall, R. A.; Dunning, T. H. *J. Chem. Phys.* **1993,** *99*, 1930.

(16)   Woon, D. E.; Dunning, T. H. *J. Chem. Phys.* **1993**, *99*, 1914.

(17)   Pople, J. A.; Beveridge, D. L.; Dobosh, P. A. *J. Chem. Phys.* **1967**, *47*, 2026.

(18)   Dixon, R. N. *Mol. Phys.* **1967**, *12*, 83.

(19)   Rydley, J.; Zerner, M. C. *Theor. Chim. Acta* **1973**, *32*, 111.

(20)   Bacon, A. D.; Zerner, M. C. *Theor. Chim. Acta* **1979**, *53*, 21.

(21)   Zerner, M. C.; Loew, G. H.; Kirchner, R. F.; Mueller-Westerhoff, U. T. *J. Am. Chem. Soc.* **1980**, *102*, 589.

(22)   Mulliken, R. S. *J. Phys. Chem.* **1952**, *56*, 295.

(23)   Del Bene, J.; Jaffe, J. J. *J. Chem. Phys.* **1968**, *48*, 1807.

(24)   Møller, C.; Plesset, M. S. *Phys. Rev.* **1934**, *46*, 618.

(25)   Parr, R. G.; Yang, W. *Density Functional Theory of Atoms and Molecules*; Oxford University Press: New York, 1989.

(26)   Koch, W.; Holthausen, M. C. *A Chemist's Guide to Density Functional Theory*; Wiley-VCH: Weinheim, 2000.

(27)   Kohn, W. *Rev. Mod. Phys.* **1998**, *71*, 1253.

(28)   Hohenberg, P.; Kohn, W. *Phys. Rev.* **1964**, *136*, B864.

(29)   Kohn, W.; Sham, L. *Phys. Rev.* **1965**, *140*, A1133.

(30)   Vosko, S. H.; Wilk, L.; Nusair, M. *Can. J. Phys.* **1980**, *58*, 1200.

(31)   Perdew, J. P.; Yang, W. *Phys. Rev. B* **1986**, *33*, 8800.

(32) Becke, A. D. *Phys. Rev. A* **1988**, *38*, 3098.

(33) Lee, C.; Yang, W.; Parr, R. G. *Phys. Rev. B* **1988**, *37*, 785.

(34) Becke, A. D. *J. Chem. Phys.* **1993**, *98*, 5648.

(35) Peuckert, V. *J. Phys. C: Solid State Phys.* **1978**, *11*, 4945.

(36) Zangwill, A.; Soven, P. *Phys. Rev. A* **1980**, *21*, 1561.

(37) Deb, B. M.; Ghosh, S. K. *J. Chem. Phys.* **1982**, *77*, 342.

(38) Ghosh, H.; Deb, B. M. *Chem. Phys.* **1982**, *71*, 295.

(39) Bartololtti, L. *J. Phys. Rev. A* **1981**, *24*, 1661.

(40) Bartololtti, L. *J. Phys. Rev. A* **1982**, *26*, 2243.

(41) Runge, E.; Gross, E. K. U. *Phys. Rev. Lett.* **1984**, *52*, 997.

(42) Gross, E. K. U.; Dobson, J. F.; Petersilka, M. In *Density Functional Theory*; Nalewajski, R. F., Ed.; Springer: Heidelberg, 1996.

(43) Leeuwen, R. *Int. J. Mod. Phys. B* **2001**, *15*, 1969.

(44) Casida, M. E. in *Recent Advances in Density Functional Methods*; Chong, D. P., Ed.; World Scientific: Singapore, 1995.

(45) Bouman, T. D.; Hansen, A. E.; Voigt, B.; Rettrup, S. *Int. J. Quant. Chem.* **1983**, *23*, 595.

(46) van Gisbergen, S. J. A.; Snijders, J. G.; Baerends, E. J. *Comp. Phys. Commun.* **1999**, *118*, 119.

(47) Hirata, S.; Head-Gordon, M. *Chem. Phys. Lett.* **1999**, *302*, 375.

Chapter 4

Opto-Electronic Properties of Positively Charged Phenylenevinylene Oligomers[*]

Time-resolved VIS/NIR Spectroscopy versus Time-Dependent DFT

A combined experimental and theoretical study of the optical properties of positively charged unsubstituted and dialkoxy-substituted phenylenevinylene (PV) oligomers in solution is presented. Cations of PV oligomers were produced by irradiation of solutions with high-energy electron pulses. The optical absorption spectra were measured using time-resolved visible/near-infrared (VIS/NIR) spectroscopy in the range 500 to 2100 nm (0.6 to 2.5 eV). The optical absorption spectra of positively charged PVs are compared with results from Time-Dependent Density Functional Theory (TDDFT) calculations and previous semi-empirical calculations. The experimental spectra of cations of partially dialkoxy substituted PVs indicate the presence of a transition with a maximum below 0.6 eV. According to earlier semi-empirical calculations the energy of this transition exhibits an oscillating behavior as a function of the length of the oligomer. This was not observed experimentally. However, the monotonic decrease of the low energy absorption band, as obtained from TDDFT calculations, is in agreement with the experimental findings.

4.1 Introduction

Conjugated polymers are polyunsaturated compounds, in which the backbone carbon atoms are sp or sp^2 hybridized. In their pure state conjugated polymers are wide band-gap semiconductors, which can become conducting by injection of charges from electrodes, photo-excitation or chemical doping.[1] Poly(p-phenylenevinylene) (PPV) and its derivatives have received considerable attention during the last two decades due to potential applications in light emitting diodes (LEDs),[2-4] solid-state lasers,[5-7] field-effect transistors,[8] optical waveguides[9,10] and photovoltaics.[11-13] The properties that make them suitable for such applications include efficient luminescence,[14-16] low weight, flexibility and low cost. The presence of alkyl or alkoxy substituents provides soluble polymers, which can be easily processed, *e.g.* by spin-coating. The introduction of such substituents also modifies the

electronic properties of the polymers, leading to changes in the optical absorption and emission spectra[17,18] and an increase of the luminescence yield in LEDs.[19,20]

The performance of PPV derivatives in opto-electronic devices is dependent on the properties of the excess charges. Optical absorption spectra of excess charges can provide valuable information about their spatial extent along the polymer chain. Therefore, both experimental and theoretical studies of the optical absorption spectra of charged phenylenevinylene (PV) oligomers have been performed. Sakamoto *et al.*[21] reported ultraviolet to infrared absorption measurements of positively charged unsubstituted PV oligomers. Van Hal *et al.*[22] measured cation spectra of fully dialkoxy-substituted PVs by photoinduced absorption spectroscopy. Using pulse radiolysis with time-resolved spectrophotometric detection, Grozema *et al.*[23] measured the optical absorption spectra of radical cations of partially dialkoxy-substituted PV oligomers.
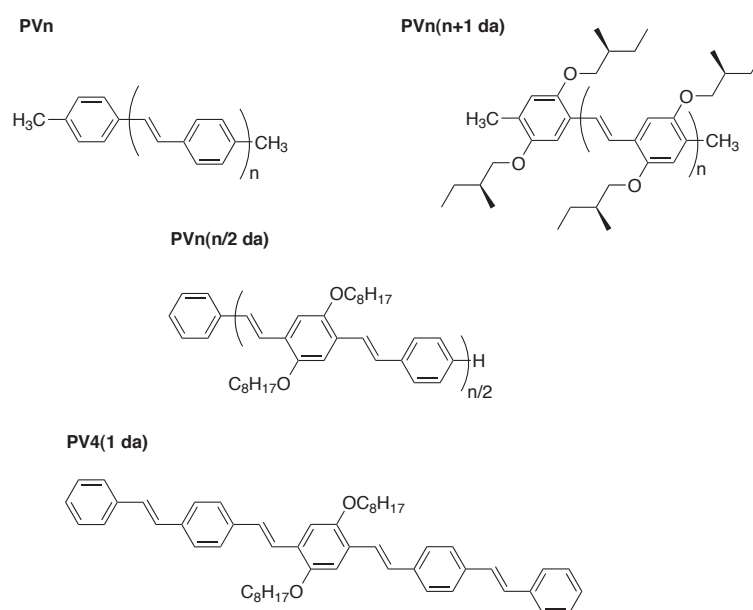
Figure 4.1: Chemical structures of phenylenevinylene (PV) oligomers (n is the number of phenylene units).

Quantum chemical calculations have been performed, to gain insight into the nature of the electronic transitions. Cornil *et al.*[24] performed semiempirical calculations on neutral and positively charged unsubstituted PV oligomers. The geometries of the cations were optimized using the Austin Model 1 (AM1). The optical absorption spectra were calculated using the Hartree-Fock intermediate neglect of differential overlap (INDO) method, combined with configuration interaction of singly excited states (CIS). According to the calculations by Cornil *et al.*[24] two subgap absorption peaks are induced by the generation of singly charged PVs. For doubly charged PVs the absorption spectrum is characterized by a single strong transition. Grozema *et al.*[23] calculated the spectra of positively charged unsubstituted and dialkoxy-substituted PVs, using the INDO/s-CIS method with geometries obtained from Density Functional Theory (DFT) calculations. It was shown that this combination of methods gives a good description of the optical absorption spectra of short derivatives of PV

oligomers. For longer chains Grozema *et al.*[23] found that the charge distributions obtained from DFT calculations are more delocalized than those calculated using the INDO/s Hartree-Fock method. The differences between the two methods are also reflected in the effect of alkoxy side-chains. The INDO/s-CIS method predicts an oscillating behavior of the low absorption energy (RC1) of partially dialkoxy-substituted PVs, as a function of chain length. This odd-even effect was determined to be consistent with the degree of charge delocalization as obtained from semi-empirical INDO/s Hartree-Fock calculations. The odd-even effect could not be verified experimentally, because of the limited accessible energy range of the optical absorption set-up.

The odd-even effect could be an artifact in the INDO/s-CIS calculations. Therefore, the measurements of the optical absorption spectra of cations of partially dialkoxy-substituted PVs have been extended to low absorption energies. Additionally, time-dependent density functional theory (TDDFT) calculations have been performed. The latter method is promising, because Hirata *et al.*[25] have shown that TDDFT provides a good description of the lowest excitation energies of polycyclic aromatic hydrocarbon radical ions. Until now, only a few TDDFT calculations on open-shell systems have been performed.[26,25] To gain further insight into the performance of this method, optical absorption spectra of unsubstituted and fully dialkoxy-substituted PV oligomers have also been calculated. The results of the TDDFT calculations are compared with those from experiments and INDO/s-CIS calculations. The structures of the PV oligomers investigated in the present work are presented in Figure 4.1.

4.2 Experimental details

The PVn(n/2 da) and PV4(1 da) oligomers, shown in Figure 4.1, were synthesized and purified as reported earlier.[27] Solutions of PVn(n/2 da) oligomers in UV-spectroscopic-grade benzene with concentrations in the range of 10^{-4}-10^{-3} M were prepared. The solutions were bubbled with benzene-saturated oxygen for about 30 minutes and maintained under a slight overpressure of the gas during the experiments. Experiments were also performed on oligomer solutions (with concentrations of the order of 10^{-5}-10^{-4} M) in UV-spectroscopic-grade chloroform. The chloroform solutions were bubbled with chloroform-saturated argon. All experiments were performed at room temperature.

The pulse radiolysis technique[28] was used to generate positive charges on isolated PV oligomers in solution. The solutions were irradiated with 20 ns pulses of 3 MeV electrons from a Van de Graaff accelerator. PV cations were detected using time-resolved visible/near-infrared (VIS/NIR) spectroscopy measurements. The detection light source was an Osram XBO high-pressure Xe-lamp (450 W). To avoid photolysis of the solution by the analyzing light, a slow shutter, suitable cut-off filters and a fast shutter were placed between the light source and the sample. The solution was flowed continuously through a quartz cell (optical path length 12.5 mm), using a switch overpressure system. For detection up to 1000 nm, a silicon photodiode was used. Between 1000 nm and 1600 nm, a short-wavelength enhanced InGaAs PIN photodiode G5125-10 (Hamamatsu, Japan) was used, while for NIR this was replaced by a long-wavelength enhanced InGaAs PIN photodiode G5853-01 (Hamamatsu,

Japan). Transient changes in the optical absorption spectrum were recorded by a Tektronix TDS680 digitizer.

The absorption spectra of the PV radical cations were measured by following the transient changes in absorbance of the solution at different wavelengths. The initial concentration of charge carriers is determined by the amount of energy that is transferred from the incident 3 MeV electrons to the solution. The radiation dose (in Gy) is defined as the amount of energy transferred per unit mass (1 Gy = 1 J/kg).[29] The change in optical absorbance is related to the radiation dose, the yield of free charge carriers per unit dose (*G*) and the molar absorption coefficient (ε). The radiation dose per pulse was determined by dosimetry using KSCN solution (10 mM) in N_2O-saturated water. For such a solution *G* and ε are accurately known ($G\varepsilon(SCN)_2^- = 5.18 \cdot 10^{-4}$ m^2J^{-1} at 475 nm[30]). In the optical absorption spectra shown in Figures 4.2 and 4.5 the absorbance changes upon irradiation are normalized to the radiation dose and optical path length.

4.3 Computational methodology

The geometries of the positively charged phenylenevinylene oligomers were optimized using the Amsterdam Density Functional (ADF) theory program.[31] The geometry optimizations were performed using the Local Density Approximation (LDA) with exchange and correlation functionals based on Vosko-Wilk-Nusair (VWN) parameterization of electron gas data.[32] The Generalized Gradient Approximation (GGA)[33] corrections by Becke[34] (exchange) and Perdew[35] (correlation) were included. For optimizing the geometries a triple zeta plus double polarization (TZ2P) basis set was used. The geometries were restricted to C_{2h} symmetry.

The electronic absorption spectra of the positively charged phenylenevinylenes were calculated with Time-Dependent Density Functional Theory (TDDFT)[36,37] as implemented in the Q-Chem program.[38] The excitation energies were computed using a correlation consistent[39] polarized Valence Double Zeta (cc-pVDZ) basis set. The Becke (exchange) and the Lee-Yang-Parr (correlation)[40] functional (BLYP) or the Becke3 (exchange) and the Lee-Yang-Parr (correlation) hybrid functional (B3LYP)[41] were used. The TDDFT results for the positively charged phenylenevinylene oligomers are compared with INDO/s-CIS calculations published previously.[23]

4.4 Results and discussion

Three different series of phenylenevinylene oligomers were studied. The first series, PVn, consists of PV oligomers that have been para-substituted with methyl groups on the first and last phenyl ring (see Figure 4.1). The experimental optical absorption spectra of the PVn cations up to n=3 are available in the literature.[21] The experimental and calculated optical absorption energies are presented in Table 4.1. The second series, PVn(n+1 da), contains two alkoxy substituents on each phenyl ring. The experimental optical absorption spectra of PVn(n+1 da) cations were published previously,[22] and the energies of the maxima in the spectra are given in Table 4.2, together with theoretical results. The third series, PVn(n/2 da),

has two alkoxy substituents on every second phenyl ring. The optical absorption spectra of the PVn(n/2 da) cations were measured using pulse radiolysis, as described below. To obtain additional insight into the effects of substituents, experiments and calculations were also performed on PV4(1 da), which is dialkoxy-substituted only on the central phenyl ring. The experimental and calculated results obtained for the third series of PV oligomers are presented in Table 4.3.

4.4.1 Measurement of cation spectra of partially dialkoxy substituted PVs

Irradiation of benzene (bz) leads to the generation of radical cations (bz$^{\bullet+}$), excited states (bz*) and solvated electrons (e$^-$)[42-44] (eq. 4.1)

$$bz \rightarrow bz^{\bullet+}, bz^*, e^- \tag{4.1}$$

The radiolytic processes that result in the formation of positively charged PVs were discussed in detail elsewhere.[45] The most important reactions are described below. In oxygen-saturated solutions ([O$_2$]=11.9 mM at 1 atm. and 25°C) the excess electrons are rapidly scavenged, according to equation 4.2.

$$e^- + O_2 \rightarrow O_2^- \tag{4.2}$$

The excited states are quenched by O$_2$ within a few nanoseconds to yield O$_2$ in the $^1\Delta$ excited state[46] (eq. 4.3).

$$bz^* + O_2 \rightarrow O_2(^1\Delta) + bz \tag{4.3}$$

The radical cations of benzene transfer their charge to the PV oligomers, because these compounds have a lower ionization potential than benzene (eq. 4.4).

$$bz^{\bullet+} + PV \rightarrow bz + PV^{\bullet+} \tag{4.4}$$

Candeias *et al.*[47] have shown that the radical cations of PV oligomers are unaffected by O$_2$.

The measured radical cation absorption spectra of PVn(n/2 da) oligomers are shown in Figure 4.2. The energies corresponding to the absorption maxima can be found in Table 4.3. For the PV2(1 da) radical cation, two bands are observed. The first band appears at 1.27 eV and is denoted RC1. The second band (denoted as RC2) has a maximum at 2.08 eV and exhibits two vibrational transitions, in agreement with previous measurements.[23] The shape of the RC2 band between 1.8 eV and 2.4 eV differs from that in ref. 23, because of improvement of the spectral resolution of the optical setup. For the longer oligomers in the PVn(n/2 da) series, the maximum of the low energy band (RC1) could not be observed in the accesible energy range. However, the RC1 absorption maxima shift below 0.6 eV.

In Figure 4.3, the optical absorption spectra of the positively charged, partially dialkoxy-substituted oligomers are superposed. The RC2 band of the PVn(n/2 da) radical cations (with n>2) exhibits no observable shift to lower energies with increasing chain length. The absorption maxima of the RC1 band could not be determined for PVs other than PV2(1 da).

However, the onset of the RC1 band in Figure 4.3 suggests that there is not a large shift, as a function of the chain length.
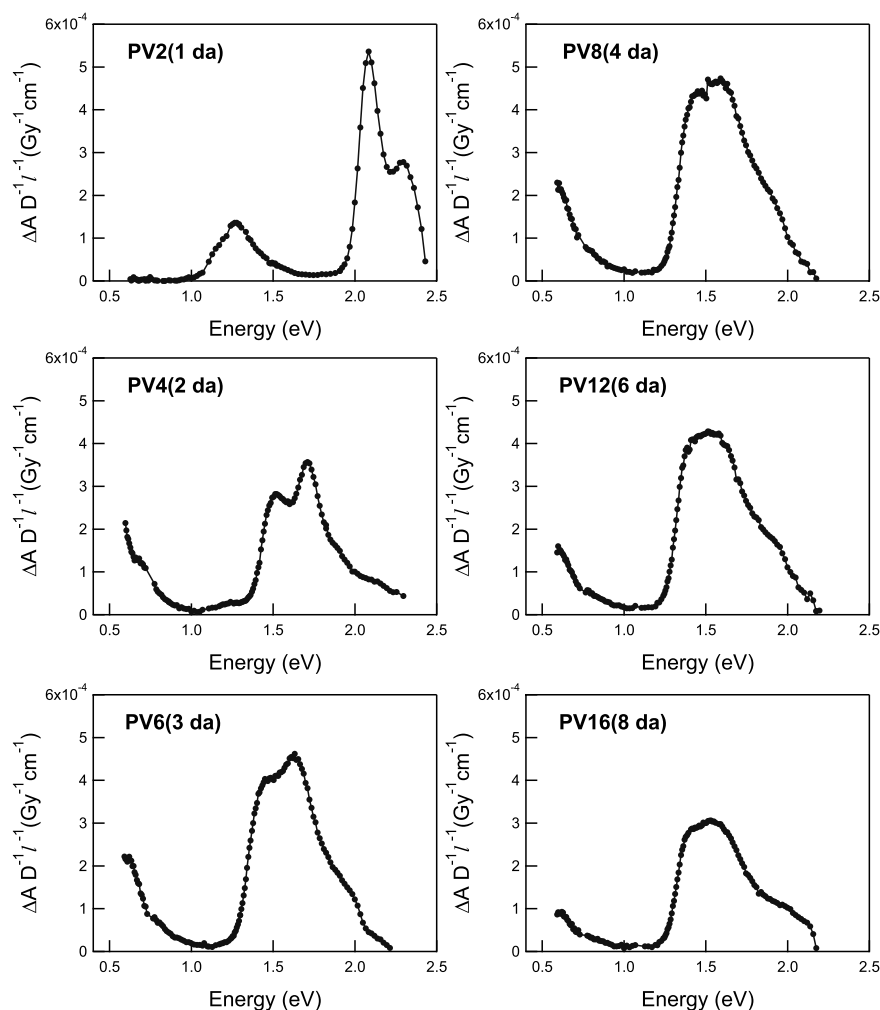
Figure 4.2: Optical absorption spectra of the radical cations of the PVn(n/2 da) series in benzene.

Additional measurements were performed in chloroform. Irradiation of chloroform ($CHCl_3$) with 3 MeV electrons leads to the formation of chloroform radical cations ($CHCl_3^{\bullet+}$) and excess electrons (e^-),[48,49] according to equation 4.5.

$$CHCl_3 \rightarrow CHCl_3^{\bullet+} + e^- \tag{4.5}$$

The $CHCl_3^{\bullet+}$ ions transfer their charge to the PV oligomers, which have a lower ionization potential. This leads to the formation of PV radical cations (eq. 4.6).

$$CHCl_3^{\bullet+} + PV \rightarrow PV^{\bullet+} + CHCl_3 \tag{4.6}$$

The excess electrons react with neutral chloroform and form the methylene chloride radical and the chloride anion[50] (eq. 4.7).

$$e^- + CHCl_3 \rightarrow {}^\bullet CHCl_2 + Cl^- \tag{4.7}$$

The methylene chloride radical can react with neutral PV oligomers, leading to formation of PV radical cations and methylene chloride anions (eq. 4.8).

$${}^\bullet CHCl_2 + PV \rightarrow PV^{\bullet+} + CHCl_2^- \tag{4.8}$$
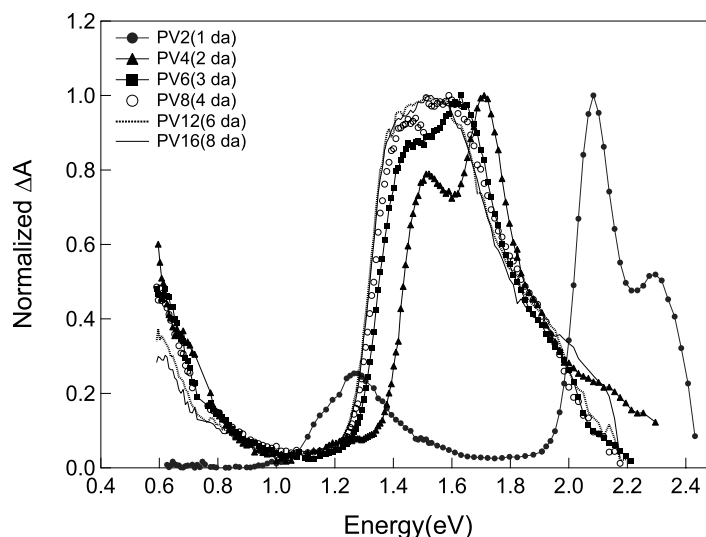
Figure 4.3: Optical absorption spectra of the radical cations of the PVn(n/2 da) series in benzene.

In Figure 4.4 the optical absorption spectra of PV2(1 da) and PV16(8 da) radical cations in chloroform are compared with the spectra in benzene. For PV2(1 da), the absorption maxima in chloroform appear at an energy, which is approximately 0.1 eV higher than that in benzene. The effect of the solvent on the cation spectrum of PV16(8 da) is much smaller. Apparently, for the longer oligomer, the solvent effect is reduced as a consequence of a larger extent of delocalization of the charge.
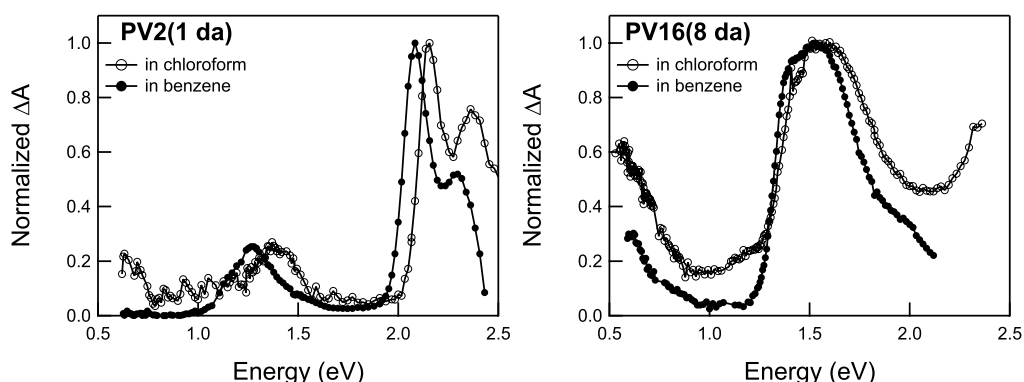
Figure 4.4: Optical absorption spectra of radical cations of the PV2(1 da) and PV16(8 da) in chloroform and benzene.

Figure 4.5 shows a comparison of the absorption spectra for the radical cations of PV4(1 da) and PV4(2 da). The number and position of the substituents clearly influence the optical absorption spectra of these PV tetramers. The low-energy band (RC1) for the PV4(1 da) radical cation has a maximum at 0.77 eV. Although the low-energy band for PV4(2 da) could not be measured completely, the data in Figure 4.5 show that the maximum of this band appears below 0.6 eV. This reduction of the transition energy suggests that the charge is more delocalized when more dialkoxy substituents are present. The RC2 bands for PV4(1 da) and PV4(2 da) appear at similar energies in the cation spectra.
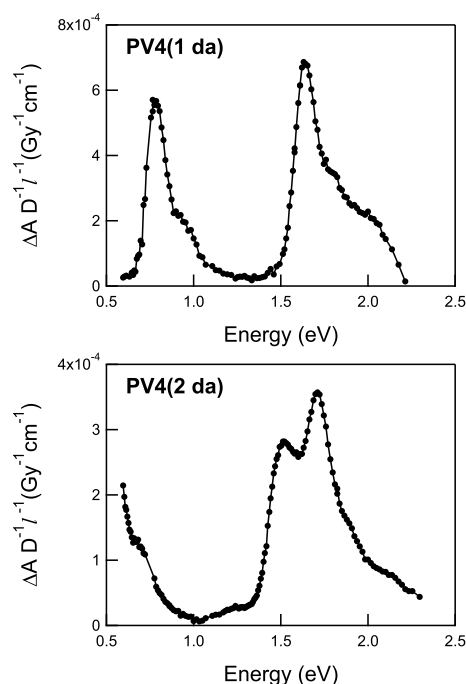
Figure 4.5: Optical absorption spectra of radical cations of the PV4(1 da) and PV4(2 da) in benzene.

4.4.2 Calculated absorption spectra of PV cations

The calculated electronic transitions of the three series of PV radical cations are listed in Tables 4.1–4.3, together with the experimental data from the present measurements and literature. In the calculations, the alkoxy substituents were taken to be methoxy groups. This simplification is not expected to influence the results significantly, with regard to electronic effects of the substituents.[23] The results from the TDDFT calculations are discussed and compared with INDO/s-CIS results and with the experimental data below.

PVn radical cations

The calculated and experimental transition energies (ΔE) and the calculated oscillator strengths (f) for radical cations of PVn oligomers are given in Table 4.1. The electronic configurations that dominate the allowed transitions, according to the INDO/s-CIS method for

the PVn radical cations, were described in a previous study.[23] It was found that the lowest transition (RC1) is dominated by excitation of an electron from the highest doubly occupied molecular orbital to the singly occupied molecular orbital. The second (RC2) and third (RC3) transition correspond mainly to excitation of an electron from the singly occupied molecular orbital to the lowest unoccupied molecular orbital with a different contribution of other excitations involving lower-lying orbitals.

Table 4.1: Calculated and experimental transition energies (ΔE in eV), and calculated oscillator strengths (f) for radical cations of PVn oligomers. Only the transitions with an oscillator strength higher than 0.1 are presented.

| | | Exptl.[a] | TDDFT | | | | INDO/s-CIS[b] | |
| | | | BLYP | | B3LYP | | | |
Oligomer	Band	ΔE	ΔE	f	ΔE	f	ΔE	f
PV1	RC1	1.54	1.91	0.11	1.99	0.15	1.71	0.04
	RC2	2.45	3.08	0.88	3.11	0.90	2.20	0.80
PV2	RC1	1.03	1.28	0.26	1.32	0.39	1.13	0.36
	RC2	1.95	2.34	1.58	2.43	1.56	1.89	1.01
PV3	RC1	0.80	0.98	0.50	1.01	0.74	0.87	0.62
	RC2	1.74	1.94	1.90	2.07	1.94	1.69	1.14
PV4	RC1		0.80	0.79	0.81	1.12	0.71	0.89
	RC2		1.74	1.04	1.85	1.44	1.65	1.03
	RC3		2.60	0.67	1.92	0.48	1.91	0.22
PV6	RC1		0.58	1.34	0.56	1.76	0.55	1.13
	RC2		1.46	1.84	1.67	1.81	1.44	0.14
	RC3		2.08	1.68	2.39	1.09	1.58	1.00
PV8	RC1		0.43	1.73	0.41	2.11	0.49	1.29
	RC2		1.36	1.58	1.57	1.13	1.57	0.80
	RC3						1.81	0.38
PV10	RC1		0.37	2.15	0.35	2.65	0.46	1.33
	RC2						1.47	0.23
	RC3						1.60	0.27
PV12	RC1		0.30	2.31	0.27	2.51	0.45	1.39
	RC2						1.60	0.43
	RC3						1.72	0.34

[a] Experimental data were taken from ref. 21
[b] Theoretical data were taken from ref. 23

The RC1 and RC2 excitation energies of PVn cations calculated with TDDFT are compared with the INDO/s-CIS calculated energies[23] and with experimental data[21] in Figure 4.6(a). The general observation is that all transition energies shift to lower values with increasing chain length, which can be understood in terms of increasing spatial delocalization of the charge. The TDDFT results obtained using BLYP and B3LYP functionals are similar. For short PVn oligomers (with n=1-3), the TDDFT transition energies are higher than the INDO/s-CIS transition energies. The INDO/s-CIS excitation energies are generally closer to the experimental values. For long PVn oligomers (with n>3), the TDDFT results for the RC1

and RC2 bands are similar to those obtained with the INDO/s-CIS method. The third absorption band (RC3) for longer PVn oligomers obtained from TDDFT calculations appears at a substantially higher energy than found by the INDO/s-CIS method (see Table 4.1). For PVn oligomers with n≥8, not all three transitions could be calculated due computer hardware limitations. The main conclusion is that both TDDFT and INDO/s-CIS methods reproduce the experimental data for the RC1 and RC2 transitions. To be able to distinguish the performance of the different theoretical methods, experimental results on the RC3 transition for longer oligomers are needed.
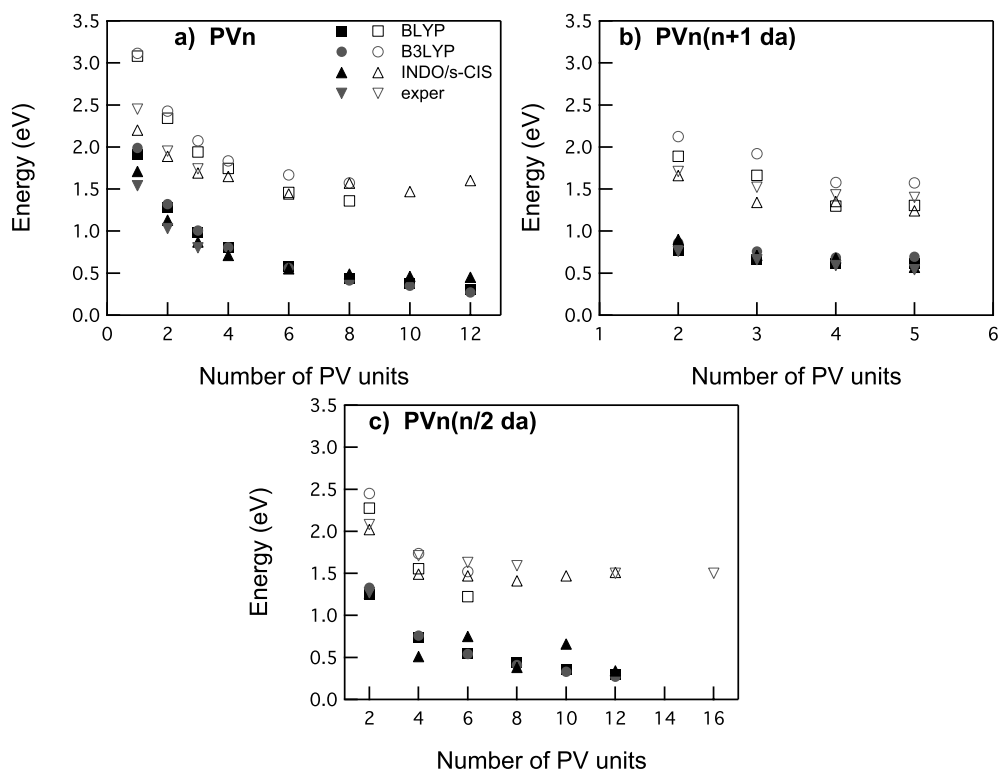
Figure 4.6: Chain length dependence of the absorption energies for PV cations ((a) PVn, (b) PVn(n+1 da), and (c) PVn(n/2 da)). Filled markers correspond to the lowest energy band (RC1) and open markers to the RC2 energy band.

The data in Table 4.1 show that the calculated oscillator strength (*f*) of the RC1 transition increases with the chain length, in agreement with previous calculations.[24] For shorter chains, the oscillator strength of the RC1 transition is higher than that for RC2, whereas for longer chains, the RC2 transition is most intense. The oscillator strength obtained from TDDFT calculations is in general higher than that from INDO/s-CIS calculations, in particular for the RC2 band of the PV6 radical cation.

PVn(n+1) radical cations

Table 4.2 shows the calculated and experimental transition energies (Δ*E*) and the calculated oscillator strengths (*f*) for radical cations of PVn(n+1 da) oligomers. Introduction of dialkoxy

substituents at each phenyl ring reduces the absorption energies (*cf.* Tables 4.1 and 4.2). As can be seen in Figure 4.6(b), both the TDDFT and the INDO/s-CIS methods reproduce the experimental RC1 and RC2 transition energies reasonably well.[22] Note that the dependence of the RC1 energy on the chain length is much smaller than for the PVn series, both in the experiment and in the calculations. A possible explanation can be the delocalization of the charge into the alkoxy side chains. This means that, for the same chain length, the charge is always more delocalized in the PVn(n+1 da) series than in the PVn series. As a consequence, the chain length at which the distance dependence becomes very small is reached already for shorter oligomers. The differences between the results obtained with the BLYP and B3LYP functionals are larger than for PVn radical cations. The transition energies obtained with the BLYP functional are more similar to the experimental data. According to both the TDDFT and the INDO/s-CIS calculations a third absorption band (RC3) appears at higher energies (see Table 4.2). For the PV2(3 da) radical cation, a third absorption band is clearly present in the experimental spectrum of van Hal *et al.*[22] However, this band has not been assigned to a separate electronic transition by those authors. The energy of the RC3 band for PV2(3 da) is reproduced quite well by the INDO/s-CIS calculations, whereas TDDFT considerably overestimates the energy of this band. For longer PVn(n+1 da) cations, a shoulder towards the high-energy side of the RC2 band can be distinguished in the experimental spectra of van Hal *et al.*[22] According to the present calculations, this shoulder could be due to the RC3 transition. The RC3 excitation energies as estimated from the experimental spectra in ref. 22 are close to the calculated values (see Table 4.2).

Table 4.2: Calculated and experimental transition energies (ΔE in eV), and calculated oscillator strengths (f) for radical cations of PVn(n+1 da) oligomers. Only the transitions with an oscillator strength higher than 0.1 are presented.

| | | Exptl.[a] | TDDFT | | | | INDO/s-CIS[b] | |
| | | | BLYP | | B3LYP | | | |
Oligomer	Band	ΔE	ΔE	f	ΔE	f	ΔE	f
PV2(3 da)	RC1	0.76	0.77	0.20	0.86	0.33	0.90	0.30
	RC2	1.71	1.89	0.87	2.12	1.21	1.66	0.64
	RC3	~2.0[c]	2.47	0.22	3.58	0.21	1.99	0.23
PV3(4 da)	RC1	0.66	0.67	0.38	0.76	0.64	0.71	0.43
	RC2	1.52	1.66	1.07	1.92	1.57	1.34	0.34
	RC3	~1.7[c]	2.17	0.37			1.56	0.61
PV4(5 da)	RC1	0.59	0.62	0.53	0.69	0.90	0.68	0.58
	RC2	1.43	1.30	0.24	1.58	1.42	1.35	0.96
	RC3	~1.6[c]	1.42	1.59	1.70	0.74	1.61	0.11
PV5(6 da)	RC1	0.54	0.62	0.52	0.69	0.88	0.57	0.74
	RC2	1.40	1.30	0.33	1.57	1.63	1.24	0.31
	RC3	~1.6[c]	1.42	1.57	1.71	0.60	1.40	0.85

[a] Experimental data were taken from ref. 22
[b] Theoretical data were taken from ref. 23
[c] The estimated absorption energies of RC3 were extracted from the spectra in ref. 22

PVn(n/2 da) radical cations

The TDDFT transition energies (ΔE) for the cations of PVn(n/2 da) oligomers are compared with the INDO/s-CIS energies and with the experimental data from the present work in Figure 4.6(c) and Table 4.3. For the PV2(1 da) cation, the agreement between the calculated and the experimental energy of the RC1 band is excellent. The RC2 transition energy of the PV2(1 da) cation is better reproduced by the INDO/s-CIS method than by the TDDFT calculation.

Table 4.3: Calculated and experimental transition energies (ΔE in eV), and calculated oscillator strengths (f) for radical cations of PVn(n/2 da) oligomers. Only the transitions with an oscillator strength higher than 0.1 are presented.

| | | | TDDFT | | | | | |
| | | Exptl.[a] | BLYP | | B3LYP | | INDO/s-CIS[b] | |
Oligomer	Band	ΔE	ΔE	f	ΔE	f	ΔE	f
PV2(1 da)	RC1	1.27	1.25	0.24	1.33	0.38	1.26	0.04
	RC2	2.08	2.27	1.07	2.45	1.20	2.02	1.08
PV4(2 da)	RC1	<0.6	0.74	0.52	0.76	0.88	0.51	0.75
	RC2	1.52	1.55	2.02	1.74	2.10	1.49	0.56
	RC3	1.71	2.41	0.33	2.69	0.12	1.74	0.53
PV6(3 da)	RC1	<0.6	0.54	1.07	0.54	1.59	0.75	0.86
	RC2	1.45	1.22	0.20	1.52	1.98	1.47	0.44
	RC3	1.63	1.31	1.82			1.56	0.72
	RC4						1.91	0.30
PV8(4 da)	RC1	<0.6	0.44	1.56	0.41	2.03	0.38	1.03
	RC2	1.59					1.41	0.77
	RC3						1.56	0.10
	RC4						1.72	0.29
PV10(5 da)	RC1		0.36	3.28	0.33	2.38	0.66	1.08
	RC2						1.47	0.30
	RC3						1.65	0.81
	RC4						1.92	0.49
PV12 (6 da)	RC1	<0.6	0.29	2.31	0.27	2.58	0.34	1.15
	RC2	1.51					1.51	0.56
	RC3						1.59	1.19
	RC4						1.72	0.38
PV16(8 da)	RC1	<0.6						
	RC2	1.50						
PV4(1 da)	RC1	0.77	0.79	0.78	0.82	1.07	1.03	0.44
	RC2	1.63	1.62	0.52	1.82	0.47	1.77	1.47
	RC3		1.77	1.33	1.98	1.39	1.94	0.14

[a] Experimental data were obtained from spectra in Figures 4.2 and 4.5
[b] Theoretical data were taken from ref. 23

    The maximum of the low-energy band (RC1) in the measured spectrum of PV4(2 da) cation is below 0.6 eV, in agreement with the results from INDO/s-CIS calculations.[23]

TDDFT overestimates the energy of the RC1 band by at least 0.15 eV. The double maximum of the high-energy band in the experimental spectrum of PV4(2 da) (see Figure 4.2) can be assigned to two separate electronic transitions, on the basis of INDO/s-CIS calculations (RC2 and RC3). In contrast, TDDFT does not predict two close-lying electronic transitions (see Table 4.3).

According to the experiments, the RC1 transition energy of the longer oligomers of the PVn(n/2 da) series is less than 0.6 eV, in agreement with the results from TDDFT calculations. The RC2 transition energies are reproduced quite well by both the INDO/s-CIS and the TDDFT calculations.
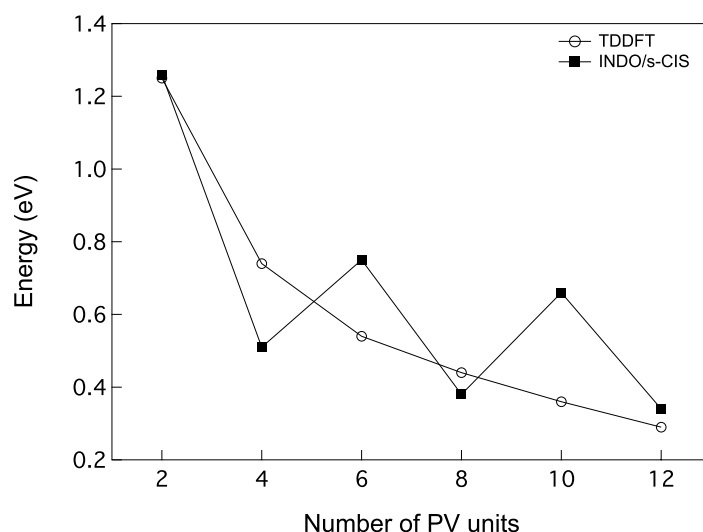
Figure 4.7: Chain length dependence of the lowest transition energy (RC1) calculated for PVn(n/2 da) radical cations, using the TDDFT and INDO/s-CIS methods.

The most interesting observation from the comparison of the TDDFT and the INDO/s-CIS results is that the former method predicts a monotonic decrease of the RC1 absorption energy with chain length (see Figure 4.7), in contrast with the latter. As shown earlier, the INDO/s-CIS calculations for PVn(n/2 da) radical cations predict the occurrence of a so-called odd-even effect.[23] The PVn(n/2 da) radical cations with an even number of dialkoxy-substituted phenyl rings were found to have the RC1 energy lower than that for the corresponding PVn radical cation. On the other hand, for PVn(n/2 da) radical cations with an odd number of dialkoxy-substituted phenyl rings the RC1 energies are always higher than those of the unsubstituted analogue. This odd-even effect, as predicted by the INDO/s-CIS method, is not observed experimentally. In particular, the RC1 band for the PV6(3 da) radical cation is not higher than the RC1 band for the PV4(2 da) radical cation (Figure 4.2). The INDO/s-CIS method seemingly overestimates the localization of charges, because of the presence of alkoxy side chains.

PV4(1 da) radical cation

To gain additional insight into the effect of the dialkoxy substitution on the optical properties of the PV radical cations, the compound PV4(1 da), which has substituents only at the central phenyl ring (see Figure 4.1) was also investigated. The optical absorption spectra of the PV4(1 da) and PV4(2 da) cations are shown in Figure 4.5. The RC1 and RC2 transition energies of the PV4(1 da) radical cation are reproduced very well by both the TDDFT and the INDO/s-CIS methods (see Table 4.3). The RC2 band in the experimental spectrum of PV4(1 da) has a shoulder towards the high-energy side (see Figure 4.5). According to both theoretical methods, a third transition (RC3) occurs at higher energy, which may be the cause of this shoulder.

4.4.3 Effect of substituents on the charge distribution

Insight into the effect of the substituents on the delocalization of a charge carrier on a PV oligomer can be obtained by analyzing the charge distribution along the chain. Charge distributions calculated with the INDO/s-CIS method have been discussed previously.[23] In the present study, the charge distribution is calculated with the DFT method and compared with the results from the INDO/s-CIS calculations. The charge distribution was obtained from a Mulliken population analysis performed on the same charge density used to calculate the absorption spectra. In the neutral molecules, the phenylene units carry some negative charge, whereas the vinylene units are positively charged. Therefore, the distribution of the excess positive charge was calculated as the difference between the charges of the atoms in the cations and in the neutral molecules. Hence, the calculated distribution corresponds to that of the excess positive charge. Figure 4.8 shows the distribution of an excess positive charge in PV tetramers with different dialkoxy substitution patterns.

The phenylene units in the unsubstituted oligomer (PV4) carry a similar amount of charge. The same holds for the vinylene units, even though the amount of charge on the latter is smaller than on the phenylene units. Note that the charge per C atom is smaller for the phenylene units (containing six C atoms) than for the vinylene units (with two C atoms). However, because the atomic orbitals on the C atoms form molecular fragment orbitals on the phenylene and vinylene units, it is most appropriate to discuss the charge distribution in terms of these units. The higher amount of charge on the phenylene units is due to the lower ionization potential of these units in comparison with that of the vinylene units. Introduction of methoxy substituents on the phenyl ring leads to a further lowering of the ionization potential of these units. As a consequence, the charge becomes more localized on the central methoxy substituted phenyl ring in PV4(1 da) (see Figure 4.8). For PV4(2 da) the charge is mainly localized on the second and the fourth phenyl ring, *i.e.*, on the phenyl rings containing methoxy substituents. When all phenyl rings are methoxy substituted, which is the case for PV4(5 da), the charge is almost uniformly distributed over the phenylene units, with somewhat more charge on the outer phenyl rings. Figure 4.8 shows that the charge distribution for PV4(5 da) is almost the same as that for PV4.

The DFT charge distribution is different from that obtained with the INDO/s-CIS method. Grozema *et al.*[23] found, using the INDO/s-CIS method, that, for PV4, the maximum

in the charge distribution is located at the central phenyl ring. For PV4(1 da), the methoxy substituents localize the charge on the central phenyl ring, but to a larger extent than according to the DFT calculations. In the PV4(2 da) oligomer, the charge is mainly localized on the substituted phenyl rings, according to the DFT calculations, whereas the charges calculated with the INDO/s-CIS method are distributed more evenly. The results also are different for the PV4(5 da) radical cation. According to INDO/s-CIS calculations, the amount of charge on the central phenylene unit is higher than on the other phenylene units, in contrast to the results obtained with DFT.
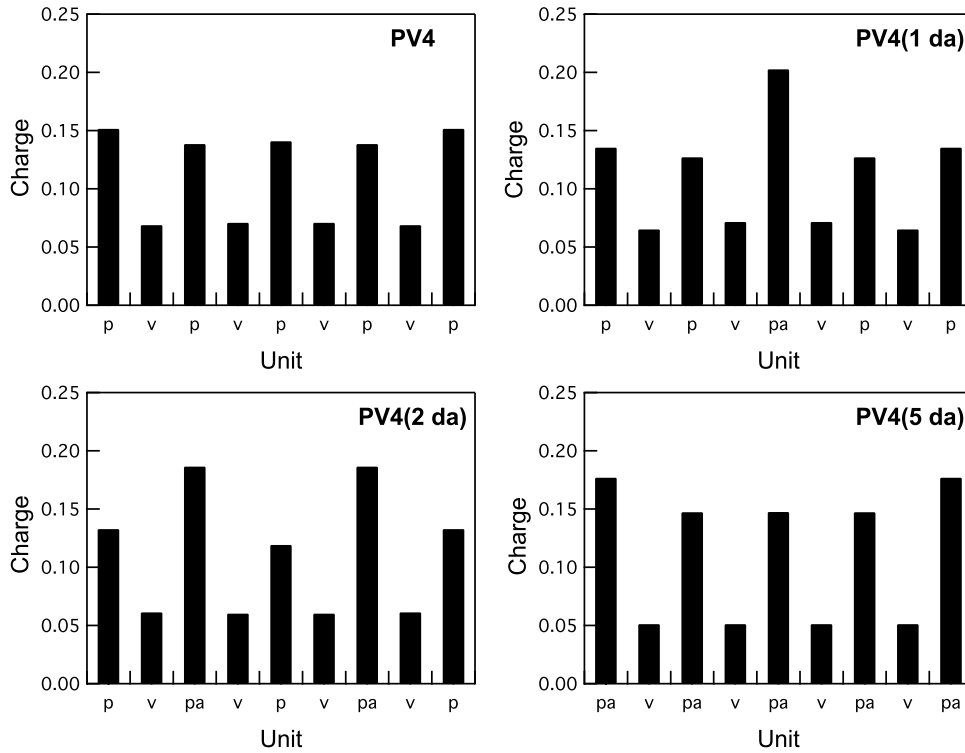
Figure 4.8: Distribution of an excess positive charge in PV tetramers with different dialkoxy substitution patterns (phenylene, vinylene and dialkoxy-substituted phenylene units are indicated as p, v and pa, respectively).

The degree of charge delocalization can be characterized in terms of the participation ratio, P (eq. 4.9).

$$P = \left[\sum_{i=1}^{N} Q_i^2 \right]^{-1} \tag{4.9}$$

Note that the aforementioned expression represents the reciprocal value of the often-used inverse participation ratio. In equation 4.9, Q_i represents the amount of charge present on the i-th unit and N is the number of units. If all the excess charge is localized on a single unit, P becomes 1. If the charge is evenly spread over all N units, than P will be equal to N. Table 4.4 shows the calculated participation ratio for the unsubstituted and dimethoxy-substituted PV radical cations. The participation ratio for the unsubstituted PV oligomers increases

smoothly with chain length, which reflects that the charge becomes more delocalized for longer oligomers. Table 4.1 shows a decrease of the low energy band, RC1 for PVn oligomers, with increasing chain length. This decrease coincides with the increased charge delocalization. The same behavior is found for PVn(n/2 da) oligomers. The participation ratio substantiates the fact that DFT does not predict the odd-even trend in the RC1 transition energies for the PVn(n/2 da) series. As can be observed in Table 4.4, the *P* values for unsubstituted oligomers are higher than those for the methoxy-substituted oligomers, which means that the charge is more localized when the substituents are present. The calculated degree of charge delocalization correlates with the calculated energy of the lowest absorption band. The only exception is PV4(1 da), which has a lower participation ratio than PV4, whereas the RC1 absorption energies are similar.

Table 4.4: Participation ratio from the DFT Mulliken population analysis.

Unsubstituted oligomer	Participation ratio, P	Dimethoxy-substituted oligomer	Participation ratio, P
PV2	4.5	PV2(1 da)	4.3
PV4	8.1	PV4(2 da)	7.5
PV6	11.7	PV6(3 da)	10.8
PV8	15.3	PV8(4 da)	14.1
PV10	18.9	PV10(5 da)	17.4
PV12	22.6	PV12(6 da)	20.7
		PV4(1 da)	5.4
		PV4(2 da)	7.2

The differences between results obtained from INDO/s-CIS and DFT calculations were noticed previously. According to DFT calculations on singly and doubly charged thiophene oligomers,[51,52,53] the charge distribution and the geometry deformations are fully delocalized over the entire length of the oligomer. There are indications that the delocalization of charge is overestimated in DFT.[54] In contrast, the charge distribution obtained from INDO/s-CIS calculations of charged oligo(phenylenevinylene)s[23,24] and oligothiophenes[55] has a rather localized character. Moreover, the comparison of experimental[56] and theoretical[55] results for thiophene oligomers indicates that semi-empirical INDO/s-CIS calculations underestimate the spatial extent of charge carriers on conjugated chains. The difference between DFT and semi-empirical INDO/s-CIS results is attributed to the fact that the two methods are developed from different monoelectronic operators with different theoretical frameworks.[57] DFT includes the electron correlation, whereas, in INDO/s-CIS calculations, the dynamic correlation is not taken into consideration. The extent to which electron correlation is taken into consideration has a large effect on the delocalization of an excess charge.

4.5 Summary and conclusions

Cations of partially dialkoxy-substituted phenylenevinylene (PV) oligomers were produced in solution using pulse radiolysis with nanosecond pulses of 3 MeV electrons. The cations were

detected using time-resolved visible/near-infrared (VIS/NIR) optical absorption measurements.

Quantum chemical calculations were performed for unsubstituted and dialkoxy-substituted PV oligomers. The geometries of the positively charged PV oligomers were optimized using the Amsterdam Density Functional (ADF) Theory program. The electronic absorption spectra of the charged PVs were calculated with time-dependent density functional theory (TDDFT) and compared with those obtained earlier from intermediate neglect of differential overlap combined with configuration interaction of singly excited states (INDO/s-CIS) calculations.

The calculated absorption energies for transition bands RC1 and RC2 for the unsubstituted PVn and fully dialkoxy-substituted PVn(n+1 da) cations were determined to be in agreement with experiments. For the shortest PVn(n+1 da) cations, TDDFT overestimates the energy of the third RC3 transition.

The experimental spectra of partially dialkoxy-substituted PVn(n/2 da) radical cations show that the maximum of the lowest optical absorption band (RC1) is below 0.6 eV. This is in agreement with the TDDFT calculations, which predict a monotonic decrease of the lowest transition energy (RC1) with chain length. INDO/s-CIS calculations predict an oscillating behavior (odd-even effect) of the RC1 transition energy with the length of the oligomer chain, which is in disagreement with the current experimental findings. The decrease of the RC1 absorption energy with chain length is consistent with the degree of charge delocalization as calculated with density functional theory (DFT).

The presence of alkoxy substituents reduces the transition energies, which is most pronounced for fully dialkoxy-substituted PV oligomers. In partially dialkoxy-substituted PV oligomers, more positive charge is present on the substituted phenylene units than on the unsubstituted ones.

DFT calculations lead to a more-delocalized charge distribution than the INDO/s-CIS method. It is of interest to establish whether the relatively localized charge distributions from INDO/s-CIS calculations and the odd-even effect are caused by the absence of dynamic electron correlation or by an artifact in the semiempirical INDO/s-CIS calculations. This issue could be solved by performing correlated quantum mechanics calculations, *e.g.* using second-order Moller-Plesset (MP2) methods. Such calculations should be performed on PV oligomers of at least eight repeat units, which requires high computational power.

4.6 References

(1)   Skotheim, T. A.; Elsenbaumer, R. L.; Reynolds, J. R. *Handbook of Conducting Polymers*; Marcel Dekker, Inc.: New York, 1998.

(2)   Burroughes, J. H.; Bradley, D. D. C.; Brown, A. R.; Marks, R. N.; Mackay, K.; Friend, R. H.; Burns, P. L.; Holmes, A. B. *Nature* **1990**, *347*, 539.

(3)   Kraft, A.; Grimsdale, A. C.; Holmes, A. B. *Angew. Chem. Int. Ed.* **1998**, *37*, 402.

(4)   Friend, R. H.; Gymer, R. W.; Holmes, A. B.; Burroughes, J. H.; Marks, R. N.; Taliani, C.; Bradley, D. D. C.; Dos Santos, D. A.; Bredas, J. L.; Logdlund, M.; Salaneck, W. R. *Nature* **1999**, *397*, 121.

(5)   McGehee, M. D.; Heeger, A. J. *Adv. Mater.* **2000**, *12*, 1655.

(6)   McGehee, M. D.; Diaz-Garcia, M. A.; Hide, F.; Gupta, R.; Miller, E. K.; Moses, D.; Heeger, A. J. *Appl. Phys. Lett.* **1998**, *72*, 1536.

(7)   Schulzgen, A.; Spiegelberg, C.; Morrell, M. M.; Mendes, S. B.; Kippelen, B. *Appl. Phys. Lett.* **1998**, *72*, 269.

(8)   Pichler, K.; Jarrett, C. P.; Friend, R. H.; Ratier, B.; Moliton, A. *J. Appl. Phys.* **1995**, *77*, 3523.

(9)   Michelotti, F.; Gabler, T.; Horhold, H.; Waldhausl, R.; Brauer, A. *Opt. Commun.* **1995**, *114*, 247.

(10)   Gymer, R. W.; Friend, R. H.; Ahmed, H.; Burn, P. L.; Kraft, A. M.; Holmes, A. B. *Synth. Met.* **1993**, *57*, 3683.

(11)   Halls, J. J. M.; Walsh, C. A.; Greenham, N. C.; Marseglla, E. A.; Friend, R. H.; Moratti, S. C.; Holmes, A. B. *Nature* **1995**, *376*, 498.

(12)   Zhou, Q.; Zheng, L.; Sun, D.; Deng, X.; Yu, G.; Cao, Y. *Synth. Met.* **2003**, *135-136*, 825.

(13)   Breeze, A. J.; Schlesinger, Z.; Carter, S. A.; Tillmann, H.; Horhold, H. H. *Sol. Energy Mater. Sol. Cells* **2004**, *83*, 263.

(14)   Braun, D.; Staring, E. G. J.; Demandt, R. C. J. E.; Rikken, G. L. J.; Kessener, Y. A. R. R.; Venhuizen, A. H. J. *Synth. Met.* **1994**, *66*, 75.

(15)   Greenham, N. C.; Samuel, I. D. W.; Hayes, G. R.; Phillips, R. T.; Kessener, Y. A. R. R.; Moratti, S. C.; Holmes, A. N.; Friend, R. H. *Chem. Phys. Lett.* **1995**, *241*, 89.

(16)   Cao, Y.; Parker, I. D.; Yu, G.; Zhang, C.; Heeger, A. J. *Nature* **1999**, *397*, 414.

(17)   Burn, P. L.; Holmes, A. B.; Kraft, A.; Bradley, D. D. C.; Brown, A. R.; Friend, R. H.; Gymer, R. W. *Nature* **1992**, *356*, 47.

(18)   Hilberer, A.; Brouwer, H. J.; Van der Scheer, B. J.; J. Wildeman, J.; Hadziioannou, G. *Macromolecules* **1995**, *28*, 4525.

(19)   Samuel, I. D. W.; Rumbles, G.; Collison, C. J. *Phys. Rev. B* **1995**, *52*, 11573.

(20)   Van Hutten, P. F.; Krasnikov, V. V.; Hadziioannou, G. *Acc. Chem. Res.* **1999**, *32*, 257.

(21)   Sakamoto, A.; Furukawa, Y.; Tasumi, M. *J. Phys. Chem.* **1994**, *98*, 4635.

(22)   van Hal, P. A.; Beckers, E. H. A.; Peeters, E.; Apperloo, J. J.; Janssen, R. A. J. *Chem. Phys. Lett.* **2000**, *328*, 403.

(23)   Grozema, F. C.; Candeias, L. P.; Swart, M.; van Duijnen, P. T.; Wildeman, J.; Hadziiannou, G.; Siebbeles, L. D. A.; Warman, J. L. *J. Chem. Phys.* **2002**, *117*, 11366.

(24)   Cornil, J.; Beljonne, D.; Bredas, J. L. *J. Chem. Phys.* **1995**, *103*, 834.

(25)   Hirata, S.; Head-Gordon, M.; Szczepanski, J.; Vala, M. *J. Phys. Chem. A* **2003**, *107*, 4940.

(26)   Hirata, S.; Lee, T. J.; Head-Gordon, M. *J. Chem. Phys.* **1999**, *111*, 8904.

(27)   Hilberer, A.; Hutten, P. F. v.; Wildeman, J.; Hadziioannou, G. *Macromol. Chem. Phys.* **1997**, *198*, 2211.

(28)   Tabata, Y. *Pulse Radiolysis*; CRC Press: Boca Raton, 1991.

(29)   Tabata, Y.; Ito, Y.; Tagawa, S. *Handbook of Radiation Chemistry*; CRC Press: Boca Raton, 1991.

(30) Buxton, G. V.; Stuart, C. R. *J. Chem. Soc., Faraday Trans.* **1995**, *91*, 279.

(31) Te Velde, G.; Bickelhaupt, F. M.; Baerends, E. J.; Guerra, C. F.; van Gisbergen, S. J. A.; Snijders, J. G.; Ziegler, T. *J. Comput. Chem.* **2001**, *22*, 931.

(32) Vosko, S. H.; Wilk, L.; Nusair, M. *Can. J. Phys.* **1980**, *58*, 1200.

(33) Jensen, F. *Introduction to Computational Chemistry*; John Wiley & Sons Ltd.: Chichester, 1999.

(34) Becke, A. D. *Phys. Rev. A* **1988**, *38*, 3098.

(35) Perdew, J. P. *Phys. Rev. B* **1986**, *33*, 8800.

(36) Runge, E.; Gross, E. K. U. *Phys. Rev. Lett.* **1984**, *52*, 997.

(37) Petersilka, M.; Gossmann, U. J.; Gross, E. K. U. *Phys. Rev. Lett.* **1996**, *76*, 1212.

(38) Kong, J.; White, C. A.; Krylov, A. I.; Sherrill, D.; Adamson, R. D.; Furlani, T. R.; Lee, M. S.; Lee, A. M.; Gwaltney, S. R.; Adams, T. R.; Ochsenfeld, C.; Gilbert, A. T. B.; Kedziora, G. S.; Rassolov, V. A.; Maurice, D. R.; Nair, N.; Shao, Y.; Besley, N. A.; Maslen, P. E.; Korambath, J. P.; Baker, J.; Byrd, E. F. C.; van Voorhis, T.; Oumi, M.; Hirata, S.; Hsu, C.; Ishikawa, N.; Florian, J.; Warshel, A.; Johnson, B. G.; Gill, P. M. W.; Head-Gordon, M.; Pople, J. A. *J. Comput. Chem.* **2000**, *21*, 1532.

(39) Dunning, T. H. *J. Chem. Phys.* **1989**, *90*, 1007.

(40) Lee, C.; Yang, W.; Parr, R. G. *Phys. Rev. B* **1988**, *37*, 785.

(41) Stephens, P. J.; Devlin, F. J.; Chabalowski, C. F.; Frisch, M. J. *J. Phys. Chem.* **1994**, *98*, 11623.

(42) Cooper, R.; Thomas, J. K. *J. Chem. Phys.* **1968**, *48*, 5097.

(43) Schmidt, W. F.; Allen, A. O. *J. Phys. Chem.* **1968**, *72*, 3730.

(44) Gee, N.; Freeman, G. R. *Can. J. Chem.* **1992**, *70*, 1618.

(45) Grozema, F. C.; Hoofman, R. J. O. M.; Candeias, L. P.; de Haas, M. P.; Warman, J. M.; Siebbeles, L. D. A. *J. Phys. Chem. A* **2003**, *107*, 5976.

(46) Gorman, A. A.; Lovering, G.; Rodgers, M. A. J. *J. Am. Chem. Soc.* **1978**, *100*, 4527.

(47) Candeias, L. P.; Wildeman, J.; Hadziioannou, G.; Warman, J. M. *J. Phys. Chem. B* **2000**, *104*, 8366.

(48) Kaiser, E. T.; Kevan, L. *Radical Ions*; Wiley-Interscience: New-York, 1968.

(49) Burrows, H. D.; Greatorex, D.; Kemp, T. J. *J. Phys. Chem.* **1972**, *76*, 20.

(50) Farhataziz, I.; Rodgers, M. A. J. *Radiation Chemistry. Principles and Applications*; VCH Publishers, Inc., 1987.

(51) Moro, G.; Scalmani, G.; Cosentino, U.; Pitea, D. *Synth. Met.* **1998**, *92*, 69.

(52) Brocks, G. *Synth. Met.* **1999**, *102*, 914.

(53) Moro, G.; Scalmani, G.; Cosentino, U.; Pitea, D. *Synth. Met.* **2000**, *108*, 165.

(54) Geskin, V. M.; Dkhissi, A.; Bredas, J. L. *Int. J. Quant. Chem.* **2003**, *91*, 350.

(55) Cornil, J.; Belijonne, D.; Bredas, J. L. *J. Chem. Phys.* **1995**, *103*, 842.

(56) Van Haare, J. A. E. H.; Havinga, E. E.; van Dongen, J. L. J.; Janssen, R. A. J.; Cornil, J.; Bredas, J. L. *Chem. Eur. J.* **1998**, *4*, 1509.

(57) Baerends, J.; Gritsenko, O. V. *J. Phys. Chem. A* **1997**, *101*, 5383.

Chapter 5

Optical Properties and Delocalization of Excess Negative Charges on Oligo(Phenylenevinylene)s[*]

A Quantum Chemical Study

A quantum chemical study of the electronic structure of negatively charged phenylenevinylene (PV) oligomers and methoxy-substituted derivatives is presented. The geometries of the PV oligomers were optimized using density functional theory (DFT). The geometry deformations are found to be delocalized along the entire oligomer chain without indication of polaron formation. The optical absorption spectra of the negatively charged PVs were calculated using both time-dependent density functional theory (TDDFT) and the singly excited configuration interaction method with an intermediate neglect of differential overlap reference wave function (INDO/s-CIS). The available experimental optical absorption energies are reproduced by the calculations. Introduction of methoxy substituents reduces the transition energies, while this does not have a strong effect on the charge distribution along the chain. DFT calculations yield a more delocalized excess negative charge than that of INDO/s-CIS calculations.

5.1 Introduction

Conjugated oligomers and polymers have attracted a great deal of attention for application in light-emitting diodes (LEDs)[1-3], field effect transistors (FETs)[4], solid state lasers,[5] and photovoltaics[6]. This is due to advantages of these materials as compared to inorganic semiconductors, including low weight, ease of processing, flexibility and low fabrication cost. LEDs based on conjugated polymers have been studied extensively since 1990, when Burroughes et al.[7] discovered the electroluminescence of poly(1,4-phenylenevinylene). An important limitation of using PV derivatives in LEDs is the poor charge transport, in particular the imbalance between the hole and electron mobility.[8] In general, electron transport in conjugated polymers is much less efficient than hole transport, probably because electrons are trapped at impurities or defects. However, it has been shown that the mobilities of electrons and holes on isolated poly(2-methoxy-5-[2'-ethyl-hexyloxy]-phenylenevinylene) (MEH-PPV) chains in solution are comparable.[9] Many attempts have been made to improve

---

the electron-hole mobility balance in devices.[10-13] It was shown experimentally that electrons and holes in MEH-PPV have comparable mobilities.[14] Recently, Choulis et al.[15] reported that poly(3-hexylthiophene) is both a good electron and hole transporting material. Because of this, it is of considerable interest to investigate the possibility of building electron transport devices. To achieve this, a detailed insight into the properties of excess electrons is needed.

Important information on the properties of charged species in conjugated molecules can be obtained from optical absorption spectroscopy. Only a few experiments have been reported concerning the radical anions of conjugated oligomers and polymers. Schenck et al.[16] reported UV/vis/near-IR measurements on anionic, *tert*-butyl-substituted PVs, having two to six phenyl rings. Deussen et al.[17] measured the absorption spectra of chemically reduced unsubstituted PVs. Optical absorption spectra of excess negative charge carriers on MEH-PPV and other conjugated polymers in tetrahydrofuran solutions have been published.[18,19]

PVn

PVn(n+1 da)

PVn(n/2 da)
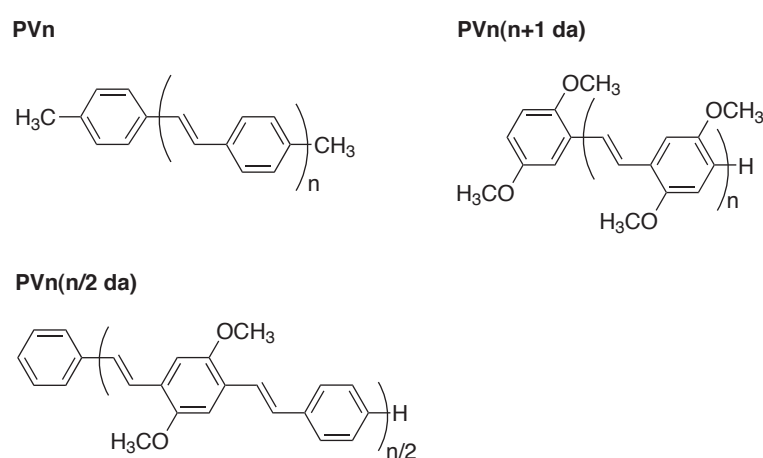
Figure 5.1: PV oligomer structures (n is the number of phenylenevinylene units).

Quantum chemical calculations provide valuable information about the electronic properties of oligomers. Usually, the electronic properties of a series of oligomers with increasing chain length are studied. Such calculations have been performed for neutral or positively charged conjugated oligomers, including phenylenevinylenes,[20-25] thiophenes,[26] thienylenevinylenes[27,28] and diacetylenes[29]. The description of the excited states is a more challenging task than the calculations of the ground state. The majority of the calculations performed to describe excited states has been limited to semi-empirical methods. The Hartree-Fock intermediate neglect of differential overlap (INDO) method combined with a single configuration interaction (SCI) (INDO/s-CIS) is the most commonly utilized semi-empirical technique for performing excited-state calculations on large organic systems, such as PV oligomers.[23] Until now, only a few calculations on the negatively charged species have been reported, most likely due to the larger basis set requirement to describe the diffuse orbitals of anions. Ottonelli et al.[29] performed calculations of negatively charged unsubstituted oligodiacetylenes, using the Austin Model 1 (AM1) optimized geometry and the INDO/s-CIS method for obtaining the optical transition energies. Recently, the INDO method was combined with the equation-of-motion coupled-cluster single and double excitations (EOM-

CCSD) method to calculate the optical properties of negatively charged polyenes, oligothiophenes, oligophenylenes and, oligo(phenylenevinylene)s.[24]

Time-dependent density functional theory (TDDFT) provides an alternative for semi-empirical INDO methods. TDDFT can also handle relatively large systems, such as polycyclic aromatic hydrocarbon (PAH) radical ions.[30] However, the applicability of this method to different systems has not been established yet. It has been shown that TDDFT considerably underestimates the transition energies in the spectra of neutral conjugated chains, especially for longer oligomers.[28] In contrast, this problem was not found to occur for doubly charged conjugated chains. Hirata et al.[30] have shown that TDDFT provides an accurate description of the lowest excitation energies of relatively large PAH radical ions.

To gain further insight into the performance of the TDDFT method for extended conjugated systems, we have calculated the optical absorption spectra of unsubstituted and dimethoxy-substituted PV anions with this method. The TDDFT results are compared with those from INDO/s-CIS calculations. The structures of the PV oligomers investigated in the present work are presented in Figure 5.1. With the present study, we also aim to provide information about the spatial extent and distribution of an excess negative charge along oligomer chains. Particular attention is paid to the extent to which the excess electron leads to the formation of a localized lattice distortion; i.e., a polaron. The chain length dependence of the optical absorption energies for the PV oligomers and the effect of the methoxy substitution on the optical spectra are investigated.

The data provided on PV oligomers are relevant to polymers, since conjugation breaks and conformational disorder in the latter cause the effective conjugation length to be limited. Theoretical knowledge about optical spectra of excess electrons is useful for the interpretation of experiments in which excess charge carriers are detected optically, for instance in optical pump-probe experiments.[31]

5.2 Computational methodology

The geometries of the negatively charged PV oligomers were optimized using the Amsterdam Density Functional (ADF) Theory program.[32] The geometry optimizations were performed using the Local Density Approximation (LDA) with exchange and correlation functionals based on Vosko-Wilk-Nusair (VWN) parameterization of electron gas data.[33] The Generalized Gradient Approximation (GGA)[34] corrections by Becke[35] (exchange) and Perdew[36] (correlation) were included. For optimization of the geometries, a triple zeta plus double polarization (TZ2P) basis set was used. The geometries were restricted to C_{2h} symmetry.

The electronic absorption spectra of the negatively charged PVs were calculated with Time-Dependent Density Functional Theory (TDDFT),[37,38] as implemented in the Q-Chem program.[39] The excitation energies were computed using a correlation consistent[40] polarized Valence Double Zeta (cc-pVDZ) basis set. The Becke (exchange) and the Lee-Yang-Parr (correlation)[41] functional (BLYP) or the Becke3 (exchange) and the Lee-Yang-Parr (correlation) hybrid functional (B3LYP)[42] were used.

The electronic absorption spectra of the negatively charged PVs were also calculated using the semi-empirical Hartree-Fock intermediate neglect of differential overlap (INDO)[43] method combined with singly excited configuration interaction (CIS)[44,45] as implemented in the ZINDO package.[46] The Coulomb repulsion terms were expressed according to Mataga-Nishimoto potential.[47] The application of this potential to the INDO Hamiltonian is known as INDO/s.[48] Electron correlation effects were included by CIS, in which the excited states are expressed as a linear combination of Slater determinants generated by promoting one electron from an occupied orbital to an unoccupied orbital. In the CIS calculations, all configurations generated by excitation from the 40 highest occupied to the 40 lowest unoccupied orbital were included. The reference determinant in INDO/s-CIS method was a restricted open-shell Hartree-Fock (ROHF) wave function.

5.3 Results and discussion

Three different series of PV oligomers were studied. The first series, PVn, consists of phenylenevinylene oligomers para-substituted with methyl groups on the first and last phenyl ring (see Figure 5.1). The experimental optical absorption spectra of the PVn anions up to n=6 are available in the literature.[16] The experimental and calculated transition energies are presented in Tables 5.1 and 5.2. The second series, PVn(n+1 da), contains two methoxy substituents on each phenyl ring. The calculated electronic transitions for PVn(n+1 da) radical anions are given in Tables 5.3 and 5.4, together with the composition of the excited states. The third series, PVn(n/2 da), has two methoxy substituents on every second phenyl ring. Data for the PVn(n/2 da) radical anions are listed in Tables 5.5 and 5.6. The results from the TDDFT calculations are discussed and compared with INDO/s-CIS results and with the available experimental data below.
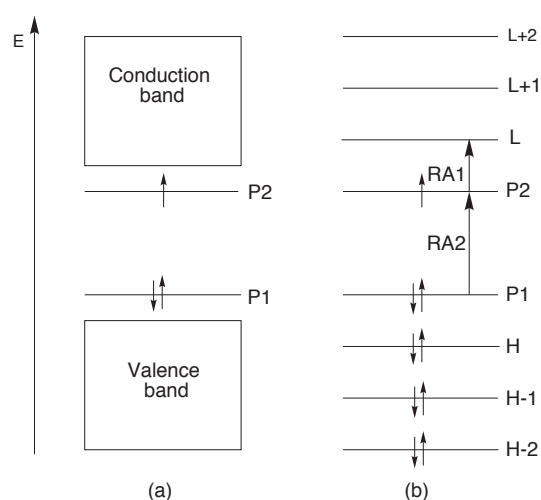
Figure 5.2: (a) Band structure model and (b) radical anion molecular orbital model for phenylenevinylene oligomers.

The absorption spectra of radical ions of conjugated polymers are generally explained in terms of the so-called "one electron band structure model".[49,50] According to this model, the

presence of a singly charged defect leads to the formation of two localized electronic levels in the gap between the valence band and the conduction band, the so-called polaron levels, P1 and P2 (Figure 5.2(a)). In a negatively charged system, P1 is doubly occupied while P2 is singly occupied. Note that P2 represents the highest occupied molecular orbital (HOMO) of the anion, while the lowest unoccupied molecular orbital (LUMO) of the anion is indicated as L. Although this model is not directly applicable to oligomers, which have a finite length and discrete energy levels, the above-mentioned nomenclature, used in the literature, will be adopted in the present study. The molecular orbital model for radical anions of oligomers is shown schematically in Figure 5.2(b).

5.3.1 PVn radical anions

The geometries of the negatively charged unsubstituted PV oligomers were optimized as described in section 5.2. The geometry deformations, as obtained from DFT calculations, were found to be evenly spread over the entire chain, which indicates that, according to DFT, no self-localized polaron is formed.
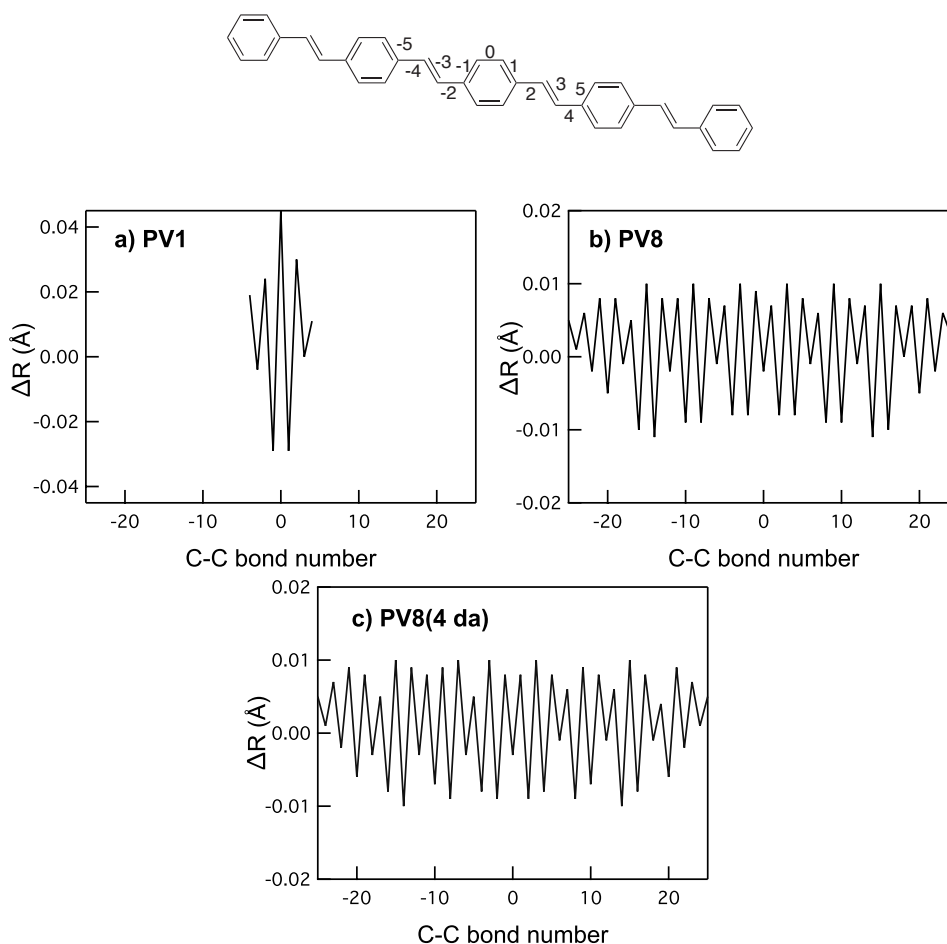
Figure 5.3: Changes in C-C bond length due to adding an electron as calculated with DFT. (The numbering of the bonds is indicated in the chemical structure.) (a) PV1, (b) PV8, and (c) PV8(4 da).

This is analogous to the DFT results for positively charged PVs.[21] Recently, Lynge et al.[25] showed that the density-functional-based tight-binding (DFTB) approach predicts no polaron formation in anions or cations of PV oligomers. The changes in C-C bond length due to adding an electron, as calculated with the DFT method, are shown in Figure 5.3. The maximum change in C-C bond length was found to be ~0.04 Å for PV1. The C-C bond changes become smaller with increasing chain length, *cf.* Figures 5.3(a) and 5.3(b). Similar results were found by DFT calculations on PV radical cations.[21] In contrast with the present findings, Ye et. al[24] showed that for an AM1 optimized geometry, there is a significant modification in the conformation of the PV chain when an electron is added. In this case, the lattice distortions are mostly located around the center of the chain, indicating the formation of a self-localized polaron. These large differences between DFT and Hartree-Fock results were observed previously for radical cations on phenylenevinylenes and oligothiophenes.[21,51] The differences between HF and DFT geometry deformations are also reflected in the charge distribution, which is discussed in section 5.3.4.

Table 5.1: TDDFT transition energies (ΔE in eV), oscillator strengths (f), and composition of excited states for radical anions of PVn oligomers. Only transitions with f higher than 0.1 are presented.

Olig.	Band	ΔE^a (exp)	Functional	ΔE (calc)	f	Composition of excited states
PV1	RA1	1.77	BLYP	2.13	0.09^b	$-0.19(P2{\rightarrow}L)+0.84(P2{\rightarrow}L+2)-0.50(P1{\rightarrow}P2)$
	RA2	2.52		3.03	1.02	$-0.23(P2{\rightarrow}L)+0.46(P2{\rightarrow}L+2)+0.83(P1{\rightarrow}P2)$
			B3LYP	2.02	0.08^b	$0.84(P2{\rightarrow}L+2)-0.53(P1{\rightarrow}P2)$
				3.01	0.97	$0.52(P2{\rightarrow}L+2)+0.84(P1{\rightarrow}P2)$
PV2	RA1	1.14	BLYP	1.29	0.23	$0.89(P2{\rightarrow}L)|+0.43(P2{\rightarrow}P2)$
	RA2	2.03		2.30	1.70	$-0.48(P2{\rightarrow}L)+0.88(P1{\rightarrow}P2)$
			B3LYP	1.35	0.37	$0.92(P2{\rightarrow}L)+0.39(P1{\rightarrow}P2)$
				2.37	1.68	$-0.40(P2{\rightarrow}L)+0.88(P1{\rightarrow}P2)$
PV3	RA1	0.85	BLYP	1.00	0.48	$0.95(P2{\rightarrow}L)-0.39(P1{\rightarrow}P2)$
	RA2	1.74		1.91	2.11	$0.43(P2{\rightarrow}L)+0.89(P1{\rightarrow}P2)$
			B3LYP	1.03	0.72	$0.96(P2{\rightarrow}L)-0.32(P1{\rightarrow}P2)$
				2.03	2.07	$0.33(P2{\rightarrow}L)+0.88(P1{\rightarrow}P2)$
PV4	RA1	0.72	BLYP	0.82	0.78	$0.99(P2{\rightarrow}L)-0.32(P1{\rightarrow}P2)$
	RA2	1.64		1.67	2.12	$0.35(P2{\rightarrow}L)+0.88(P1{\rightarrow}P2)-0.31(P2{\rightarrow}L+4)$
			B3LYP	0.83	1.13	$0.98(P2{\rightarrow}L)+0.24(P1{\rightarrow}P2)$
				1.83	2.16	$-0.26(P2{\rightarrow}L)+0.87(P1{\rightarrow}P2)$
PV6	RA1	0.63	BLYP	0.59	1.37	$1.09(P2{\rightarrow}L)$
	RA2	1.56		1.43	2.02	$-0.26(P2{\rightarrow}L)+0.94(P1{\rightarrow}P2)$
			B3LYP	0.58	1.82	$1.04(P2{\rightarrow}L)$
				1.62	1.75	$-0.31(H{\rightarrow}L)+0.76(P1{\rightarrow}P2)$
PV8	RA1		BLYP	0.45	1.80	$1.17(P2{\rightarrow}L)$
	RA2			1.32	1.73	$0.95(P1{\rightarrow}P2)$
			B3LYP	0.43	2.21	$1.10(P2{\rightarrow}L)$
				1.53	1.53	$0.71(P1{\rightarrow}P2)-0.35(H{\rightarrow}L)$

[a] Experimental data were taken from ref. 16
[b] For unsubstituted PV1 the calculated oscillator strength was found to be smaller than 0.1

Tables 5.1 and 5.2 show the TDDFT and INDO/s-CIS transition energies, oscillator strengths, and composition of excited states for unsubstituted PV radical anions. The calculated energies are compared with the experimental data of Schenk et al.[16] The electronic transitions are described in detail below in terms of the configuration state functions that contribute to the excited state to which the excitation takes place.

Table 5.2: INDO/s-CIS transition energies (ΔE in eV), oscillator strengths (f), and composition of excited states for radical anions of PVn oligomers. Only transitions with f higher than 0.1 are presented.

Oligomer	Band	ΔE^a (exp)	ΔE (calc)	f	Composition of excited states
PV1	RA1	1.77	1.34	0.11	$0.84(P2\rightarrow L)$
	RA2	2.52	2.03	0.58	$0.79(P1\rightarrow P2)+0.38(P2\rightarrow L)$
PV2	RA1	1.14	0.89	0.28	$0.89(P2\rightarrow L)$
	RA2	2.03	1.65	0.65	$0.74(P1\rightarrow P2)$
PV3	RA1	0.85	0.73	0.40	$0.84(P2\rightarrow L)$
	RA2	1.74	1.48	0.87	$0.71(P1\rightarrow P2)$
PV4	RA1	0.72	0.61	0.57	$0.85(P2\rightarrow L)+0.32(P2\rightarrow L+2)$
	RA2	1.64	1.36	0.55	$0.57(P1\rightarrow P2)+0.34(L-1\rightarrow H)$
	RA3		1.55	0.31	$-0.51(P1\rightarrow P2)-0.52(P2\rightarrow L+2)$
PV6	RA1	0.63	0.53	0.81	$-0.74(P2\rightarrow L)-0.52(P2\rightarrow L+1)$
	RA2	1.56	1.48	1.02	$0.37(P2\rightarrow L)+0.66(P1\rightarrow P2)$
PV8	RA1		0.50	0.93	$-0.56(P2\rightarrow L)-0.63(P2\rightarrow L+2)-0.36(P2\rightarrow L+4)$
	RA2		1.43	0.65	$0..43(P1\rightarrow P2)+0.39(P2\rightarrow L)$
	RA3		1.70	0.46	$-0.46(P2\rightarrow L+2)+0.57(P1\rightarrow P2)$

[a] Experimental data were taken from ref. 16

As Table 5.1 shows, both experimental and TDDFT data exhibit two allowed transitions, RA1 and RA2. The INDO/s-CIS calculations predict two allowed transitions for the shorter PVn anions (n=1-3), while for some of the longer chains (n=4-8) a third allowed transition appears at higher energy, denoted RA3 in Table 5.2. For the PV4 and PV5 anions, a shoulder towards the high energy side of the RA2 band can be distinguished in the experimental spectra of Schenk et al.[16] According to the INDO/s-CIS calculations, this shoulder could be due to the RA3 transition. Note that this shoulder has not been assigned to a separate electronic transition by Schenk et al.

For the shortest oligomer PV1, both theoretical methods do not reproduce accurately the measured RA1 and RA2 transition energies. According to the TDDFT results, the RA1 transition is very weak (see the oscillator strength in Table 5.1) and is shifted by ~0.3 eV to higher energy as compared with the experimental value. The RA1 transition is dominated by an excitation of an electron from the singly occupied molecular orbital, P2, to the third unoccupied molecular orbital, L+2. (This excited-state configuration is denoted as P2→L+2.) In contrast, the RA1 transition of the PV1 anion, as calculated with the INDO/s-CIS method, is lower in energy than the experimental value, see Table 5.2. In addition, according to the INDO/s-CIS method, the RA1 transition is mainly due to excitation of an electron from the

singly occupied molecular orbital, P2 to the lowest unoccupied molecular orbital, L. The second transition, RA2, has higher oscillator strength and corresponds according to both methods, mainly to excitation from the highest doubly occupied molecular orbital, P1, to the singly occupied molecular orbital, P2. This configuration is indicated as P1→P2 in Tables 5.1 and 5.2.

For the third transition (RA3), the excited state contains excitations involving higher-lying orbitals, such as P2→L+2, P2→L+1, and P2→L+4.

In Figure 5.4, the chain length dependence of the radical anion transition energies RA1 and RA2 is presented. The general observation is that all transition energies shift to lower values with increasing chain length, which can be understood in terms of increasing spatial delocalization of the charge. Since the TDDFT results obtained using BLYP and B3LYP functionals are similar (see Table 5.1), only the values calculated with the BLYP functional are shown in Figure 5.4. For short PVn oligomers with n=1-4, the TDDFT transition energies are higher than the INDO/s-CIS transition energies. The experimental energies are between the results obtained by the two different theoretical methods. The agreement between the theoretical and experimental data improves considerably from PV1 to PV6. For longer PVn oligomers with n>4, the RA1 and RA2 transitions, as calculated with TDDFT, have a lower energy than obtained with the INDO/s-CIS method.
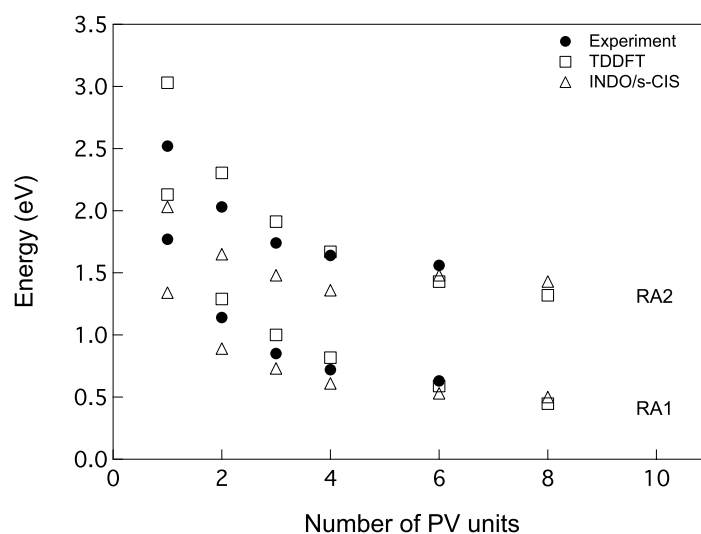
Figure 5.4: Chain length dependence of the transition energies for PVn anions.

The present INDO/s-CIS absorption spectra are similar to the calculated INDO/EOM-CCSD spectra[24] of PV anions. In general, we can conclude that both the TDDFT and INDO/s-CIS methods give a reasonable description of the excited states of unsubstituted PV anions.

5.3.2 PVn(n+1) radical anions

In Tables 5.3 and 5.4 the calculated transition energies (ΔE) and oscillator strengths (f) for radical anions of PVn(n+1 da) oligomers are presented. The introduction of two methoxy

substituents on each phenyl ring reduces the transition energies (*cf.* Tables 5.1-5.4). The lowest energy band (RA1) is dominated by the P2→L transition in all cases, as was also observed for the PVn radical anions, with the exception of the RA1 transition of the PV1 oligomer calculated with TDDFT (Table 5.1). The second energy band (RA2) is mainly due to the P1→P2 excitation. The only exception is the PV2(3 da) anion, for which TDDFT with BLYP as functional predicts a coefficient of 0.55 for the P1→P2 transition, while the dominant one (with coefficient 0.78) is P2→L+2. A third absorption band (RA3) is predicted by TDDFT even for the shortest oligomer. This is a mixture of configurations, including P2→L+2, P1→P2, H→L, and P1→L+1. The transition energies obtained with the INDO/s-CIS method are somewhat lower than those obtained by TDDFT (Figure 5.5), especially for the short chains. However, both methods give the same trend in the excitation energies, as was the case for the unsubstituted PVn.

Table 5.3: TDDFT transition energies (ΔE in eV), oscillator strengths (f), and composition of excited states for radical anions of PVn(n+1 da) oligomers. Only transitions with f higher than 0.1 are presented.

Oligomer	Band	Functional	ΔE	f	Composition of excited states
PV2(3 da)	RA1	BLYP	1.19	0.18	0.88(P2→L)-0.49(P1→P2)
	RA2		1.99	0.47	-0.31(P2→L)+0.78(P2→L+2)-0.55(P1→P2)
	RA3		2.11	1.13	0.62(P2→L+2)+0.66(P1→P2)
		B3LYP	1.27	0.32	0.91(P2→L)-0.42(P1→P2)
			2.16	1.53	0.42(P2→L)+0.86(P1→P2)
PV3(4 da)	RA1	BLYP	0.93	0.29	0.89(P2→L)-0.48(P1→P2)
	RA2		1.69	2.24	0.52(P2→L)+0.86(P1→P2)
	RA3		2.69	0.12	0.48(H→L)+0.56(P2→L+6)+0.49(H→L)
		B3LYP	0.99	0.54	0.92(P2→L)-0.39(P1→P2)
			1.81	2.25	0.39(P2→L)+0.88(P1→P2)
PV4(5 da)	RA1	BLYP	0.76	0.50	0.93(P2→L)-0.44(P1→P2)
	RA2		1.46	2.63	-0.48(P2→L)-0.88(P1→P2)
	RA3		2.26	0.44	0.49(H→L)-0.48(P1→L+1)
		B3LYP	0.81	0.89	0.96(P2→L)-0.32(P1→P2)
			1.59	2.58	0.34(P2→L)+0.88(P1→P2)
			2.62	0.14	0.52(H→L)-0.53(P1→L+1)
PV5(6 da)	RA1	BLYP	0.65	0.74	0.97(P2→L)+0.39(P1→P2)
	RA2		1.29	2.69	-0.42(P2→L)+0.88(P1→P2)
	RA3		1.43	0.18	0.91(P2→L+2)+0.23(P1→P2)
		B3LYP	0.67	1.27	0.98(P2→L)+0.26(P1→P2)
			1.45	2.67	0.86(P1→P2)
			2.30	0.33	0.54(H→L)-0.55(P1→L+1)

5.3.3 PVn(n/2 da) radical anions

Introduction of methoxy substituents was not found to change the calculated spatial extent of the charge on the oligomer chain, as compared to the unsubstituted oligomer. This is obvious

from Figures 5.3(b) and 5.3(c), where the changes in C-C bond lengths for PV8 and PV8(4 da) are compared. Similar results were found for the other oligomers of the series.

Table 5.4: INDO/s-CIS transition energies (ΔE in eV), oscillator strengths (f), and composition of excited states for radical anions of PVn oligomers. Only transitions with f higher than 0.1 are presented.

Oligomer	Band	ΔE	f	Composition of excited states
PV2(3 da)	RA1	0.88	0.24	0.86(P2→L)
	RA2	1.59	0.63	0.70(P1→P2)
PV3(4 da)	RA1	0.72	0.34	0.82(P2→L)
	RA2	1.38	0.87	0.71(P1→P2)
PV4(5 da)	RA1	0.64	0.51	0.83(P2→L)
	RA2	1.33	0.84	0.63(P1→P2)+0.34(H→L)
	RA3	1.54	0.21	0.45(P1→P2)-0.58(P2→L+2)
PV5(6 da)	RA1	0.59	0.61	0.77(P2→L)+0.40(P2→L+2)
	RA2	1.29	0.70	0.32(P2→L+2)-0.57(P1→P2)+0.35(H→L)
	RA3	1.44	0.62	0.59(P1→P2)+0.35(P2→L+2)

The calculated transition energies (ΔE), oscillator strengths (f), and the composition of excited states for radical anions of PVn(n/2 da) oligomers are listed in Tables 5.5 and 5.6. The TDDFT results are compared with the INDO/s-CIS energies in Figure 5.6. For the shortest oligomer PV2(1 da), both the TDDFT and the INDO/s-CIS methods predict two sub-gap absorption bands. As for the unsubstituted radical anions, the low-energy band (RA1) is dominated by an excitation from the singly occupied molecular orbital, P2, to the lowest unoccupied molecular orbital, L (P2→L).
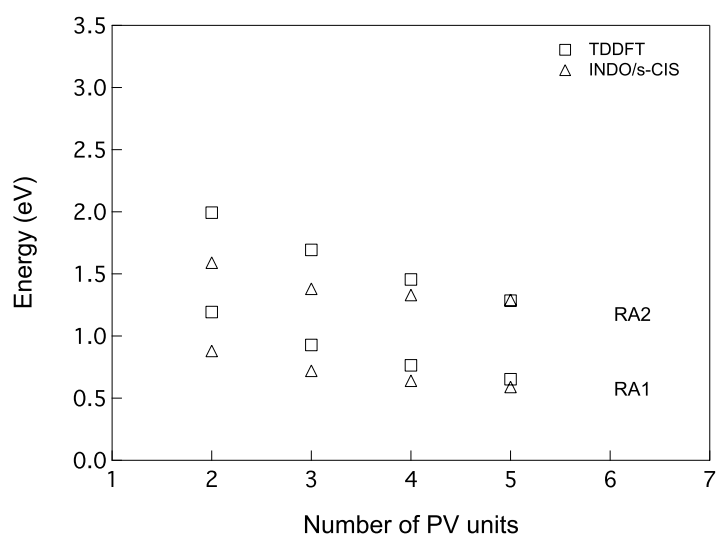

Figure 5.5: Chain length dependence of the transition energies for PVn(n+1 da) anions.

The second transition (RA2) is due to the excitation denoted as P1→P2 and has much higher oscillator strength than the first absorption band (RA1). For PVn(n/2 da) oligomers with n>1, a third allowed transition (RA3) appears in the spectra (Tables 5.5 and 5.6). The excited state is composed of a mixture of excitations involving higher-lying orbitals.

Table 5.5: TDDFT transition energies (ΔE in eV), oscillator strengths (f), and composition of excited states for radical anions of PVn(n/2 da) oligomers. Only transitions with f higher than 0.1 are presented.

Oligomer	Band	Functional	ΔE	f	Composition of excited states
PV2(1 da)	RA1	BLYP	1.28	0.14	0.86(P2→L)
	RA2		2.20	1.67	0.84(P1→P2)
		B3LYP	1.38	0.24	0.88(P2→L)
			2.28	1.77	0.84(P1→P2)
PV4(2 da)	RA1	BLYP	0.80	0.62	0.97(P2→L)
	RA2		1.55	1.63	0.56(P2→L+2)+0.75(P1→P2)
	RA3		1.57	0.78	0.79(P2→L+2)-0.50(P1→P2)
		B3LYP	0.81	0.99	0.97(P2→L)
			1.71	2.32	-0.30(P2→L)+0.87(P1→P2)
			2.31	0.10	0.56(H→L)-0.43(P1→L+1)
PV6(3 da)	RA1	BLYP	0.58	1.21	1.06(P2→L)
	RA2		1.24	0.58	0.85(P2→L+2)+0.44(P1→P2)
	RA3		1.30	1.75	-0.43(P2→L+2)+0.83(P1→P2)
		B3LYP	0.57	1.73	1.03(P2→L)
			1.40	0.16	0.94(P2→L+2)
			1.49	2.01	0.34(H→L)+0.80(P1→P2)
PV8(4 da)	RA1	BLYP	0.45	1.70	1.14(P2→L)
	RA2		1.16	2.00	0.94(P1→P2)
		B3LYP	0.43	2.23	1.09(P2→L)
PV10(5 da)	RA1	BLYP	0.37	2.20	1.20(P2→L)
		B3LYP	0.35	2.64	1.14(P2→L)

For the shorter oligomers PV2(1 da) and PV4(2 da), the RA1 and RA2 transition energies, as calculated using TDDFT, are considerably higher than the INDO/s-CIS energies (see Figure 5.6). The TDDFT transition energies of the PV6(3 da) anion are similar to the INDO/s-CIS energies. For longer PVn(n/2 da) chains (n>6), the TDDFT transition energies become smaller than the INDO/s-CIS results. Interestingly, the INDO/s-CIS transition energies show deviations from the monotonic decrease with increasing chain length. A strong oscillating behavior of the low-energy band as a function of the length of the oligomer was previously noticed for PV radical cations, using the INDO/s-CIS method.[21] This oscillatory behavior was attributed to the strong charge-localizing effect of the methoxy groups present on some of the phenyl rings. For the anion, this effect of substituents on the excitation energies from INDO/s-CIS calculations is less pronounced than previously found for cation spectra.

Table 5.6: INDO/s-CIS transition energies (ΔE in eV), oscillator strengths (f), and composition of excited states for radical anions of PVn(n/2 da) oligomers. Only transitions with f higher than 0.1 are presented.

Oligomer	Band	ΔE	f	Composition of excited states
PV2(1 da)	RA1	0.95	0.23	0.87(P2→L)
	RA2	1.61	0.68	0.77(P1→P2)
PV4(2 da)	RA1	0.57	0.57	0.87(P2→L)
	RA2	1.32	0.64	-0.33(H→L)+0.65(P1→P2)
	RA3	1.56	0.23	0.41(P1→P2)+0.56(P2→L+2)
PV6(3 da)	RA1	0.57	0.78	0.50(P2→L+2)+0.73(P2→L)
	RA2	1.27	0.14	0.40(P2→L+2)+0.38(P2→L+6)
	RA3	1.44	1.04	0.67(P1→P2)-0.41(P2→L)
PV8(4 da)	RA1	0.47	0.89	0.56(P2→L)-0.66(P2→L+2)
	RA2	1.37	0.94	0.54(P1→P2)+0.42(P2→L+2)
	RA3	1.68	0.25	0.49(P1→P2)-0.33(P2→L)-0.43(P2→L+2)
PV10 (5 da)	RA1	0.54	1.00	0.39(P2→L)-0.60(P2→L+2)-0.47(P2→L+4)
	RA2	1.39	0.23	0.36(P2→L)
	RA3	1.53	0.19	0.39(P2→L+2)
	RA4	1.62	0.86	0.54(P1→P2)+0.35(P2→L+2)

For the PV10(5 da) oligomer, only the first transition could be calculated with the TDDFT method due to the limited computer memory available.
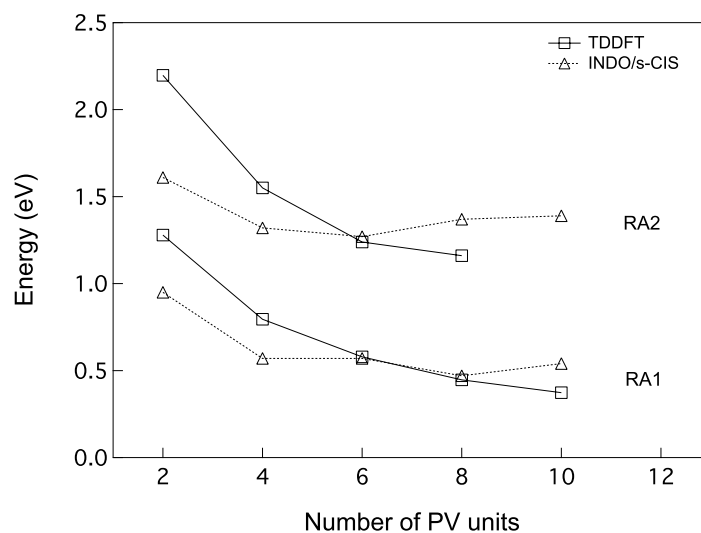

Figure 5.6: Chain length dependence of the transition energies for PVn(n/2 da) anions.

5.3.4. Charge distribution in PV radical anions

Information on the charge distribution along the oligomer chain is useful to gain insight into the occurence of polaronic effects, which influence the mechanism of charge transport in the

materials investigated. In this paragraph, the charge distribution is discussed, and particular attention is paid to effects of methoxy substituents. The charge distribution was calculated with both the DFT and the INDO/s-CIS methods. The charge distribution was obtained from a Mulliken population analysis performed on the same wave function or charge density in the case of DFT, used to calculate the absorption spectra. The distribution of charge will be discussed in terms of the phenylene (containing six C atoms) and vinylene (containing two C atoms) units. In the neutral molecules, the phenylene units carry some negative charge, while the vinylene units are positively charged. Therefore, the distribution of the excess negative charge was calculated as the difference between the charges of the atoms in the anions and in the neutral molecules.

In Figure 5.7 the DFT charge distribution of an excess negative charge in PV oligomers is compared with the INDO/s-CIS charge distribution. For the shortest unsubstituted radical anion (PV1), the DFT and the INDO/s-CIS results are similar. The phenylene units carry an equal amount of charge, which is higher than the charge on the vinylene units. For longer oligomers, there is a significant difference between the charge distributions obtained by the two methods. As can be seen in the second graph from Figure 5.7, the charge distribution in the PV8 radical anion calculated with DFT suggests that the excess negative charge is delocalized along the chain. According to the INDO/s-CIS calculations, a maximum in the charge distribution is found at the central phenylene unit of the chain, indicating that most of the charge is localized in the middle of the oligomer.
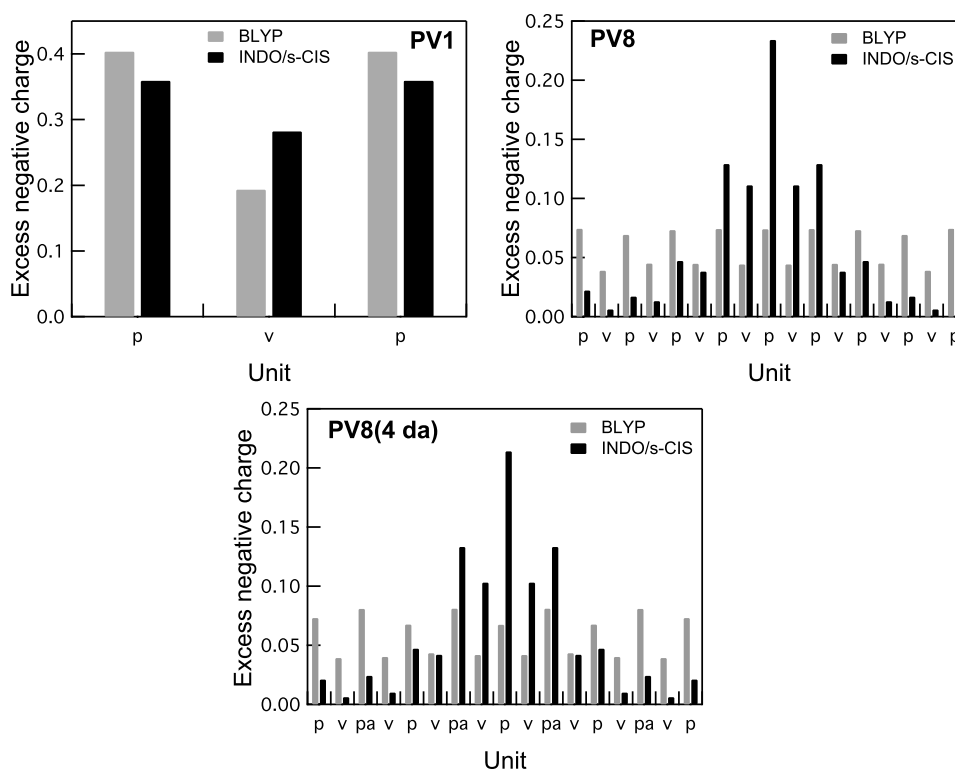

Figure 5.7: Distribution of excess negative charge in PV oligomers (phenylene, vinylene, and dimethoxy-substituted phenylene units are indicated as p, v, and pa, respectively).

A possible explanation for the higher degree of delocalization in DFT is the presence of electron correlation, which is absent in Hartree-Fock-based methods. Electron correlation in general leads to more distributed charge distributions. However, it has also been suggested that the delocalization in DFT is an artifact due to the approximate description of the exchange interaction.[51,52] To gain insight in to the effects of the exchange part of the functional on the charge delocalization, the charge distribution obtained using the hybrid B3LYP functional was analyzed. In the B3LYP functional the exchange is partly described as the (exact) HF exchange. The BLYP and B3LYP charge distributions are compared in Figure 5.8. The difference between the two charge distributions is rather small. Although B3LYP predicts that there is slightly more charge in the middle part of the chain, the charge is still delocalized over the entire chain. From these results, it can be concluded that the effect of improving the description of the exchange interaction does not lead to a significant localization of the charge. It appears that the presence of electron correlation is responsible for the increased delocalization of the charge. However, additional correlated calculations, e.g., using MP2, are called for to clearly establish this effect of correlation on the charge delocalization. It is also of importance to obain more experimental data on the charge delocalization, e.g., by ESR measurements. Recent ESR experiments seem to indicate that radical cations are delocalized over considerable distances in PV oligomers,[53] which seems to favour the DFT results; however, additional work is needed also in this respect.
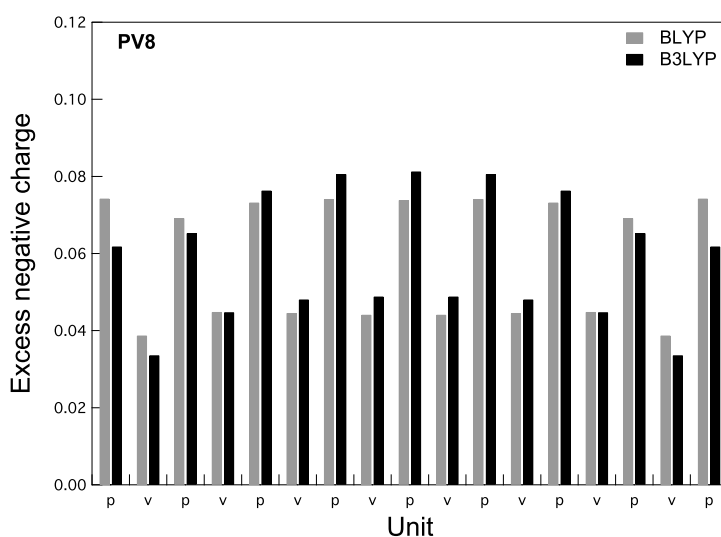
Figure 5.8: Comparison of the distribution of excess negative charge in a PV8 anion, using two different functionals.

When two methoxy substituents are introduced, either on every second phenylene unit (see the PV8(4 da) charge distribution in Figure 5.7) or on all phenylene units, the charge distribution only changes slightly. In contrast, methoxy substituents were found to have a strong effect on the charge distribution in positively charged PV oligomers.[21,22] The latter is due to the significant reduction of the ionization energy of the phenyl rings by addition of a methoxy substituent. (The ionization energy of benzene is 9.24 eV,[54] while the ionization energy of methoxybenzene is 8.25 eV.[55])

5.4 Summary and conclusions

Quantum chemical calculations were performed on anions of unsubstituted and dimethoxy-substituted phenylenevinylene oligomers. The geometries of the negatively charged phenylenevinylene oligomers were optimized using the Amsterdam Density Functional (ADF) Theory program. Geometry deformations were found to be delocalized along the entire oligomer chain without indication of polaron formation.

The electronic absorption spectra of the negatively charged phenylenevinylenes were calculated with both Time-Dependent Density Functional Theory (TDDFT) and the INDO/s-CIS method. It was found that the low energy band in the optical absorption spectra of anions of phenylenevinylene oligomers is dominated by a configuration corresponding to an excitation from the singly occupied molecular orbital to the lowest unoccupied molecular orbital. The second transition in the spectrum corresponds mainly to a transition of an electron from the highest doubly occupied molecular orbital to the singly occupied molecular orbital. For longer oligomers, a third allowed transition appears in the spectra, which corresponds to an excited state consisting of a mixture of configurations involving higher lying orbitals.

For unsubstituted PV anions both DFT and INDO/s-CIS give a reasonable description of the lowest two absorption bands, as compared to experiment. For short chains DFT tends to overestimate the transition energy somewhat, whereas the energies from INDO/s-CIS calculations are lower than the experimental results. For longer chains the differences between the two methods become smaller and the experimental data is well-reproduced by both.

The TDDFT method predicts a monotonous decrease with increasing chain length of the low absorption energy (RA1) of PV anions which are partially dimethoxy substituted. In this case the INDO/s-CIS method shows deviations from the monotonous decrease of the low energy band (RA1) with chain length.

The two methods give different results for longer oligomers when the distribution of charge along the chain is considered. DFT calculations lead to a more delocalized charge distribution than the INDO/s-CIS method. More extensive theoretical and experimental work is called for in order to establish which method gives a more correct description of the charge distribution. The presence of substituents does not strongly affect the distribution of an excess negative charge along the oligomer chain, in contrast to previous findings for excess positive charges. However, methoxy substituents cause a reduction of the transition energies of the phenylenevinylene radical anions.

The agreement between the TDDFT and INDO/s-CIS transition energies and the available experimental data is good. In particular, the performance of the TDDFT method to describe the spectra of PV anions is very promising, in contrast to the performance for neutral systems.

5.5 References

(1)   Kraft, A.; Grimsdale, A. C.; Holmes, A. B. *Angew. Chem. Int. Ed.* **1998**, *37*, 402.

(2)   Friend, R. H.; Gymer, R. W.; Holmes, A. B.; Burroughes, J. H.; Marks, R. N.; Taliani, C.; Bradley, D. D. C.; Dos Santos, D. A.; Bredas, J. L.; Logdlund, M.; Salaneck, W. R. *Nature* **1999**, *397*, 121.

(3)   Cao, Y.; Parker, I. D.; Yu, G.; Zhang, C.; Heeger, A. J. *Nature* **1999**, *397*, 414.

(4)   Reese, C.; Roberts, M.; Ling, M.; Bao, Z. *Mater. Today* **2004**, *7*, 20.

(5)   McGehee, M. D.; Heeger, A. J. *Adv. Mater.* **2000**, *12*, 1655.

(6)   Breeze, A. J.; Schlesinger, Z.; Carter, S. A.; Tillmann, H.; Horhold, H. H. *Sol. Energy Mater. Sol. Cells* **2004**, *83*, 263.

(7)   Burroughes, J. H.; Bradley, D. D. C.; Brown, A. R.; Marks, R. N.; Mackay, K.; Friend, R. H.; Burns, P. L.; Holmes, A. B. *Nature* **1990**, *347*, 539.

(8)   Blom, P. W. M.; Vissenberg, M. C. J. M. *Mater. Sci. Eng.* **2000**, *27*, 53.

(9)   Hoofman, R. O. M.; de Haas, M. P.; Siebbeles, L. D. A.; Warman, J. M. *Nature* **1998**, *392*, 54.

(10)   Nguyen, T.-Q.; Kwong, R. C.; Thompson, M. E.; Schwartz, B. J. *Appl. Phys. Lett.* **2000**, *76*, 2454.

(11)   Blom, P. W. M.; Martens, H. C. F.; Schoo, H. E. M.; Vissenberg, M. C. J. M.; Huiberts, J. N. *Synth. Met.* **2001**, *122*, 95.

(12)   Yu, L.-S.; Chen, S.-A. *Synth. Met.* **2002**, *132*, 81.

(13)   Jang, J. W.; Lee, C. E.; Lee, D. W.; Jin, J.-I. *Solid State Commun.* **2004**, *130*, 265.

(14)   Scott, J. C.; Brock, P. J.; Salem, J. R.; Ramos, S.; Malliaras, G. G.; Carter, S. A.; Bozano, L. *Synth. Met.* **2000**, *111-112*, 289.

(15)   Choulis, S. A.; Kim, Y.; Nelson, J.; Bradley, D. D. C.; Giles, M.; Shkunov, M.; McCulloch, I. *Appl. Phys. Lett.* **2004**, *85*, 1.

(16)   Schenk, R.; Gregorius, H.; Mullen, K. *Adv. Mater.* **1991**, *3*, 492.

(17)   Deussen, M.; Bassler, H. *Chem. Phys.* **1992**, *164*, 247.

(18)   Burrows, H. D.; da G.Miguel, M.; Monkman, A. P.; Horsburgh, L. E.; Hamblett, I.; Navaratnam, S. *J. Chem. Phys.* **2000**, *112*, 3082.

(19)   Burrows, H. D.; da G.Miguel, M.; Monkman, A. P.; Hamblett, I.; Navaratnam, S. *J. Mol. Struct.* **2001**, *563-564*, 41.

(20)   Cornil, J.; Beljonne, D.; Bredas, J. L. *J. Chem. Phys.* **1995**, *103*, 834.

(21)   Grozema, F. C.; Candeias, L. P.; Swart, M.; van Duijnen, P. T.; Wildeman, J.; Hadziiannou, G.; Siebbeles, L. D. A.; Warman, J. L. *J. Chem. Phys.* **2002**, *117*, 11366.

(22)   Fratiloiu, S.; Candeias, L. P.; Grozema, F. C.; Wildeman, J.; Siebbeles, L. D. A. *J. Phys. Chem. B* **2004**, *108*, 19967.

(23)   Tomlinson, A.; Yaron, D. *J. Comp. Chem.* **2003**, *24*, 1782.

(24)   Ye, A.; Shuai, Z.; Kwon, O.; Bredas, J. L.; Beljonne, D. *J. Chem. Phys.* **2004**, *121*, 5567.

(25)   Lynge, T. B.; Pedersen, T. G. *Comput. Mater. Sci.* **2004**, *30*, 212.

(26)   Cornil, J.; Belijonne, D.; Bredas, J. L. *J. Chem. Phys.* **1995**, *103*, 842.

(27)   Krzeminski, C.; Delerue, C.; Allan, G.; Haguet, V.; Stievenard, D. *J. Chem. Phys.* **1999**, *111*, 6643.

(28)   Grozema, F. C.; van Duijnen, P. T.; Siebbeles, L. D. A.; Goossens, A.; de Leeuw, S. W. *J. Phys. Chem. B* **2004**, *108*, 16139.

(29)   Ottonelli, M.; Moggio, I.; Musso, G. F.; Comoretto, D.; Cuniberti, C.; Dellepiane, G. *Synth. Met.* **2001**, *124*, 179.

(30) Hirata, S.; Head-Gordon, M.; Szczepanski, J.; Vala, M. *J. Phys. Chem. A* **2003**, *107*, 4940.

(31) Gadermaier, C.; Lanzani, G. *J. Phys.:Condens. Matter* **2002**, *14*, 9785.

(32) Te Velde, G.; Bickelhaupt, F. M.; Baerends, E. J.; Guerra, C. F.; van Gisbergen, S. J. A.; Snijders, J. G.; Ziegler, T. *J. Comput. Chem.* **2001**, *22*, 931.

(33) Vosko, S. H.; Wilk, L.; Nusair, M. *Can. J. Phys.* **1980**, *58*, 1200.

(34) Jensen, F. *Introduction to Computational Chemistry*; John Wiley & Sons Ltd.: Chichester, 1999.

(35) Becke, A. D. *Phys. Rev. A* **1988**, *38*, 3098.

(36) Perdew, J. P. *Phys. Rev. B* **1986**, *33*, 8800.

(37) Runge, E.; Gross, E. K. U. *Phys. Rev. Lett.* **1984**, *52*, 997.

(38) Petersilka, M.; Gossmann, U. J.; Gross, E. K. U. *Phys. Rev. Lett.* **1996**, *76*, 1212.

(39) Kong, J.; White, C. A.; Krylov, A. I.; Sherrill, D.; Adamson, R. D.; Furlani, T. R.; Lee, M. S.; Lee, A. M.; Gwaltney, S. R.; Adams, T. R.; Ochsenfeld, C.; Gilbert, A. T. B.; Kedziora, G. S.; Rassolov, V. A.; Maurice, D. R.; Nair, N.; Shao, Y.; Besley, N. A.; Maslen, P. E.; Korambath, J. P.; Baker, J.; Byrd, E. F. C.; van Voorhis, T.; Oumi, M.; Hirata, S.; Hsu, C.; Ishikawa, N.; Florian, J.; Warshel, A.; Johnson, B. G.; Gill, P. M. W.; Head-Gordon, M.; Pople, J. A. *J. Comput. Chem.* **2000**, *21*, 1532.

(40) Dunning, T. H. *J. Chem. Phys.* **1989**, *90*, 1007.

(41) Lee, C.; Yang, W.; Parr, R. G. *Phys. Rev. B* **1988**, *37*, 785.

(42) Stephens, P. J.; Devlin, F. J.; Chabalowski, C. F.; Frisch, M. J. *J. Phys. Chem.* **1994**, *98*, 11623.

(43) Rydley, J.; Zerner, M. C. *Theor. Chim. Acta* **1973**, *32*, 111.

(44) Bene, J. E. D.; Ditchfield, R.; Pople, J. A. *J. Chem. Phys.* **1971**, *55*, 2236.

(45) Foresman, J. B.; Head-Gordon, M.; Pople, J. A.; Frisch, M. J. *J. Phys. Chem.* **1992**, *96*, 135.

(46) Zerner, M. C. *ZINDO, A General Semiempirical Program Package*; University of Florida: Gainesville, 1998.

(47) Mataga, N.; Nishimoto, K. *Z. Physik. Chem.* **1957**, *13*, 140.

(48) Zerner, M. C. *Reviews in Computational Chemistry*; VCH: New York, 1991; Vol. 2.

(49) Fesser, K.; Bishop, A. R.; Campbell, D. K. *Phys. Rev. B* **1983**, *27*, 4804.

(50) Furukawa, Y. *Synth. Met.* **1995**, *69*, 629.

(51) Moro, G.; Scalmani, G.; Cosentino, U.; Pitea, D. *Synth. Met.* **2000**, *108*, 165.

(52) Geskin, V. M.; Dkhissi, A.; Bredas, J. L. *Int. J. Quantum Chem.* **2003**, *91*, 350.

(53) Zezin, A. A.; Feldman, V. I.; Warman, J. M.; Wildeman, J.; Hadziioannou, G. *Chem. Phys. Lett.* **2004**, *389*, 108.

(54) Nemeth, G. I.; Selzle, H. L.; Schlag, E. W. *Chem. Phys. Lett.* **1993**, *215*, 151.

(55) Maier, I. P.; Turner, D. W. *J. Chem. Soc., Faraday Trans. 2* **1973**, *69*, 521.

Chapter 6

Two-Dimensional Charge Delocalization in X-Shaped Phenylenevinylene Oligomers[*]

Optical Absorption, Charge Distribution and Charge Transport

A combined experimental and theoretical study of the opto-electronic properties of charged two-dimensional X-shaped phenylenevinylene oligomers (X-mers) is presented. Cations and anions of X-mers were produced by irradiation of solutions with high-energy electron pulses. The optical absorption spectra were measured using time-resolved visible/near-infrared spectroscopy in the range of 500-1600 nm (0.8-2.5 eV). The optical absorption spectra were also calculated using the singly excited configuration interaction method with an intermediate neglect of differential overlap reference wave function (INDO/s-CIS) together with a density functional theory (DFT) optimized geometry. The INDO/s-CIS calculations reproduce the main absorption features of charged X-mers near 1.6-1.7 eV. The charge distributions calculated with DFT show that the excess positive charge is mostly localized on the phenylene units containing methoxy substituents. In contrast, the excess negative charge is delocalized over the entire oligomer. Charge transport calculations indicate that high charge carrier mobilities can be achieved for transport along π-π stacks of X-mers at small mutual twist angles.

6.1 Introduction

Phenylenevinylene (PV) oligomers and polymers are promising candidates for application in plastic electronic devices, such as light-emitting diodes,[1,2] field effect transistors[3,4] and photovoltaics.[5] The advantages of using PV oligomers and polymers in devices include the following: efficient luminescence,[6,7] low molecular weight, flexibility, and low cost. Most PVs are linear, leading to one-dimensional charge delocalization. The charge transport properties of these linear phenylenevinylenes have been found to be highly dependent on the order in the material on a supramolecular scale. Charge carrier mobilities measured in light-emitting diodes based on poly-phenylevinylenes (PPVs) are very low, on the order of 10^{-5} $cm^2V^{-1}s^{-1}$.[8] Much higher mobilities (up to 0.1 $cm^2V^{-1}s^{-1}$) have been obtained from time-resolved microwave conductivity (TRMC) experiments.[9,10] In particular, TRMC experiments

---

[*] This chapter is based on: S. Fratiloiu, K. Senthilkumar, F.C. Grozema, H. Christian-Pandya, Z.I. Niazimbetova, Y.J. Bhandari, M.E. Galvin and L.D.A. Siebbeles, *Chem. Mater.*, **18** (2006), 2118-2129.

by Warman et al.[9] give a direct indication that improved supramolecular order can increase the charge carrier mobility by more than one order of magnitude. It was shown that symmetrically substituted PPVs have a more ordered backbone structure than asymetrically substituted PPVs, which lead to a considerably higher charge carrier mobility in the former. A possible approach to achieve improved molecular ordering is synthesizing oligomers and polymers that are not restricted to linear structures, *e.g.* two-dimensional conjugated molecules. In such molecules the distribution of an excess charge is expected to occur in two dimensions. Different nonlinear conjugated organic molecules have been synthesized for opto-electronic applications: spyro-type molecules,[11] tetrahedral structures,[12] self-organized discotic liquid crystals[13,14] and star-shaped compounds.[15,16] The charge carrier mobility has been measured only for the last two classes of organic molecules mentioned above. In discotic liquid crystals one-dimensional transport of charge can occur through the core with a very high mobility (0.5 $cm^2V^{-1}s^{-1}$ for alkylated hexabenzocoronene compounds).[13] Field-effect transistors based on star-shaped oligothiophenes with truxene cores have been designed with mobilities up to 1.03×10^{-3} $cm^2V^{-1}s^{-1}$.[16]

Recently, a new series of two-dimensional conjugated phenylenevinylene oligomers[17,18] were synthesized, characterized, and evaluated for use in light-emitting diodes. These PV oligomers contain a central phenyl ring, which is substituted with four arms, see Figure 6.1. The chemical structure of the arms can be varied so that these materials are either hole or electron conductors.[17] Due to their X shape, these PV oligomers are called X-mers. It was shown that the position of the arms has a large effect on supramolecular order. Changes in structural symmetry affect the properties of these materials, including absorption and emission spectra, thermal stability, HOMO/LUMO energy levels, tendency to crystallize or to form π-π stacks in films, and device characteristics.[17,18] X-ray diffraction studies performed on powdered samples[17,18] indicate that these X-shaped molecules form π-π stacks with a stacking distance of 3.5 Å. In this way these materials have the potential to provide pathways for charge transport along the stacking direction. The conjugation through the arms and central phenyl ring is maintained, so it is expected that charge delocalization will occur in two dimensions. It was suggested previously[17,18] that the delocalization of the charge in the excited state may occur over all arms.

We present a combined experimental and theoretical study of the electronic structure of charged X-mers with particular attention to the optical absorption spectra of cations and anions of these oligomers. Optical absorption spectra of excess charges provide information about the spatial extent in the oligomer structure. The optical absorption spectra of charged X-mers were measured using pulse radiolysis with time-resolved visible/near-infrared spectroscopy in the range of 500-1600 nm (0.8-2.5 eV). In addition, the optical absorption spectra of charged X-mers were calculated using the singly excited configuration interaction method with an intermediate neglect of differential overlap reference wave function (INDO/s-CIS). Comparison of calculated and measured optical absorption spectra provides insight into the nature of the electronic transitions. Information about the spatial extent and distribution of an excess positive and negative charge along the four arms of the X-mers is obtained from quantum chemical calculations. As noted above, these molecules form π-π stacks, which can provide a pathway for charge transport. Calculations on charge transport along the stacks were carried out with the aim to estimate the mobility of charge carriers in X-mers.

Figure 6.1: Chemical structure of X-shaped phenylenevinylene oligomers.
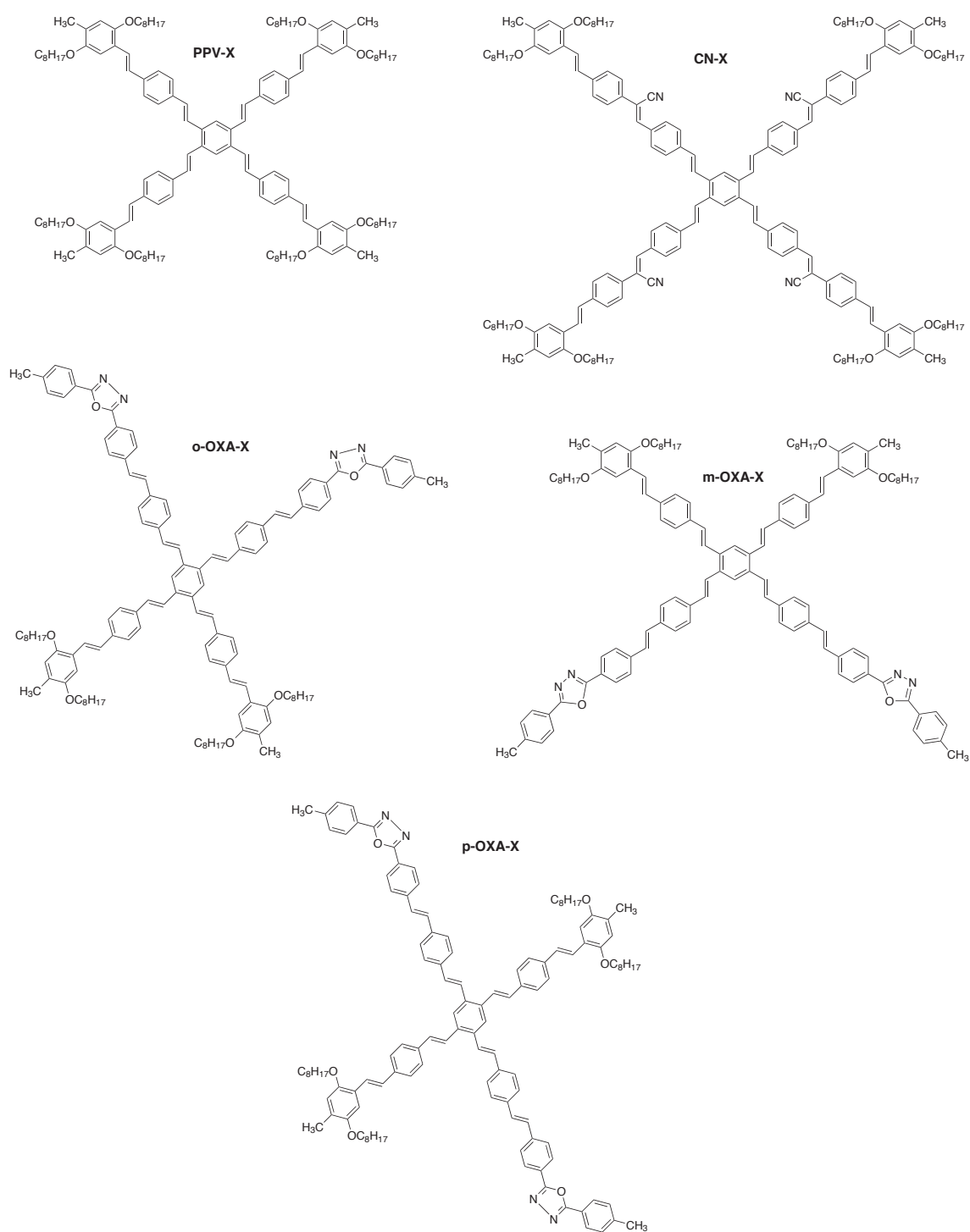
The structures of the X-shaped phenylenevinylene oligomers investigated in this work are presented in Figure 6.1. The PPV-X oligomer contains four phenylenevinylene arms with solubilizing octyloxy substituents. Three oligomers (*o*-OXA-X, *m*-OXA-X and *p*-OXA-X) have two phenylenevinylene arms and two oxadiazole arms, which are placed *ortho*-, *meta*- or

para- with respect to each other. The oxadiazole moieties were introduced in order to improve electron transport, LED efficiency, and photoluminescence stability.[19] It was shown previously that cyano-containing phenylenevinylene polymers are highly efficient electron-transporting materials.[20] Therefore, a cyano-substituted X-mer has also been synthesized and studied.

6.2 Experimental details

The synthesis and characterization of the X-shaped oligomers is described elsewhere.[17,18] The experiments presented in this work were performed using dilute solutions of X-mers (with concentrations in the range of 10^{-5}-10^{-4} M) in UV spectroscopic grade benzene. The solutions were bubbled with benzene-saturated oxygen for 20 minutes. Pulse radiolysis with time-resolved visible/near-infrared (VIS/NIR) spectroscopy[21] was used to generate and detect charges. The X-mer solutions were irradiated with 5 ns pulses of 3 MeV electrons from a Van de Graaff accelerator in order to form charged X-mer molecules. The optical absorption detection of the charged X-mer molecules is essentially the same as used previously for the measurement of the optical absorption spectra of linear positively charged phenylenevinylenes.[21] The detection light source was an Osram XBO high-pressure Xe-lamp (450 W). To avoid photolysis of the solution by the analyzing light, a fast shutter, a chopper, and suitable cut-off filters were placed between the light source and the cell. For detection up to 1000 nm a silicon photodiode was used. Between 1000 nm and 1600 nm this was replaced by a short-wavelength enhanced InGaAs PIN photodiode G5125-10 (Hamamatsu, Japan). Transient changes in the optical absorption spectrum were recorded by a LeCroy LT374L digitizer. The optical absorption spectra of the charged X-mers were obtained by measuring the transient changes in absorbance (ΔA) of the solution at different wavelengths. The spectra are normalized using the radiation dose in the electron pulse, which is proportional to the charge, Q.

6.3 Computational methodology

The geometries of the neutral and charged X-mers were optimized using the Amsterdam Density Functional (ADF) Theory program.[22] The geometry optimizations were performed using the Local Density Approximation (LDA) with exchange and correlation functionals based on Vosko-Wilk-Nusair (VWN) parameterization of electron gas data.[23] The Generalized Gradient Approximation (GGA)[24] corrections by Becke[25] (exchange) and Perdew[26] (correlation) were included. All Density Functional Theory (DFT) calculations were performed with an atomic basis set of Slater-type orbitals (STOs) of double-ζ quality including one set of polarization functions on each atom (DZP basis set in ADF). For open shell systems restricted DFT calculations have been used.

The optical absorption spectra of charged X-mers were calculated using the semi-empirical Hartree-Fock intermediate neglect of differential overlap (INDO)[27] method combined with singly excited configuration interaction (CIS)[28,29] as implemented in the ZINDO package.[30] The Coulomb repulsion terms were expressed according to the Mataga-

Nishimoto potential.[31] The application of this potential to the INDO Hamiltonian is known as INDO/s.[32] Electron correlation effects were included by CIS, in which the excited states are expressed as a linear combination of Slater determinants generated by promoting one electron from an occupied orbital to an unoccupied orbital. In the CIS calculations all configurations generated by excitation from the 40 highest occupied orbitals to the 40 lowest unoccupied orbitals were included. The reference determinant in INDO/s-CIS method was a restricted open shell Hartree-Fock (ROHF) wavefunction.

In the mobility calculations the rate for charge transfer between neighboring X-mers was evaluated according to the Marcus equation[33]

$$\nu = \frac{J_{eff}^2}{\hbar} \sqrt{\frac{\pi}{\lambda k_B T}} e^{\left(-\frac{\lambda}{4 k_B T}\right)} \tag{6.1}$$

where J_{eff} is the effective charge transfer integral, λ is the reorganization energy, and k_B is Boltzmann's constant. The effective charge transfer integral (J_{eff}) is defined as[34]

$$J_{eff} = J - \frac{1}{2} S(\varepsilon_1 + \varepsilon_2) \tag{6.2}$$

where S is the spatial overlap and ε_1 and ε_2 are the site energies (ε_n is the energy of a charge when it is localized on site *n*). The optimized geometry for an individual, neutral X-mer was used to construct a dimer consisting of two X-mers with a stacking distance of 3.5 Å.[17] The charge transfer integrals (J), the spatial overlap integrals, and the site energies were computed for different angles between two stacked X-mers using DFT with the fragment orbital approach[35] as implemented in ADF. In this approach the orbitals of the π-π stacked dimer are expressed as a linear combination of the molecular orbitals of the individual X-mer molecules. This procedure provides a direct and exact calculation of the charge transfer integrals and site energies, as discussed previously.[35] The charge transfer integrals for hole transport are obtained from the highest-occupied molecular orbitals (HOMOs), while those for electron transport are calculated from the lowest unoccupied molecular orbitals (LUMOs). The reorganization energy (λ) for hole transport is given by[36]

$$\lambda = \left[E^+\left(g^0\right) - E^+\left(g^+\right) \right] + \left[E^0\left(g^+\right) - E^0\left(g^0\right) \right]. \tag{6.3}$$

In eq. 6.3 $E^+\left(g^0\right)$ is the energy of the cation with the optimized geometry of the neutral molecule, $E^+\left(g^+\right)$ is the energy of the cation with the optimized cation geometry, etc. The reorganization energy for electron transport is calculated analogously. The energies in eq. 6.3 were calculated using DFT, as implemented in the ADF program. The charge carrier mobility (μ) can be calculated according to

$$\mu = \frac{e}{k_B T} \nu d^2 \tag{6.4}$$

where d is the stacking distance between two X-mers and e is the elementary charge. Eq. 6.4 is valid only for a regular sequence of stacked molecules, which implies that all charge transfer integrals along the stack are equal.

Molecular dynamics simulations were performed using the TINKER program[37] with standard molecular mechanics, MM2 force field parameters.[38] The simulations were performed at a time step of 1 fs and the atomic coordinates in trajectories were saved every 0.1 ps. The dynamics simulations were done up to 1 ns.

6.4 Results and discussion

6.4.1 Optical absorption spectra of charged X-mers

Measurements of the optical absorption spectra of charged X-mers were performed as described in section 6.2. Transient changes in optical absorption observed upon irradiation of an oxygen-saturated solution ($[O_2]$=11.9 mM at 1 atm and 25 $^{\circ}$C) of *p*-OXA-X in benzene at different wavelengths are shown in Figure 6.2. Irradiation of benzene solutions leads to the formation of benzene radical cations ($bz^{\bullet+}$), excited states (bz^*) and excess electrons (e^-)[39-41]

$$bz \rightarrow bz^{\bullet+}, bz^*, e^- \qquad (6.5)$$

The excess electrons generated during irradiation are highly mobile (0.13 $cm^2V^{-1}s^{-1}$)[42] and can react rapidly (<1 ns) with the oxygen molecules (O_2) with a rate constant of 1.5×10^{11} $M^{-1}s^{-1}$,[43] yielding oxygen anions (O_2^-)

$$e^- + O_2 \rightarrow O_2^- \qquad (6.6)$$

In competition with the reaction in eq. 6.6 the excess electrons can also react with *p*-OXA-X according to

$$e^- + p\text{-OXA-X} \rightarrow p\text{-OXA-X}^- \qquad (6.7)$$

The time scale on which the diffusion controlled reactions in eqs. 6.6 and 6.7 occur can be calculated knowing the rate constant and the concentration. The rate constant (k) for a charge transfer reaction controlled by diffusion of the charge can be calculated according to

$$k = 4\pi RD \qquad (6.8)$$

In eq. 6.8 R is the reaction radius and D is the diffusion coefficient of the charge. The diffusion coefficient can be obtained from the charge carrier mobility using the Einstein relation

$$D = \frac{\mu k_B T}{e} \qquad (6.9)$$

Taking the known electron mobility in benzene equal to 0.13 $cm^2V^{-1}s^{-1}$ at room temperature[42] and assuming a typical reaction radius of 1 nm,[44] the rate constant of the reaction of excess

electrons with *p*-OXA-X is estimated to be 2.46×10^{12} M^{-1}s^{-1}. At the concentration of *p*-OXA-X in benzene used in this work (0.057 mM) the reaction of excess electrons with *p*-OXA-X (eq. 6.7) takes place in about 10 ns. Indeed, in the optical absorption transient at 700 nm from Figure 6.2, it can be seen that directly after the pulse *p*-OXA-X anions have already been formed. Note that not all electrons react with the *p*-OXA-X molecules. The time scale on which the reaction from eq. 6.6 occurs is estimated around 0.6 ns for a rate constant of 1.5×10^{11} M^{-1}s^{-1} and a O$_2$ concentration of 11.9 mM. This means that a large fraction of electrons will react with O$_2$. Transient optical absorption at short times is due to the fraction of electrons that does react with *p*-OXA-X. The decay of the *p*-OXA-X anion is attributed to the abstraction of electrons from the *p*-OXA-X anions by O$_2$

$$p\text{-OXA-X}^- + O_2 \rightarrow p\text{-OXA-X} + O_2^- \tag{6.10}$$

The reaction in eq. 6.10 occurs due to the higher electron affinity of O$_2$. Since the ionization potential of *p*-OXA-X will be lower than that of benzene, the benzene radical cations formed upon irradiation will undergo charge transfer to *p*-OXA-X , according to
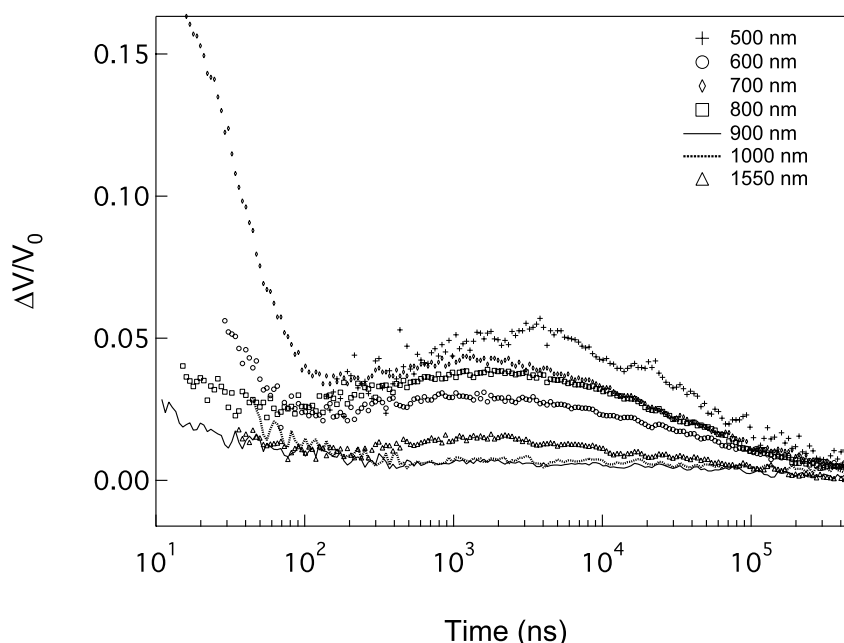
$$bz^{\bullet+} + p\text{-OXA-X} \rightarrow bz + p\text{-OXA-X}^{\bullet+} \tag{6.11}$$

Figure 6.2: Optical absorption transients due to the positive and negative charges on *p*-OXA-X oligomers observed upon irradiation of O$_2$-saturated benzene solutions at different wavelengths (the concentration of the *p*-OXA-X solution was 57 μM). The data during and directly after the electron pulse could not be measured due to Cerenkov radiation, which is present during the pulse and varies with wavelength.

The time scale of formation of *p*-OXA-X$^{\bullet+}$ can be estimated from the rate constant and the concentration of the solution. The hole mobility in benzene is 0.0004 cm^{2}V^{-1}s^{-1} at room temparature.[45] Assuming a reaction radius of 1 nm[44] in eq. 6.7 the rate constant is calculated

to be 7.56×10^9 $M^{-1}s^{-1}$. For the *p*-OXA-X concentration of 0.057 mM, this yields a cation formation time of ~2300 ns. This is in agreement with the rise of the optical absorption transients on a time scale of a few thousands nanoseconds in Figure 6.2. The decay of the optical absorption in Figure 6.2 on a time scale of tens of microseconds is due to the reaction of the *p*-OXA-X radical cations with O_2 anions

$$\text{*p*-OXA-X}^{\bullet+} + O_2^- \rightarrow \text{*p*-OXA-X} + O_2. \qquad (6.12)$$

Due to the fact that the formation of the *p*-OXA-X radical cations takes place at longer times than the formation of the radical anions, we could obtain the optical absorption spectra of radical cations and anions from the same transient absorption data by integrating the change in optical absorption at different time intervals.

Cation spectra of three X-mers were obtained by integrating the optical absorption transients for different wavelengths between 500 and 3000 ns. These spectra are presented in Figure 6.3(a). For the three X-mers investigated the spectra show absorption features at short wavelengths. A distinct absorption peak is observed only for the *p*-OXA-X cation. The maximum of the absorption of the *p*-OXA-X cation is near 750 nm. In addition, there are weak absorption features at longer wavelengths, which are most pronounced for the CN-X cation.
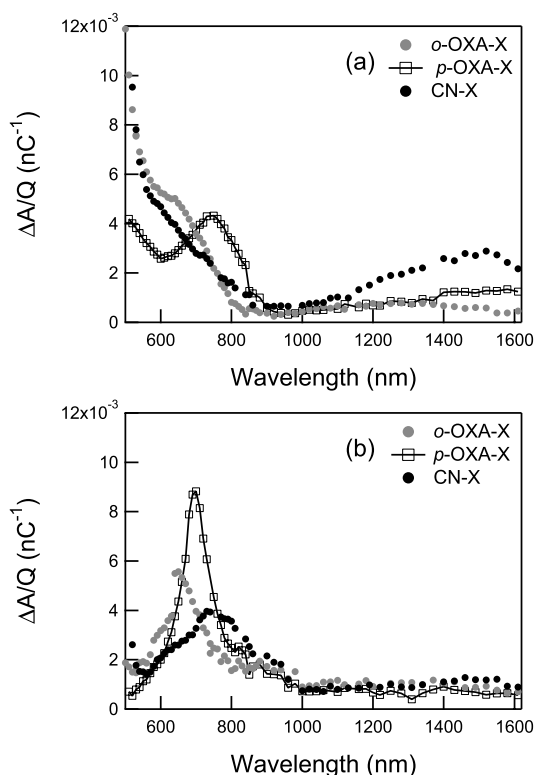

Figure 6.3: Optical absorption spectra of radical cations (a) and anions (b) of three different X-mers obtained by integrating the optical absorption transients between 500 and 3000 ns (for cations) and 10-100 ns (for anions).

In Figure 6.3(b) the optical absorption spectra of X-mer anions obtained by integrating the transient change in absorbance between 10 and 100 ns are shown. The spectra of the X-mer anions exhibit an absorption band at short wavelength. Changing the position of the phenylenevinylene and oxadiazole arms from *ortho-* to *para-* leads to a red shift of 50 nm. The introduction of cyano substituents at the vinylene units of the phenylenevinylene arms induces a further red shift of the optical absorption band.

Similar absorption features were reported for the linear phenylene vinylene radical cations[21] and anions.[46] The optical absorption spectrum of linear dialkoxy-substituted PV radical cations with three phenyl rings (the size of one arm of the X-shaped PVs) exhibits absorption features below 0.6 eV together with two distinguished peaks at 1.52 and 1.71 eV, respectively.[21] These peaks are close to the 750 nm (1.65 eV) absorption of the *p*-OXA-X cation. The optical absorption spectrum of the *tert*-butyl-substituted PV3 anion measured by Schenck et al.[46] shows an absorption peak at 1.74 eV, similar to that found for the *p*-OXA-X anion. The low energy band near 0.85 eV for the linear PV anions was not observed in the case of the X-shaped anions.

The optical absorption spectra of X-mer radical cations and anions were also calculated using the INDO/s-CIS method and a geometry obtained from DFT. This methodology has been applied successfully to linear PV radical cations and anions.[47,48] The octyloxy substituents were replaced by methoxy groups, similar to previous calculations on linear phenylenevinylene radical cations.[47] The INDO/s-CIS calculations predict a large number of allowed transitions with relatively small oscillator strength. The electronic configurations that dominate the allowed transitions of the X-mer radical cations and anions are given in Tables 6.1 and 6.2. The orbital notation in the last column of Tables 6.1 and 6.2 refers to the radical ion molecular orbital model described elsewhere.[21,47,48] In previous work it was found for linear PV radical cations that the lowest transition (RC1) is dominated by excitation of an electron from the highest doubly occupied molecular orbital to the singly occupied molecular orbital (H→P1).[47] The second transition (RC2) of the linear radical cation corresponds mainly to excitation of an electron from the singly occupied molecular orbital to the lowest unoccupied molecular orbital (P1→P2).[47] The data in Table 6.1 show that the lowest energy transition (RC1) of the X-mer radical cation contains a large contribution of an H→P1 excitation, similar to the case for linear PV cations. For all X-mer cations there is a transition (RC3 or RC4 in Table 6.1) dominated by a P1→P2 excitation, which was also found for linear PV radical cations. In addition to transitions mainly due to H→P1 and P1→P2 excitations, transitions involving lower lying orbitals (H-10, H-9, H-8 etc.) are also found for X-mers.

The lowest energy transition of linear PV anions (RA1) was found to be dominated by an excitation from the singly occupied molecular orbital to the lowest unoccupied molecular orbital (P2→L), while the second transition in the spectrum (RA2) corresponds mainly to excitation of an electron from the highest doubly occupied molecular orbital to the singly occupied molecular orbital (P1→P2).[48] According to INDO/s-CIS calculations on negatively charged X-mers, the first two or three transitions are due to excitations of electrons from the singly occupied molecular orbital (P2) to higher-lying orbitals. The electronic transition which has the highest oscillator strength (RA3 or RA4 in Table 6.2) is dominated by

excitation of an electron from the highest doubly occupied molecular orbital to the singly occupied molecular orbital (P1→P2), similar to the case for linear PV anions. Several electronic transitions at higher energy (above 1.8 eV) are present in the calculated optical absorption spectra of X-mer anions. These transitions have small oscillator strength and involve excitations to high-lying orbitals.

Table 6.1: Calculated transition energies (ΔE in eV), calculated oscillator strengths (f), and main CI-expansion coefficients for radical cations of X-mers. Only the transitions with oscillator strength higher than 0.1 are given.

X-mer	Band	ΔE	f	Main CI-expansion coefficients
PPV-X	RC1	0.79	0.55	0.42(H-9→P1)-0.80(H→P1)
	RC2	1.14	0.33	-0.34(H-10→P1)+0.79(H-2→P1)
	RC3	1.64	0.67	-0.37(H-2→P1)+0.66(P1→P2)
	RC4	1.77	0.14	-0.36(H-9→P1)
	RC5	2.02	0.48	-0.42(H-9→P1)-0.50(H→P1)-0.41(P1→L)
o-OXA-X	RC1	0.58	0.14	0.34(H-6→P1)-0.35(H-1→P1)+0.67(H→P1)
	RC2	0.77	0.65	0.34(H-5→P1)+0.65(H-1→P1)+0.36(H→P1)
	RC3	1.05	0.31	0.49(H-4→P1)-0.57(H-2→P1)-0.34(H→P1)
	RC4	1.71	0.52	0.60(P1→P2)
	RC5	1.82	0.23	0.33(P1→L)
	RC6	1.94	0.11	0.44(H-3→P1)-0.43(H-1→P1)
	RC7	2.14	0.11	0.40(P1→P2)
	RC8	2.41	0.37	0.35(H-5→P1)+0.44(P1→P2)
m-OXA-X	RC1	0.82	0.54	0.53(H-4→P1)+0.61(H→P1)
	RC2	1.10	0.40	-0.46(H-3→P1)+0.61(H-2→P1)
	RC3	1.74	0.65	-0.62(P1→P2)
	RC4	1.95	0.38	0.54(H→P1)-0.32(P1→L)
	RC5	2.45	0.28	-0.42(H-4→P1)+0.38(P1→L)
p-OXA-X	RC1	0.65	0.77	-0.79(H→P1)
	RC2	1.18	0.27	-0.39(H-5→P1)-0.33(H-4→P1)-0.63(H-4→P1)
	RC3	1.66	0.75	-0.56(P1→P2)
	RC4	1.87	0.21	no contribution>0.1
	RC5	2.15	0.16	-0.45(H-6→P1)-0.46(H-2→P1)+0.35(P1→P2)
	RC6	2.41	0.17	no contribution>0.1
	RC7	2.48	0.12	0.35(H-12→P1)+0.35(H-4→P1)
CN-X	RC1	0.26	0.68	0.65(H-3→P1)+0.36(H-2→P1)+0.32(H→P1)
	RC2	1.99	0.18	-0.36(P1→P2)
	RC3	2.14	0.19	0.38(P1→P2)
	RC4	2.59	0.19	0.33(P1→P2)-0.37(P1→L)

The optical absorption spectra of charged X-mers have been calculated using a 40×40 set of orbitals, as described in section 6.3. The use of a reduced set of orbitals for calculating the spectra leads to a shift of the transition energies in the INDO/s-CIS spectra. In addition to the calculations using a 40×40 set of orbitals, the spectra of *p*-OXA-X cation was calculated with

a 10×10 set of orbitals. The results show that the low-energy band shift by 0.1 eV towards a higher energy. This shift becomes more pronounced for the higher energy bands (up to 0.4 eV).

Table 6.2: Calculated transition energies (ΔE in eV), calculated oscillator strengths (f), and main CI-expansion coefficients for radical anions of X-mers. Only transitions with oscillator strength higher than 0.1 are given.

X-mer	Band	ΔE	f	Main CI-expansion coefficients
PPV-X	RA1	0.76	0.41	-0.71(P2→L+1)+0.54(P2→L+5)
	RA2	1.11	0.23	-0.75(P2→L+2)-0.36(P2→L+10)
	RA3	1.62	0.69	0.65(P1→P2)+0.39(P2→L+2)
	RA4	1.99	0.49	0.34(H→P2)+0.46(P2→L)+0.32(P2→L+4)
	RA5	2.00	0.17	0.50(P2→L+3)
	RA6	2.83	0.31	-0.32(H→P2)+0.50(P2→L+4)
o-OXA-X	RA1	0.80	0.50	-0.62(P2→L+1)+0.47(P2→L+2)+0.42(P2→L+9)
	RA2	1.08	0.25	-0.45(P2→L)-0.59(P2→L+4)+0.39(P2→L+12)
	RA3	1.69	0.69	0.60(P1→P2)
	RA4	1.87	0.29	0.48(P2→L+1)
	RA5	2.07	0.10	0.47(P2→L+5)-0.40(P2→L+9)
	RA6	2.20	0.16	-0.69(P2→L+2)
	RA7	2.41	0.14	no contribution>0.1
m-OXA-X	RA1	0.60	0.19	0.65(P2→L)-0.48(P2→L+8)
	RA2	0.79	0.30	0.43(P2→L+3)+0.57(P2→L+4)-0.46(P2→L+12)
	RA3	1.04	0.30	0.66(P2→L+1)
	RA4	1.70	0.61	-0.56(P1→P2)
	RA5	1.84	0.23	0.45(P2→L)
	RA6	1.99	0.13	0.33(P1→P2)-0.41(P2→L+5)
	RA7	2.08	0.17	-0.45(P2→L+4)
	RA8	2.46	0.16	no contribution>0.1
	RA9	2.64	0.20	-0.50(P2→L+8)
p-OXA-X	RA1	0.69	0.56	0.70(P2→L)-0.35(P2→L+2)+0.41(P2→L+8)
	RA2	1.13	0.22	0.70(P2→L+4)+0.37(P2→L+12)
	RA3	1.69	0.75	-0.59(P1→P2)
	RA4	1.87	0.21	no contribution>0.1
	RA5	2.03	0.16	-0.34(P1→P2)
	RA6	2.18	0.17	-0.78(P2→L+13)
	RA7	2.39	0.12	-0.32(P2→L+4)
CN-X	RA1	0.61	0.30	-0.61(P2→L)+0.46(P2→L+1)+0.32(P2→L+5)
	RA2	0.64	0.33	0.50(P2→L)+0.45(P2→L+1)-0.35(P2→L+2)
	RA3	0.93	0.39	0.72(P2→L+2)-0.38(P2→L+6)
	RA4	1.75	0.55	-0.61(P1→P2)
	RA5	1.90	0.19	0.38(P2→L+6)
	RA6	2.17	0.13	-0.36(P1→P2)-0.44(P2→L+6)
	RA7	2.62	0.11	0.45(P2→L+23)
	RA8	2.67	0.44	no contribution>0.1

Comparison of the experimental and calculated optical absorption spectra of charged X-mers shows that for both cations and anions the measured high-energy band near 1.6-1.7 eV is reproduced by the INDO/s-CIS calculations. In Figures 6.4(a) and 6.4(b) the experimental and calculated spectra of the *p*-OXA-X cation and anion are superimposed. Indeed, the high-energy band near 1.65 eV is well-reproduced by the INDO/s-CIS calculations. Both experimental and theoretical results show that this band has high oscillator strength. Apart from the high-energy band near 1.65 eV, the INDO/s-CIS calculations predict a large number of allowed transitions, most of them having a small oscillator strength. This large number of electronic transitions predicted by the INDO/s-CIS method was not found experimentally. For energies above 2 eV the measured oscillator strengths of the *p*-OXA-X radical cation are higher than the calculated results. The low energy band of the *p*-OXA-X cation and anion (RC1 and RA1) with relatively large oscillator strength, as predicted by INDO/s-CIS, exceeds the accessible experimental range towards lower energy.
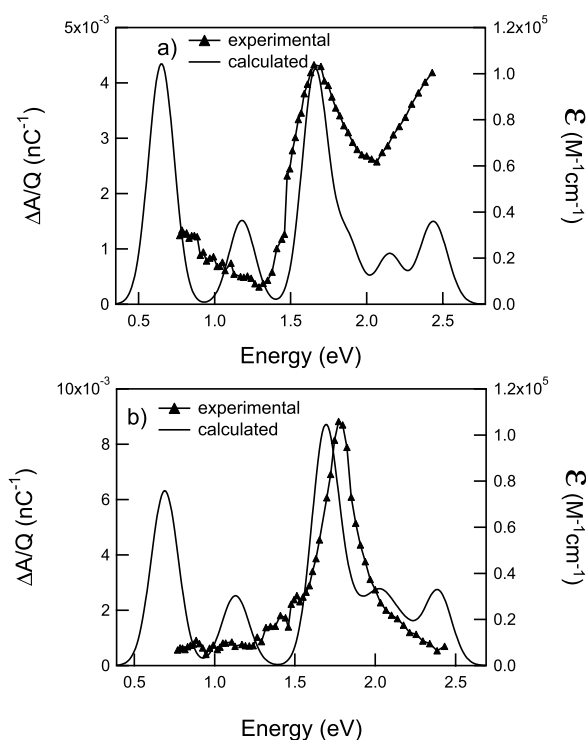

Figure 6.4: Experimental and calculated optical absorption spectra of *p*-OXA-X radical (a) cation and (b) anion. The calculated spectra were simulated using a Gaussian distribution centered at the computed transition energy with an arbitrary width of 0.1 eV and an integrated amplitude equal to the computed oscillator strength.

6.4.2 Charge distribution in X-mers

To investigate the delocalization of charges in the X-shaped oligomers, a Mulliken population analysis was performed using the DFT density. The distribution of an excess charge will be discussed in terms of unsubstituted phenylene units (p), methoxy-substituted phenylene units (mp), oxadiazole units (oa), vinylene units (v) and cyano-substituted vinylene units (cv). The

distribution of an excess charge was calculated as the difference between the charges of the atoms in the charged state and in the neutral molecule. Analysis of the charge distribution of the PPV-X cation in Figure 6.5(a) shows that the unsubstituted phenylene units carry a similar amount of charge. The amount of charge on the vinylene units is smaller than that on the phenylene units. The higher amount of charge on the phenylene units is attributed to the lower ionization potential of these units in comparison with that of the vinylene units. The presence of methoxy substituents on the phenyl rings leads to a further reduction of the ionization potential of these units. As a consequence the charge becomes more localized on the phenylene units containing methoxy substituents. The same features of the DFT charge distribution have been found previously for a series of linear phenylenevinylene tetramers (PV4).[21] Comparison of Figures 6.5(a) and 6.5(b) shows that the distribution of an excess positive charge for PPV-X is similar to that of a negative charge, although the localization of the negative charge on the mp-units is less pronounced.
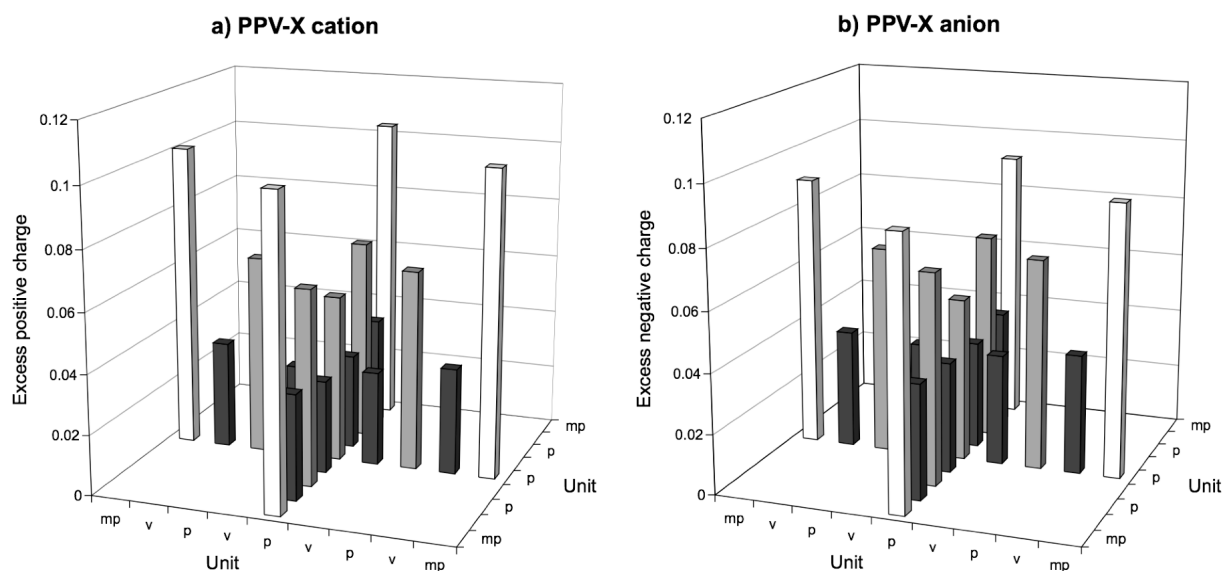

Figure 6.5: DFT distribution of an excess (a) positive and (b) negative charge in PPV-X. Charges on the unsubstituted phenylene units (p) are shown in grey, on the methoxy-substituted phenylene units (mp) in white and on the vinylene units (v) in black.

The distribution of an excess positive and negative charge on PPV-X has been also investigated using the INDO/s-CIS method. The maximum in the charge distribution for the PPV-X cation and anion is located at the central phenyl ring, see Figures 6.6(a) and 6.6(b). It has been previously published that a INDO/s-CIS analysis of the distribution of charge on linear PVs leads to a localization of the charge at the central phenyl ring.[47,48] One explanation for the different charge distributions obtained from INDO/s-CIS and DFT is electron correlation, leading to a more delocalized charge distribution in DFT. It has been also suggested that DFT leads to more delocalized charge distributions because of the approximate description of the exchange interaction.[49,50] However, the comparison of the distribution of an excess negative charge in a linear PV anion using BLYP and B3LYP functionals (in the B3LYP functional the exchange is partly described as the exact Hartree-Fock exchange)

shows that the exchange interaction does not lead to a significant localization of the charge.[48] In summary, it has not been unanimously established which method gives a more accurate description of the charge distribution. Correlated calculations, other than DFT, are required to resolve this issue.
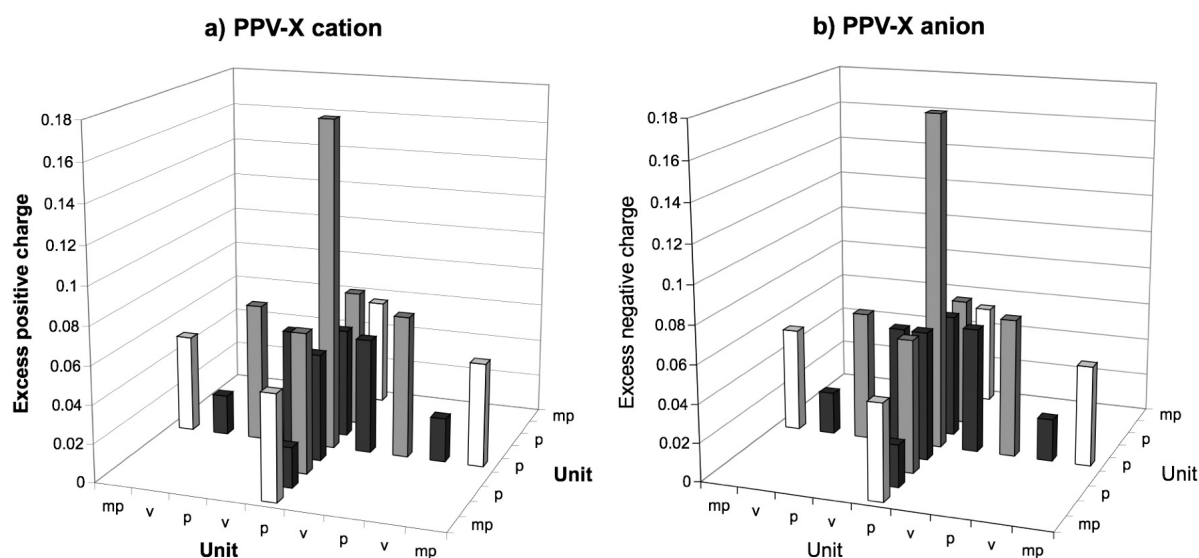

Figure 6.6: INDO/s-CIS distribution of an excess (a) positive and (b) negative charge in PPV-X. Charges on the unsubstituted phenylene units (p) are shown in grey, on the methoxy-substituted phenylene units (mp) in white and on the vinylene units (v) in black.

In Figure 6.7(a) the DFT distribution of an excess positive charge for the *p*-OXA-X oligomer is presented. The excess positive charge of *p*-OXA-X is mostly localized on the phenylene units containing methoxy substituents. The arms containing only phenylene and vinylene units carry a higher amount of charge than the arms containing the oxadiazole unit. Interestingly, the distribution of an excess negative charge is different from that of an excess positive charge. The negative charge is evenly distributed over all arms, see Figure 6.7(b). The excess negative charge does not localize on the oxadiazole units, as might have been expected on basis of the electron-withdrawing nature of the oxadiazole group. Nevertheless, the phenylene units adjacent to the oxadiazole units carry a somewhat higher amount of charge than the other phenylene units. The calculated charge distributions for *o*-OXA-X and *m*-OXA-X were found to be similar to that of *p*-OXA-X.

The introduction of cyano substituents at the vinylene units in CN-X does not have a large influence on the distribution of the excess charge. The excess positive charge is mostly localized on the methoxy-substituted phenylene units (see Figure 6.8(a)), while the distribution of an excess negative charge shows a delocalization over the four arms (see Figure 6.8(b)). For the negatively charged CN-X the amount of charge present on the cyano-substituted vinylene units is higher than that on the unsubstituted ones, reflecting the electron-withdrawing properties of the cyano group.
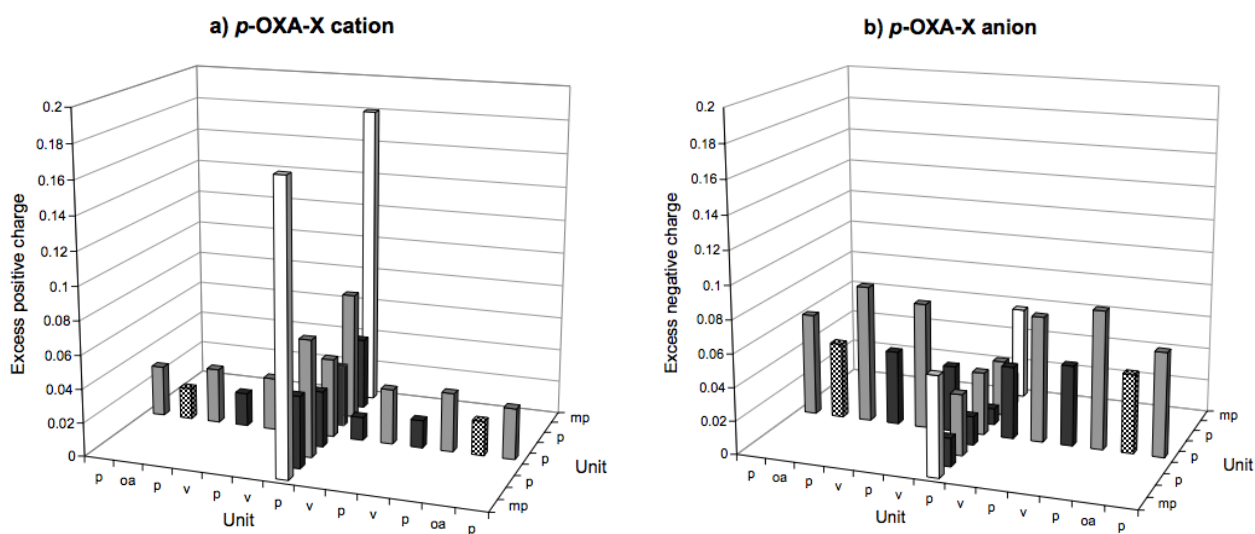
Figure 6.7: DFT distribution of an excess (a) positive and (b) negative charge in
p-OXA-X. Charges on the unsubstituted phenylene units (p) are shown in grey,
on the methoxy-substituted phenylene units (mp) in white, on the vinylene units
(v) in black, and on the oxadiazole (oa) units with the checker board pattern.

In summary, the DFT calculations predict two-dimensional charge delocalization over the X-mer arms, in agreement with indications derived from absorption/emission and cyclic voltammetry measurements.[18]
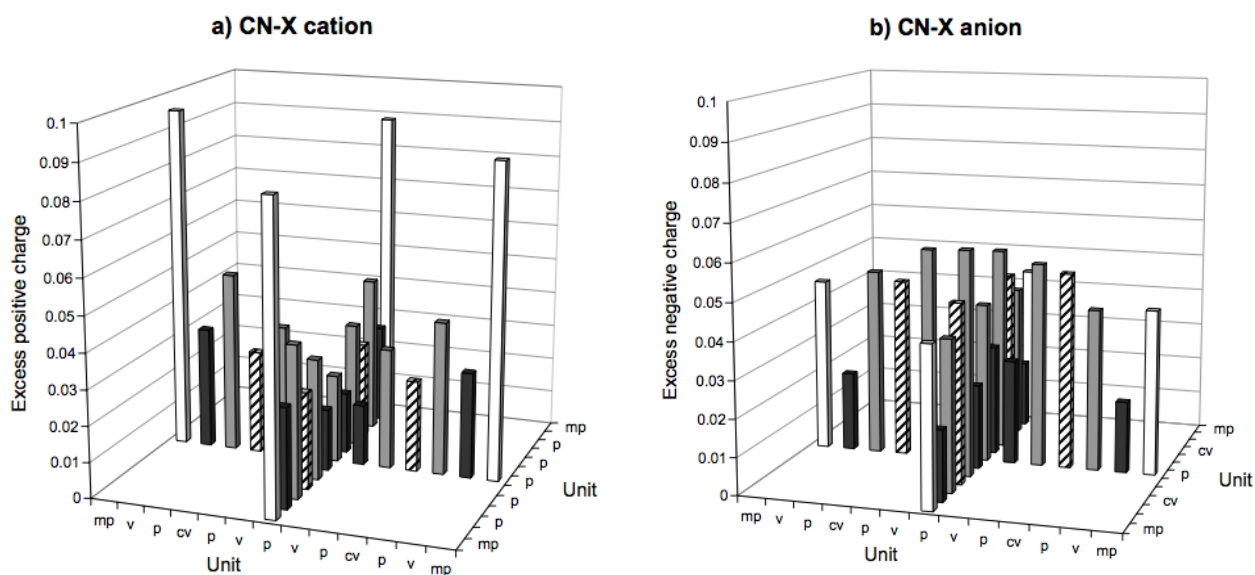

Figure 6.8: DFT distribution of an excess (a) positive and (b) negative charge in
CN-X. Charges on the unsubstituted phenylene units (p) are shown in grey, on
the methoxy-substituted phenylene units (mp) in white, on the vinylene units (v)
in black, and on the cyano-substituted vinylene units (cv) with the diagonal lines
pattern.

6.4.3 Charge transport calculations

Thermal and morphological studies performed previously[18] indicate that π-π interactions are prominent in stacks of X-mer molecules. X-ray diffraction experiments show that columnar structures can be formed in which the X-mer molecules stack at a distance of 3.5 Å.[17] To gain insight into the charge carrier mobility along these stacks, charge transport calculations have been performed. The charge transport calculations are discussed only for the *p*-OXA-X oligomer. Similar results were found for the other X-mers. The charge transfer integrals, the spatial overlap integrals, and the site energies were calculated for different twist angle around the stacking axis, as described in the section 6.3. Note that in the present charge transport calculations the central phenyl rings of the oligomers are superimposed in the stack. This gives a higher limit of the charge transfer integrals, spatial overlap integrals, and site energies. If the central phenyl rings are shifted in a direction perpendicular on the stacking axis, the coupling between the two oligomers in the stack becomes smaller, leading to lower values of the charge transfer integrals and mobilities.

The effective charge transfer integrals for holes and electrons for a stack with superimposed central phenyl rings are presented in Table 6.3 for different twist angles. The effective charge transfer integral is maximum for zero twist angle, where the contact between arms is optimal. The effective charge transfer integrals for both holes and electrons rapidly decrease with increasing twist angle from 0 to 50 degrees. A further increase of the twist angle up to 90 degrees leads to a slight increase of the effective charge transfer integral for the electrons.

Table 6.3: Effective charge transfer integrals (J_{eff}) and charge carrier mobilities (μ) for holes and electrons of *p*-OXA-X dimer at a stacking distance of 3.5 Å.

Angle (degrees)	$J_{eff, hole}$ (eV)	$J_{eff, electron}$ (eV)	μ_{hole} ($cm^2V^{-1}s^{-1}$)	$\mu_{electron}$ ($cm^2V^{-1}s^{-1}$)
0	0.255	0.270	33.5	38.4
10	0.089	0.126	4.1	8.3
20	0.046	0.078	1.1	3.2
30	0.035	0.049	0.6	1.3
40	0.019	0.019	0.2	0.2
50	0.015	0.008	0.1	0.03
60	0.001	0.032	0.05	0.5
70	0.005	0.048	0.01	2.1
80	0.003	0.094	0.005	4.6
90	0.021	0.105	0.2	5.8

The reorganization energies defined by eq. 6.3 were found to be 0.145 eV and 0.144 eV for the hole and the electron, respectively. These values are smaller than the reorganization energies reported for the excess charges on a linear phenylenevinylene trimer or tetramer.[51] The smaller values of the reorganization energies for *p*-OXA-X are consistent with a higher degree of delocalization of the charge along the X-mer in comparison with linear PVs.

The rate for charge transfer between two *p*-OXA-X oligomers and the charge carrier mobility of holes and electrons were calculated according to eqs. 6.1 and 6.4, respectively, using the values of the effective charge transfer integrals and reorganization energies discussed above. The calculated charge carrier mobility is shown as a function of the twist angle in Figure 6.9. The calculated hole mobility of *p*-OXA-X is 33.5 cm^{2}V^{-1}s^{-1} for a twist angle of 0°. Increase of the twist angle leads to a dramatic decrease of the charge carrier mobility of holes. At 10° the charge carrier mobility of holes is eight times smaller than the mobility at 0° and decreases further as the twist angle increases.
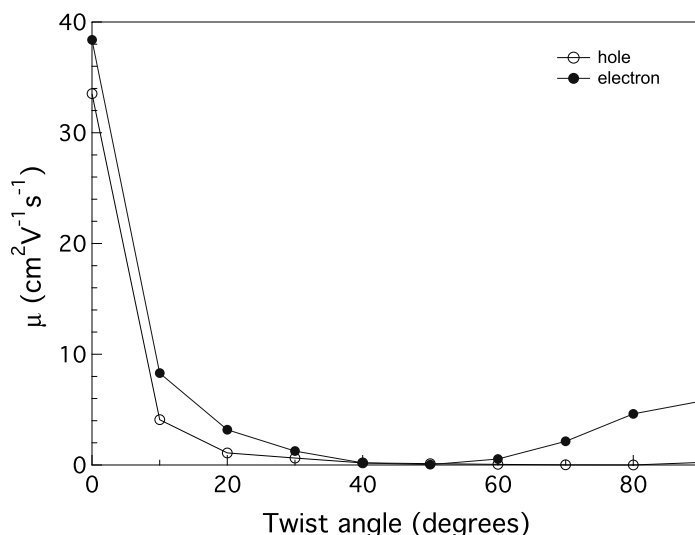

Figure 6.9: Dependence of the hole and electron mobility on the twist angle for *p*-OXA-X stacks.

The electron mobility at 0° is slightly higher than the hole mobility. The electron mobility decreases strongly with increasing twist angle; however, the decrease is less pronounced than for holes. The electron mobility for *p*-OXA-X decreases by a factor of ~4.5 when going from 0 to 10°. The electron mobility exhibits an additional decrease with increasing the twist angle from 10 to 45°. A further increase of the twist angle up to 90° leads to a slight increase of the electron mobility. This is the main difference between the angular dependence of the hole and electron mobility for *p*-OXA-X.

The difference between the angular dependence of the hole and electron mobility for *p*-OXA-X can be explained on basis of the spatial distribution of the HOMO and LUMO orbitals. In Figure 6.10 the HOMO and LUMO orbitals are shown for *p*-OXA-X together with a schematic representation. The HOMO has the highest density on the phenylenevinylene arms, while there is hardly any density on the oxadiazole arms. In contrast, for the LUMO the density is almost evenly distributed over the phenylenevinylene and oxadiazole arms. The shape of the HOMO and LUMO orbitals in Figure 6.10 is consistent with the charge distribution of an excess positive and negative charge shown in Figure 6.7. This justifies the use of these orbitals to calculate the charge transfer integrals for hole and electron transport. At a twist angle of 0° the electronic coupling between the HOMOs (LUMOs) of two stacked

p-OXA-X oligomers is maximum, due to a strong overlap of the arms of the same nature, see Table 6.3 and Figure 6.9.
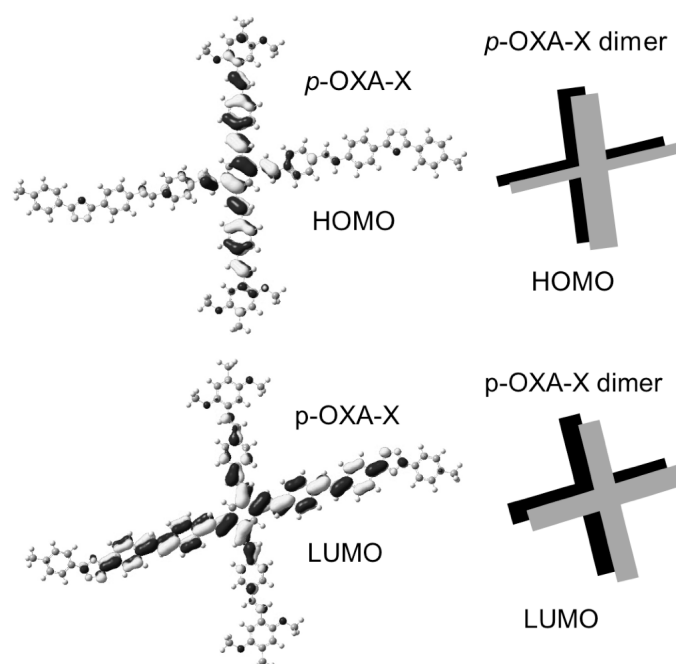

Figure 6.10: HOMO and LUMO orbitals for the *p*-OXA-X oligomer (in left side) together with the schematic representation of the HOMO and LUMO orbitals of the *p*-OXA-X dimer (right side).

When one *p*-OXA-X oligomer is rotated over 90° around the stacking axis, the phenylenevinylene arms on which the positive charge delocalizes have negligible overlap, see Figure 6.11. As a result, the charge transfer integral and, consequently, the hole mobility, are close to zero.
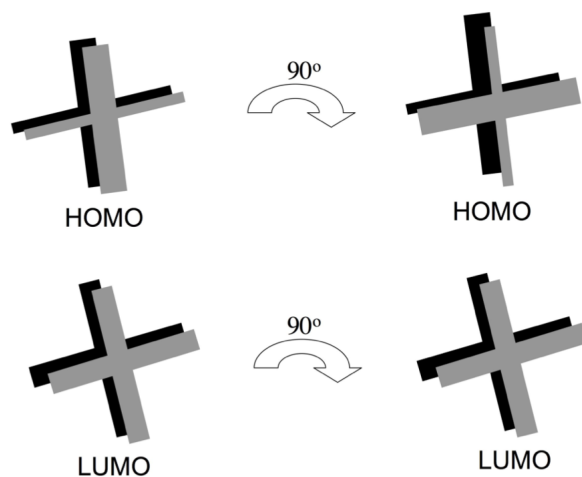

Figure 6.11: Schematic representation of the HOMO and LUMO orbitals of the *p*-OXA-X dimer explaining the dependence of the charge carrier mobilities on the twist angle.

For the electron mobility the situation is different. A rotation of 90° of one *p*-OXA-X oligomer leads to a situation in which the phenylenevinylene arms of one X-mer overlap with the arms containing the oxadiazole unit on the other X-mer. Since the density of the LUMO is appreciable on both types of arms, the charge transfer integral and the electron mobility do not vanish at 90°.

As discussed above, the mobility depends to a large extent on the mutual orientation of the molecules. To gain insight into the twist angle between *p*-OXA-X oligomers in a stack, molecular dynamics simulations were performed. The results of the molecular dynamics simulations in Figure 6.12 indicate that the most favorable conformation occurs at a twist angle of 10°. According to the charge transport calculations a twist angle of 10° implies a mobility of 4.1 cm^{2}V^{-1}s^{-1} for the hole and 8.3 cm^{2}V^{-1}s^{-1} for the electron at 3.5 Å stacking distance. The mobility calculations discussed above involve ordered static molecular stacks. However, in reality, the stacks exhibit dynamic structural fluctuations, which cause the charge transfer integrals to differ from place to place along the stack. For π-π stacked OPV molecules it was shown that if dynamic structural fluctuations are taken into account, the mobility is determined by the slowest hopping steps, which correspond to the largest twist angles.[51] Hence, the mobility of charges on a disordered X-mer stack will be lower than the values obtained for the equilibrium angle of 10°. From the present study it is clear that high charge carrier mobilities can be achieved for X-mers at small twist angles around the stacking distance. The charge transport calculations described in this section give a qualitative picture of the mobilities along stacks of X-shaped oligo(phenylenevinylene)s.
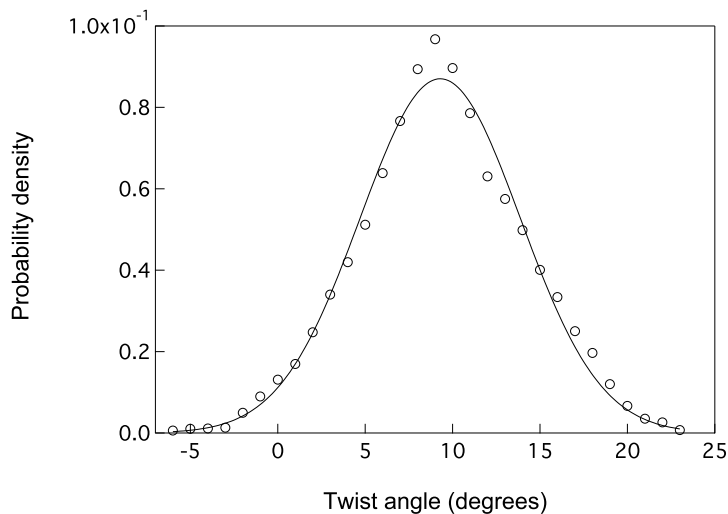
Figure 6.12: Probability distribution of the twist angle for the *p*-OXA-X dimer. The circles represent the probability density obtained by molecular dynamics simulations, while the line is a gaussian fit.

6.5 Summary and conclusions

Pulse radiolysis with time-resolved VIS/NIR spectroscopy was used to measure transient optical absorption spectra of charges on X-shaped phenylenevinylene oligomers in the wavelength range of 500-1600 nm (0.8-2.5 eV). The experimental spectra of the X-mer

cations and anions exhibit a strong absorption band near 1.6-1.7 eV. For the CN-X cation an additional weak absorption was found at low energy.

Optical absorption spectra of charged X-mers were calculated using the INDO/s-CIS method with a geometry obtained by density functional theory (DFT). The calculations reproduce the measured optical absorption band near 1.6-1.7 eV. The calculations predict additional weak absorption bands at lower energy.

The distribution of positive and negative charges on the X-mers was investigated using DFT and INDO/s-CIS. According to DFT calculations, the excess positive charge is mostly localized on the methoxy-substituted phenylene units, while the excess negative charge is delocalized over the entire oligomer. In contrast, the INDO/s-CIS calculations predict a localization of the excess positive and negative charges at the central phenyl ring.

We have also calculated the charge carrier mobility on static stacks of *p*-OXA-X oligomers using parameters obtained from DFT calculations. It was found that the charge carrier mobility strongly depends on the twist angle between adjacent oligomers in the stack. The mobilities of electrons are higher than those of holes and exhibit a somewhat different dependence on the twist angle.

Molecular dynamics simulations show that the most favorable conformation of the *p*-OXA-X dimer is reached for a twist angle of 10°. For this angle the calculated hole mobility is 4.1 $cm^2V^{-1}s^{-1}$ and the electron mobility is 8.3 $cm^2V^{-1}s^{-1}$. According to the charge transport calculations the mobility can be significantly enhanced by reduction of the twist angle. The high mobility values obtained from the calculations make these materials attractive candidates for application in opto-electronic devices.

6.6 References

(1)   Kraft, A.; Grimsdale, A. C.; Holmes, A. B. *Angew. Chem. Int. Ed.* **1998**, *37*, 402.
(2)   Friend, R. H.; Gymer, R. W.; Holmes, A. B.; Burroughes, J. H.; Marks, R. N.; Taliani, C.; Bradley, D. D. C.; Dos Santos, D. A.; Bredas, J. L.; Logdlund, M.; Salaneck, W. R. *Nature* **1999**, *397*, 121.
(3)   Garnier, F. *Chem. Phys.* **1998**, 253.
(4)   Reese, C.; Roberts, M.; Ling, M.; Bao, Z. *Mater. Today* **2004**, *7*, 20.
(5)   Brabec, C.; Dyakonov, V.; Parisi, J.; Sariciftci, N. S. *Organic Photovoltaics*; Springer: Berlin, 2003.
(6)   Braun, D.; Staring, E. G. J.; Demandt, R. C. J. E.; Rikken, G. L. J.; Kessener, Y. A. R. R.; Venhuizen, A. H. J. *Synth. Met.* **1994**, *66*, 75.
(7)   Greenham, N. C.; Samuel, I. D. W.; Hayes, G. R.; Phillips, R. T.; Kessener, Y. A. R. R.; Moratti, S. C.; Holmes, A. N.; Friend, R. H. *Chem. Phys. Lett.* **1995**, *241*, 89.
(8)   Blom, P. W. M.; Vissenberg, M. C. J. M. *Mater. Sci. Eng.* **2000**, *27*, 53.
(9)   Warman, J. M.; Gelinck, G. H.; de Haas, M. P. *J. Phys.: Condens. Matter* **2002**, *14*, 9935.
(10)   Krebs, F. C.; Jorgensen, M. *Macromolecules* **2003**, *36*, 4374.

(11) Johansson, N.; Dos Santos, D. A.; Guo, S.; Cornil, J.; Fahlman, M.; Salbeck, J.; Schenk, H.; Arwin, H.; Bredas, J. L.; Salanek, W. R. *J. Chem. Phys.* **1997**, *107*, 2542.

(12) Robinson, M. R.; Wang, S.; Heeger, A. J.; Bazan, G. C. *Adv. Funct. Mater.* **2001**, *11*, 413.

(13) Van de Craats, A. M.; Warman, J. M.; Fechtenkotter, A.; Brand, J. D.; Harbison, M. A.; Mullen, K. *Adv. Mater.* **1999**, *11*, 1469.

(14) Schmidt-Mende, L.; Fechtenkotter, A.; Mullen, K.; Moons, E.; Friend, R. H.; MacKenizie, J. D. *Science* **2001**, *293*, 1119.

(15) Ponomarenko, S. A.; Kirchmeyer, S.; Elschner, A.; Huisman, B.-H.; Karbach, A.; Drechsler, D. *Adv. Funct. Mater.* **2003**, *13*, 591.

(16) Sun, Y.; Xiao, K.; Liu, Y.; Wang, J.; Pei, J.; Yu, G.; Zhu, D. *Adv. Funct. Mater.* **2005**, *15*, 818.

(17) Niazimbetova, Z. I.; Christian, H. Y.; Bhandari, Y. J.; Beyer, F. L.; Galvin, M. E. *J. Phys. Chem. B* **2004**, *108*, 8673.

(18) Christian-Pandya, H.; Niazimbetova, Z. I.; Beyer, F. L.; Galvin, M. E., to be published.

(19) Peng, Z.; Bao, Z.; Galvin, M. E. *Adv. Mater.* **1998**, *10*, 680.

(20) Peng, Z.; Galvin, M. E. *Chem. Mater.* **1998**, *10*, 1785.

(21) Fratiloiu, S.; Candeias, L. P.; Grozema, F. C.; Wildeman, J.; Siebbeles, L. D. A. *J. Phys. Chem. B* **2004**, *108*, 19967.

(22) Te Velde, G.; Bickelhaupt, F. M.; Baerends, E. J.; Guerra, C. F.; van Gisbergen, S. J. A.; Snijders, J. G.; Ziegler, T. *J. Comput. Chem.* **2001**, *22*, 931.

(23) Vosko, S. H.; Wilk, L.; Nusair, M. *Can. J. Phys.* **1980**, *58*, 1200.

(24) Jensen, F. *Introduction to Computational Chemistry*; John Wiley & Sons Ltd.: Chichester, 1999.

(25) Becke, A. D. *Phys. Rev. A* **1988**, *38*, 3098.

(26) Perdew, J. P. *Phys. Rev. B* **1986**, *33*, 8800.

(27) Rydley, J.; Zerner, M. C. *Theor. Chim. Acta* **1973**, *32*, 111.

(28) Bene, J. E. D.; Ditchfield, R.; Pople, J. A. *J. Chem. Phys.* **1971**, *55*, 2236.

(29) Foresman, J. B.; Head-Gordon, M.; Pople, J. A.; Frisch, M. J. *J. Phys. Chem.* **1992**, *96*, 135.

(30) Zerner, M. C. *ZINDO, A General Semiempirical Program Package*; University of Florida: Gainesville, 1998.

(31) Mataga, N.; Nishimoto, K. *Z. Physik. Chem.* **1957**, *13*, 140.

(32) Zerner, M. C. *Reviews in Computational Chemistry*; VCH: New York, 1991; Vol. 2.

(33) Mikkelsen, K. V.; Ratner, M. A. *Chem. Rev.* **1987**, *87*, 113.

(34) Newton, M. D. *Chem. Rev.* **1991**, *91*, 767.

(35) Senthilkumar, K.; Grozema, F. C.; Bickelhaupt, F. M.; Siebbeles, L. D. A. *J. Chem. Phys.* **2003**, *119*, 9809.

(36) Bredas, J.-L.; Beljonne, D.; Coropceanu, V.; Cornil, J. *Chem. Rev.* **2004**, *104*, 4971.

(37) Ponder, J. *Tinker 4.2- Software Tools for Molecular Design*; Washington University: St. Louis, 2004.

(38) Sprague, J. T.; Tai, J. C.; Yuh, Y.; Allinger, N. L. *J. Comput. Chem.* **1987**, *8*, 581.

(39) Cooper, R.; Thomas, J. K. *J. Chem. Phys.* **1968**, *48*, 5097.

(40) Schmidt, W. F.; Allen, A. O. *J. Phys. Chem.* **1968**, *72*, 3730.

(41)   Gee, N.; Freeman, G. R. *Can. J. Chem.* **1992**, *70*, 1618.

(42)   Shinsaka, K.; Freeman, G. R. *Can. J. Chem.* **1974**, *52*, 3495.

(43)   Grozema, F. C.; Hoofman, R. J. O. M.; Candeias, L. P.; de Haas, M. P.; Warman, J. M.; Siebbeles, L. D. A. *J. Phys. Chem. A* **2003**, *107*, 5976.

(44)   Warman, J. M.; Infelta, P. P.; de Haas, M. P.; Hummel, A. *Chem. Phys. Lett.* **1976**, *43*, 321.

(45)   Huang, S. S.-S.; Freeman, G. R. *J. Chem. Phys.* **1980**, *72*, 1989.

(46)   Schenk, R.; Gregorius, H.; Mullen, K. *Adv. Mater.* **1991**, *3*, 492.

(47)   Grozema, F. C.; Candeias, L. P.; Swart, M.; van Duijnen, P. T.; Wildeman, J.; Hadziiannou, G.; Siebbeles, L. D. A.; Warman, J. L. *J. Chem. Phys.* **2002**, *117*, 11366.

(48)   Fratiloiu, S.; Grozema, F. C.; Siebbeles, L. D. A. *J. Phys. Chem. B* **2005**, *109*, 5644.

(49)   Moro, G.; Scalmani, G.; Cosentino, U.; Pitea, D. *Synth. Met.* **2000**, *108*, 165.

(50)   Geskin, V. M.; Dkhissi, A.; Bredas, J. L. *Int. J. Quant. Chem.* **2003**, *91*, 350.

(51)   Prins, P.; Senthilkumar, K.; Grozema, F. C.; Jonkheijm, P.; Schenning, A. P. H. J.; Meijer, E. W.; Siebbeles, L. D. A. *J. Phys. Chem. B* **2005**, *109*, 18267.

Chapter 7

Electronic Structure and Optical Properties of Charged Oligofluorenes[*]

Time-Resolved VIS/NIR Spectroscopy versus Time-Dependent DFT

The electronic structure and optical properties of charged oligofluorenes were studied experimentally and theoretically. Measurements of the optical absorption spectra of charged oligofluorenes in dilute solutions have been performed using the pulse radiolysis technique. In addition, optical absorption spectra of radical cations and anions in a solid matrix were measured after γ-irradiation at 77K. The optical absorption spectra were measured in the range of 440-2100 nm (0.6-2.8 eV) and compared with results from time-dependent density functional theory (TDDFT) calculations. The calculated charge induced deformations and charge distribution do not indicate the occurrence of polaronic effects. The potential energy profiles for rotation around the inter-unit bond show that oligofluorenes are nonplanar in their neutral state, while they tend to more planar structures in their charged state. The optical absorption spectra of charged oligofluorenes are dependent on the angle between neighboring units. TDDFT absorption energies shift to lower values with increasing chain length, which suggests that the charge delocalizes along the oligomer chain.

7.1 Introduction

Conjugated polymers and oligomers offer an alternative to inorganic semiconductors for applications in optoelectronic devices, such as field-effect transistors (FETs),[1] light-emitting diodes (LEDs),[2] solar cells[3] and nanoscale molecular electronic devices.[4] Semiconducting polyfluorenes[5] have been intensively studied in the last years for LED applications[6-9] due to their high fluorescence yield[10] and high charge carrier mobility.[11] Alkyl chains are introduced at the fluorene 9-position to induce polymer solubility, liquid crystallinity and chirality without affecting the π-conjugated backbone. The applicability of fluorenes in LEDs critically depends on their charge transport properties. Radical cations and anions of fluorenes correspond to the charged species (holes and excess electrons) that are produced by charge injection from electrodes in a LED. Therefore the properties of charged fluorenes are of great

---

interest. Optical absorption spectra of excess charges can provide valuable information about their spatial extent along the π-conjugated backbone.
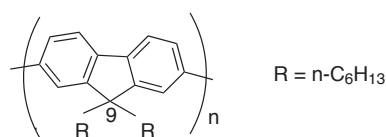

Figure 7.1: Chemical structure of the fluorene oligomers investigated. The optical absorption spectra of charged Fn oligomers were measured in dilute solution, while the DHFn series was studied in solid matrix (n is the number of phenylene units).

Fluorene oligomers can be considered as model systems for conjugated polyfluorenes. For instance, the effect of chain length on the optical properties of charged oligofluorenes provides information about the delocalization of charge carriers, which can be extrapolated to the polymer. In the present study we report optical absorption spectra of positively and negatively charged oligofluorenes in dilute solution. Additional information on vibrational transitions in charged oligofluorenes was obtained by measuring the optical absorption spectra in a solid matrix at low temperature. Quantum chemical calculations were performed to gain insight into the nature of electronic transitions and into the spatial distribution of an excess charge. Quantum chemical calculations are an important tool to investigate the relation between the electronic structure and the optical properties of π-conjugated materials. The majority of the calculations reported in the literature describe neutral oligomers, while less work has been addressed to charged oligomers.[12-20] Most of the calculations performed on charged oligomers have been limited to semi-empirical methods. Recently, time-dependent density functional theory (TDDFT) was used to calculate the optical absorption spectra of charged polycyclic aromatic hydrocarbons[16] and oligo(phenylenevinylene)s.[19,20] On the basis of the reported accuracy of this method to describe the lowest excited state of the charged systems,[16] we apply TDDFT to oligofluorene cations and anions. The experimental results in solution and solid matrix are compared with the calculated absorption spectra for oligomer chains with different length. The structures of the fluorene oligomers studied in this chapter are presented in figure 7.1.

7.2 Experimental details

Experiments were performed on two series of fluorene oligomers with *n*-hexyl substituents at the 9-position (see Figure 7.1). Both series of fluorene oligomers were prepared by similar synthetic strategies envolving step-by-step Suzuki cross-coupling reactions. The complete synthesis of the first series of fluorene oligomers (Fn; n is the number of fluorene monomer units) has been published.[21] The second series of fluorene oligomers (DHFn; n is the number of fluorene monomer units) has been synthesized as reported earlier by Koizumi et al.[22]

Fn solutions were prepared using either UV-spectroscopic grade benzene (bz) or tetrahydrofuran (THF), depending on the nature of charges (positive or negative) to be studied. Solutions of Fn in benzene were used for generating positive charges (Fn radical

cations), while the negative charges (Fn radical anions) were created in THF. The benzene solutions (3 mM in monomer units) were bubbled with benzene-saturated oxygen for about 20 minutes. The tetrahydrofuran solutions (3 mM in monomer units) were bubbled with THF-saturated argon. The experiments on dilute solutions were carried out at room temperature.

Positive and negative charge carriers on isolated Fn oligomers in solution were generated using pulse radiolysis. The Fn solutions were irradiated with 5 ns pulses of 3 MeV electrons from a Van de Graaff accelerator. The positive and negative charge carriers were detected by time-resolved visible/near-infrared (VIS/NIR) spectroscopy, as reported previously for phenylenevinylene radical cations.[15,19] The absorption spectra of the Fn radical cations and anions were measured by following the transient changes in absorbance of the solution at different wavelengths.

DHFn oligomers were dissolved in n-butyl chloride (BuCl) or methyl-tetrahydrofuran (MTHF), in order to study cationic and anionic species, respectively. The solutions (5-10 mM) were bubbled with dry argon for 2 minutes. Charge carriers were produced by γ-ray irradiation of DHFn solutions at 77 K with a dose of 4.0 kGy.[23] Optical absorption spectra of charged DHFn oligomers in solid matrix were recorded in the range 440-2100 nm at a temperature of 80-150 K, using a Shimadzu UV-3100PC spectrometer and an Oxford Optistat DN cryostat system.

7.3 Computational methodology

The geometries of neutral and charged fluorenes were optimized using the Amsterdam Density Functional (ADF) Theory program.[24] The geometry optimizations were performed by using the Local Density Approximation (LDA) with exchange and correlation functionals based on Vosko-Wilk-Nusair (VWN) parametrization of electron gas data.[25] The Generalized Gradient Approximation (GGA)[26] corrections by Becke[27] (exchange) and Perdew[28] (correlation) were included. For optimizing the geometries a double-zeta polarized (DZP) basis set was used.

The torsional potential energy profiles of neutral and charged bifluorenes were calculated using Density Functional Theory (DFT)[26] by taking the minimum energy conformation from the geometry optimization calculations and varying the inter-unit angle in steps of 15°. The geometry was not optimized for each angle. The DFT calculations were performed with the Q-Chem program,[29] using the Becke (exchange) and the Lee-Yang-Parr (correlation)[30] functional (BLYP), in a correlation consistent[31] polarized valence double-zeta (cc-pVDZ) basis set.

The optical absorption spectra of charged oligofluorenes were calculated with Time-Dependent Density Functional Theory (TDDFT),[32,33] as implemented in the Q-Chem program. The absorption energies were computed using the cc-pVDZ basis set and the BLYP functional.

In the calculations the alkyl chains at the 9-position were replaced by hydrogen atoms. This simplification is not expected to affect the optical spectra of the charged oligofluorenes

significantly. The presence of the alkyl substituents does not create any significant steric effects[34] and should not affect the electronic transitions.

7.4 Results and discussion

7.4.1 Measurement of optical absorption spectra of charged fluorene oligomers

Oligofluorenes (Fn) in oxygen-saturated benzene ([O_2]=11.9 mM at 1 atm and 25 ^{o}C) were irradiated with pulses of 3 MeV electrons from a Van de Graaff accelerator. This leads to the formation of benzene radical cations (bz$^{•+}$), excited states (bz*), and excess electrons (e$^-$),[35-37] according to

$$bz \rightarrow bz^{•+}, bz^*, e^- \tag{7.1}$$

The excess electrons generated during irradiation are highly mobile (μ=0.13 cm^{2}V^{-1}s^{-1})[38] and react with the oxygen molecules within a few nanoseconds, yielding oxygen anions (O_2^-).

$$e^- + O_2 \rightarrow O_2^- \tag{7.2}$$

The excited states of benzene molecules are quenched by O_2, leading to formation of O_2 in the $^1\Delta$ excited state.[39]

$$bz^* + O_2 \rightarrow O_2(^1\Delta) + bz \tag{7.3}$$

Benzene radical cations (bz$^{•+}$) can react with the fluorene oligomers (Fn) leading to the formation of fluorene radical cations (Fn$^{•+}$).

$$bz^{•+} + Fn \rightarrow bz + Fn^{•+} \tag{7.4}$$

The occurrence of the reaction in eq. (7.4) is evident from Figure 7.2(a), which shows the change in optical absorption (ΔA) at 1920 nm (0.65 eV) due to formation of F3 cations upon irradiation. The absorbance at 1920 nm increases as reaction (7.4) proceeds. This reaction is possible due to the lower ionization potential of the fluorene oligomers as compared to benzene. The rate constant (k) for the diffusion-controlled reaction (7.4) can be calculated using the relation:

$$k = 4\pi RD \tag{7.5}$$

where R is the reaction radius and D is the diffusion coefficient. The diffusion coefficient can be calculated from the known mobility of holes in benzene (μ=4x10^{-4} cm^{2}V^{-1}s^{-1}),[40] using the Einstein relation:

$$D = \frac{\mu k_B T}{e} \tag{7.6}$$

Taking a typical reaction radius of 1 nm[41] and a monomer concentration of 3 mM the calculated rate coefficient (k=7.6x10^9 M^{-1}s^{-1}) corresponds to a rise time of the optical absorption signal near 50 ns, in agreement with the transient in Figure 7.2(a). The decay of the transient absorption in Figure 7.2(a) on a timescale of hundreds of nanoseconds is attributed to second-order charge recombination.

$$Fn^{\bullet+} + O_2^- \rightarrow Fn + O_2 \qquad\qquad (7.7)$$

A detailed discussion of diffusion-controlled reactions analogous to those in eqs. 7.2-7.4 and 7.7, describing the formation and recombination kinetics of positively charged species in solution, has been published previously.[42]
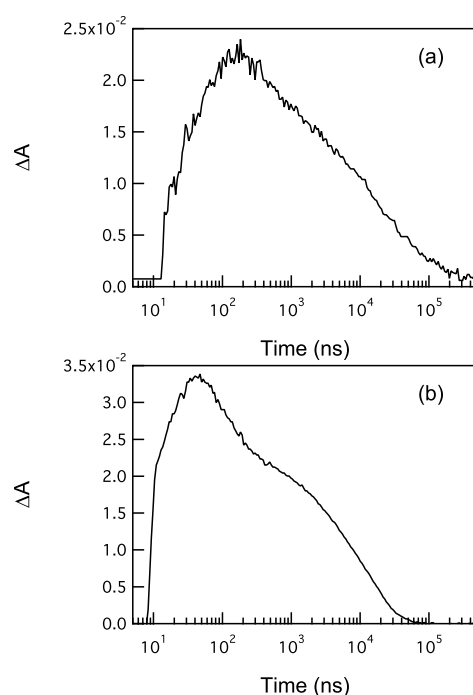

Figure 7.2: Optical absorption transients of F3 oligomers in solution at their maxima: (a) formation and recombination of Fn$^{\bullet+}$ in O$_2$-saturated benzene. (b) formation and decay of Fn$^{\bullet-}$ in Ar-saturated THF.

The optical absorption spectra of radical cations of fluorene oligomers (Fn) in solution were measured in the range of 440-2100 nm (0.6- 2.8 eV), see Figure 7.3 and Table 7.1. For the shortest radical cation (F1) the absorption was found to increase with the photon energy. However, the absorption maximum could not be observed in the accessible energy range and must thus occur at an energy above 2.8 eV. The spectrum of the F3 radical cation exhibits two absorption peaks at low energy (RC1) with maxima at 0.65 eV and 0.83 eV together with an absorption peak at high energy (RC2) (see Figure 7.3). Increasing the chain length from three to five fluorene units leads to one absorption peak at low energy (RC1), while no significant shift of the high-energy absorption peak (RC2) is observed. Data of the absorption maxima of the positively charged fluorene oligomers can be extended to data on polymers. Burrows et al.[43] have found the high-energy band (RC2) of the poly[9,9-di(ethylhexyl)fluorene] radical

cation at 2.2 eV. The RC2 energy of the F5 radical cation reported here (see Table 7.1) is similar to that of the polymer, indicating that the charged states in these systems saturate quickly.
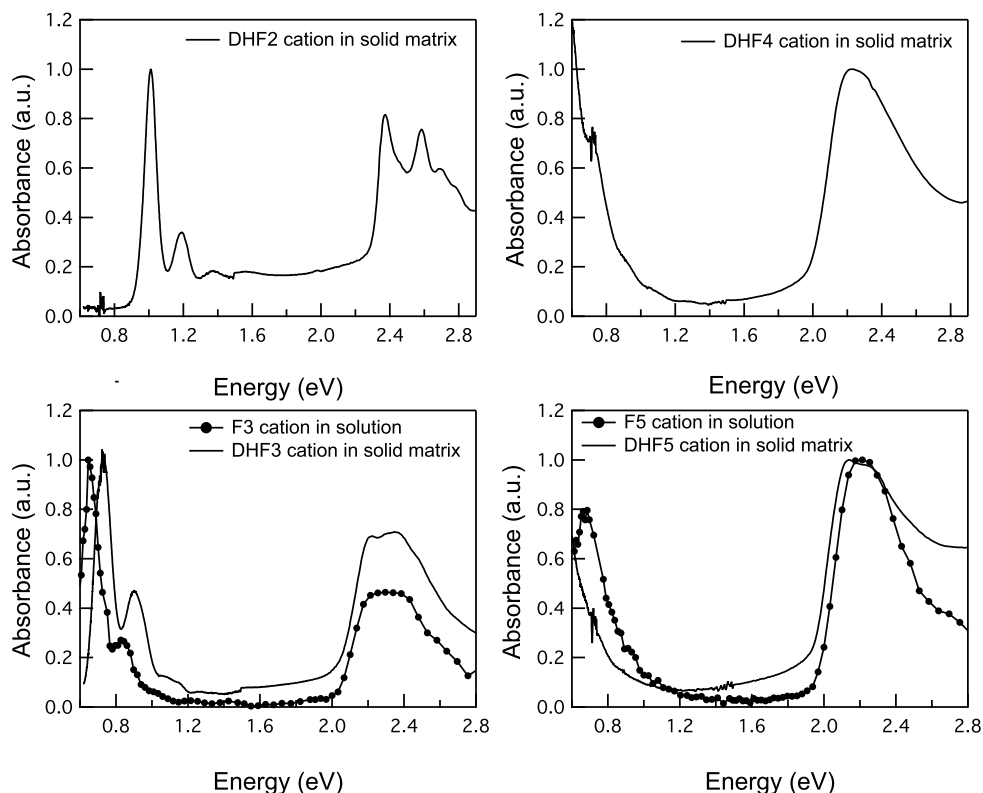

Figure 7.3: Optical absorption spectra of fluorene cations in solution (benzene) at room temperature together with the spectra in solid matrix (2-chlorobutane) at 100 K.

To obtain the spectra of fluorene radical anions in solution, measurements were performed using tetrahydrofuran (THF) as a solvent.[44] Irradiation of THF leads to the formation of solvated electrons (e^-) and radical cations ($THF^{\bullet+}$), with a very small concentration of short-lived excited states.[45,46]

$$THF \rightarrow e^-, THF^{\bullet+}, THF^* \tag{7.8}$$

Solvent radical cations ($THF^{\bullet+}$) react with neutral THF, according to[46,47]

$$THF^{\bullet+} + THF \rightarrow THF(-H)\bullet + THF(+H)^+ \tag{7.9}$$

Solvated electrons can undergo transfer to fluorene oligomers to form fluorene radical anions.

$$e^- + Fn \rightarrow Fn^{\bullet-} \tag{7.10}$$

A small fraction of the solvated electrons is lost due to reaction with counterions (cations and radicals in THF).[46]

$$e^- + THF^+ \rightarrow THF^* \text{ (or THF)} \tag{7.11}$$

$$e^- + THF(-H)\bullet \rightarrow THF(-H)^{\bullet-} \tag{7.12}$$

The formation and decay of the F3 radical anion can be observed in the optical absorption transient at 1620 nm in Figure 7.2(b). The formation of $Fn^{\bullet-}$ in tetrahydrofuran according to eq. 7.10 occurs much faster than that of $Fn^{\bullet+}$ in benzene (see eq. 7.4) due to the fact that the electron mobility in THF ($\mu = 3 \times 10^{-3}$ cm^{2}V^{-1}s^{-1})[48] is much higher than the hole mobility in benzene (4×10^{-4} cm^{2}V^{-1}s^{-1}).[40] If it is assumed that the reaction radius is 1 nm for the fluorene oligomer, a rate constant of 5.7×10^{10} M^{-1}s^{-1} is obtained, leading to a rise time less than 10 ns for a concentration of 3×10^{-3} mM (in monomer units), in agreement with the data in Figure 7.2(b). The decay of the transient absorption in Figure 7.2(b) is attributed to the recombination of the fluorene radical anions with THF(+H)$^+$.

Table 7.1: Calculated and experimental transition energies (ΔE in eV), experimental extinction coefficients (ε in Lmol^{-1}cm^{-1}), calculated oscillator strengths (f), and relative contribution of excited state configurations for radical cations of fluorene oligomers. Only the transitions with an oscillator strength higher than 0.1 are given.

Fn	Band	Exptl.[a] ΔE	Exptl.[b] ΔE	Exptl.[a] $\varepsilon, 10^4$	Calcd. ΔE	Calcd. f	Rel. contribution of excited state config.
F1	RC1	>2.8	2.05		2.18	0.11	$-0.32(P1{\rightarrow}P2)+0.95(H{-}2{\rightarrow}P1)$
F2	RC1		1.01		1.24	0.45	$1.01(H{\rightarrow}P1)$
			1.19				
	RC2		2.37		2.82	0.83	$0.96(P1{\rightarrow}P2)+0.23(H{\rightarrow}P1)$
			2.58				
F3	RC1	0.65	0.73	9.0	0.85	0.79	$1.08(H{\rightarrow}P1)$
		0.83	0.90	2.4			
	RC2	2.30	2.35	4.2	2.46	0.94	$0.97(P1{\rightarrow}P2)+0.17(H{\rightarrow}P1)$
F4	RC1		<0.6		0.63	1.00	$1.15(H{\rightarrow}P1)$
	RC2		2.23		2.30	0.88	$0.96(P1{\rightarrow}P2)$
F5	RC1	0.67	<0.6	4.7	0.49	1.14	$1.22(H{\rightarrow}P1)$
	RC2	2.21	2.14	5.9	2.22	0.84	$0.96(P1{\rightarrow}P2)$

[a] Experimental data obtained from Fn spectra measured in solution
[b] Experimental data obtained from DHFn spectra measured in solid matrix

The optical absorption spectra of fluorene radical anions and cations are found to be similar, see Figures 7.3 and 7.4. No absorption was found for the F1 anion in the accessible wavelength range. The spectrum of the F3 radical anion exhibits two absorption maxima at low energy (RA1 and RA1') and two maxima at high energy (see Figure 7.4 and Table 7.2). The maximum of the lowest energy band (RA1) is found near 0.7 eV. When the chain length of the fluorene anion is increased to five fluorene units (F5), there is only one maximum in the optical absorption spectrum at low energy (RA1), while two maxima appear at higher energy (see Figure 7.4).
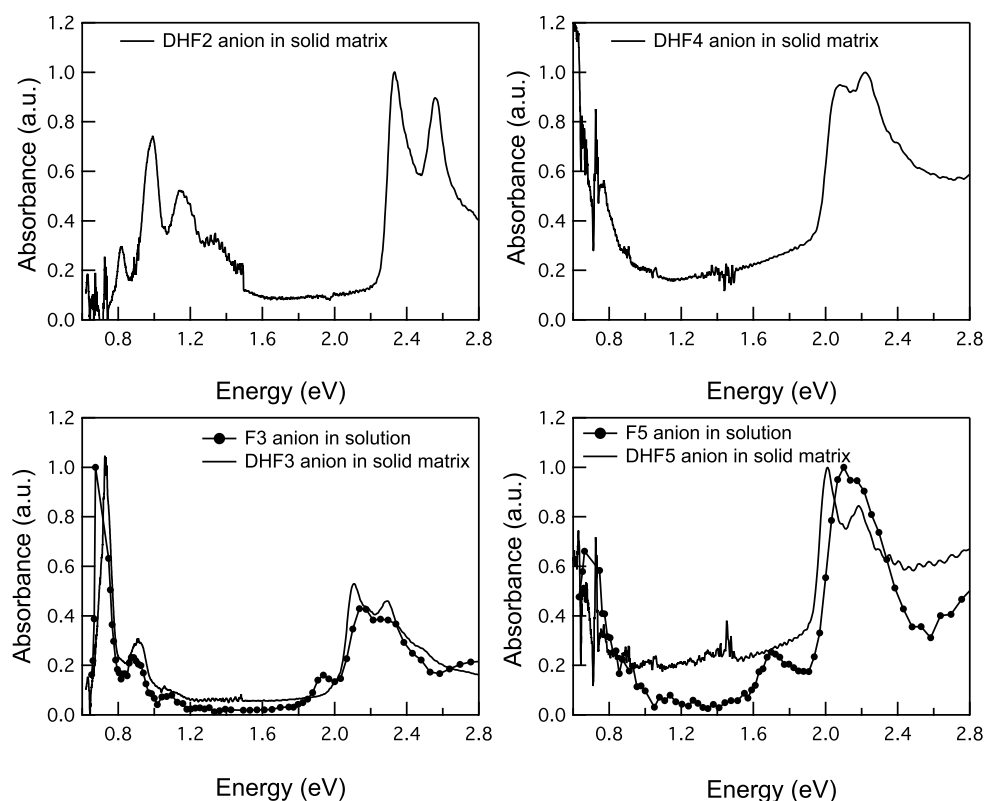
Figure 7.4: Optical absorption spectra of fluorene anions in solution (THF) at room temperature together with the spectra in solid matrix (MTHF) at 100 K.

From dosimetry measurements and pulse radiolysis data an estimation of the lower limit of the experimental extinction coefficients (ε) can be made, if it is assumed that all the charges generated during pulse radiolysis experiments react with the fluorene oligomers. The change in optical absorbance is related to the radiation dose, the yield of free charge carriers per unit dose (G), and the molar extinction coefficient (ε). The radiation dose per pulse was determined by dosymetry, using KSCN solution (10 mM) in N_2O-saturated water. For such a solution G and ε are accurately known ($G\varepsilon(SCN)_2^- = 5.18 \times 10^{-4}$ m^2/J at 475 nm).[49] For the present optical experiments the radiation dose was determined to be 1.4 Gray per nC of beam charge and the yield of free charge carriers in benzene was taken from literature $0.053(100eV)^{-1}$.[50] For experiments performed in THF the yield of free ions is $0.3(100$ eV$)^{-1}$.[51] In this way the molar extinction coefficients were determined for both cations and anions of Fn oligomers and they are listed in Tables 7.1 and 7.2.

Measurements of the optical absorption spectra were also performed for a second series of fluorene oligomers (DHFn) in a solid matrix after γ-irradiation, as described in section 7.2. Fluorene radical cations (DHFn$^{\bullet+}$) were produced by γ-irradiation of a frozen solution of DHFn in butylchloride (BuCl) at 77 K. DHFn$^{\bullet+}$ is formed by charge transfer from mobile BuCl$^+$ to fluorene oligomers,[52] according to

$$BuCl \rightarrow BuCl^+, e^- \qquad (7.13)$$

$$\text{BUCl}^+ + \text{DHFn} \rightarrow \text{DHFn}^+ + \text{BuCl} \tag{7.14}$$
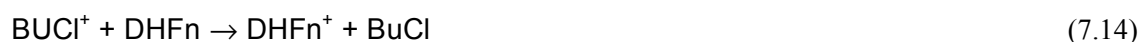
BuCl$^-$ is not produced on irradiation because of the predominant dissociative electron attachment to the BuCl molecules.[52]

$$\text{e}^- + \text{BuCl} \rightarrow \text{Bu}\bullet + \text{Cl}^- \tag{7.15}$$

Table 7.2: Calculated and experimental transition energies (ΔE in eV), experimental extinction coefficients (ε in Lmol^{-1}cm^{-1}), calculated oscillator strengths (f), and relative contribution of excited state configurations for radical anions of fluorene oligomers. Only the transitions with an oscillator strength higher than 0.1 are given.

Fn	Band	Exptl.[a] ΔE	Exptl.[b] ΔE	Exptl.[a] $\varepsilon, 10^4$	Calcd. ΔE	Calcd. f	Rel. contribution of excited state config.
F1	RA1′				2.24	0.13	0.94(P2→L+2)-0.33(P1→P2)
F2	RA1		0.82		1.24	0.34	-0.72(P2→L)-0.61(P2→L+1)
			0.99				
	RA1′		1.14		1.48	0.14	0.28(P2→L)+0.94(P2→L+2)
	RA2		2.33		2.74	0.94	0.21(P2→L)+0.95(P1→P2)
			2.56				
F3	RA1	~0.7	0.73	>10.6	0.83	0.44	0.85(P2→L)+|0.59(P2→L+2)
	RA1′	0.87	0.90	2.5	0.93	0.37	0.63(P2→L)-0.80(P2→L+2)
	RA2	1.94	2.11	1.7	2.37	1.09	0.96(P1→P2)
		2.14	2.29	4.5			
F4	RA1		<0.6		0.65	1.05	1.12(P2→L)
	RA2		2.08		2.20	1.06	0.97(P1→P2)
			2.22				
F5	RA1	~0.7	<0.6	>2.4	0.51	1.23	1.19(P2→L)
	RA2	1.70	2.01	0.9	2.13	0.97	0.97(P1→P2)
		2.10	2.18	3.6			

[a] Experimental data obtained from Fn spectra measured in solution
[b] Experimental data obtained from DHFn spectra measured in solid matrix

Figure 7.3 shows the absorption spectra of radical cations of DHFn oligomers at 100 K. The spectrum of DHFn radical cations exhibit absorption maxima at low energy and at high energy (see also Table 7.1), similar to the spectra measured in solution.

The formation of fluorene radical anions (DHFn$^{\bullet-}$) in γ-irradiated 2-methyltetrahydrofuran (MTHF) is attributed to attachment of electrons to oligofluorene molecules, analogous to experiments performed by Kira et al.[53]

$$\text{e}^- + \text{DHFn} \rightarrow \text{DHFn}^{\bullet-} \tag{7.16}$$

The optical absorption spectra of DHFn radical anions in solid matrix are similar to those measured in solution, see Figure 7.4 and Table 7.2.

7.4.2 Calculation of geometry deformations and charge distributions in oligofluorene cations and anions

The geometries of neutral and charged oligofluorenes were optimized as described in section 7.3. It was found that oligofluorenes have a nonplanar structure in both neutral and charged states. Figure 7.5 shows the energies of neutral and charged bifluorenes as a function of the twist angle between the monomers, as calculated with DFT. The potential energy profile of neutral bifluorene has a minimum at an inter-unit angle $\theta_{tor} = 41.6^{\circ}$. A further twisting of the two fluorene units leads to less stable conformations, with a maximum energy close to $\theta_{tor} = 90^{\circ}$. A second minimum of the torsional energy is found near $\theta_{tor} = 140^{\circ}$. Our results agree with those of Belletete et al.,[34] who found a minimum energy for a torsion angle of 45.3°, using the Hartree-Fock method at the 6-31G* level. The potential energy surface of bifluorene is similar to that obtained for 1-(fluoren-2-yl)phenylene by Tirapattur et al.,[54] which shows that an increase of the conjugation length does not affect the conformation of the molecule. From a geometry optimization of the neutral fluorene pentamer it was found that the optimum torsion angle between the fluorene units is between 40.4 and 41.4°. Thus, the inter-unit torsion angles do not change significantly with increasing conjugation length.
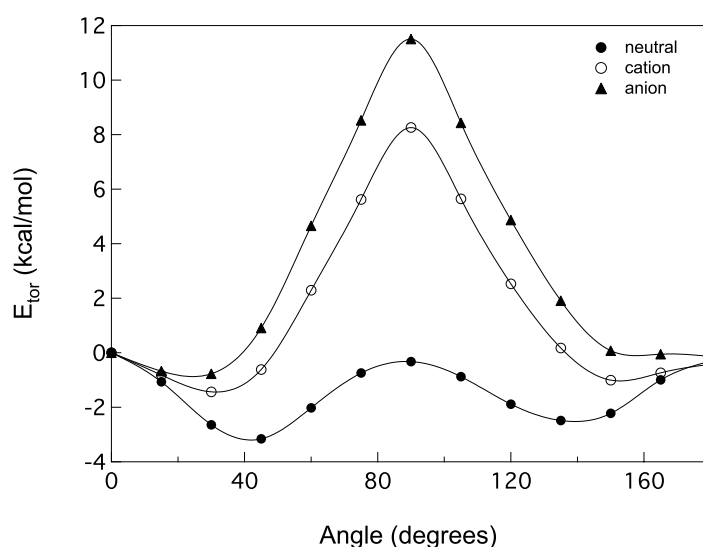

Figure 7.5: Potential energy profiles for torsional motion of the fluorene units. The zero point of the torsional energy (E_{tor}) is taken equal to the energy at zero torsional angle (θ_{tor}).

The potential energy profiles of the bifluorene cation and anion differ significantly from that for neutral bifluorene. The potential energy profile of the charged bifluorene has a minimum that corresponds to a conformation with an inter-unit angle of $\theta_{tor} = 31.7^{\circ}$ for the bifluorene cation and $\theta_{tor} = 24.4^{\circ}$ for the anion. Upon rotation around the inter-unit bond, the energy steeply increases to reach a maximum near $\theta_{tor} = 90^{\circ}$ and then decreases to a second minimum around 150° and 160° for the bifluorene cation and anion, respectively.

The rotation barrier for neutral bifluorene is 2.9 kcal/mol. For charged bifluorenes the rotation barriers are much higher than for neutral bifluorene: 9.7 kcal/mol for the cation and 12.4 kcal/mol for the anion, respectively. This leads to a more narrow distribution around the

torsion angle for which the potential energy is minimum for the charged bifluorenes in comparison with the neutral molecule.

Information about the changes in C-C bond lengths when an electron is removed or added can be obtained by comparison of the optimized geometries of neutral and charged oligofluorenes. The changes in C-C bond lengths for the cations and anions of the fluorene dimer and pentamer are shown in Figure 7.6. The maximum change in C-C bond length was found to be 0.027 Å for both the bifluorene cation and anion (see the upper graph from Figure 7.6). The C-C bond changes become smaller with increasing chain length: a maximum change of 0.01 Å for the F5 cation and 0.013 Å for the F5 anion, respectively (see the lower graph in Figure 7.6). This can be understood in terms of the degree of charge delocalization. For longer chains the amount of charge per monomer unit is less and hence the geometry deformations are smaller. The geometry deformations, as obtained from DFT calculations, are spread over the oligofluorene chains with no indication of the formation of a self-localized polaron.
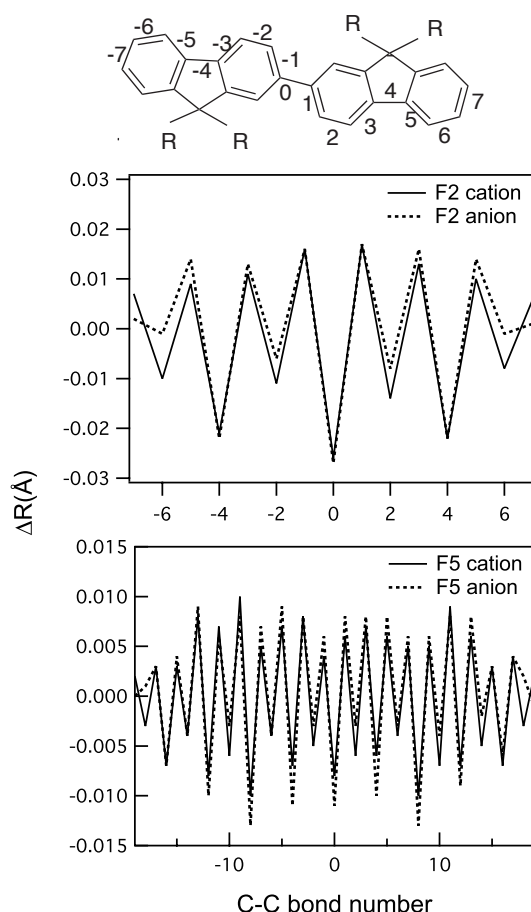

Figure 7.6: Changes in C-C bond length for the fluorene dimer and pentamer after removing or adding an electron as calculated with DFT. (The numbering of the bonds is indicated in the chemical structure.)

Information about the charge distribution along the oligomer chain is useful to gain insight into the occurrence of polaronic effects. Therefore, we have also analyzed the charge distribution of an excess positive and negative charge for the longest oligomer, F5 (see Figure 7.7). The charge distribution was obtained from a Mulliken population analysis performed

using DFT. The charge distribution is presented in terms of fluorene units and was calculated as the difference between the charges of the atoms in the charged state and in the neutral state. The excess positive and negative charge of the F5 cation and anion, respectively, are delocalized along the chain. This means that no self-localized polaron is formed. Geometry deformations and charge distributions of phenylenevinylene cations and anions calculated using the DFT method were also found to be delocalized over the entire chain.[15,20]
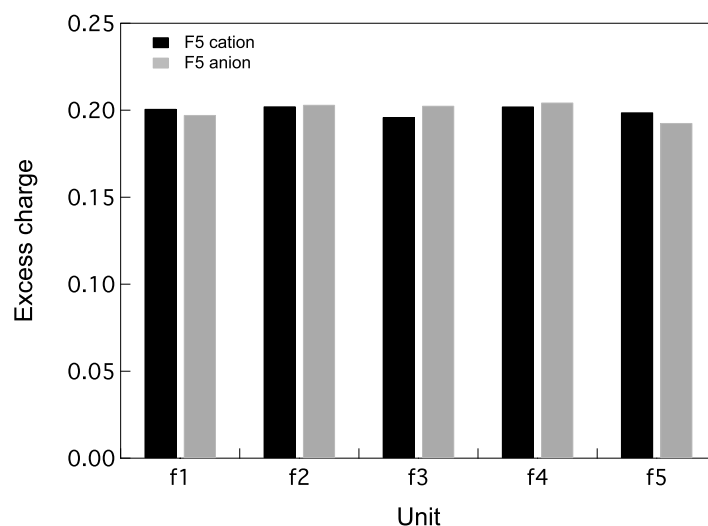

Figure 7.7: Distribution of an excess charge in F5 oligomer. Fluorene units are indicated as fn (n=1-5).

7.4.3 Comparison of experimental and calculated optical absorption spectra of charged oligofluorenes

The absorption spectra of charged conjugated oligomers and polymers are usually explained in terms of so-called "one electron band structure model".[55,56] The model considers that the presence of a singly charged defect leads to the formation of two localized electronic levels in the gap between the valence band and the conduction band, the so-called polaron levels P1 and P2. Since oligomers have discrete energy levels instead of bands, the model was adapted to a "molecular orbital model" and it was presented previously for phenylenevinylene cations and anions.[15,20] According to this model, a positively charged system has the P1 level singly occupied, while P2 is empty. In a negatively charged system the situation is different: P1 is doubly occupied, while P2 is singly occupied. Note that P2 represents the lowest unoccupied molecular orbital (LUMO) for cations and the highest occupied molecular orbital (HOMO) for anions. According to this nomenclature, the level indicated as L is actually the second empty level for cations and the first empty molecular orbital (LUMO) for anions. The molecular orbital model was adopted in this study to describe the spectra of charged fluorenes.

Fluorene cations

The optical absorption spectra of oligofluorene cations were calculated using the TDDFT method, as described in Section 7.3. The calculated transition energies are presented in Table 7.1 and Figure 7.8 together with the experimental data .

According to the TDDFT calculations there is only one allowed transition for the fluorene monomer in the energy range considered. This transition corresponds mainly to excitation of an electron from a doubly occupied molecular orbital (H-2) to the singly occupied molecular orbital (P1). From the experiments performed in solution the maximum of absorption could not be determined, while from the measurements on oligofluorenes in a solid matrix an absorption maximum was found at 2.05 eV, which is very close to the calculated energy of 2.18 eV.

When a second fluorene unit is added, two peaks appear at lower energy (1.01 eV and 1.19 eV) in the experimental absorption spectrum of DHF2 in a solid matrix of BuCl, in addition to the absorption features at higher energy (2.37 eV and 2.58 eV), see Figure 7.3. According to the calculations only a single electronic transition occurs at the lower energy. This suggests that the two peaks near 1 eV are due to different vibrational transitions with a spacing of ~0.2 eV for the same electronic excitation. Infrared absorption and Raman spectroscopy[57] on fluorene indicate that several vibrational transitions occur near 0.2 eV; i.e., close to the energetic spacing between the peaks in the spectrum of the F2 cation. The TDDFT calculations predict only one electronic transition at higher energy (2.82 eV for the RC2 band in Table 7.1). This means that the absorption features at higher energy in the experimental spectrum (2.37 eV and 2.58 eV) correspond to two different vibrational transitions for the same electronic excitation.
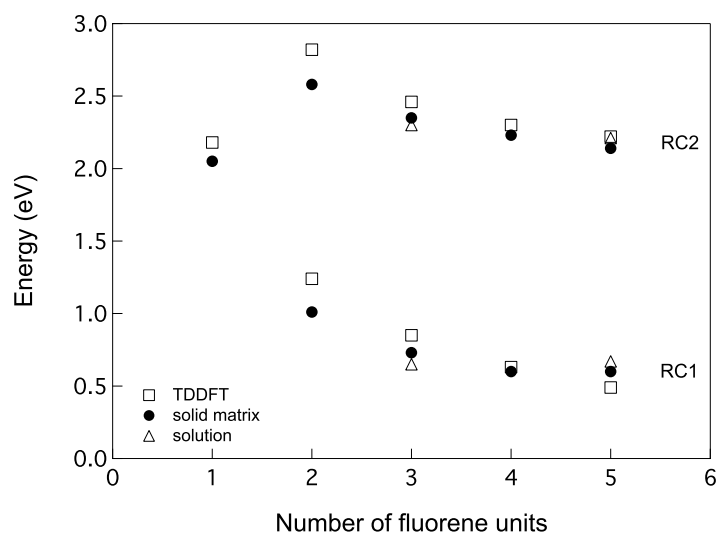

Figure 7.8: Chain length dependence of the transition energies for fluorene radical cations. The transition energies presented for the solid matrix correspond to the energies of the lowest RC1 transition (see Table 7.1) and the highest RC2 transition.

For longer Fn (n>2) cations the TDDFT absorption spectra exhibit two absorption bands: the RC1 band at energy of 0.85 eV or lower and the RC2 band at energies just above 2.2 eV.

By inspection of the electronic configurations which dominate the calculated allowed transitions of the Fn (n>1) cations, it was found that the lowest transition (RC1) is dominated by excitation of an electron from the highest doubly occupied molecular orbital (H) to the singly occupied molecular orbital (P1). The second (RC2) transition corresponds mainly to excitation of an electron from the singly occupied molecular orbital (P1) to the lowest unoccupied molecular orbital (P2).

From comparison of the experimental and calculated transition energies in Table 7.1, it can be concluded that the experimental spectra of fluorene radical cations exhibit two absorption bands (RC1 and RC2), with different vibrational transitions for the same electronic excitation.
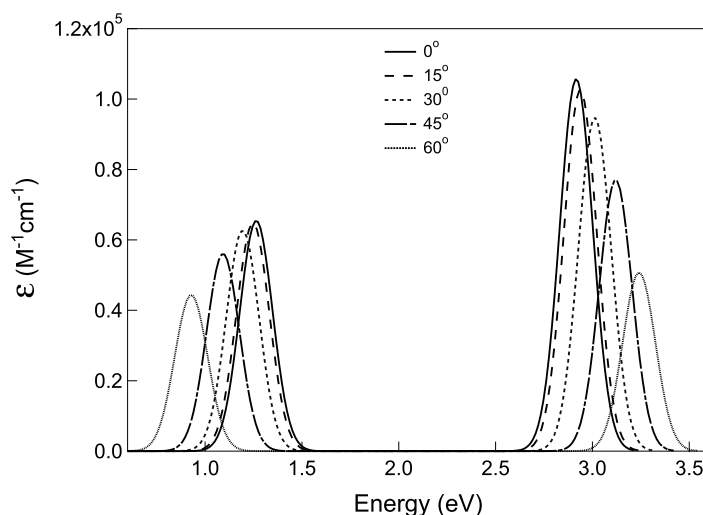

Figure 7.9: Angular dependence of the optical absorption spectra of the F2 cation. (The spectra were simulated by using a Gaussian distribution centered at the computed transition energy with an arbitrary width of 0.1 eV and an integrated amplitude equal to the computed oscillator strength.)

Analyzing the absorption energies of the Fn cations as a function of the number of fluorene units in Figure 7.8, we can conclude that both the calculated RC1 and RC2 absorption energies decrease with increasing chain length. This can be understood as an increased delocalization of the charge with the number of fluorene units. The same behavior was found previously for phenylenevinylene[19] and thiophenevinylene[17] radical cations. The calculated red shift of the low-energy band with increasing chain length was also found in experiments performed on shorter oligofluorenes in a solid matrix. For the longer Fn (n=4, 5) cations in a solid matrix the RC1 band shifts to an energy below the instrumental lower limit of 0.6 eV, see Table 7.1 and Figure 7.3. In contrast, the energy of the RC1 band of fluorene cations in solution does not shift to lower energy on increasing the chain length from 3 to 5 fluorene units. This is attributed to a larger amount of disorder in the torsion angles between the fluorene units in solution, leading to a smaller average electronic coupling between the

orbitals on the monomer units and hence a smaller energy change upon increasing the chain length.

To study to what extent the inter-unit angle of the charged oligofluorenes affects their optical properties, the absorption spectrum of the bifluorene cation was calculated for different inter-unit angles. The angular dependence of the optical absorption spectrum of bifluorene cations is presented in Figure 7.9. The low-energy band (RC1), obtained by TDDFT, shifts to lower energies as the inter-unit angle increases, while the high-energy band (RC2) is blue shifted. This can be understood based on the molecular orbital model illustrated in Figure 7.10. The energies of the RC1 and RC2 electronic transitions are determined by the electronic couplings J and J' between the HOMO and LUMO orbitals, respectively, on the two fluorene monomers. It was found from the TDDFT calculations that the RC1 transition is dominated by an H→P1 excitation. The electronic coupling (J) decreases with increasing the inter-unit angle and becomes zero at 90°. This implies that the energy difference between H and P1 orbitals becomes smaller as the inter-unit angle (θ) increases. It can thus be concluded that an increase of the inter-unit angle (θ) of fluorene units leads to a decrease of the RC1 transition energy (see Figure 7.9). The RC2 electronic transition corresponds mainly to a P1→P2 excitation. The electronic couplings J and J' decrease with increasing the inter-unit angle of the fluorene units. As a concequence the energetic difference RC2 between the P1 and P2 orbitals increases. Thus, the high-energy band (RC2) will be shifted towards higher energies, see Figure 7.9.
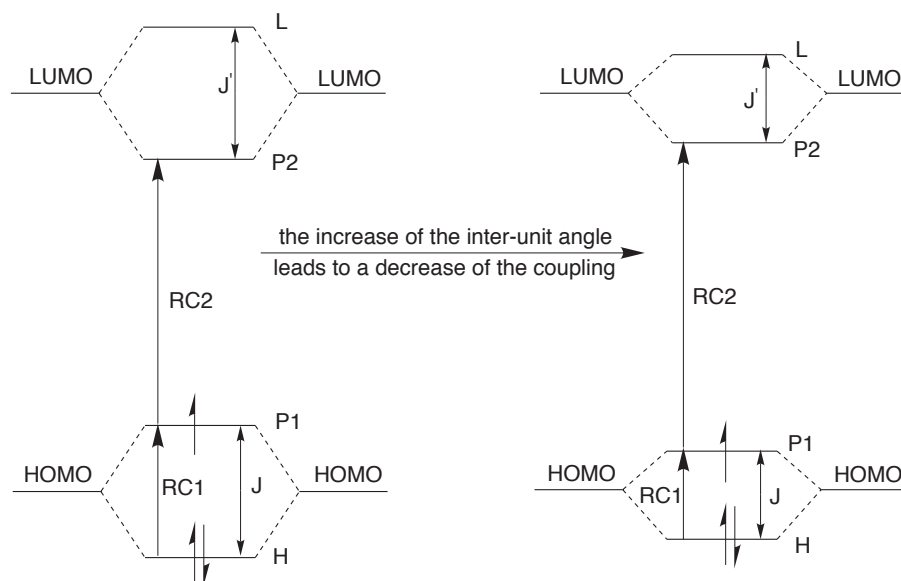

Figure 7.10: Molecular orbital model for oligofluorene cations, which explains the shifting of the absorption bands in Figure 7.9.

Fluorene anions

Table 7.2 shows the calculated and experimental transition energies (ΔE) and the calculated oscillator strength (f) for fluorene anions. The chain length dependence of the transition

energies of fluorene anions is shown in Figure 7.11. The RA1 transition energies, as calculated by TDDFT, shift to lower values with increasing chain length, which suggests that the charge delocalizes along the oligomer chain. The measurements performed on shorter Fn (n=2, 3) oligomers in a solid matrix reproduce the red shift of the transitions at low energy with increasing the number of fluorene units. For the longer Fn (n=4, 5) anions in a solid matrix the RA1 band exceeds the accessible experimental range towards lower energies. The chain length dependence of the lower absorption band RA1 of the negatively charged oligofluorene cannot be obtained from the measurements performed in solution.

As mentioned in section 7.4.1, no absorption band was observed for the monomer radical anion in solution or solid matrix. The TDDFT calculations yield an electronic transition at 2.24 eV in the absorption spectrum of the F1 anion. According to the calculations, this electronic transition is dominated by excitation of an electron from the singly occupied molecular orbital (P2) to the third empty molecular orbital (L+2). Note that the calculated oscillator strength of the F1 electronic transition is very small (0.13 in Table 7.2) and could be below the experimental sensitivity.

A low-energy band consisting of different peaks (with maxima at 0.82, 0.99, and 1.14 eV) is observed for the fluorene dimer (DHF2) in solid matrix (see Figure 7.4). The TDDFT calculations on F2 give two electronic transitions at low energy (RA1 at 1.24 eV and RA1' at 1.48 eV) and one at high energy (RA2 at 2.74 eV). Thus, according to the TDDFT calculations, the three well-resolved peaks at low energy in the experimental spectrum of the DHF2 anion can be attributed to two different electronic transitions (RA1 and RA1') with the lowest electronic transition (RA1) having an additional vibrational transition. The lowest energy transition (RA1) was found to be dominated by excitation of an electron from the singly occupied molecular orbital (P2) to the lowest unoccupied molecular orbital (L). The second low-energy transition (RA1') corresponds mainly to a P2→L+2 excitation, similar to that of the fluorene monomer anion. The high-energy transition (RA2) is dominated by a P1→P2 excitation.
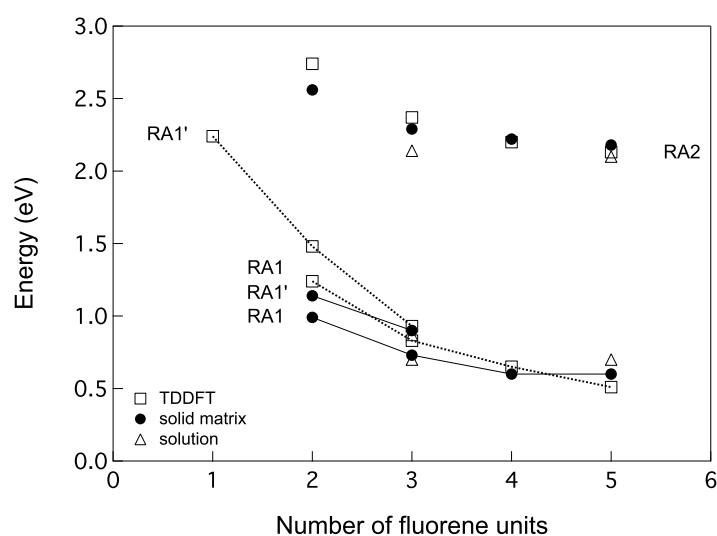

Figure 7.11: Chain length dependence of the transition energies for fluorene radical anions.

For the F3 radical anion both calculations and measurements yield two absorption bands at low energy (RA1 and RA1'). According to the TDDFT calculations, there is only one electronic transition at higher energy (RA2). This means that the two absorption peaks from the experimental spectra of the F3 anion correspond to different vibrational transitions belonging to the same electronic excitation.

For longer Fn (n>3) radical anions the TDDFT calculations predict two electronic transitions, from which it can be concluded that the additional peaks in the experimental spectra are due to different vibrational transitions.

The data in Table 7.2 and Figure 7.11 show that the experimental transition energies of Fn and DHFn anions are in general reproduced by the TDDFT calculations.

7.5 Summary and conclusions

A combined experimental and theoretical study of the optical properties of charged oligofluorenes was carried out. Experiments were performed on oligofluorenes in solution and in a solid-matrix at low temperature. Positive and negative charges in solution were generated by irradiation with high-energy electrons from a Van de Graaff accelerator, while the charges in the solid-matrix were created by γ irradiation. The charged species were detected by time-resolved VIS/NIR spectroscopy in the range of 0.6-2.8 eV. The experimental spectra exhibit distinct absorption bands at lower and higher energy with different vibrational transitions.

Quantum chemical calculations were performed on the cations and anions of oligofluorenes. The geometries of the charged oligofluorenes were optimized using density functional theory (DFT). The geometry deformations and charge distribution were found to be delocalized along the entire oligomer chain without indication of polaron formation.

The optical absorption spectra of the charged fluorene oligomers were calculated with time-dependent density functional theory (TDDFT). Calculations performed for the charged fluorene dimer show that the optical absorption spectra are dependent on the inter-unit angle between the two-fluorene units. Therefore we have studied the potential energy profiles for rotation around the inter-unit bond. It was found that charged oligofluorenes have a much more planar structure than in the neutral state.

The TDDFT method predicts a monotonic decrease of the absorption energies with increasing chain length, which suggests an increased delocalization of the charge, as the oligomer chain becomes longer. The calculated monotonic decrease of the absorption energies is less pronounced in the measurements. The good agreement between the theoretical absorption energies and the experimental data for the charged oligofluorenes stimulates the application of the TDDFT method to other charged systems.

7.6 References

(1)   Reese, C.; Roberts, M.; Ling, M.; Bao, Z. *Mater. Today* **2004**, *7*, 20.
(2)   Kraft, A.; Grimsdale, A. C.; Holmes, A. B. *Angew. Chem. Int. Ed.* **1998**, *37*, 402.

(3)   Brabec, C.; Dyakonov, V.; Parisi, J.; Sariciftci, N. S. *Organic Photovoltaics*; Springer: Berlin, 2003.

(4)   Carroll, R. L.; Gorman, C. B. *Angew. Chem. Int. Ed.* **2002**, *41*, 4378.

(5)   Scherf, U.; List, E. J. W. *Adv. Mater.* **2002**, *14*, 477.

(6)   Leclerc, M. *J. Polym. Sci. Part A: Polym. Chem.* **2001**, *39*, 2867.

(7)   Pogantsch, A.; Wenzl, F. P.; List, E. J. W.; Leising, G.; Grimsdale, A. C.; Mullen, K. *Adv. Mater.* **2002**, *14*, 1061.

(8)   Kulkarni, A. P.; Jenekhe, S. A. *Macromolecules* **2003**, *36*, 5285.

(9)   Gruber, J.; Li, R. W. C.; Aguiar, L. H. J. M. C.; Benvenho, A. R. V.; Lessmann, R.; Hummelgen, I. A. *J. Mater. Chem.* **2005**, *15*, 517.

(10)   Belletete, M.; Ranger, M.; Beaupre, S.; Mario, L.; Durocher, G. *Chem. Phys. Lett.* **2000**, *316*, 101.

(11)   Redecker, M.; Bradley, D. D. C. *Appl. Phys. Lett.* **1999**, *74*, 1400.

(12)   Cornil, J.; Beljonne, D.; Bredas, J. L. *J. Chem. Phys.* **1995**, *103*, 834.

(13)   Cornil, J.; Belijonne, D.; Bredas, J. L. *J. Chem. Phys.* **1995**, *103*, 842.

(14)   Ottonelli, M.; Moggio, I.; Musso, G. F.; Comoretto, D.; Cuniberti, C.; Dellepiane, G. *Synth. Met.* **2001**, *124*, 179.

(15)   Grozema, F. C.; Candeias, L. P.; Swart, M.; van Duijnen, P. T.; Wildeman, J.; Hadziiannou, G.; Siebbeles, L. D. A.; Warman, J. L. *J. Chem. Phys.* **2002**, *117*, 11366.

(16)   Hirata, S.; Head-Gordon, M.; Szczepanski, J.; Vala, M. *J. Phys. Chem. A* **2003**, *107*, 4940.

(17)   Grozema, F. C.; van Duijnen, P. T.; Siebbeles, L. D. A.; Goossens, A.; de Leeuw, S. W. *J. Phys. Chem. B* **2004**, *108*, 16139.

(18)   Ye, A.; Shuai, Z.; Kwon, O.; Bredas, J. L.; Beljonne, D. *J. Chem. Phys.* **2004**, *121*, 5567.

(19)   Fratiloiu, S.; Candeias, L. P.; Grozema, F. C.; Wildeman, J.; Siebbeles, L. D. A. *J. Phys. Chem. B* **2004**, *108*, 19967.

(20)   Fratiloiu, S.; Grozema, F. C.; Siebbeles, L. D. A. *J. Phys. Chem. B* **2005**, *109*, 5644.

(21)   Dudek, S. P.; Pouderoijen, M.; Abbel, R.; Schenning, A. P. H. J.; Meijer, E. W. *J. Am. Chem. Soc.* **2005**, *127*, 11763.

(22)   Koizumi, Y.; Seki, S.; Acharya, A.; Saeki, A.; Tagawa, S. *Chem. Lett.* **2004**, *33*, 1290.

(23)   Seki, S.; Yoshida, Y.; Tagawa, S.; Asai, K. *Macromolecules* **1999**, *32*, 1080.

(24)   Te Velde, G.; Bickelhaupt, F. M.; Baerends, E. J.; Guerra, C. F.; van Gisbergen, S. J. A.; Snijders, J. G.; Ziegler, T. *J. Comput. Chem.* **2001**, *22*, 931.

(25)   Vosko, S. H.; Wilk, L.; Nusair, M. *Can. J. Phys.* **1980**, *58*, 1200.

(26)   Jensen, F. *Introduction to Computational Chemistry*; John Wiley & Sons Ltd.: Chichester, 1999.

(27)   Becke, A. D. *Phys. Rev. A* **1988**, *38*, 3098.

(28)   Perdew, J. P. *Phys. Rev. B* **1986**, *33*, 8800.

(29)   Kong, J.; White, C. A.; Krylov, A. I.; Sherrill, D.; Adamson, R. D.; Furlani, T. R.; Lee, M. S.; Lee, A. M.; Gwaltney, S. R.; Adams, T. R.; Ochsenfeld, C.; Gilbert, A. T. B.; Kedziora, G. S.; Rassolov, V. A.; Maurice, D. R.; Nair, N.; Shao, Y.; Besley, N. A.; Maslen, P. E.; Korambath, J. P.; Baker, J.; Byrd, E. F. C.; van Voorhis, T.; Oumi, M.; Hirata, S.; Hsu, C.; Ishikawa, N.; Florian, J.; Warshel, A.; Johnson, B. G.; Gill, P. M. W.; Head-Gordon, M.; Pople, J. A. *J. Comput. Chem.* **2000**, *21*, 1532.

(30)   Lee, C.; Yang, W.; Parr, R. G. *Phys. Rev. B* **1988**, *37*, 785.

(31)   Dunning, T. H. *J. Chem. Phys.* **1989**, *90*, 1007.

(32)   Runge, E.; Gross, E. K. U. *Phys. Rev. Lett.* **1984**, *52*, 997.

(33)   Petersilka, M.; Gossmann, U. J.; Gross, E. K. U. *Phys. Rev. Lett.* **1996**, *76*, 1212.

(34)   Belletete, M.; Beaupre, S.; Bouchard, J.; Blondin, P.; Leclerc, M.; Durocher, G. *J. Phys. Chem. B* **2000**, *104*, 9118.

(35)   Cooper, R.; Thomas, J. K. *J. Chem. Phys.* **1968**, *48*, 5097.

(36)   Schmidt, W. F.; Allen, A. O. *J. Phys. Chem.* **1968**, *72*, 3730.

(37)   Gee, N.; Freeman, G. R. *Can. J. Chem.* **1992**, *70*, 1618.

(38)   Shinsaka, K.; Freeman, G. R. *Can. J. Chem.* **1974**, *52*, 3495.

(39)   Gorman, A. A.; Lovering, G.; Rodgers, M. A. J. *J. Am. Chem. Soc.* **1978**, *100*, 4527.

(40)   Huang, S. S.-S.; Freeman, G. R. *J. Chem. Phys.* **1980**, *72*, 1989.

(41)   Warman, J. M.; Infelta, P. P.; de Haas, M. P.; Hummel, A. *Chem. Phys. Lett.* **1976**, *43*, 321.

(42)   Grozema, F. C.; Hoofman, R. J. O. M.; Candeias, L. P.; de Haas, M. P.; Warman, J. M.; Siebbeles, L. D. A. *J. Phys. Chem. A* **2003**, *107*, 5976.

(43)   Burrows, H. D.; Seixas de Melo, J.; Forster, M.; Guntner, R.; Scherf, U.; Monkman, A. P.; Navaratnam, S. *Chem. Phys. Lett.* **2004**, *385*, 105.

(44)   Burrows, H. D.; da G.Miguel, M.; Monkman, A. P.; Horsburgh, L. E.; Hamblett, I.; Navaratnam, S. *J. Chem. Phys.* **2000**, *112*, 3082.

(45)   Jou, F. Y.; Dorfman, L. M. *J. Chem. Phys.* **1973**, *58*, 4715.

(46)   Tran-Thi, T. H.; Koulkes-Pujo, A. M. *J. Phys. Chem.* **1983**, *87*, 1166.

(47)   Baxendale, J. H.; Beaumond, D.; Rodgers, M. A. J. *Int. J. Radiat. Phys. Chem.* **1970**, *2*, 39.

(48)   Dodelet, J.-P.; Freeman, G. R. *Can. J. Chem.* **1975**, *53*, 1263.

(49)   Buxton, G. V.; Stuart, C. R. *J. Chem. Soc. Faraday Trans.* **1995**, *91*, 279.

(50)   Schmidt, W. F.; Allen, A. O. *J. Chem. Phys.* **1970**, *52*, 2345.

(51)   Shaede, E. A.; Kurihara, H.; Dorfman, L. M. *Int. J. Radiat. Phys. Chem.* **1974**, *6*, 47.

(52)   Kira, A.; Nakamura, T.; Imamura, M. *J. Phys. Chem.* **1978**, *82*, 1961.

(53)   Kira, A.; Imamura, M. *J. Phys. Chem.* **1978**, *82*, 1966.

(54)   Tirapattur, S.; Belletete, M.; Leclerc, M.; Durocher, G. *J. Mol. Struct. (THEOCHEM)* **2003**, *625*, 141.

(55)   Fesser, K.; Bishop, A. R.; Campbell, D. K. *Phys. Rev. B* **1983**, *27*, 4804.

(56)   Furukawa, Y. *Synth. Met.* **1995**, *69*, 629.

(57)   Thormann, T.; Rogojerov, M.; Jordanov, B.; Thulstrup, E. W. *J. Mol. Struct.* **1999**, *509*, 93.

Chapter 8

Opto-Electronic Properties of Fluorene-Based Derivatives as Precursors for Light-Emitting Diodes[*]

Copolymers versus Co-oligomers

This chapter reports optical absorption spectra of oxidized fluorene copolymers obtained by chemical oxidation with Ce(IV) and by pulse radiolysis experiments in chlorinated solvents. Comparison of the results observed by the two techniques is used to provide spectral data on the copolymer radical ions and information on stability of the oxidized species. In addition a detailed quantum chemical characterization is presented, concerning the electronic and optical properties of three series of charged oligomers containing alternating fluorene and phenylene or thienylene or benzothiadiazole units, respectively. The introduction of the co-monomer strongly influences the optical properties, leading to a red shift in the absorption spectra of the charged oligomers. This shift is more pronounced in case of fluorene benzothiadiazole anions due to the strong electron accepting character of the benzothiadiazole moieties. The charge distribution of the fluorene benzothiadiazole anion is different from that corresponding to fluorene phenylene and fluorene thienylene anions. The negative charge of the latter oligomers is evenly distributed over the fluorene units, while the former oligomer localizes the negative charge on the benzothiadiazole units. The charge distribution correlates with the optical absorption spectra. When the positive charge is localized on a different unit than the negative charge, the cation and anion spectra are different. Similar spectra are obtained if both the positive and negative charges are localized on the same unit.

8.1 Introduction

The development of tunable and flexible light-emitting diodes (LEDs) from conjugated polymers has received considerable attention in the last years. Fluorene oligomers and polymers are highly fluorescent compounds,[1] which makes them suitable for applications in LEDs. They have good stability due to the rigidly planar biphenyl structure in the fluorene unit. The introduction of substituents at the C-9 position makes fluorene soluble, and thus easy to process from organic solvents. One disadvantage, which limits the use of polyfluorenes in blue-light-emitting diodes, is the difficulty to inject charges in these

materials. In order to improve the charge injection different electron-donating or accepting units have been incorporated into the structure of polyfluorenes. In this way the energy of the HOMO and LUMO levels can be varied, making it easier to inject charges. Using quantum chemical calculations, Yang et al.[2] have shown that the introduction of the electron-donating 3,4-ethylenedioxythiophene units in the backbone increases the HOMO energy, which greatly improves the hole injection. Alternatively, the presence of 1,3,4-oxadiazole moieties leads to a lowering of the LUMO level and thus to an improvement of the electron-accepting properties.[2]

Structural, electronic and optical properties of fluorene copolymers containing phenylene,[3-6] thienylene[3,5,7-9] and benzothiadiazole[10-12] moieties have been investigated experimentally and theoretically. Particular attention has been paid to the application of these copolymers in LEDs. Donat-Bouillud et al.[13] have shown that the electroluminescent properties can be changed to a large extent by incorporating phenylene or thienylene moieties in the fluorene backbone. The spectral emission varies from blue to green or yellow, depending on the composition of the copolymers. Beaupre et al.[14] have synthesized a fluorene-thiophene copolymer, which is promising for applications in orange and red-light-emitting diodes. A bright red polymer light-emitting device was fabricated by Kim et al.[15] with blends of regioregular poly(3-hexylthiophene) and poly (9,9-dioctylfluorene-co-benzothiadiazole) (F8BT) as the emissive layer.
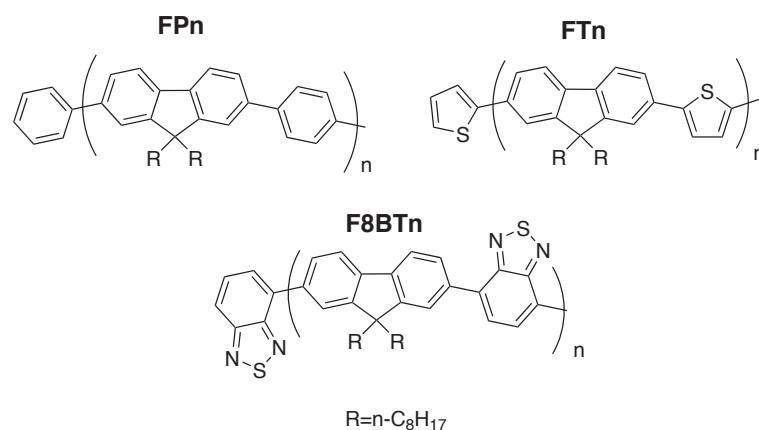

Figure 8.1: Chemical structure of the monomer units of the fluorene-based oligomers studied (n is the number of repeat units).

In order to improve the understanding of the experimental data, quantum chemical calculations have been performed at different levels of theory. *Ab initio* or density functional-based methods have been used to calculate structural properties, ionization potentials, electron affinities, energy gaps and optical absorption spectra of fluorene based co-oligomers.[2-9,12] No experimental or theoretical work has been reported yet on optical absorption of charged fluorene co-oligomers and copolymers. Therefore, this study aims at the investigation of these properties for a better understanding of the effect of introducing different moieties on the fluorene backbone.

Chemical oxidation and reduction have been used to study the charged species of a variety of conjugated polymers and oligomers.[16-21] Initially, one electron oxidized (radical cation) or reduced (radical anion) species are produced. However, it has been shown that multistep oxidation and reduction reactions can occur,[22,23] and, in addition, the initial product can undergo degradation processes,[24-26] such that the first species detected by conventional techniques may not be the one electron oxidized or reduced charge carrier species. In contrast, pulse radiolysis has been shown to be an excellent technique for characterizing the initially formed charge carriers produced on one electron oxidation or reduction.[27,28] Comparison of behaviour of the species prepared by the two techniques provides valuable information on their reactivity, which may be relevant to what happens in devices, and, in particular, to their long term stability.

This chapter presents experimental optical absorption spectra of oxidized species of three fluorene copolymers studied by both chemical oxidation and pulse radiolysis techniques. In order to examine to what extent the nature of charges in fluorene co-oligomers is influenced by adding electron donating or accepting units to the backbone, the absorption spectra of charged fluorene-thienylene, fluorene-phenylene and fluorene-benzothiadiazole oligomers have been studied theoretically. The results are compared with the absorption spectra of the corresponding charged fluorene oligomers.[29] The spectra of charged fluorene-based oligomers can also provide valuable information about the spatial extent of charges along the chain. A detailed discussion about the distribution of an excess positive and negative charge along the fluorene-based oligomers chains is presented. The opto-electronic properties of the fluorene-based oligomers are shown as a function of chain length. This makes it possible to extrapolate the data from oligomers to polymers and to compare these theoretical results with the experimental data. The chemical structures of the fluorene co-oligomers containing phenylene, thienylene and benzothiadiazole moieties are shown in Figure 8.1.

8.2 Experimental details

Details of the synthesis and photophysical properties of the three copolymers used in this study have been given elsewhere.[30-32] The fluorene copolymers were dissolved in carbon tetrachloride (with concentrations less than 10^{-4} M, in terms of monomer unit). Two techniques were tested to prepare the one-electron oxidized species. In the first, the copolymers were subjected to chemical oxidation, adding small quantities of a concentrated solution (50 mM) of the strong oxidant cerium(IV) ammonium nitrate in acetonitrile (or CD_3CN for the near IR region). This has previously been shown to be an excellent technique for the quantitative preparation of the radical cations of a variety of aromatic compounds.[33,34] UV/visible absorption spectra were measured on solutions in 1 cm quartz cuvettes on Shimadzu UV-2100 or Ocean Optics spectrophotometers. For the near infrared region ($\lambda > 850$ nm) a Cary 14 Olis modified spectrometer was used. However, these chemical oxidation studies permit the observation of the radical cations only for a few seconds after they have been formed, and during this time they may undergo secondary reactions. We have, therefore, also used pulse radiolysis technique to prepare and investigate the cations of fluorene copolymers in carbon tetrachloride solutions. The pulse radiolysis experiments were carried out at the Free Radical Research Facility, Daresbury, UK. High-energy electron pulses with

duration of 200 ns up to 2 μs were sent from a 12 MeV linear accelerator to the copolymer solutions. The copolymer solutions were placed in a 2.5 cm optical path length quartz cuvette attached to a flow system. All solutions were bubbled with argon for about 30 minutes before experiments. The experimental setup and radiation chemistry of these solvents has been described in detail elsewhere.[35]

From the chemical oxidation experiments the molar absorption coefficients for the oxidized species were calculated from the slope of the plot of the copolymer absorption values (at the maximum wavelength of absorption corrected for the baseline) *versus* the Ce(IV) concentration values, assuming 100% efficiency in the oxidation process. In pulse radiolysis experiments, molar absorption coefficients were determined as functions of dose from the initial absorbance using tri(*p*-tolyl)amine (TTA, 10 mM) in carbon tetrachloride as dosimeter.[33]

8.3 Computational methodology

The geometries of the three different series of fluorene oligomers were optimized using the Amsterdam Density Functional (ADF) Theory program.[36] The geometry optimizations were performed using the Local Density Approximation (LDA) with exchange and correlation functionals based on Vosko-Wilk-Nusair (VWN) parameterization of electron gas data.[37] The Generalized Gradient Approximation (GGA)[38] corrections by Becke[39] (exchange) and Perdew[40] (correlation) were included. For optimizing the geometries a double zeta plus polarization (DZP) basis set was used.

The electronic absorption spectra of the charged fluorene oligomers were calculated with Time-Dependent Density Functional Theory (TDDFT),[41,42] as implemented in the Q-Chem program.[43] The excitation energies were computed using a correlation consistent[44] polarized Valence Double Zeta (cc-pVDZ) basis set. The Becke (exchange) and the Lee-Yang-Parr (correlation)[45] functional (BLYP) was used.

The distribution of an excess positive and negative charge was calculated using Density Functional Theory (DFT). The charge distribution was obtained from a Mulliken population analysis performed on the same charge density used to calculate the absorption spectra.

8.4 Results and discussion

8.4.1 Experimental optical absorption spectra of one-electron oxidized species

As indicated in the experimental section, copolymer radical cations were prepared initially by chemical oxidation, using as one-electron oxidant, cerium(IV) ammonium nitrate. Figure 8.2 shows the absorption spectra of the species observed upon chemical oxidation of the three fluorene copolymers upon increasing the Ce(IV) concentration. Oxidation of the fluorene phenylene copolymer (PFP) with Ce(IV) induces an absorption band at 480 nm through the proposed reaction
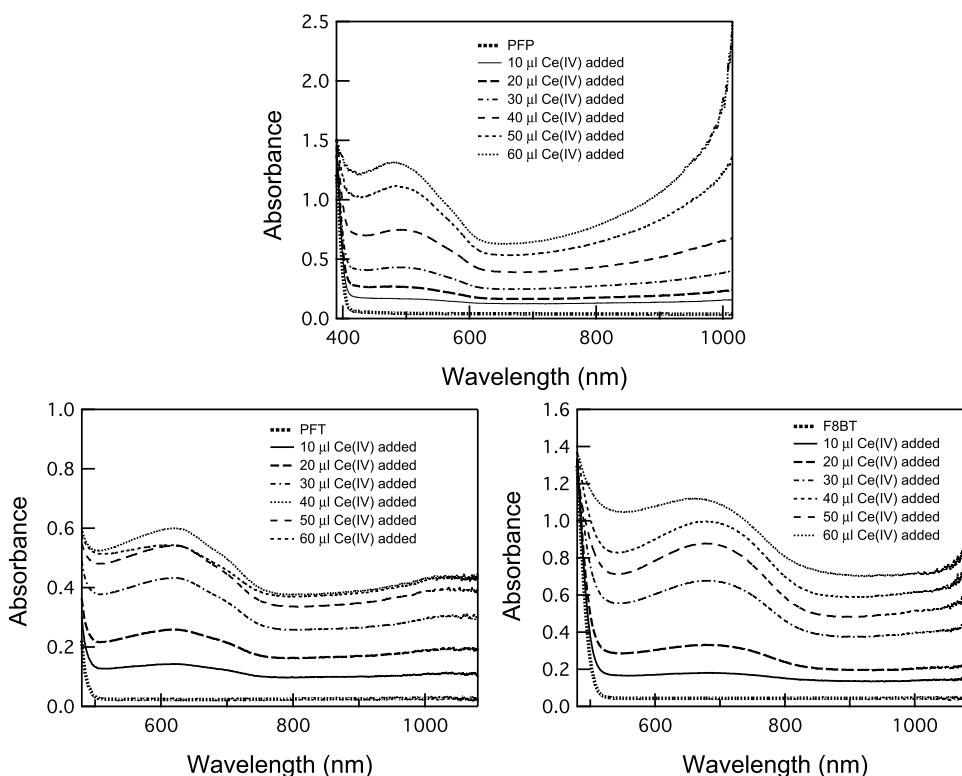
$$Ce(IV) + PFP \rightarrow Ce(III) + PFP^{\bullet+} \tag{8.1}$$

Figure 8.2: Optical absorption spectra of fluorene copolymer cations in solution (3 ml) obtained by adding increasing amounts of cerium (IV) ammonium nitrate in acetonitrile. (The data have been offset vertically to facilitate comparison.)

This absorption becomes more intense upon increasing the amount of Ce(IV). Good evidence for one electron oxidation by this species has previously been presented for a number of systems, including aromatic amines.[33,34] The replacement of the phenyl ring with a thiophene ring, or with a benzothiadiazole unit leads to a considerable red shift of the absorption maximum to 620 nm and 680 nm, respectively. Molar absorption coefficients of the oxidized species of the three copolymers investigated have been calculated as described in section 8.2 and their values and absorption maxima are listed in Table 8.1.

Table 8.1: Absorption maxima and molar absorption coefficients of the one-electron oxidized copolymers determined from pulse radiolysis and chemical oxidation. The rate constants for the kinetics of the decay of the radical cations determined from pulse radiolysis and obtained from chemical oxidation experiments are also presented.

Copolymer	Pulse radiolysis			Chemical oxidation		
	λ_{max} (nm)[a]	ε ($M^{-1}cm^{-1}$)	k (s^{-1})	λ_{max} (nm)[a]	ε ($M^{-1}cm^{-1}$)	k ($M^{-1}s^{-1}$)
PFP	540 (2.30)	2600	1.80×10^5	480 (2.58)	555	see text
PFT	680 (1.82)	5130	3.99×10^5	620 (2.00)	255	36.3
F8BT	510 (2.43)	2460	7.10×10^3	680 (1.82)	510	9.1
	720 (1.72)	1090	6.89×10^3			

[a] Values in eV are given in brackets

For the PFT and F8BT copolymers, the oxidized species decay over several minutes, following pseudo-first-order kinetics. The decay of the PFT cation is shown in Figure 8.3(a). The exponential fit of the decay of this transient gives a lifetime of 35.28 s for an added Ce(IV) concentration of 0.74 mM. This corresponds to pseudo-first-order rate constant (k_{obs}) of 2.84×10^{-2} s^{-1}. The pseudo-first-order rate constants (k_{obs}) increase as a function of the added Ce(IV) concentration (see Figure 8.3(b)). However, according to reaction (1), all the Ce(IV) has been quantitatively converted to Ce(III). The trend, therefore, indicates some more complex decay sequence, possible involving multiple charges on the chain. An empirical fit of the overall kinetic behavior of PFT and F8BT was made to the second-order rate law:

$$i = k[Ce(IV)][X] = k_{obs}[X] \qquad (8.2)$$

where [Ce(IV)] is the added cerium(IV) concentration, [X] represents the oxidized polymer species and k is the apparent second-order rate constant obtained from a plot of k_{obs} against Ce(IV) concentration. Values of k for the two copolymers are given in Table 8.1.
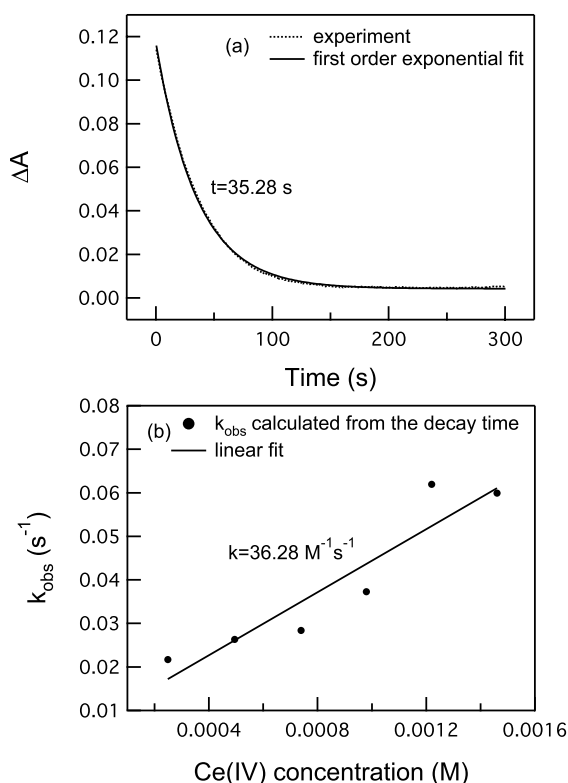

Figure 8.3: (a) Optical absorption transient of the PFT polymer at the absorption maximum, indicating the decay kinetics of the cation. The exponential fit of such transient gives a decay time of 35.28 s for a Ce(IV) concentration of 0.74 mM. (b) Plot of pseudo-first-order rate constants against Ce(IV) concentration. The linear fit (with a poor correlation coefficient 0.934) gives an apparent second-order rate constant of 36 M^{-1}s^{-1}.

For PFP, somewhat different behaviour was observed. At low Ce(IV) concentration (4.95×10^{-4} M), the decay was pseudo-first-order with the rate constant k = 2.90×10^{-3} s^{-1}. Increase of the

Ce(IV) concentration leads to a change of the kinetics, such that at [Ce(IV)] = 1.22×10^{-3} M, the decay could be fitted by a double exponential with fitting constants $k_1 = 7.23 \times 10^{-3}$ s^{-1} and $k_2 = 2.94 \times 10^{-4}$ s^{-1}.

One-electron oxidation of the polymers may be accompanied by side reactions, such as chain scission, leading to polymer degradation.[24-26] In some cases, it is, therefore, difficult to distinguish between the absorption spectrum of the initial positive charge carrier and of a side product. Therefore, pulse radiolysis experiments have been carried out, which allow direct observation of the initially formed positive charge carrier (radical cation). Radiolysis of chlorinated aliphatic solvents is known to quantitatively produce solvent radical cations, and using pulse radiolysis under these conditions, the copolymer radical cations (S$^{\bullet+}$) are selectively generated,[28,33,35] according to the reaction scheme (given for carbon tetrachloride):

$$2CCl_4 \rightarrow CCl_4^{\bullet+} + {}^{\bullet}CCl_3 + Cl^- \tag{8.3}$$

$$CCl_4^{\bullet+} + S \rightarrow CCl_4 + S^{\bullet+} \tag{8.4}$$

The optical absorption spectra of copolymer cations obtained by pulse radiolysis are presented in Figure 8.4, while spectral data of the species produced on pulse radiolysis and chemical oxidation are compared in Table 8.1.
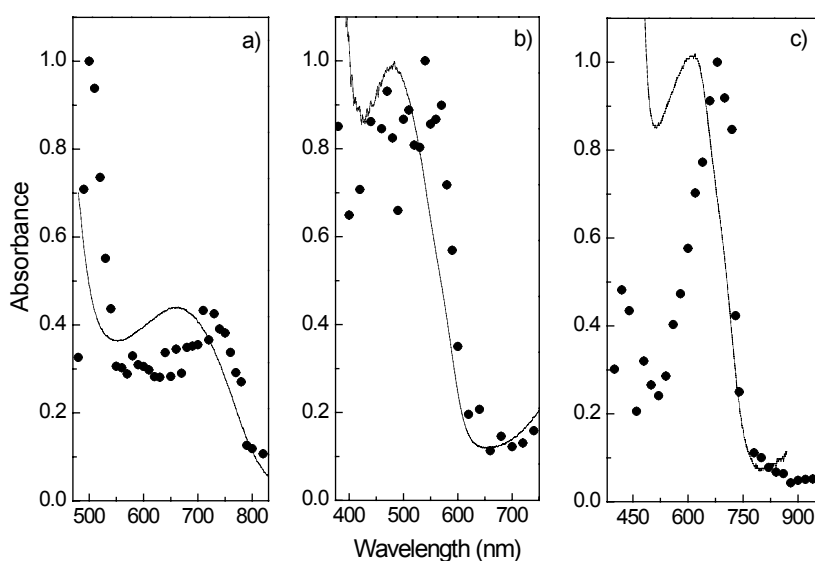
Figure 8.4: Optical absorption spectra of fluorene copolymer cations in solution obtained by pulse radiolysis (dots) compared with their optical absorption spectra obtained by chemical oxidation (line) (a) F8BT, (b) PFP and (c) PFT.

Clear differences are seen in the spectral behavior of the species formed by pulse radiolysis and chemical oxidation. For all three copolymers, the visible absorption band seen in pulse radiolysis is red shifted by 0.1- 0.3 eV relative to that seen by chemical oxidation. In addition, the molar absorption coefficients obtained by pulse radiolysis are at least five times

greater than those obtained by chemical oxidation. Two factors can be assumed to be responsible for this. From the concentrations (in mg/mL) and the average molecular weights of the copolymers,[32] their molar concentrations can be estimated to be less than 10^{-6} M (based on the polymer chain), which is considerably lower than the Ce(IV) concentration. Under these conditions, it is possible to have more than one positive charge on each copolymer chain. In contrast, under the conditions of the pulse radiolysis experiments, the concentrations of solvent radical cation produced are lower than those of the copolymers, such that, on average, each chain contains at most one positive charge. We believe that the presence of multiple charged copolymers may explain the differences in molar absorption coefficients and in the absorption maxima. Studies in progress show that upon oxidation, fluorene based systems may undergo chemical degradation via bond cleavage. This may lead to a decrease of the conjugation length, and to the observed blue shift in absorption. Formation of such defects may have implications on the long term stability of devices containing these polymers. In addition, pulse radiolysis of fluorene polymers using time-resolved microwave conductivity detection has shown that positive charges on fluorene based polymers have very high mobility.[46] It is possible that for the species produced by chemical oxidation there may be interactions between the multiple charged states on the polymer chain to produce other states.

In contrast, the species produced on pulse radiolysis in carbon tetrachloride can be identified with the initial one electron positive charge carrier, and used for comparison with the theoretical calculations of the spectra.

8.4.2 Computational results

In order to gain more insight in the nature of positive charges on fluorene co-polymers and to understand the changes in optical absorption spectra when different moieties are introduced in the fluorene backbone, a DFT study of the charged fluorene co-oligomers have been performed. Geometry deformations, distributions of excess positive and negative charges and optical absorption spectra were calculated for the cations and anions of the following series of fluorene-based oligomers: fluorene-phenylene (FPn), fluorene-thienylene (FTn) and fluorene-benzothiadiazole (F8BTn). In the calculations the substituents at the fluorene 9-position were taken to be hydrogen. This approximation simplifies the calculation without affecting the accuracy. All calculations were performed on symmetric oligomers. The shortest oligomer of each series contains one fluorene unit functionalized with two phenylene, thienylene and benzothiadiazole units, respectively.

8.4.2.1 Geometry deformations and charge distributions along chains of fluorene-based oligomers

The distribution of excess positive and negative charge along chains of fluorene-based oligomers will be discussed in terms of fluorene units (containing 13 C atoms), phenylene units (containing 6 C atoms), thienylene units (containing 4 C atoms and one S atom) and benzothidiazole units (with 6 C atoms, 2 N atoms and one S atom). The distribution of an excess positive or negative charge was calculated as the difference between the charges of the

atoms in the cations or anions, and in the neutral molecules. The DFT results are described in detail below for the three series of oligomers with varying chain length.

Fluorene phenylene oligomers

The geometries of fluorene phenylene oligomers were optimized as described in section 8.3. Both neutral and charged FPn have a nonplanar structure. For example, the dihedral angle between the fluorene and phenylene units is 42.4° for neutral FP3. In case of the FP3 cation and anion, the inter-unit angle becomes smaller: 36.3° and 31.2°, respectively.
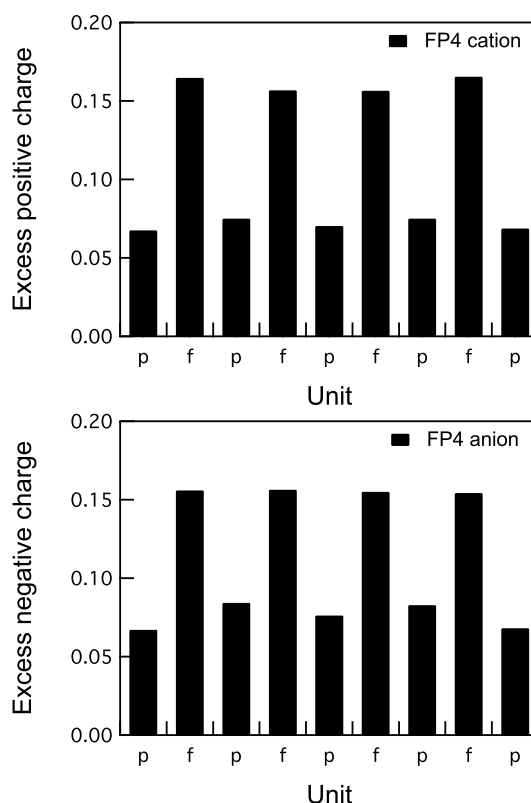

Figure 8.5: Distribution of an excess positive and negative charge in the FP4 oligomer. Fluorene units are indicated as f, while phenylene units are indicated as p.

In Figure 8.5 the calculated distribution of an excess positive and negative charge is presented for the fluorene phenylene tetramer. Similar results were found for the fluorene phenylene oligomers with other chain lengths. The phenylene units carry a similar amount of charge, which is lower than the charge on the fluorene units. The higher amount of positive charge on the fluorene unit coincides with the lower ionization potential of this unit (7.91 eV[47]) in comparison with that of the phenylene units (9.24 eV[48]). The DFT results suggest that both the excess positive and negative charges are evenly distributed along the chains. Taking into consideration that one fluorene unit consists of two phenylene units, it is found that the positive and negative charges are equaly distributed over the fluorene phenylene

chains, indicating a complete delocalization of the charge. This is similar to previous results on phenylenevinylene[49,50] and fluorene[29] oligomers.

Fluorene thienylene oligomers

DFT geometry optimization indicates a smaller value for the inter-unit angle of fluorene thienylene oligomers in comparison with the one of the fluorene phenylene oligomers. For FT3 neutral, cation and anion the angles are 27.9°, 23.7° and 20.3°, respectively. As found for fluorene phenylene oligomers, the inter-unit angle decreases slightly upon introduction of a charge.

Figure 8.6: Distribution of an excess positive and negative charge in the FT4 oligomer. Fluorene units are indicated as f, while thienylene units are indicated as t.

The distribution of an excess positive and negative charge of fluorene thienylene tetramer (see Figure 8.6) is similar to that of the fluorene phenylene tetramer. The charge is delocalized along the entire chain, the fluorene units carry a higher amount of charge than the thienylene units. For positive charges this effect is explained by a lower ionization potential of the fluorene units (7.91 eV[47]) than the ionization potential of the thienylene unit (8.85 eV[51]).

Fluorene benzothiadiazole oligomers

The DFT geometry optimization shows that the inter-unit angle for the F8BT1 oligomer in its neutral state is 45.5^o, the cation has an inter-unit angle of 35.9^o, while the angle for the F8BT1 anion is 41.9^o. This is in contrast with the FPn and FTn oligomers, where the inter-unit angle corresponding to the cation is larger than the angle for the anion.

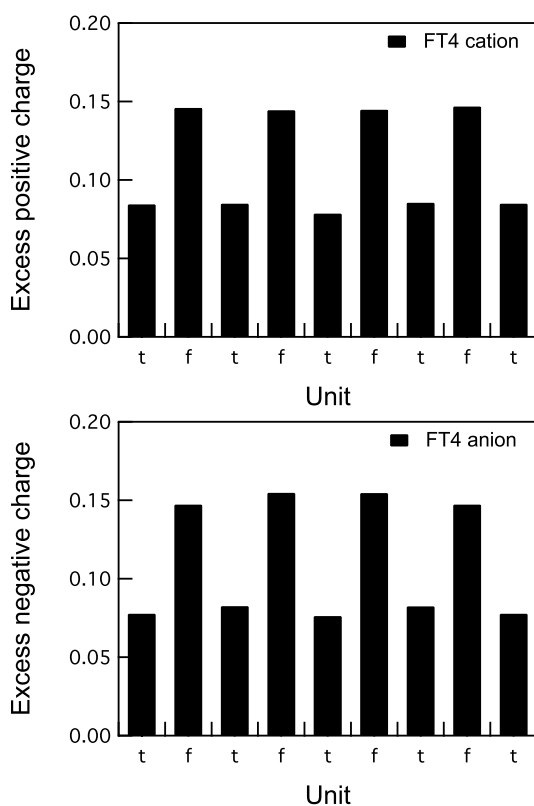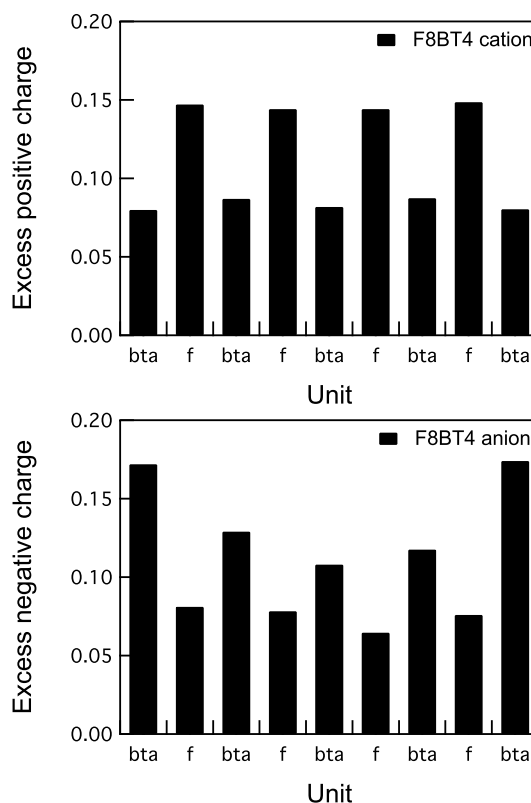**Figure 8.7**: Distribution of an excess positive and negative charge in the F8BT4 oligomer. Fluorene units are indicated as f, while benzothiadiazole units are indicated as bta.

When the thienylene or phenylene units are replaced with benzothiadiazole units the charge distribution of an excess positive charge is quite different from the charge distribution of an excess negative charge. This is due to the strong electron accepting character of the benzothiadiazole unit. The DFT charge distribution of the positively charged fluorene benzothiadiazole tetramer shows that the fluorene units carry a higher amount of charge than the benzothiadiazole units (see the first graph of Figure 8.7). About 58% of the positive charge is distributed over the fluorene units, while the benzothiadiazole units carry 42%. In contrast, for the F8BT4 anion the highest amount of charge is present on the benzothiadiazole units (70%) (see the second graph of Figure 8.7). Moreover, the excess negative charge is not uniformly distributed over the benzothiadiazole units, but the charge has a tendency to localize towards the edges of the tetramer.

8.4.2.2 Calculated optical absorption spectra of charged fluorene-based oligomers

Optical absorption spectra have been calculated for the three series of oligomers using Time-Dependent Density Functional Theory (TDDFT).

Fluorene phenylene oligomers

The calculated transition energies for fluorene phenylene cations are presented in Table 8.2, together with the oscillator strength and the composition of the excited states. In Figure 8.8(a) the absorption maxima of FPn cations are shown as a function of chain length. The maximum of absorption decreases with increasing chain length, indicating delocalization of the positive charge along the chain. A similar monotonous decrease of the transition energies with increasing chain length was previously found from TDDFT calculations on phenylenevinylene[49,50] and fluorene[29] cations.

Table 8.2: Calculated transition energies, oscillator strengths and relative contribution from excited state configuration for cations of fluorene phenylene oligomers (FPn). Only the transitions with an oscillator strength higher than 0.1 are given.

Oligomer	Band	Energy (eV)	Oscillator strength	Relative contribution of excited state configuration
FP1	RC1	1.22	0.42	0.98(H→P1)
	RC2	2.94	0.71	0.91(P1→P2)
FP2	RC1	0.71	0.85	1.13(H→P1)
	RC2	2.48	0.79	0.92(P1→P2)
FP3	RC1	0.46	0.99	1.25(H→P1)
	RC2	2.38	0.67	0.94(P1→P2)
FP4	RC1	0.33	1.04	1.37(H→P1)
FP5	RC1	0.25	0.98	1.51(H→P1)

TDDFT indicates that the low energy absorption (RC1) is the most intense (with the highest oscillator strength) except for the shortest oligomer (FP1 cation). The optical absorption spectra of fluorene phenylene cations can be discussed using a molecular orbital model, shown schematically in Figure 8.9(a). This model considers that adding or removal of an electron introduces additional transitions with lower energy than the one of the neutral compound. Since the molecular orbital model is derived from the polaron model[52] the energy levels between additional transitions will be named after the polaronic levels, P1 and P2. According to this model, in fluorene phenylene cations the P1 level is singly occupied, while P2 represents the lowest unoccupied molecular orbital. The highest doubly occupied molecular orbital is indicated as H, while the second empty level for cations is denoted L (see Figure 8.9(a)). In the last column of Table 8.2 the relative contributions of excited state configurations are presented in terms of this model. The lowest transition (RC1) of FPn cations is dominated by the configuration in which an electron from the highest doubly occupied molecular orbital is excited to the singly occupied molecular orbital (H→P1). Experimentally, it was not possible to see this lowest energy transition in the pulse radiolysis

measurements due to lack of suitable detectors for the near infrared region. However, evidence of its presence comes from the chemical oxidation studies. The second RC2 transition corresponds mainly to excitation of an electron from the singly occupied molecular orbital to the lowest unoccupied molecular orbital (P1→P2).
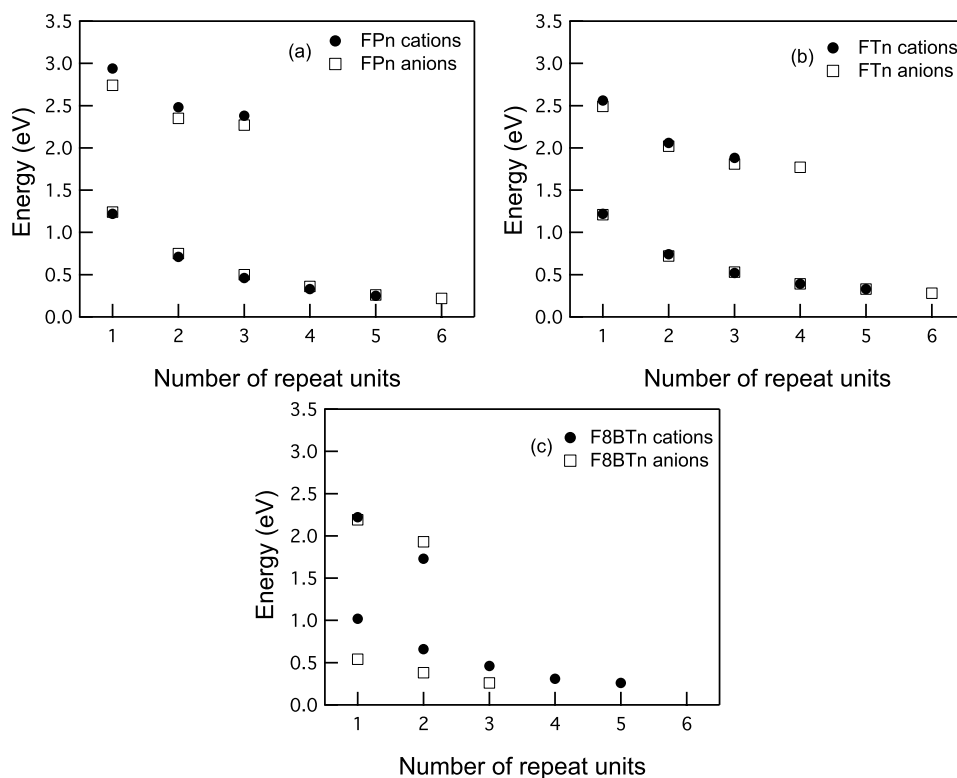

Figure 8.8: Chain length dependence of the transition energies for cations and anions of (a) fluorene phenylene, (b) fluorene thienylene and (c) fluorene benzothiadiazole oligomers.

Table 8.3: Calculated transition energies, oscillator strengths and relative contribution from excited state configuration for anions of fluorene phenylene oligomers (FPn). Only the transitions with an oscillator strength higher than 0.1 are given.

Oligomer	Band	Energy (eV)	Oscillator strength	Relative contribution of excited state configuration
FP1	RA1	1.24	0.46	0.98(P2→L)
	RA2	2.74	0.80	-0.89(P1→P2)
FP2	RA1	0.75	0.96	1.09(P2→L)
	RA2	2.35	0.99	0.97(P1→P2)
FP3	RA1	0.50	1.16	-1.20(P2→L)
	RA2	2.27	0.81	0.96(P1→P2)
FP4	RA1	0.36	1.21	1.32(P2→L)
FP5	RA1	0.26	1.13	1.45(P2→L)
FP6	RA1	0.22	1.28	1.51(P2→L)

Similar results have been obtained for fluorene phenylene anions. The maxima of the optical absorption shift as function of chain lengths, see Table 8.3 and Figure 8.8(a). The optical absorption transitions of phenylene fluorene anions are explained using the molecular orbital model illustrated in Figure 8.9(b). According to the TDDFT results the low energy band (RA1) in the optical absorption spectra of FPn anions is due to an excitation of an electron from the singly occupied molecular orbital (P2) to the lowest unoccupied molecular orbital (L): (P2→L). The second transition in the spectra from Table 8.3 corresponds mainly to a transition of an electron from the highest doubly occupied molecular orbital (P1) to the singly occupied molecular orbital (P2): (P1→P2). The composition of excited states of FPn anions and cations are very similar to those calculated for charged phenylenevinylene[50,53] and fluorene oligomers.[29]
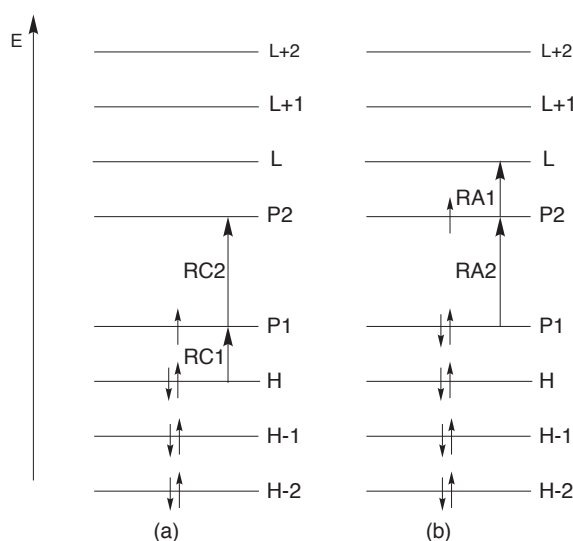
Figure 8.9: Molecular orbital model for (a) cations and (b) anions for fluorene-based oligomers. The electronic transitions are also represented.

The RC2 and RA2 transitions could not be calculated for FPn (n>3) due to the limited computer memory available. The similarity between the results obtained for fluorene phenylene cations and anions is reflected both in the optical absorption spectra and in the charge distribution.

Fluorene thienylene oligomers

The results obtained for fluorene thienylene oligomers are similar to those obtained for fluorene phenylene oligomers. Both cations and anions of the FTn oligomers exhibit two absorption bands, whose energies decrease with increasing chain length. The values of the absorption maxima are shown in Tables 8.4 and 8.5 and in Figure 8.8(b). The RC1 transition is mainly due to an H→P1 excitation, while RC2 is dominated by a P1→P2 excitation. The FTn anion absorption features are very similar to those for the FPn anions.

Fluorene benzothiadiazole oligomers

The absorption maxima of F8BTn cations and anions are presented in Tables 8.6 and 8.7, respectively, and in Figure 8.8(c).

Table 8.4: Calculated transition energies, oscillator strengths and relative contribution from excited state configuration for cations of fluorene thienylene oligomers (FTn). Only the transitions with an oscillator strength higher than 0.1 are given.

Oligomer	Band	Energy (eV)	Oscillator strength	Relative contribution of excited state configuration
FT1	RC1	1.22	0.37	0.99(H→P1)
	RC2	2.56	0.91	0.94(P1→P2)
FT2	RC1	0.74	0.83	0.62(H→P1)
	RC2	2.06	0.85	0.92(P1→P2)
FT3	RC1	0.52	1.16	1.18(H→P1)
	RC2	1.88	0.85	0.90(P1→P2)
FT4	RC1	0.39	1.33	1.28(H→P1)
FT5	RC1	0.33	1.73	-1.35(H→P1)

Table 8.5: Calculated transition energies, oscillator strengths and relative contribution from excited state configuration for anions of fluorene thienylene oligomers (FTn). Only the transitions with an oscillator strength higher than 0.1 are given.

Oligomer	Band	Energy (eV)	Oscillator strength	Relative contribution of excited state configuration
FT1	RA1	1.21	0.35	0.98(P2→L)
	RA2	2.49	0.63	0.79(P1→P2)+0.54(P2→L+6)
FT2	RA1	0.72	0.78	1.08(P2→L)
	RA2	2.02	1.07	0.96(P1→P2)
FT3	RA1	0.53	1.17	-1.15(P2→L)
	RA2	1.81	1.01	0.94(P1→P2)
FT4	RA1	0.39	1.34	1.25(P2→L)
	RA2	1.77	0.91	0.95(P1→P2)
FT5	RA1	0.33	1.66	-1.32(P2→L)
FT6	RA1	0.28	1.83	1.39(P2→L)

For the F8BT1 cation the low energy band (RC1) is at 1.02 eV, while the F8BT1 anion absorbs at 0.54 eV (RA1). The energy difference of approximately 0.5 eV between RA1 and RC1 as found for F8BT1 was not observed for the other fluorene series. This energy difference between the F8BT1 cation and anion absorption can be correlated with the very different charge distribution for the anion and cation, as discussed in section 8.4.2.1. It was shown that for F8BTn cations the charge is localized on the fluorene units, while for F8BTn anions most of the charge is distributed over the benzothiadiazole units. This is reflected in different values of the absorption energy of the F8BTn cations and anions. This is in contrast

with the results found for fluorene phenylene and fluorene thienylene oligomers, where the positive and negative charges are localized on the same unit (fluorene), leading to a similar cation and anion spectra. The energy difference between the transitions for F8BT cations and anions decreases with increasing chain length. This is explained by the fact that the amount of negative charge localized on benzothiadiazole units decreases with increasing chain length from 80% for the F8BT1 anion to 68% for the F8BT5 anion, while the amount of positive charge on the benzothiadiazole units is close to constant (58%) for all chain lengths.

Table 8.6: Calculated transition energies, oscillator strengths and relative contribution from excited state configuration for cations of fluorene benzothiadiazole oligomers (F8BTn). Only the transitions with an oscillator strength higher than 0.1 are given.

Oligomer	Band	Energy (eV)	Oscillator strength	Relative contribution of excited state configuration
F8BT1	RC1	1.02	0.41	1.02(H→P1)
	RC2	2.22	0.24	0.85(P1→P2)
F8BT2	RC1	0.66	0.81	1.10(H→P1)
	RC2	1.73	0.41	0.89(P1→P2)
F8BT3	RC1	0.46	1.02	1.20(H→P1)
F8BT4	RC1	0.31	0.91	1.37(H→P1)
F8BT5	RC1	0.26	1.11	1.45(H→P1)

The optical absorption spectra of charged fluorenes have been calculated previously using TDDFT.[29] The comparison of fluorene spectra with the present calculations leads to the conclusion that the absorption maxima for the fluorene co-oligomers are red shifted.

Table 8.7: Calculated transition energies, oscillator strengths and relative contribution from excited state configuration for anions of fluorene benzothiadiazole oligomers (F8BTn). Only the transitions with an oscillator strength higher than 0.1 are given.

Oligomer	Band	Energy (eV)	Oscillator strength	Relative contribution of excited state configuration
F8BT1	RA1	0.54	0.18	1.35(P2→L)
	RA2	2.19	0.12	0.83(P1→P2)
F8BT2	RA1	0.38	0.34	1.43(P2→L)
	RA2	1.93	0.14	0.64(P1→P2)+0.56(P1→L+1)
F8BT3	RA1	0.26	0.40	1.57(P2→L)

In Figure 8.10 the high-energy band (RC2) of cations of FPn, FTn and F8BTn co-oligomers is plotted as function of the reciprocal value of the number of repeat units. Linear extrapolation of the calculated data on co-oligomers gives absorption energies for the radical cations of PFP, PFT and F8BT copolymers at 2.08 eV (600 nm), 1.55 eV (800 nm) and 1.24 eV (1000 nm), respectively. As discussed in section 8.4.1 and presented in Table 8.1, the energies measured in the chemical oxidation experiments for the PFP, PFT and F8BT copolymers are: 2.58 eV (480 nm), 2.00 eV (620 nm) and 1.82 eV (680 nm). The results of the pulse radiolysis experiments are: 2.30 eV (540 nm) for the PFP radical cation, 1.82 eV

(680 nm) for the PFT radical cation and 1.72 eV (720 nm) for the F8BT radical cation. Comparison of the extrapolated values with those determined by chemical oxidation and pulse radiolysis shows that the calculated transition energies are closest to those found in the pulse radiolysis experiments (only the F8BT cation has the absorption maximum approximately 280 nm lower than found in the pulse radiolysis experiments).
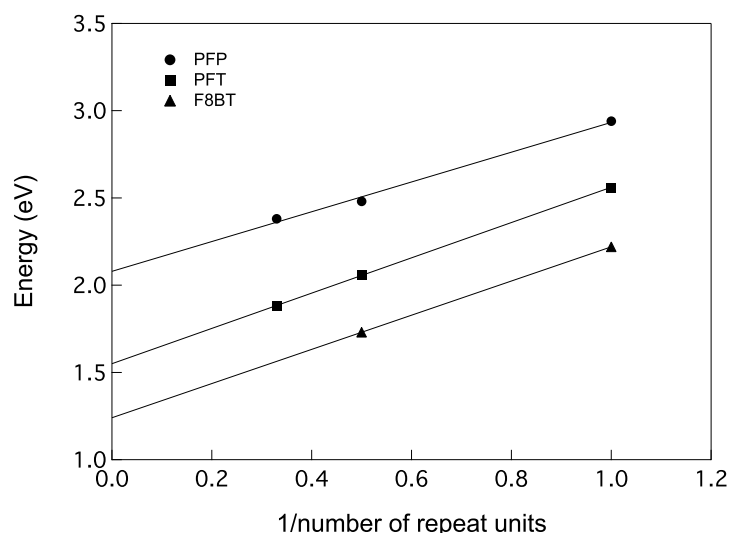

Figure 8.10: RC2 transition energies plotted against the inverse chain length for FPn, FTn and F8BTn. The extrapolation of the linear fit gives the RC2 transition energy for an infinite chain (the corresponding copolymer).

The linear extrapolation of the calculated data yields transition energies that are lower than the experimental data for the copolymers. The difference between the extrapolated results and the pulse radiolysis data reflects the approximate nature of the assumed linear dependence of the absorption energy on the reciprocal of the number of repeat units. Considerable deviations from such a linear dependence can be expected if the charge is not fully delocalized along the chain. Such (partial) localization of the charge can occur because of structural disorder. For the copolymers studied here, substantial disorder in the rotation angles between neighboring units is expected, since the potential energy for rotation around the inter-unit bond between two fluorene units was found to be relatively low.[29] An additional source of localization leading to deviation from a linear behavior can be the self-localization of the charge leading to a polaron.

8.5 Summary and conclusions

In this chapter a combined experimental and theoretical study of structural and opto-electronic properties of charged fluorene-based oligomers and polymers is described. Radical cations of fluorene copolymers were produced by chemical oxidation with Ce(IV) and by pulse radiolysis. Differences in both spectral and kinetic behaviour were observed. It is believed that the species observed in the chemical oxidation experiments correspond to products formed following decay of the initial one-electron oxidized charged species. However, the

introduction of different moieties to the fluorene backbone was found to have a large effect on the optical absorption spectra of the copolymer cations.

DFT calculations on the geometry optimization of charged oligomers show nonplanar structures. An analysis of the charge distribution along the fluorene-based oligomer chains show that for FPn and FTn the charge is evenly distributed over the fluorene units. Similar behavior has been found for F8BTn cations. In contrast, the excess negative charge of F8BTn oligomers is localized on the benzothiadiazole units, with higher amounts on the edges of the chain. This is explained by the electron accepting character of the benzothiadiazole moieties.

TDDFT calculations of the cation and anion optical absorption spectra show a monotonous decrease of the low energy band with increasing chain length. This indicates the delocalization of charge along the chains. RA1 absorption band of F8BTn anions has a lower energy than the RC1 band of F8BTn cations. This correlates with the different distribution of the charge in F8BTn anions and cations. When the positive and negative charges are localized on different units (as in F8BTn cations and anions) the optical absorption spectra are different. If charges are localized on the same units (fluorene units in case of FPn and FTn cations and anions) similar absorption spectra are obtained.

The absorption maxima calculated for cations of the fluorene co-oligomers are red-shifted compared with those for oligomers containing fluorene units only.

Data of the absorption maxima of the positively charged fluorene-based oligomers have been extended to data on polymers. The extrapolation of high-energy data of the oligomers indicates the following absorption maxima: 2.08 eV (600 nm), 1.55 eV (800 nm) and 1.24 eV (1000 nm) for PFP, PFT and F8BT, respectively, which are in reasonable agreement with the values from pulse radiolysis experiments.

TDDFT calculations give also indications about the energy levels, in between which the electronic transitions take place. In this context TDDFT predicts that the RC1 transition is dominated by an excitation of an electron from H→P1, RC2 corresponds to a P1→P2 excitation, RA1 to P2→L and RA2 to P1→P2, in agreement with previous results found for different charged oligomers.

8.6 References

(1)   Nijegorodov, N. I.; Downey, W. S. *J. Phys. Chem.* **1994**, *98*, 5639.
(2)   Yang, L.; Liao, Y.; Feng, J.-K.; Ren, A.-M. *J. Phys. Chem. A* **2005**, *109*, 7764.
(3)   Belletete, M.; Beaupre, S.; Bouchard, J.; Blondin, P.; Leclerc, M.; Durocher, G. *J. Phys. Chem. B* **2000**, *104*, 9118.
(4)   Belletete, M.; Morin, J.-F.; Beaupre, S.; Leclerc, M.; Durocher, G. *Synth. Met.* **2002**, *126*, 43.
(5)   Tirapattur, S.; Belletete, M.; Leclerc, M.; Durocher, G. *J. Mol. Struct. (THEOCHEM)* **2003**, *625*, 141.
(6)   Gong, Z.; Lagowski, J. B. *J. Mol. Struct. (THEOCHEM)* **2005**, *729*, 211.
(7)   Belletete, M.; Morin, J.-F.; Beaupre, S.; Ranger, M.; Leclerc, M.; Durocher, G. *Macromolecules* **2001**, *34*, 2288.

(8) Poolmee, P.; Ehara, M.; Hannongbua, S.; Nakatsuji, H. *Polymer* **2005**, *46*, 6474.

(9) Yang, L.; Feng, J.-K.; Ren, A.-M. *J. Mol. Struct. (THEOCHEM)* **2006**, *758*, 29.

(10) Grell, M.; Redecker, M.; Whitehead, K. S.; Bradley, D. D. C.; Inbasekaran, M.; Woo, E. P.; Wu, W. *Liq. Cryst.* **1999**, *26*, 1403.

(11) Donley, C. L.; Zaumseil, J.; Andreasen, J. W.; Nielsen, M. M.; Sirringhaus, H.; Friend, R. H.; Kim, J.-S. *J. Am. Chem. Soc.* **2005**, *127*, 12890.

(12) Cornil, J.; Gueli, I.; Dkhissi, A.; Sancho-Garcia, J. C.; Hennebicq, E.; Calbert, J. P.; Lemaur, V.; Beljonne, D.; Bredas, J. L. *J. Chem. Phys.* **2003**, *118*, 6615.

(13) Donat-Bouillud, A.; Levesque, I.; Tao, Y.; D'Iorio, M.; Beaupre, S.; Blondin, P.; Ranger, M.; Bouchard, J.; Leclerc, M. *Chem. Mater.* **2000**, *12*, 1931.

(14) Beaupre, S.; Leclerc, M. *Adv. Funct. Mater.* **2002**, *12*, 192.

(15) Kim, Y.; Bradley, D. D. C. *Curr. Appl. Phys.* **2005**, *5*, 222.

(16) Sprangler, C. W.; Hall, T. J.; Sapochak, L. S.; Liu, P.-K. *Polymer* **1989**, *30*, 1166.

(17) Deussen, M.; Bassler, H. *Chem. Phys.* **1992**, *164*, 247.

(18) Sakamoto, A.; Furukawa, Y.; Tasumi, M. *J. Phys. Chem.* **1994**, *98*, 4635.

(19) Schenk, R.; Gregorius, H.; Mullen, K. *Adv. Mater.* **1991**, *3*, 492.

(20) Furukawa, Y.; Sakamoto, A.; Tasumi, M. *Macromol. Symp.* **1996**, *101*, 95.

(21) Oberski, J. M.; Greiner, A.; Bassler, H. *Chem. Phys. Lett.* **1991**, *184*, 391.

(22) Schenk, R.; Gregorius, H.; Meerholz, K.; Heinze, J.; Mullen, K. *J. Am. Chem. Soc.* **1991**, *113*, 2634.

(23) Gebhardt, V.; Bacher, A.; Thelakkat, M.; Stalmach, U.; Meier, H.; Schmidt, H.-W.; Haarer, D. *Adv. Mater.* **1999**, *11*, 119.

(24) Scott, J. C.; Kaufman, J. H.; Brock, P. J.; DiPietro, R.; Salem, J.; Goita, J. A. *J. Appl. Phys.* **1996**, *79*, 2745.

(25) Gamertih, S.; Nothover, H.-G.; Scherf, U.; List, E. J. W. *Jpn. J. Appl. Phys.* **2004**, *43*, L891.

(26) Narwark, O.; Peetz, R.; Thorn-Csanyi, E.; Burrows, H. D.; Monkman, A. P.; Hamblett, I.; Navaratnam, S. *Chem. Mater.*, *submitted for publication*.

(27) Hoofman, R. O. M.; de Haas, M. P.; Siebbeles, L. D. A.; Warman, J. M. *Nature* **1998**, *392*, 54.

(28) Burrows, H. D.; da G.Miguel, M.; Monkman, A. P.; Horsburgh, L. E.; Hamblett, I.; Navaratnam, S. *J. Chem. Phys.* **2000**, *112*, 3082.

(29) Fratiloiu, S.; Grozema, F. C.; Koizumi, Y.; Seki, S.; Saeki, A.; Tagawa, S.; Dudek, S. P.; Siebbeles, L. D. A. *J. Phys. Chem. B* **2006**, *110*, 5984.

(30) Asawapirom, U.; Guntner, R.; Forster, M.; Farrell, T.; Scherf, U. *Synthesis* **2002**, *9*, 1136.

(31) Charas, A.; Morgado, J.; Martinho, J. M. G.; Alcacer, L.; Lim, S. F.; Friend, R. H.; Cacialli, F. *Polymer* **2003**, *44*, 1843.

(32) Fonseca, S. M.; Pina, J.; Arnaut, L. G.; Seixas de Melo, J.; Burrows, H. D.; Chattopadhyay, N.; Alcacer, L.; Charas, A.; Morgado, J.; Monkman, A. P.; Asawapirom, U.; Scherf, U.; Edge, R.; Navaratnam, S. *J. Phys. Chem. B* **2006**, *110*, 8278.

(33) Burrows, H. D.; Greatorex, D.; Kemp, T. J. *J. Phys. Chem.* **1972**, *76*, 20.

(34) Burrows, H. D.; Castro, R. A. E.; Esteves, M. A.; Gigante, B.; Leitao, M. L. P.; Pauleta, A. C. *Mater. Sci. Forum* **2006**, *504/506*, 8.

(35)   Burrows, H. D.; Seixas de Melo, J.; Forster, M.; Guntner, R.; Scherf, U.; Monkman, A. P.; Navaratnam, S. *Chem. Phys. Lett.* **2004**, *385*, 105.

(36)   Te Velde, G.; Bickelhaupt, F. M.; Baerends, E. J.; Guerra, C. F.; van Gisbergen, S. J. A.; Snijders, J. G.; Ziegler, T. *J. Comput. Chem.* **2001**, *22*, 931.

(37)   Vosko, S. H.; Wilk, L.; Nusair, M. *Can. J. Phys.* **1980**, *58*, 1200.

(38)   Jensen, F. *Introduction to Computational Chemistry*; John Wiley & Sons Ltd.: Chichester, 1999.

(39)   Becke, A. D. *Phys. Rev. A* **1988**, *38*, 3098.

(40)   Perdew, J. P.; Yang, W. *Phys. Rev. B* **1986**, *33*, 8800.

(41)   Runge, E.; Gross, E. K. U. *Phys. Rev. Lett.* **1984**, *52*, 997.

(42)   Petersilka, M.; Gossmann, U. J.; Gross, E. K. U. *Phys. Rev. Lett.* **1996**, *76*, 1212.

(43)   Kong, J.; White, C. A.; Krylov, A. I.; Sherrill, D.; Adamson, R. D.; Furlani, T. R.; Lee, M. S.; Lee, A. M.; Gwaltney, S. R.; Adams, T. R.; Ochsenfeld, C.; Gilbert, A. T. B.; Kedziora, G. S.; Rassolov, V. A.; Maurice, D. R.; Nair, N.; Shao, Y.; Besley, N. A.; Maslen, P. E.; Korambath, J. P.; Baker, J.; Byrd, E. F. C.; van Voorhis, T.; Oumi, M.; Hirata, S.; Hsu, C.; Ishikawa, N.; Florian, J.; Warshel, A.; Johnson, B. G.; Gill, P. M. W.; Head-Gordon, M.; Pople, J. A. *J. Comput. Chem.* **2000**, *21*, 1532.

(44)   Dunning, T. H. *J. Chem. Phys.* **1989**, *90*, 1007.

(45)   Lee, C.; Yang, W.; Parr, R. G. *Phys. Rev. B* **1988**, *37*, 785.

(46)   Grozema, F. C.; Siebbeles, L. D. A.; Warman, J. M.; Seki, S.; Tagawa, S.; Scherf, U. *Adv. Mater.* **2002**, *14*, 228.

(47)   Ruscic, B.; Kovac, B.; Klasinc, L.; Gusten, H. *Z. Naturforsch. A* **1978**, *33*, 1006.

(48)   Nemeth, G. I.; Selzle, H. L.; Schlag, E. W. *Chem. Phys. Lett.* **1993**, *215*, 151.

(49)   Fratiloiu, S.; Candeias, L. P.; Grozema, F. C.; Wildeman, J.; Siebbeles, L. D. A. *J. Phys. Chem. B* **2004**, *108*, 19967.

(50)   Fratiloiu, S.; Grozema, F. C.; Siebbeles, L. D. A. *J. Phys. Chem. B* **2005**, *109*, 5644.

(51)   Klasinc, L.; Sabljic, A.; Kluge, G.; Rieger, J.; Scholz, M. *J. Chem. Soc. Perkin Trans. 2* **1982**, 539.

(52)   Fesser, K.; Bishop, A. R.; Campbell, D. K. *Phys. Rev. B* **1983**, *27*, 4804.

(53)   Grozema, F. C.; Candeias, L. P.; Swart, M.; van Duijnen, P. T.; Wildeman, J.; Hadziiannou, G.; Siebbeles, L. D. A.; Warman, J. L. *J. Chem. Phys.* **2002**, *117*, 11366.

Chapter 9

Charge Delocalization in Phenylenevinylene and Thiophene Oligomers Studied by Hartree-Fock, Density Functional Theory and MP2 Calculations[*]

Effects of Geometry, Electron Correlation, Methoxy Substitution and Spin Contamination on the Charge Distribution

The distribution of an excess positive charge on phenylenevinylene (PV) and thiophene (T) oligomers was studied by Density Functional Theory (DFT), Hartree-Fock (HF) theory and second-order Møller-Plesset perturbation (MP2) theory. The method used for geometry optimization has only minor effects on the charge distribution. In contrast, the quantum chemical method used to calculate the electron density (wave function) for a given geometry, has a large effect on the charge distribution. DFT calculations yield a high degree of charge delocalization, the HF method gives more localized charges, while the results from MP2 calculations are intermediate between those from DFT and HF. For all three methods the introduction of methoxy substituents on a phenylene unit in a PV4 oligomer leads to an increase of the amount of positive charge on the substituted unit. The effect of methoxy substitution is most pronounced for DFT calculations. Comparison of results from restricted and unrestricted HF or MP2 calculations, shows that spin contamination is important and correlates with enhanced localization of the excess positive charge.

9.1 Introduction

Conjugated oligomers can be considered as model systems[1,2] for conjugated polymers with applications in opto-electronic devices (light-emitting diodes,[3] field-effect transistors,[4] photovoltaics,[5] etc.). Advantages of conjugated oligomers over polymers include their well-defined chain length, absence of chain defects, ease of purification and characterization. Introduction of a charge in a conjugated oligomer material can lead to changes of the geometrical structure. A charged defect that induces structural relaxation leading to self-

---

[*] This chapter is based on: S. Fratiloiu, F.C. Grozema and L.D.A. Siebbeles, manuscript in preparation.

localization of the charge, is known as a polaron in solid state physics.[6] The extent to which polaronic effects play a role in conjugated oligomers and polymers is still under debate.[7,8]

According to quantum chemical calculations performed at the Hartree-Fock (HF) level of theory excess, positive charges and associated geometry deformations are localized in the middle of an oligomer chain, which is typical for the formation of a self-localized polaron.[9-11] According to Hartree-Fock calculations, the delocalization length ("size") of a polaron is three units for phenylenevinylene oligomers[8] and five units for thiophene oligomers.[10] This would imply that the optical absorption spectra would not depend on chain length for phenylenevinylene oligomers longer than three units and for oligothiophenes longer than five units. However, the lowest optical transition energy of positively charged dialkoxy-substituted phenylenevinylenes[12] was found to decrease for chain length up to the longest oligomer studied, which contains six units. Such a chain length dependence of the lowest transition energy was also found for thiophene cations up to the longest oligomer studied, which contains twelve thiophene rings.[13]
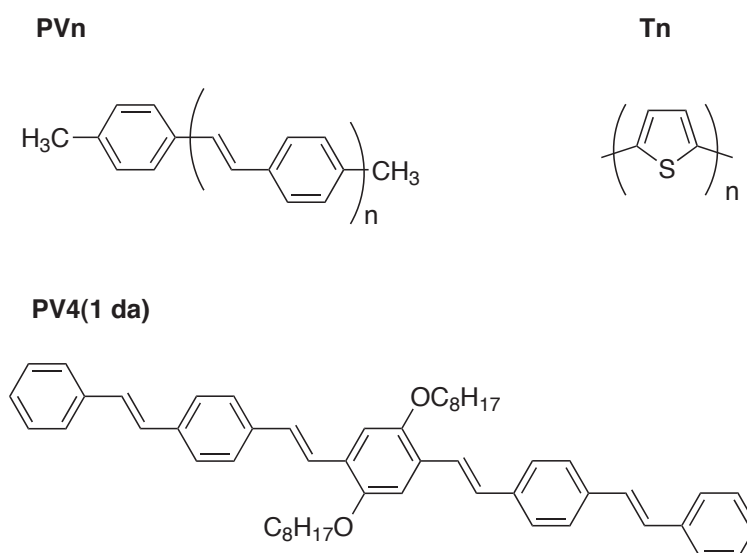

Figure 9.1: Chemical structures of phenylenevinylene (PV) and thiophene (T) oligomers (n is the number of repeat units).

In contrast with the HF results, Density Functional Theory calculations yield that an excess positive charge is delocalized over the entire oligomer chain with no indication of the formation of a self-localized polaron.[8,11,14-16] A possible explanation for the higher degree of delocalization obtained with DFT is the inclusion of electron correlation, which is not taken into account in the Hartree-Fock methods. In DFT the electron correlation is taken into account by an exchange-correlation functional, which includes the non-classical contribution of the electron-electron interaction, the correction for self-interaction and the component of the kinetic energy that is not covered by a non-interacting reference system. Despite these corrections, the exchange-correlation functional, as expressed in DFT, is still approximate. Specifically, the Local Density Approximation assumes that the electronic density can be treated locally as that of a uniform electron gas.[17] In DFT, none of the exchange-correlation

functionals is self-interaction free (there is a non-zero correlation energy for a single electron).[17] In this context, it is of considerable interest to establish whether the higher degree of delocalization is due to the inclusion of electron correlation or that it is an artifact of the DFT method. It has been suggested that the delocalization in DFT is an artifact due to the approximate description of the exchange interaction in the non-hybrid functional.[7,11] Therefore, hybrid functionals (e.g. B3LYP[18] or BHandHLYP) have been used to include partially the exact Hartree-Fock exchange contribution and the exchange-correlation contributions of a gradient-corrected functional.

To investigate the effect of the exchange part of the functional on charge delocalization, the charge distribution of a PV8 anion using the B3LYP functional was calculated previously and compared with that obtained using the BLYP functional.[15] The geometry was optimized with the Becke-Perdew functional. The results obtained with the B3LYP and BLYP functionals are similar with the excess negative charge being delocalized over the entire oligomer chain. In contrast, calculations on thiophene oligomers using the BHandHLYP functional (the exchange part is based on one half of HF exchange and one half of DFT exchange including local (LSDA) and gradient corrected terms (Becke88); correlation is based on the LYP functional) have shown to give a charge distribution that is more localized in the middle of the chain.[7] The geometry of the thiophene oligomers was optimized using the BHandHLYP functional. Until now, it has not been established whether the partial localization of the charge is due to improving the description of the exchange interaction or to the use of a different method for geometry optimization. Therefore, in the present work all calculations were performed for geometries optimized at HF level of theory or by using DFT.

Effects of electron correlation on the charge distribution can be studied by comparison of results from second-order Møller-Plesset perturbation (MP2) theory [19] with those from HF and DFT calculations. The MP2 method takes electron correlation into account on a completely different basis than the DFT approach. MP2 calculations have been performed previously for the radical cation of the thiophene octamer.[7] Specifically, the spin-unresticted MP2 (UMP2) method has been used and the results were similar to those from unrestricted Hartree-Fock calculations. The excess positive charge of the thiophene octamer cation was found to be localized in the middle of the chain. Usually, open-shell systems (e.g. radical cations and anions) are described using unrestricted wave functions. Unrestricted calculations can be affected by spin contamination.[20] Spin contamination of cations and anions corresponds to the mixing with higher-lying quartet and sextet states in the wave function of the doublet state.[21] This effect will be reflected in the charge distribution. In the present work, problems associated with spin contamination are avoided by using a spin-restricted open-shell MP2 method.

The aim of the present study is to investigate the effects of the level of theory (HF, DFT, MP2) on molecular geometry and charge distribution in phenylenevinylene and thiophene oligomers. Charge distributions from restricted calculations are compared with those from unrestricted calculations to gain insight into effects associated with spin contamination. Also the effect of methoxy substituents on the charge distribution of positively charged phenylenevinylene oligomers is studied.

9.2 Computational methodology

Two different series of conjugated oligomers were studied. The chemical structures of the oligomers are presented in Figure 1. The first series consists of phenylenevinylene (PVn, n indicating the number of repeat units) oligomers. In order to gain insight into the effect of substituents on the charge distribution, calculations were also performed on a phenylenevinylene tetramer with methoxy substituents at the central phenylene unit, denoted PV4(1 da). The second series concerns thiophene (Tn, n indicating the number of repeat units) oligomers with a chain length of five or eight repeat units. The oligomer geometries were restricted to C_{2h} or C_{2v} symmetry. The geometries of the neutral and singly charged oligomers were optimized at two levels of theory: Density Functional Theory (DFT) and Hartree-Fock (HF). The DFT optimizations were performed using the Amsterdam Density Functional (ADF) program[22] in the Local Density Approximation (LDA) with exchange and correlation functionals based on Vosko-Wilk-Nusair (VWN) parameterization of electron gas data.[23] The Generalized Gradient Approximation (GGA) corrections by Becke[24] (exchange) and Perdew[25] (correlation) were included. The geometry optimizations were performed with an atomic basis set consisting of Slater-type orbitals (STOs) of double-zeta quality including one set of polarization functions on each atom (DZP basis set in ADF). For cations (which are open-shell systems) restricted DFT geometry optimizations have been performed.

At the Hartree-Fock level of theory the geometries were optimized using the Gaussian 03 program.[26] For the oligomer cations the geometry optimizations were performed with the spin-restricted open shell (ROHF) method. All HF calculations have been performed using the correlation consistent-polarized valence double zeta (cc-pVDZ)[27] basis set, which is of similar quality as the DZP-type used in ADF.

The charge distribution was calculated using DFT, restricted and unrestricted HF and restricted MP2. Note that the cation charge distribution could be calculated with a spin-restricted open-shell MP2 method in the Gaussian program by first performing a ROHF calculation and writing a set of orbitals for alpha and beta spin (which are the same) in a separate file. These orbitals were used next in an unrestricted-MP2 calculation on the same wave function, without carrying out any additional SCF calculation. This method is reliable for the present calculations since there is only one unpaired electron.

The charge distribution was obtained from a Mulliken population analysis. The distribution of charge is discussed in terms of phenylene and vinylene units (for PVs) and thiophene units (for Ts). In the neutral PVs, the phenylene units carry some negative charge, while the vinylene units are positively charged. Therefore the distribution of an excess positive charge was calculated from the difference between the charges on the atoms in the cations and in the neutral molecules.

In order to investigate the effect of the basis set on the charge distribution, the MP2 calculations have also been performed using a smaller basis set, 4-31G, which does not contain any polarization functions.

The effect of spin contamination is studied by comparison of results from restricted and unrestricted HF and MP2 calculations for PV4 and T8.

9.3 Results and discussion

9.3.1 Effect of geometry and electron correlation on the charge distribution

The geometries of phenylenevinylene and thiophene oligomers have been optimized as described in the Computational Section. In Figure 9.2 the charge distribution for the PV4 cation obtained from three different quantum chemical methods (DFT, HF and restricted MP2) is presented for geometries optimized with DFT or HF. It can be seen that the method used for geometry optimization has only little effect on the charge distribution. For a given quantum chemical method, the distribution of charge for the PV4 cation with DFT optimized geometry is similar to the charge distribution of the PV4 cation whose geometry was optimized at the HF level. A similar effect was found by Geskin et al.,[28] who investigated effects of molecular geometry on calculated optical absorption characteristics. They found that the calculated optical absorption spectra depend on the quantum mechanical method used for the electronic density (wave function) calculations, while the computational method employed to optimize the geometry has relatively little effect on the results.
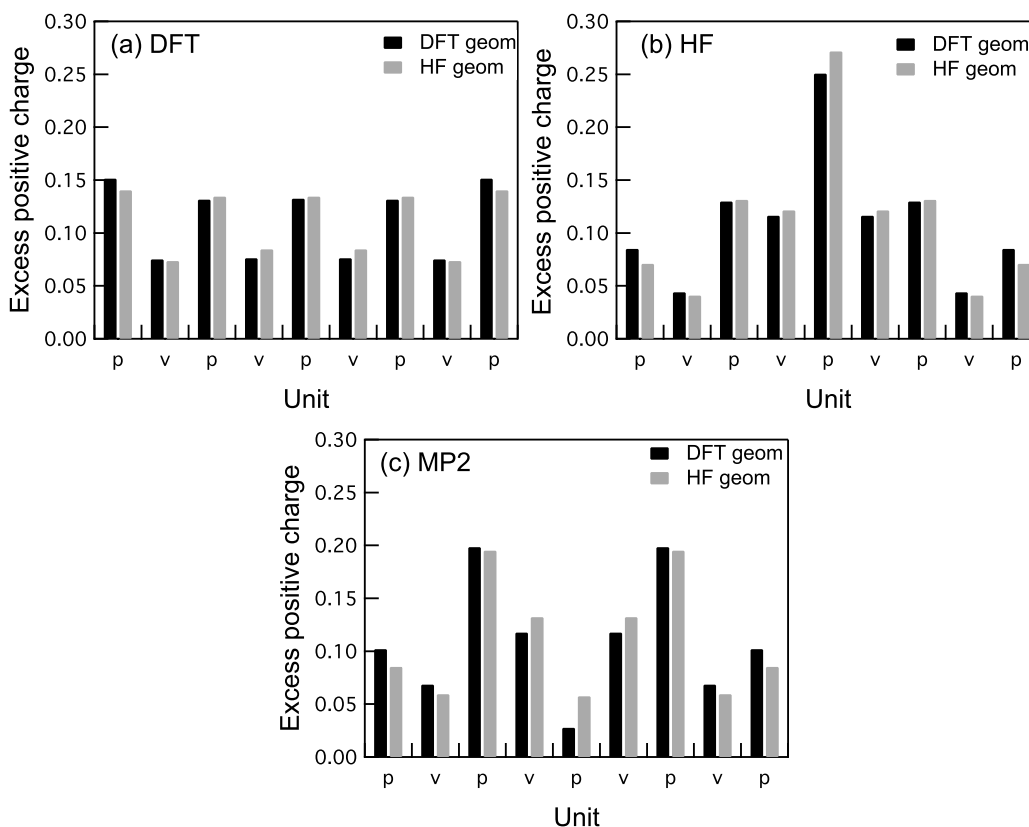

Figure 9.2: Distribution of an excess positive charge over the phenylene (p) and vinylene (v) units in the PV4 oligomer, as calculated using (a) DFT, (b) HF and (c) MP2 for geometries optimized with DFT or HF.

The DFT calculations yield a delocalized excess positive charge along the oligomer chain (see Figure 9.2(a)), in agreement with earlier work.[14] The phenylene units carry a similar amount of charge. The same holds for the vinylene units, but the amount of charge on these

units is smaller than on the phenylene units. This is explained by the lower ionization energy of a benzene molecule (9.24 eV[29]) in comparison with that of an ethylene molecule (10.51 eV[30]). In contrast to the DFT results, the Hartree-Fock distribution of an excess positive charge (see Figure 9.2(b)) is typical for the formation of a polaron in the PV4 cation, in agreement with data from literature.[8] Most of the excess positive charge is localized at the central phenylene unit. The MP2 results differ from those obtained with DFT and HF (see Figure 9.2 (c)). According to the MP2 calculations, most of the excess positive charge localizes on the second and fourth phenylene unit with a smaller amount of charge on the central phenylene unit. The results in Figure 9.2 show, that inclusion of electron correlation in DFT and MP2 calculations leads to a higher degree of delocalization of the excess positive charge. The extent of charge delocalization obtained with MP2 calculations is intermediate between that obtained with DFT and HF. The higher degree of delocalization obtained with DFT as compared with MP2 must be due to the approximations in the description of the exchange-correlation potential in DFT.

The degree of charge delocalization can be quantified in terms of the participation ratio, P, defined as

$$P = \left[\sum_{i=1}^{N} Q_i^2 \right]^{-1} \qquad (9.1)$$

In equation 9.1, Q_i represents the amount of charge present on the i-th unit and N is the number of units. If all the excess charge is localized on a single unit, P becomes 1. If the charge is evenly spread over all N units, than P will be equal to N. Table 9.1 shows the participation ratio for the PV4 cation for different computational methods. The participation ratio obtained with DFT has the highest value, indicating the highest degree of delocalization. The participation ratio obtained from the MP2 calculations is smaller than that for DFT. The smallest participation ratio, which indicates the lowest degree of delocalization, is found for the HF method.

Table 9.1: Participation ratio (*P*) from DFT, HF and MP2 Mulliken population analysis for PV4 and PV4(1 da) cations.

Method	PV4		PV4(1 da)
	P for DFT geometry	*P* for HF geometry	*P* for HF geometry
DFT	8.1	8.4	7.4
HF	7.1	6.6	5.2
MP2	7.3	7.4	7.6

Charge distributions were also calculated for thiophene oligomers. In Figure 9.3(a) the distribution of an excess positive charge is shown for T5, as calculated with restricted MP2, using the cc-pVDZ basis set. The MP2 charge distribution is different from those obtained from DFT or HF calculations,[7,11] analogous to the results for phenylenevinylene cations. According to the MP2 calculations, the excess positive charge is neither completely delocalized over the thiophene units (as found with DFT[7,11]) nor predominantly located on the

central thiophene unit (as found from HF calculations[7,11]). According to the present restricted MP2 calculations for the thiophene pentamer, the amount of charge on the central thiophene unit is smallest (in contrast to HF calculations). Most of the charge is delocalized over the other four thiophene units with a slightly higher amount on the second and fourth units (see Figure 9.3(a)).
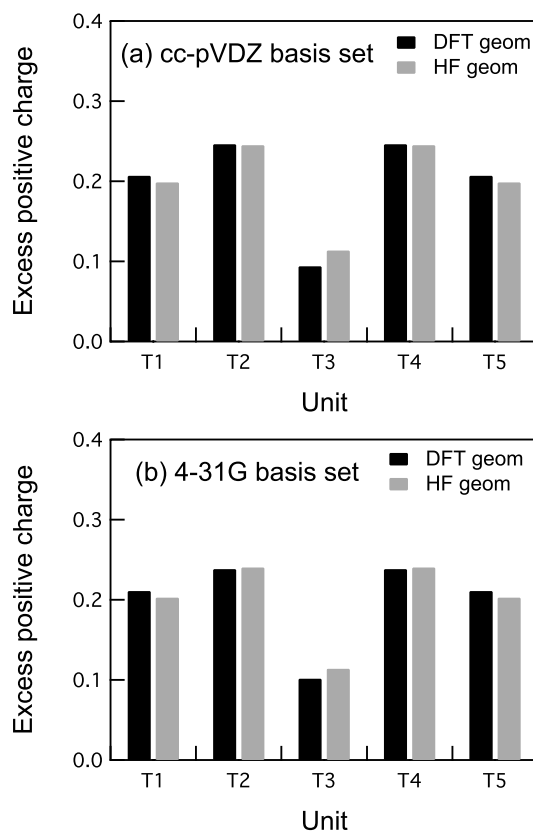

Figure 9.3: Distribution of an excess positive charge over the thiophene (T) units in the T5 oligomer, as calculated using MP2 and the (a) cc-pVDZ or the (b) 4-31G basis set for geometries optimized with DFT or HF.

Moro et al.[11] have shown that an extended basis set does not lead to any significant changes in the optimized geometries. In order to investigate whether the size of the basis set affects the distribution of a charge, MP2 calculations have been also performed for phenylenevinylene and thiophene cations using a smaller basis set, 4-31G, which does not account for polarization effects. The charge distribution for the T5 cation, calculated with restricted MP2 with a 4-31G basis set, is presented in Figure 9.3(b). The results are similar to those in Figure 9.3(a), which were obtained using a cc-pVDZ basis set. This indicates that the size of the cc-pVDZ basis set is sufficiently large, so that the size of the basis does not affect the results to a significant extent.

9.3.2 Effect of methoxy substitution on the charge distribution

The effect of methoxy substitution on the charge distribution was calculated for a PV4(1 da) oligomer, which has two methoxy substituents at the central phenylene unit. The charge distribution of the PV4(1 da) cation as calculated using DFT, HF and restricted MP2 is shown in Figure 9.4. The geometry was optimized at the HF level. According to the DFT calculations, introduction of methoxy substituents on the central phenylene unit leads to a significant increase of the excess positive charge on the substituted phenylene unit, as compared with the charge distribution for the PV4 cation, *cf.* Figures 9.2(a) and 9.4(a). A similar effect was found previously for the PV4(1 da) cation with a DFT optimized geometry.[14] The HF calculations (see Figure 9.4(b)) yield an even higher degree of localization of the excess positive charge on the central phenylene unit containing the methoxy substituents. The MP2 charge distribution is different from those obtained with the DFT and HF methods. Figure 9.4(c) shows that the excess positive charge is distributed over the PV4(1 da) chain in such a way that the highest amount of charge is present on the second and fourth phenylene units. Comparison of the charge distribution for the PV4(1 da) cation in Figure 9.4(c) and that for the PV4 cation in Figure 9.2(c), shows that according to restricted MP2 calculations the amount of positive charge on the central phenylene unit is only slightly enhanced by the presence of methoxy substituents (from 5.7% to 9.4%).
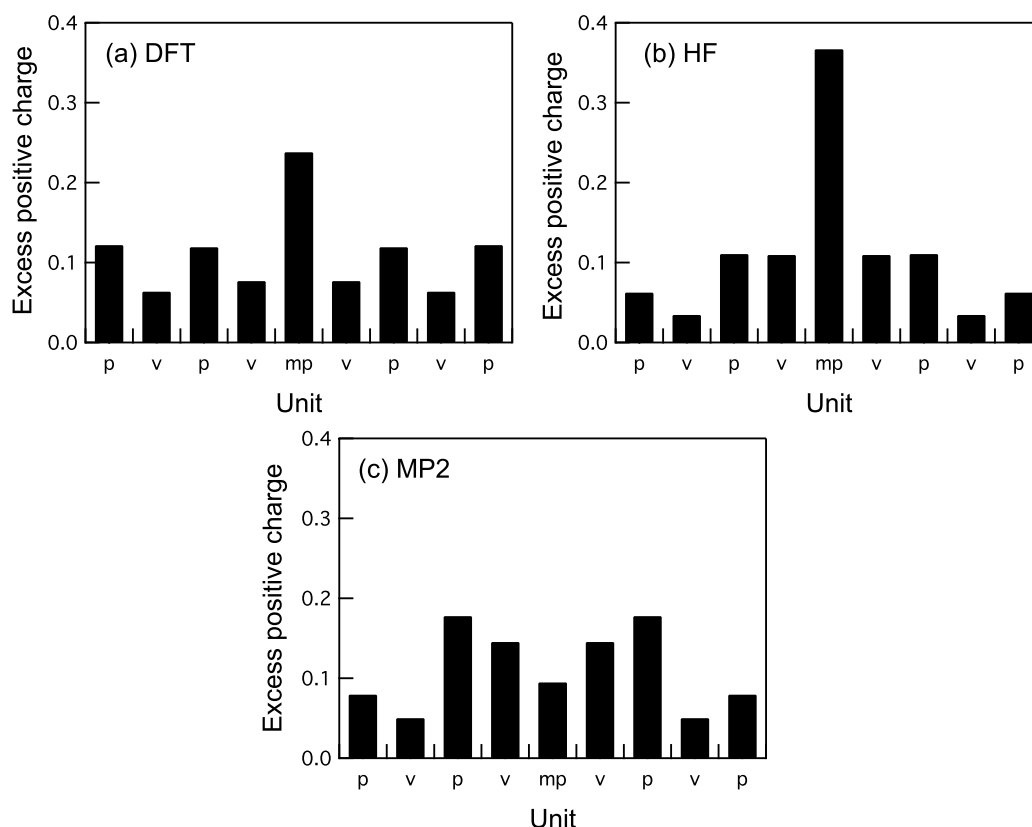

Figure 9.4: Distribution of an excess positive charge over the phenylene (p), vinylene (v) and methoxy substituted phenylene (mp) units for the PV4(1 da) oligomer, as calculated using (a) DFT, (b) HF and (c) MP2 for geometries optimized with HF.

Until now it has been shown that the distribution of an excess positive charge for PV4(1 da) is different, depending on the computational method used. Even though DFT and HF yield a higher degree of localization of the positive charge on the central methoxy substituted phenylene unit as compared with MP2 (see Figure 9.4), the values for the participation ratio in Table 9.1 indicate a similar degree of delocalization for DFT and MP2 (7.4 and 7.6). This means that on basis on participation ratio only, the differences in the charge distribution obtained with MP2 and DFT are not clearly elucidated.

9.3.3 Effect of spin contamination on the charge distribution

As mentioned in section 9.1, spin contamination can have a significant influence on the results of an unrestricted calculation. In Figure 9.5 the charge distributions for the PV4 and T8 cations are shown for both restricted and unrestricted HF calculations. The geometries of the PV4 and T8 cations were optimized using DFT. For the PV4 cation the difference between the results from the restricted and the unrestricted HF calculations is small (see Figure 9.5(a)).
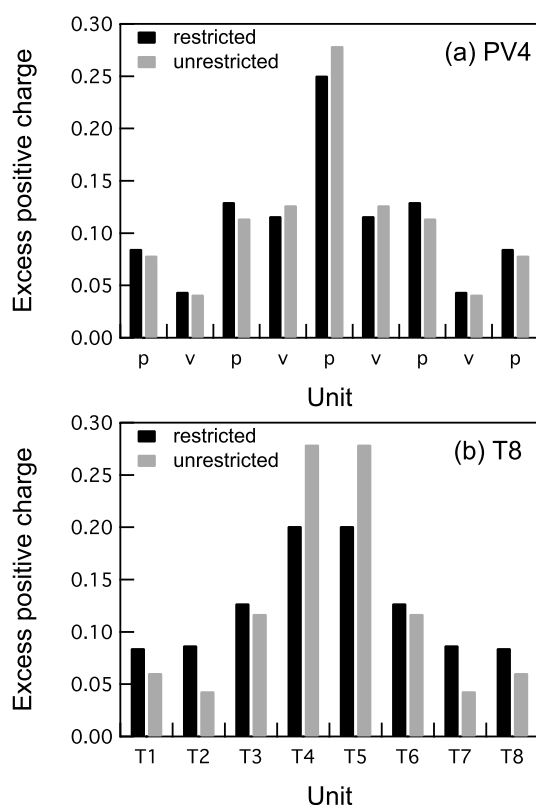

Figure 9.5: Charge distribution of the (a) PV4 and (b) T8 oligomers as obtained from restricted and unrestricted HF calculations with a geometry optimized with DFT.

Both restricted and unrestricted calculations show that the positive charge is predominantly present at the central phenylene unit, with the effect being slightly larger for

the unrestricted calculation. In the absence of spin contamination the eigenvalue of the spin S^2 operator is 0.75. The spin S^2 operator is an indication of the degree of spin contamination and it is expected that the presence of spin contamination leads to a higher value of S^2. Indeed, the value of $S^2 = 0.98$ for the unrestricted calculation for the PV4 cation indicates that spin contamination plays an important role. Spin contamination is more pronounced in the case of the T8 cation. The value of spin operator S^2 is 2.64 for the unrestricted HF calculation. Figure 9.5(b) shows that most of the excess positive charge is located on the central thiophene units, with the effect being largest for the unrestricted calculation. This is similar to previous results of Geskin et al.[7]
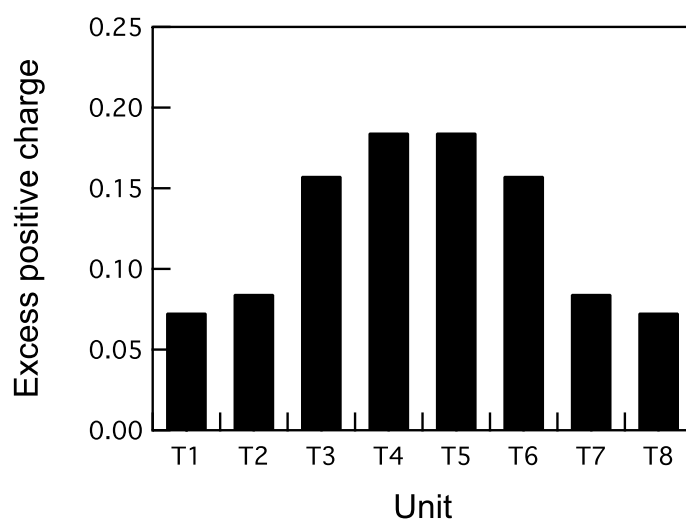

Figure 9.6: Charge distribution of the T8 cation obtained from restricted MP2 calculations with a geometry optimized with DFT.

Figure 9.6 shows the charge distribution for a T8 cation, as obtained form restricted MP2 calculations and geometry optimization with DFT. Comparison of these data with those from unrestricted MP2 calculations performed by Geskin et al.[7] shows that the amount of charge on the central thiophene units is smaller in case of the restricted calculation. Comparison of the results in Figure 9.6 with those of Geskin et al.[7] is reasonable even though the T8 cation geometry has been optimized using different functionals, since it has been shown in section 9.3.1 that the effect of geometry on the charge distribution is very small. According to the unrestricted MP2 calculations by Geskin et al.[7] the fourth and fifth thiophene units in the center of the oligomer each contain about 28% of the excess positive charge. About 12% of the charge is localized on the third (sixth) unit, while the remaining thiophene units each contain less than 5% of the excess positive charge. In contrast, the restricted MP2 calculations yield a more delocalized charge distribution. Approximately 18% of the charge is localized on the fourth (fifth) unit, while the third (sixth) thiophene unit contains about 16%. The amount of positive charge decreases towards the edge of the molecule with 8% on the second (seventh) unit and about 7% on the first (last) unit. The results discussed above, show that unrestricted MP2 and HF calculations yield considerable spin contamination together with a higher degree of localization of the excess positive charge.

9.4 Summary and conclusions

Different quantum chemical approaches were used to assess the effects of geometry and electron correlation on the distribution of an excess positive charge on phenylenevinylene (PV) and thiophene (T) oligomers. The geometries of the positively charged PV and T oligomers were optimized at the level of HF theory or DFT. The distribution of an excess positive charge of the PV and T oligomers was obtained from a Mulliken population analysis. The method used to optimize the geometry has no significant effect on the charge distribution. However, the distribution of a positive charge on an oligomer depends on the quantum chemical method used to calculate the electron density (wave function). The charge distribution evolves from being localized with HF to a high degree of delocalization with DFT. An intermediate degree of localization is found from restricted MP2 calculations.

The presence of methoxy substituents on the central phenylene unit in the PV4(1 da) cation increases the amount of positive charge on this unit. Nevertheless, according to MP2 calculations, most of the positive charge is localized on the second and fourth phenylene units. This is different from results obtained with DFT and HF calculations, which yield localization of the positive charge at the central phenylene unit.

Comparison of results from restricted and unrestricted HF or MP2 calculations, shows that spin contamination correlates with enhanced localization of the excess positive charge.

In conclusion, this chapter resolves a standing issue concerning the spatial extent of polarons in conjugated oligomers. It was shown by MP2 calculations that the spatial extent of a positive charge on phenylenevinylene and thiophene chains is considerably larger than initially predicted by Hartree-Fock calculations. This indicates that the inclusion of electron correlation in the calculations leads to an increased delocalization of the charge.

The large degree of delocalization is in agreement with results from EPR experiments on a series of phenylenevinylene oligomers of increasing length.[31] It was shown in those experiments that the charge is delocalized over at least eight units, considerably more than a delocalization over three units as predicted by HF calculations.

It was also confirmed that DFT calculations predict a charge distribution that is even more delocalized than that obtained by MP2. This overestimation of the degree of delocalization by DFT is attributed to the approximate (local) description of the exchange and correlation between the electrons and the non-zero self-interaction.

9.5 References

(1)   Van Hutten, P. F.; Hadziiannou, G. A Model Oligomer Approach to Semiconducting Polymers; in *Semiconducting Polymers: Chemistry, Physics and Engineering*; Hadziiannou, G., van Hutten, P. F., Eds.; Wiley-VCH: Weinheim, 2000.
(2)   Müllen, K.; Wegner, G. *Electronic Materials: The Oligomer Approach*; Wiley-VCH: Weinheim, 1998.
(3)   Kraft, A.; Grimsdale, A. C.; Holmes, A. B. *Angew. Chem. Int. Ed.* **1998**, *37*, 402.
(4)   Reese, C.; Roberts, M.; Ling, M.; Bao, Z. *Mater. Today* **2004**, *7*, 20.

(5) Brabec, C.; Dyakonov, V.; Parisi, J.; Sariciftci, N. S. *Organic Photovoltaics*; Springer: Berlin, 2003.

(6) Kittel, C. *Introduction to Solid State Physiscs*, 8th ed.; John Wiley & Sons, Inc.: New York, 1995.

(7) Geskin, V. M.; Dkhissi, A.; Bredas, J. L. *Int. J. Quant. Chem.* **2003**, *91*, 350.

(8) Grozema, F. C.; Candeias, L. P.; Swart, M.; van Duijnen, P. T.; Wildeman, J.; Hadziiannou, G.; Siebbeles, L. D. A.; Warman, J. L. *J. Chem. Phys.* **2002**, *117*, 11366.

(9) Cornil, J.; Beljonne, D.; Bredas, J. L. *J. Chem. Phys.* **1995**, *103*, 834.

(10) Cornil, J.; Belijonne, D.; Bredas, J. L. *J. Chem. Phys.* **1995**, *103*, 842.

(11) Moro, G.; Scalmani, G.; Cosentino, U.; Pitea, D. *Synth. Met.* **2000**, *108*, 165.

(12) Van Hal, P. A.; Beckers, E. H. A.; Peeters, E.; Apperloo, J. J.; Janssen, R. A. J. *Chem. Phys. Lett.* **2000**, *328*, 403.

(13) Van Haare, J. A. E. H.; Havinga, E. E.; van Dongen, J. L. J.; Janssen, R. A. J.; Cornil, J.; Bredas, J.-L. *Chem. Eur. J.* **1998**, *4*, 1509.

(14) Fratiloiu, S.; Candeias, L. P.; Grozema, F. C.; Wildeman, J.; Siebbeles, L. D. A. *J. Phys. Chem. B* **2004**, *108*, 19967.

(15) Fratiloiu, S.; Grozema, F. C.; Siebbeles, L. D. A. *J. Phys. Chem. B* **2005**, *109*, 5644.

(16) Fratiloiu, S.; Grozema, F. C.; Koizumi, Y.; Seki, S.; Saeki, A.; Tagawa, S.; Dudek, S. P.; Siebbeles, L. D. A. *J. Phys. Chem. B* **2006**, *110*, 5984.

(17) Koch, W.; Holthausen, M. C. *A Chemist's Guide to Density Functional Theory*; Wiley-VCH: Weinheim, 2000.

(18) Becke, A. D. *J. Chem. Phys.* **1993**, *98*, 5648.

(19) Møller, C.; Plesset, M. S. *Phys. Rev.* **1934**, *46*, 618.

(20) Young, D. *Computational Chemistry: A Practical guide for Applying Techniques to Real-World Problems*; Wiley-Interscience: New-York, 2001.

(21) Binkley, J. S.; Pople, J. A.; Dobosh, P. A. *Mol. Phys.* **1974**, *28*, 1423.

(22) Te Velde, G.; Bickelhaupt, F. M.; Baerends, E. J.; Guerra, C. F.; van Gisbergen, S. J. A.; Snijders, J. G.; Ziegler, T. *J. Comput. Chem.* **2001**, *22*, 931.

(23) Vosko, S. H.; Wilk, L.; Nusair, M. *Can. J. Phys.* **1980**, *58*, 1200.

(24) Becke, A. D. *Phys. Rev. A* **1988**, *38*, 3098.

(25) Perdew, J. P.; Yang, W. *Phys. Rev. B* **1986**, *33*, 8800.

(26) Frisch, M. J.; Trucks, G. W.; Schlegel, H. B.; Scuseria, G. E.; Robb, M. A.; Cheeseman, J. R.; Montgomery, J. A. J.; Vreven, T.; Kudin, K. N.; Burant, J. C.; Millam, J. M.; Iyengar, S. S.; Tomasi, J.; Barone, V.; Mennucci, B.; Cossi, M.; Scalmani, G.; Rega, N.; Petersson, G. A.; Nakatsuji, H.; Hada, M.; Ehara, M.; Toyota, K.; Fukuda, R.; Hasegawa, J.; Ishida, M.; Nakajima, T.; Honda, Y.; Kitao, O.; Nakai, H.; Klene, M.; Li, X.; Knox, J. E.; Hratchian, H. P.; Cross, J. B.; Bakken, V.; Adamo, C.; Jaramillo, J.; Gomperts, R.; Stratmann, R. E.; Yazyev, O.; Austin, A. J.; Cammi, R.; Pomelli, C.; Ochterski, J. W.; Ayala, P. Y.; Morokuma, K.; Voth, G. A.; Salvador, P.; Dannenberg, J. J.; Zakrzewski, V. G.; Dapprich, S.; Daniels, A. D.; Strain, M. C.; Farkas, O.; Malick, D. K.; Rabuck, A. D.; Raghavachari, K.; Foresman, J. B.; Ortiz, J. V.; Cui, Q.; Baboul, A. G.; Clifford, S.; Cioslowski, J.; Stefanov, B. B.; Liu, G.; Liashenko, A.; Piskorz, P.; Komaromi, I.; Martin, R. L.; Fox, D. J.; Keith, T.; Al-Laham, M. A.; Peng, C. Y.; Nanayakkara, A.; Challacombe, M.; Gill, P. M. W.;

Johnson, B.; Chen, W.; Wong, M. W.; Gonzalez, C.; Pople, J. A. *Gaussian 03, Revision D.01*; Wallingford CT, 2004.

(27) Dunning, T. H. *J. Chem. Phys.* **1989**, *90*, 1007.

(28) Geskin, V. M.; Grozema, F. C.; Siebbeles, L. D. A.; Beljonne, D.; Bredas, J. L.; Cornil, J.; Bredas, J. L. *J. Phys. Chem. B* **2005**, *109*, 20237.

(29) Nemeth, G. I.; Selzle, H. L.; Schlag, E. W. *Chem. Phys. Lett.* **1993**, *215*, 151.

(30) Ohno, K.; Okamura, K.; Yamakado, H.; Hoshino, S.; Takami, T.; Yamauchi, M. *J. Phys. Chem.* **1995**, *99*, 14247.

(31) Zezin, A. A.; Feldman, V. I.; Warman, J. M.; Wildeman, J.; Hadziioannou, G. *Chem. Phys. Lett.* **2004**, *389*, 108.

Summary

Conjugated polymers are polyunsaturated compounds containing an alternating sequence of single and double (or triple) bonds between the backbone carbon atoms. During the last two decades conjugated polymers have received considerable attention due to their potential applications in light emitting diodes (LEDs), field effect transistors, optical waveguides or photovoltaics. In their pure state conjugated polymers are wide band-gap semiconductors, which can become conducting by injection of charges from electrodes, photo-excitation or chemical doping. The properties that make them suitable for applications in opto-electronic devices include efficient luminescence, flexibility, low weight and relatively low processing cost. The presence of alkyl or alkoxy substituents on the backbone provides solubility to these polymers, so that processing from solution, *e.g.* by spin coating, becomes possible. The introduction of such substituents can also modify the electronic properties of the polymers, leading to changes in the optical absorption and emission spectra and an increase of the luminescence yield in LEDs.

The performance of conjugated polymers in opto-electronic devices critically depends on the properties of the excess charges in the material. A detailed understanding of the properties of these excess charges is therefore of obvious importance. Among these properties, optical absorption spectra of excess charges can provide valuable information about their spatial extent along the polymer chain. A useful and common approach is to study the optical absorption spectra of the charged species for series of short corresponding conjugated chains (known as oligomers) with increasing chain length. The results for oligomers with a well-defined chain length can be extrapolated to infinitely long chains of the corresponding polymer. In this way, information about the spatial extent of the charges on a defect-free polymer chain can be obtained. (It is well known that in conjugated polymers, chemical or structural defects are present, which limit the spatial extent of the charges on the polymer.) All these aspects are discussed in detail in the general introduction presented in Chapter 1.

Charged species of conjugated molecules can be produced in several ways. Most commonly, charged conjugated polymers and oligomers are produced by chemical or electrochemical oxidation or reduction, depending on the nature of charged species desired to obtain (oxidation in the case of positively charged species, called cations and reduction in the

case of negatively charged species, called anions). The formation of side products in chemical or electrochemical oxidations or reductions is often inevitable, which makes it difficult to distinguish between the absorption band of the cation or anion and that of the side product. An alternative method to produce charged species is pulse radiolysis, which circumvents the problem mentioned above. The most important advantage is the pulsed nature of the technique. This makes it possible to study the formation and decay of the charged species in a time resolved way, e.g. by time-resolved optical absorption spectroscopy. This technique was used in the present work to measure the optical absorption spectra of cations or anions of different conjugated oligomers and polymers. The experimental methodology including this technique is described in Chapter 2.

Quantum chemical calculations can provide additional information, *e.g.* insight into the nature of the electronic transitions, which lead to a better understanding of the electronic properties of conjugated oligomers. Quantum chemical calculations can also provide information about the distribution of an excess positive or negative charge along the oligomer chain, which is impossible to obtain directly from experimental data. Computational methods are a powerful tool to investigate the relation between the electronic structure and optical properties of π-conjugated materials. Therefore, the experimental results are compared with the calculated absorption spectra of the charged oligomers with different chain lengths. The theoretical approach used in this thesis is to calculate the opto-electronic properties of a series of conjugated oligomers with increasing chain length. The methods used in this thesis for the electronic structure calculations are briefly discussed in Chapter 3. The discussion includes Hartree-Fock theory, configuration interaction and Møller-Plesset perturbation theory, density functional theory and time-dependent density functional theory.

In chapter 4 the results of a combined experimental and theoretical study of the opto-electronic properties of positively charged phenylenevinylene (PV) oligomers is presented. The optical absorption spectra for PV cations with different chain lengths and substitution patterns were measured using pulse radiolysis with time-resolved VIS/NIR spectroscopy in the range 2100 nm to 500 nm (0.6 eV to 2.5 eV). In the theoretical studies the geometries of the PV cations were optimized using density functional theory (DFT). The optical absorption spectra of positively charged PVs were calculated using time-dependent density functional theory (TDDFT) and compared with the present experimental results and semi-empirical calculations reported in the literature. The experimental spectra of cations of partially dialkoxy substituted PVs indicate the presence of a low absorption band (denoted RC1) with a maximum below 0.6 eV. This is in agreement with the TDDFT calculations, which predict a monotonic decrease of the lowest energy transition (RC1) with chain length. According to semi-empirical calculations from the literature, the energy of this transition exhibits an oscillating behavior as a function of the length of the oligomer, which is in disagreement with the current experimental findings. DFT calculations lead to a more delocalized charge distribution than found previously by the semi-empirical method. The degree of delocalization of the charge calculated by DFT correlates with the energy of the lowest absorption band, calculated by TDDFT. In partially dialkoxy-substituted PV oligomers, more positive charge is present on the substituted phenylene units than on the unsubstituted ones.

Chapter 5 presents a quantum chemical study of the electronic structure and optical absorption spectra of negatively charged PV oligomers and methoxy-substituted derivatives. The geometries of the PV oligomers and derivatives were optimized using DFT. Geometry deformations were found to be delocalized along the entire oligomer chain without indication of the formation of a self-localized polaron. The optical absorption spectra of the negatively charged PVs were calculated using both TDDFT and the singly excited configuration interaction method with an intermediate neglect of differential overlap reference wave function (INDO/s-CIS). A molecular orbital model was used to asses the electronic transitions of the PV anions. According to this model, the low energy transition (RA1) is dominated by a configuration corresponding to an excitation from the singly occupied molecular orbital to the lowest unoccupied molecular orbital. The second transition in the spectrum (RA2) corresponds mainly to a transition of an electron from the highest doubly occupied molecular orbital to the singly occupied molecular orbital. The available experimental optical absorption spectra (from literature) are reproduced by the calculations. TDDFT predicts a monotonic decrease of the RA1 of partially dimethoxy-substituted PV anions with increasing chain length. INDO/s-CIS shows deviations from the monotonic decrease of RA1 with chain length. The main conclusion of this chapter is that the two methods give different results for longer oligomers when the distribution of charge along the chain is considered. DFT calculations yield a more delocalized excess negative charge than INDO/s calculations.

Improved supramolecular order can increase the charge carrier mobility in conjugated molecules. Therefore, synthesizing materials with a high degree of order is of interest. One approach to achieve improved molecular ordering is to use oligomers that are not restricted to linear structures, e.g. two-dimensional conjugated molecules. Chapter 6 presents a combined experimental and theoretical study of the opto-electronic properties of such charged two-dimensional PV oligomers. These oligomers contain a central phenyl ring substituted with four arms. The chemical structure of these arms varies, so that these materials can be either hole or electron conductors. Due to their X shape, these PV oligomers are called X-mers. The optical absorption spectra of charged X-mers were measured using time-resolved VIS/NIR spectroscopy in the range of 1600 to 500 nm (0.8 eV to 2.5 eV). The experimental spectra of the X-mer cations and anions exhibit a strong absorption band near 1.6-1.7 eV. Optical absorption spectra of charged X-mers were calculated using the INDO/s-CIS method with a geometry obtained by DFT. The calculations reproduce the measured optical absorption band near 1.6-1.7 eV. Additional weak absorption bands at low energy are predicted by the calculations. The distribution of the positive and negative charges on the X-mer arms was calculated using both the DFT and the INDO/s methods. According to the DFT calculations, the excess positive charge is mostly localized on the phenylene units containing methoxy substituents, while the excess negative charge is delocalized over the entire oligomer. In contrast, the INDO/s calculations predict a localization of the excess positive and negative charge at the central phenyl ring. Charge transport calculations have also been performed on static stacks of one of the X-mers, *p*-OXA-X. It was found that charge carrier mobility strongly depends on the twist angle between adjacent oligomers in the stack. Moreover, the charge carrier mobility can be significantly enhanced by reduction of the twist angle.

The next two chapters present the opto-electronic properties of a different class of conjugated molecules. Fluorene based oligomers and polymers are of current interest due to

their applicability in LEDs. Therefore, the properties of charged fluorenes are intensively investigated. The optical absorption spectra of fluorene cations and anions, which are presented in Chapter 7, have been measured both in solution and in a solid matrix. The positive and negative charges have been produced in solution by irradiation with high energy electrons from a Van de Graaff accelerator, while the charges in the solid matrix were created by γ-irradiation at 77 K. The optical absorption spectra were measured in the range of 2100 nm to 440 nm (0.6 eV- 2.8 eV) and compared with results from TDDFT calculations. The TDDFT method predicts a monotonic decrease of the absorption energies with increasing chain length, which suggests an increased delocalization of the charge, as the oligomer chain becomes longer. In agreement with this, geometry deformations and charge distributions were found to be delocalized along the oligomer chain without indication of polaron formation. The calculated monotonic decrease of the absorption energies is less pronounced in the experimental results. Calculations performed for the charged fluorene dimer show that the optical absorption spectra depend on the inter-unit angle. Therefore, the potential energy profiles for the rotation around the inter-unit bond have been studied. It was found that the oligofluorenes are nonplanar in their neutral state, while they tend to more planar structures in their charged state.

Chapter 8 presents the optical absorption spectra of cations of fluorene copolymers obtained by chemical oxidation with Ce (IV) and by pulse radiolysis. Differences in the optical absorption spectra obtained using the two techniques were observed. These can be explained by the fact that the species observed in the chemical oxidation experiments correspond to products formed by multiple oxidations. Introduction of different moieties in the fluorene backbone has a large effect on the optical absorption spectra of the copolymer cations. In addition to these experimental results, Chapter 8 presents a quantum chemical study of the electronic and optical properties of three series of charged oligomers containing alternating fluorene and phenylene (FPn) or thienylene (FTn) or benzothiadiazole (F8BTn) moieties, respectively. As was the case for the fluorene copolymers, introduction of phenylene, thienylene or benzothiadiazole moieties leads to a red shift of the optical absorption spectra of the charged co-oligomers as compared with the spectra of the charged oligomers containing fluorene units only. TDDFT calculations of the cation and anion absorption spectra of the fluorene co-oligomers show a monotonic decrease of the low energy band with increasing chain length, as also found for charged PVs, see Chapters 4 and 5. Interestingly, it was found that the RA1 absorption band of F8BTn anions has a lower energy than the RC1 band of F8BTn cations. This correlates with a different charge distribution of the charge in F8BT cations and anions. In F8BTn cations the charge is evenly distributed over the fluorene units. In contrast, the negative charge of F8BTn co-oligomers is localized on the benzothiadiazole units, with higher amounts on the edges of the chain. This difference is explained by the electron accepting character of the benzothiadiazole moieties.

The calculated geometry deformation and charge distribution calculations depend on the quantum chemical method used, see Chapters 4 to 8. It was found that DFT yields delocalization of the excess charge along the oligomer chain, while (semi-empirical or *ab initio*) Hartree-Fock has the tendency to localize the charge in the middle of the chain. A possible explanation for the higher degree of delocalization obtained with DFT is the inclusion of electron correlation, which is not taken into account in the Hartree-Fock methods.

In order to establish whether the higher degree of delocalization is due to the electron correlation, a more conventional correlated quantum mechanical method was employed in Chapter 9. Second order Møller-Plesset perturbation theory (MP2) was performed in addition to DFT and *ab initio* Hartree-Fock to calculate the charge distribution in PV and thiophene (T) cations. Effects of geometry, electron correlation, methoxy substitution and spin contamination on the charge distribution have been investigated. It was found that the method used to optimize the geometry has no significant effect on the charge distribution. However, the quantum chemical method used to calculate the electron density (wave function) has a large effect on the charge distribution. Restricted MP2 calculations yield an intermediate degree of localization, between HF and DFT. This means that the degree of delocalization, as found with MP2 is larger than obtained from Hartree-Fock calculations. This confirms that the inclusion of electron correlation in the calculations leads to an increased delocalization of the charge. Nevertheless, the DFT calculations yield a charge distribution that is even more delocalized than that obtained by MP2. This overestimation of the degree of delocalization by DFT can be attributed to the approximate (local) description of the exchange and correlation between the electrons and the non-zero self-interaction. It was found also that the presence of methoxy substituents on the central phenylene unit in PV4(1 da) cation leads to an increased amount of charge on this unit. Comparison of results from restricted and unrestricted HF and MP2 calculations shows that spin contamination correlates with enhanced localization of the excess positive charge.

Silvia Frățiloiu

Samenvatting

Geconjugeerde polymeren zijn meervoudig onverzadigde verbindingen die bestaan uit een alternerende sequentie van enkele en dubbele (of drievoudige) bindingen tussen de koolstof atomen in de hoofdketen van het polymeer. Gedurende de afgelopen twintig jaar is er erg veel aandacht geweest voor geconjugeerde polymeren als gevolg van mogelijke toepassingen in licht uitzendende diodes (LEDs), veld effect transitoren en zonnecellen. In hun pure vorm zijn geconjugeerde polymeren halfgeleiders met een grote band-gap. Ze kunnen echter geleidend worden wanneer ladingen geïnjecteerd worden bijvoorbeeld vanuit elektrodes, door fotoexcitatie of door chemische doping. De eigenschappen die deze materialen aantrekkelijk maken voor opto-elektronische toepassingen zijn onder meer efficiënte luminescentie, flexibiliteit een laag gewicht en relatief lage verwerkingskosten. De aanwezigheid van alkyl of alkoxy zijketens zorgt er voor dat conjugeerde polymeren oplosbaar worden in organische oplosmiddelen, waardoor het mogelijk wordt om ze vanuit oplossing te verwerken, bijvoorbeeld door middel van spin-coaten. De introductie van zulke substituenten kan ook leiden tot veranderingen in de optische absorptie en emissie spectra en tot verandering in de lumiscentie opbrengst in LEDs.

De prestaties van geconjugeerde polymeren in opto-elektronische componenten is sterk afhankelijk van de eigenschappen van ladingen in het materiaal. Een gedetailleerd begrip van de eigenschappen van deze ladingen is daarom van groot belang. Optische absorptie spectra van geladen moleculen kunnen waardevolle informatie opleveren over de uitgebreidheid van de lading langs de polymeer keten.Een veelgebruikte benadering is het bestuderen van de optische absorptie spectra voor ladingen op een serie korte geconjugeerde moleculen (oligomeren) van toenemende lengte. De resultaten voor een serie oligomeren kunnen worden geëxtrapoleerd naar oneindige lengte, wat overeenkomt met het corresponderende polymeer. Op deze manier wordt informatie verkregen over de uitgebreidheid van ladingen op polymeer ketens zonder defecten. (Het is bekend dat er in het algemeen defecten aanwezig zijn in geconjugeerde polymeren die leiden tot beperkingen in de mate van uitspreiding van de lading op het polymeer.) Al deze aspecten worden uitgebreid behandeld in Hoofdstuk 1.

Ladingen in geconjugeerde moleculen kunnen op verschillende manieren worden aangemaakt. De meest gebruikelijke methode is het genereren van positieve ladingen door

middel van chemische of elektrochemische oxidatie (of reductie in het geval van negatieve ladingen). Chemische of elektrochemische oxidatie en reductie gaan vaak gepaard met de vorming van bijproducten. Dit maakt het moeilijk om te beoordelen of de geobserveerde absorptiebanden toegeschreven moeten worden aan de gewenste kationen en anionen van het bestudeerde molecuul of aan zulke bijproducten. Een alternatieve manier om ladingen aan te maken in geconjugeerde moleculen is pulse radiolyse, waarbij de bovengenoemde problemen grotendeels worden voorkomen. Het belangrijkste voordeel van deze techniek is gelegen in het gepulste karakter. Hierdoor wordt het mogelijk om de vorming en verdwijning van geladen moleculen te bestuderen op een tijdsopgeloste manier, bijvoorbeeld door tijdsopgeloste optische absorptie spectroscopie. Deze techniek is gebruikt in de experimenten die beschreven worden in dit proefschrift om de optische absorptie spectra van positief of negatief geladen geconjugeerde oligomeren te meten. De methodes gebruikt in deze experimenten worden beschreven in Hoofdstuk 2.

Kwantumchemische berekeningen kunnen belangrijke toegevoegde informatie opleveren over bijvoorbeeld de aard van elektronische overgangen. Zulke berekeningen kunnen daardoor leiden tot een beter begrip van de elektronische eigenschappen van geconjugeerde oligomeren. Kwantumchemische berekeningen kunnen ook informatie geven over de distributie van positieve of negatieve ladingen langs de oligomeerketens. Het verkrijgen van zulke informatie uit experimenten is onmogelijk. Deze rekenmethoden zijn daarom een krachtige techniek om de relatie tussen de elektronenstructuur en de optische eigenschappen van geconjugeerde materialen te bestuderen. Daarom worden de experimentele resultaten die beschreven worden in dit proefschrift vergeleken met berekende absorptie spectra voor geconjugeerde oligomeren van verschillende lengtes. De kwantumchemische methodes die gebruikt worden in dit proefschrift worden kort beschreven in Hoofdstuk 3. De beschrijving omvat Hartree-Fock theorie, configuratie interactie, Møller-Plesset storingrekening, dichtheidsfunctionaaltheorie en tijdsafhankelijke dichtheidsfunctionaaltheorie.

In Hoofdstuk 4 worden de resultaten beschreven van een gecombineerd experimenteel en theoretisch onderzoek naar de opto-elektronische eigenschappen van positief geladen phenylenevinylene (PV) oligomeren. De optische absorptie spectra voor positief geladen PV moleculen met verschillende ketenlengtes en posities van zijketens zijn gemeten met behulp van pulse radiolyse gecombineerd met tijdopgeloste VIS/NIR spectroscopie in een golflengte bereik tussen 2100 nm en 500 nm (0.6 eV tot 2.5 eV). In het theoretische onderzoek werd de geometrie van de bestudeerde positief geladen moleculen geoptimaliseerd met behulp van dichtheidsfunctionaal (DFT) theorie. De optische absorptie spectra werden berekend door middel van tijdsafhankelijke dichtheidsfunctionaaltheorie (TDDFT) en vergeleken met de experimentele resultaten en met semi-empirische berekeningen in de literatuur. De experimentele spectra van gedeeltelijk met alkoxy zijketens gesubstitueerde PVs wijzen op het bestaan van een lage-energie absorptieband (RC1) met een maximum beneden 0.6 eV. Dit is in overeenstemming met de resultaten van TDDFT berekeningen die een monotone daling van de RC1 energie met toenemende ketenlengte laten zien. Volgens semi-empirische berekeningen uit de literatuur vertoont de energie van de RC1 overgang een oscillerend gedrag als functie van de ketenlengte. Dit is niet in overeenstemming met de huidige experimentele resultaten. De DFT berekeningen leiden tot een meer gedelocaliseerde ladingsverdeling dan in voorgaande semi-empirische berekeningen. De mate van delocalisatie

van de lading verkregen uit DFT berekeningen vertoont een correlatie met de energie van de RC1 band berekend door middel van TDDFT. In PVs die gedeeltelijk gesubstitueerd zijn met alkoxy zijketens is er meer lading aanwezig op de gesubstitueerde phenyl eenheden dan op de ongesubstitueerde.

In Hoofdstuk 5 word een kwantumchemisch onderzoek beschreven naar de elektronische structuur en optische absorptie spectra van negatief geladen PV oligomeren met en zonder methoxy zijketens. De geometrie van de PV oligomeren werd geoptimaliseerd door middel van DFT berekeningen. De geometrie deformaties die ontstaan door introductie van een negatieve lading zijn geheel gedelocaliseerd langs de oligomeer keten, zonder indicatie van de vorming van een zelflocaliserend polaron. De optische absorptie spectra van negatief geladen PVs zijn berekend met zowel TDDFT als met de semi-empirische INDO/s-CIS methode. De elektronische overgangen worden beschreven in termen van de molekulaire orbitalen. In dit model wordt de lage energie overgang (RA1) gedomineerd door een configuratie waarin een elektron vanuit de enkel bezette orbital naar de laagste onbezette orbital geëxciteerd wordt. De tweede overgang in het spectrum wordt voornamelijk veroorzaakt door de excitatie van een elektron uit de hoogste dubbel bezette orbital naar de enkel bezette orbital. De in de literatuur beschikbare experimentele optische absorptie spectra worden goed beschreven door deze berekeningen. TDDFT voorspelt een monotone daling van de RA1 energie met de ketenlengte voor PVs die gedeeltelijk gesubstitueerd zijn met alkoxy zijketens. INDO/s-CIS berekeningen laten afwijkingen van een monotoon dalend gedrag zien. De belangrijkste conclusie van dit hoofdstuk is dat de twee gebruikte methodes verschillende resultaten geven voor de ladingverdeling op langere oligomeren. DFT berekeningen leiden tot een meer uitgespreide lading dan INDO/s berekeningen.

Een verbeterde supramoleculaire organisatie kan leiden tot een verhoging van de mobiliteit van ladingen in geconjugeerde moleculen. Daarom is het van belang om materialen te synthetiseren met een hoge mate van orde. Een mogelijke benadering om een hogere mate van ordening te bereiken is het gebruik van moleculen die niet beperkt worden tot een lineaire structuur, bijvoorbeeld twee dimensionale moleculen. In Hoofdstuk 6 wordt een gecombineerd experimenteel en theoretisch onderzoek beschreven naar de opto-elektronische eigenschappen van zulke twee dimensionale PV oligomeren. Deze oligomeren bevatten een centrale phenyl ring waaraan vier 'armen' gekoppeld zijn. De chemische structuur van deze armen varieert zodat ze zowel elektronen- als gatengeleiders kunnen zijn. Op basis van hun structuur worden deze PV oligomeren X-meren genoemd. De optische absorptie spectra van geladen X-meren zijn gemeten door middel van tijdsopgeloste VIS/NIR spectroscopie in een golflengte bereik tussen 1600 nm en 500 nm (0.8 ev tot 2.5 eV). De experimentele spectra van de X-meer kationen en anionen vertonen een sterke absorptie band in de buurt van 1.6-1.7 eV. Optische absorptie spectra van geladen X-meren zijn berekend door middel van INDO/s-CIS berekeningen met een geometrie verkregen uit DFT berekeningen. De berekeningen reproduceren de gemeten absorptieband rond de 1.6-1.7 eV. De berekeningen voorspellen hiernaast nog verschillende zwakke absorptiebanden bij lage energie. De distributie van positieve en negatieve ladingen over de armen van de X-meren zijn bestudeerd met behulp van DFT en INDO/s berekeningen. Volgens de DFT berekeningen zijn positieve lading vooral gelokaliseerd op de armen die phenyl eenheden bevatten, terwijl negatieve ladingen over het hele molecuul verdeeld zijn. In tegenstelling tot deze resultaten voorspelt de INDO/s

methode dat zowel de poitieve als de negatieve lading gelokaliseerd zijn rond de centrale phenyl ring. Hiernaast zijn ook ladingstransport berekeningen uitgevoerd voor statische stacks van één type X-meer, *p*-OXA-X. Uit deze berekeningen blijkt dat de mobiliteit van ladingsdragers langs de stack sterk afhankelijk is van de twist hoek tussen aangrenzende moleculen in de stack. Daarom kan de ladingdrager mobiliteit sterk verhoogd worden door te zorgen voor een gereduceerde twist hoek in deze materialen.

In de volgende twee hoofdstukken worden de opto-elektronische eigenschappen besproken van een andere klasse van geconjugeerde moleculen. Fluorene gebaseerde oligomeren en polymeren zijn momenteel van groot belang naar aanleiding van hun toepasbaarheid in LEDs. Daarom worden de eigenschappen van geladen fluorenen intensief bestudeerd. De optische absorptie spectra van fluorene kationen en anionen, gemeten zowel in oplossing als in een vaste matrix, worden beschreven in Hoofdstuk 7. De positive en negatieve lading in oplossing zijn geproduceerd door middel van pulse radiolyse terwijl de ladingen in de vaste matrix geproduceerd werden door γ-bestraling bij een temperatuur van 77 K. De optische absorptie spectra zijn gemeten in een golflengte gebied van 2100 nm to 440 nm (0.6 eV tot 2.8 eV) en worden vergeleken met resultaten van TDDFT berekeningen. De TDDFT methode voorspelt een monotone daling van de absorptie energie met toenemende ketenlengte, wat suggereert dat de lading meer gedelokaliseerd raakt als de keten langer wordt. In overeenstemming met dit resultaat is ook gevonden dat de deformaties van de geometrie na introductie van een lading geheel gedelokaliseerd zijn langs de keten. Er is geen indicatie gevonden van een zichzelf lokaliserend polaron. De berekende afname van de absorptie energie met toenemende ketenlengte is minder prominent aanwezig in de experimentele resultaten. Uit berekeningen aan een fluorene dimeer blijkt dat het optische absorptie spectrum sterk afhankelijk is van de rotatie hoek tussen de twee fluorene eenheden. Daarom zijn ook de rotatie energie profielen voor de rotatie rond de binding tussen de twee eenheden bestudeerd. Uit deze berekeningen is gevonden dat oligofluorenen niet plat zijn in hun neutrale vorm maar dat ze een meer vlakke structuur gaan vertonen in hun geladen toestand.

In Hoofdstuk 8 worden de optische absorptie spectra van positief geladen fluorene co-polymeren beschreven die verkregen zijn door middel van chemische oxidatie met Ce(IV) en door pulse radiolyse. Tussen de resultaten verkregen met de verschillende technieken zijn significante verschillen. Deze verschillen worden verklaard door het feit dat in de chemische oxidatie experimenten producten als gevolg van meervoudige oxidaties gevormd kunnen worden. De introductie van verschillende eenheden in de fluorene hoofdketen heeft een groot effect op de optische absorptie spectra van de positief geladen copolymeren. Naast de experimentele resultaten beschrijft Hoofdstuk 8 ook een kwantumchemische studie naar de elektronische en optische eigenschappen van drie series geladen oligomeren. Deze verbindingen bestaan uit een alternerende sequentie van fluorene met phenyl, thienyl en benzothiadiazool. Evenals in de experimentele resultaten voor de copolymeren leidt de introductie van phenyl, thienyl of benzothiadiazole tot een roodverschuiving van het absorptie spectrum van positief geladen oligomeren ten opzichte van die van oligomeren die enkel bestaan uit fluorene eenheden. TDDFT berekeningen laten een monotone daling zien van de lage energie absorptie band met toenemende lengte van het oligomeer, evenals gevonden voor PVs, zie Hoofdstukken 4 en 5.Een interessante observatie is dat de RC1 band van F8BTn

anionen een stuk lager is dan voor de F8BTn kationen. In F8BTn kationen werd gevonden dat de lading evenredig verdeeld is over de fluorene eenheden, terwijl de negatieve lading verdeeld is over de benzothiadiazole eenheden. Dit verschil is te verklaren op grond van het hogere elektron accepterend vermogen van de benzothiadiazole eenheden.

De berekende geometrie deformaties en ladingsverdelingen hangen in grote mate af van de gebruikte kwantumchemische methode zoals beschreven in Hoofdstukken 4 tot 8. DFT leidt in het algemeen tot een gedelokaliseerde lading terwijl (semi-empirische of ab initio) Hartree-Fock berekeningen leiden tot lokalisatie van de lading in het midden van de keten. Een mogelijke verklaring voor de meer gedelokaliseerde ladingsverdeling verkregen uit DFT berekeningen is gelegen in de beschrijving van elektron correlatie, wat niet in rekening gebracht wordt in Hartree-Fock methodes. Om vast te stellen of de hogere mate van delokalisatie wordt veroorzaakt door electron correlatie is in Hoofdstuk 9 een meer conventionele gecorreleerde rekenmethode gebruikt. In dit hoofdstuk is naast DFT en Hartree-Fock ook tweede orde Møller-Plesset storingrekening (MP2) gebruikt om de ladingsverdeling in PV en thiophene kationen te bestuderen. De effecten van de geometrie, de ladings verdeling, de aanwezigheid van alkoxy zijketens en spin-contaminatie op de ladings verdeling zijn bestudeerd. Hier uit is gebleken dat de methode waarmee de geometrie geoptimaliseerd is geen significant effect op de ladingverdeling heeft. Echter, de kwantumchemische methode die gebruikt wordt om de elektronendichtheid te berekenen heeft wel een groot effect op de ladingverdeling. Uit restricted MP2 berekeningen werd een ladingverdeling verkregen die tussen die uit Hartree-Fock en DFT berekeningen valt. Dat wil zeggen dat de mate van delokalisatie gevonden door middel van MP2 berekeningen groter is dan die uit Hartree berekeningen. Dit laat zien dat het in rekening brengen van elektron correlatie leidt tot een grotere mate van delokalisatie van de lading. Echter, uit de DFT berekeningen werd een nog grotere mate van delocalisatie gevonden. Het overschatten van de delokalisatie door DFT wordt toegeschreven aan de niet-exacte (lokale) beschrijving van de exchange en correlatie interacties tussen elektronen en aan de zelfinteractie die niet nul is in DFT. De berekeningen laten ook zien dat de aanwezigheid van methoxy zijketens op de centrale phenyl ring in PV4(1 da) leidt tot een toename van de hoeveelheid lading op deze eenheid. Vergelijking van de resultaten van restricted en unrestricted HF en MP2 berekeningen laten zien dat spin contaminatie leidt tot een sterkere lokalisatie van de positieve lading.

Translated in Dutch by Ferdinand Grozema

Acknowledgements

The book that you are holding in your hands is not the result of the effort of one single person, but of a whole team. Therefore, I would like to express my gratitude to all those who were involved in this project. Many thanks to you all! And if I will forget to name somebody, please forgive me!

First, I would like to thank prof. dr. Joop Schoonman, for giving me the opportunity to come in 2002 to Delft to work on my final project for my studies in Romania. In the time spent in Delft I discovered how challenging a research project is. Because of this experience I decided to continue my studies by starting a PhD. I would like to thank prof. dr. Siebbeles, who accepted me as a PhD student in his group. Thank you for your confidence in my ability to complete this project. In the beginning, quantum mechanics was an unexplored field for me, but you had the trust that I will become a good theoretician as well. I appreciate our discussions that made me see things from a different perspective.

I would like to thank to my former supervisor, dr. Luis Candeias for initiating me in the pulse radiolysis technique and time-resolved VIS/NIR optical absorption spectroscopy. The work presented in Chapter 4 was completed under his supervision. I was fortunate in having dr. Ferdinand Grozema, as a daily supervisor in my second part of my PhD project. I am impressed by your knowledge in quantum mechanics and I assure you that my quantum mechanics improved due to our discussions. I liked your intuition and the ability of seeing things in perspective. You were always listening to my ideas and helping me to find answers for my questions. You guided and support me (especially in the difficult moments) and I believe that this thesis won't be in the present form without your contribution. Thank you!

John Warman I would like to thank you for the valuable scientific discussions that we had. You were a kind of *"scientific guru"* for me, the person to whom I would of come when nobody had answers to my questions. Even though we did not always find the right answer, at least you would of give me some ideas about possible solutions.

The experiments, whose results are described in this thesis, would not be possible without the help of Martien Vermeulen. Martien, you were preparing, maintaining and fixing the optical absorption setup for me anytime when I need it. Thank you for improving the time

resolved VIS/NIR optical absorption apparatus to be as accurate as possible and as handy as possible for me. Thanks as well for conditioning the electron accelerator in the morning, so that it will be ready for me to start the experiments. Also Marinus Hom is acknowledged for *"conditioning the machine"*.

The work in this thesis has also greatly benefited from several national and international collaborations. In particular, I want to mention dr. Senthilkumar Kittusami from N. G. M. College, Pollachi, India, and dr. Hermona Christian-Pandya and prof. dr. Mary Galvin from University of Delaware, USA. The work that we have done together is presented in Chapter 6. Senthil, special thanks to you for teaching me to perform charge transport calculations and molecular dynamics simulations! Another important collaboration I had with Yoshiko Koizumi and prof. dr. Seiichi Tagawa from Osaka University, Japan. We worked together on fluorene oligomers and the results are presented in Chapter 7. In the last year of my PhD project I was studying opto-electronic properties of fluorene copolymers and co-oligomers together with dr. Sofia Fonseca and prof. dr. Hugh Burrows from Coimbra University, Portugal. It has been a great pleasure working with you all! Several other groups have contributed by supplying the materials used in the experiments in this thesis: Jurjen Wildeman (Groningen University) and Albert Schenning (Eindhoven University).

The realization of the work described in this thesis would have not been possible without the use of the computer facilities from our group. I would like to thank John Suijkerbuijk for help with the computational programs (Qchem, ADF, etc.) and Paul Rijkers for assistance in changing computers (three in four years). Although not directly involved in this project, I would like to thank to Ruben Abellon (for helping me in the lab), Thijs de Haas (who always talked to me as my parents would do), Cecilia Quick (for all the administrative work, especially my immigration and insurance papers), Tom Savenije, Juleon Schins, Walter Knulst, Lee Luthjens and Albert Goossens.

I would like to thank to my colleagues with whom I was sharing an office room during my stay at IRI: Gary, Pieter and Wojtek and recently (since we moved in DCT) Paulette, Avi, Joris and Sander. I have spent also nice moments with the former PhD students Jorge and Jessica. Good luck to all the PhD students that will finish in the next years: Annemarie, Ruben, Tuan and Elise.

My further words are addressed to my friends and my family. Loïc and Agnès *merci beaucoup* for you friendship! My French improved a lot since I hang with you guys (not mentioning how delicious is the French cuisine). Lena and Nicolas thanks for the *"beer evenings"* that we spent together; Joost, Mario and Corado thanks for the *"gezellige nederlandse avonds"*. And of course I cannot forget my Romanian friends. We spent nice moments together for which I would like to thank you. I hope we will remain friends despite the geographical distances that separate us! I cannot mention all of you here, but in particular I want to thank to Camelia and Florin, Diana and Marius, Ioana, Delia, Cristina and Bogdan.

Last, but not at least, aș vrea să mulțumesc părinților mei. Mamă și tată, teza aceasta de doctorat vă este dedicată în întregime. Ani întregi, zi de zi, v-ați sacrificat pentru mine să mă duceți și să mă aduceți de la școală. Niciodată nu ați spus "nu". Vă mulțumesc din suflet! Sunt convinsă că fără dragostea si suportul dumneavoastră nu aș fi ajuns aici! Clau, tu ai

crezut întotdeauna în forțele mele. Alături de Mădă m-ai încurajat si susținut în tot ceea ce am vrut să fac. Vă mulțumesc! Gândurile mele se îndreaptă acum către Leana și Nenea Mihai, Răzvi și Mădă, Miță și bunica.

Dan, this is the most difficult paragraph to write. I know that I did it all until here, but I cannot find my words anymore. All I can say is "Thank you very much for everything!" The rest I will tell you other time in different circumstances…

Silvia Frățiloiu
Delft, February 2007

Curriculum Vitae

Silvia Frățiloiu was born on the 26th of May 1979 in *Brașov,* Romania. She attended primary and secondary school in *Brașov.* After following "*C. D. Nenițescu*" high-school she started in 1998 her studies at the Faculty of Sciences, Transilvania University in *Brașov.* In 2002 she was awarded a Socrates-Erasmus scholarship and she came to Delft University of Technology in The Netherlands and studied proton inserion in $Li_4Ti_5O_{12}$ spinel for battery applications under the supervision of Prof. dr. Joop Schoonman and dr. Eric Kelder. In February 2003 she graduated in physics and chemistry at Transilvania University.

From April 2003 to April 2007 she was a PhD student in the Opto-Electronic Materials Section, Faculty of Applied Sciences, Delft University of Technology. In this group she performed a combined theoretical and experimental study of the opto-electronic properties of charged conjugated molecules, under the supervision of Prof. dr. Laurens Siebbeles and dr. Ferdinand Grozema.

List of Publications

1. *VIS/NIR Absorption Spectra of Positively Charged Oligo(phenylenevinylene)s and Comparison with Time-Dependent Density Functional Theory Calculations*
   S. Fratiloiu, L.P. Candeias, F.C. Grozema, J. Wildeman and L.D.A. Siebbeles, *J. Phys. Chem. B*, **108** (2004), 19967-19975.

2. *Optical Properties and Delocalization of Excess Negative Charges on Oligo(phenylenevinylene)s: A Quantum Chemical Study*
   S. Fratiloiu, F.C. Grozema and L.D.A. Siebbeles, *J. Phys. Chem. B*, **109** (2005), 5644-5652.

3. *Electronic Structure and Optical Properties of Charged Oligofluorenes Studied by VIS/NIR Spectroscopy and Time-Dependent Density Functional Theory*
   S. Fratiloiu, F.C. Grozema, Y. Koizumi, S. Seki, A. Saeki, S. Tagawa, S.P. Dudek and L.D.A. Siebbeles, J. Phys. Chem. B, **110** (2006), 5984-5993.

4. *Two-dimensional Charge Delocalization in X-shaped Phenylenevinylene Oligomers*
   S. Fratiloiu, K. Senthilkumar, F.C. Grozema, H. Christian-Pandya, Z.I. Niazimbetova, Y.J. Bhandari, M.E. Galvin and L.D.A. Siebbeles, Chem. Mater., **18** (2006), 2118-2129.

5. *Opto-electronic Properties of Fluorene-based Derivatives as Precursors for Light-Emitting Diodes*
   S. Fratiloiu, S.M. Fonseca, F.C. Grozema, H.D.Burrows, M.L. Costa, A. Charas, J. Morgado, and L.D.A. Siebbeles, J. Phys. Chem. C, *accepted for publication*.

6. *Optical Properties of Charged Conjugated Molecules Studied by Pulse Radiolysis and Quantum Chemistry*
   S. Fratiloiu, F.C. Grozema and L.D.A. Siebbeles in *Recents Trends in Radiation Chemistry*, Eds. J. Wishart and B.S.M. Rao, World Scientific Publishing Company, Singapore, *accepted for publication*.

7. *Charge Delocalization in Phenylenevinylene and Thiophene Oligomers Studied by Hartree-Fock, Density Functional Theory and MP2 Calculations*
   S. Fratiloiu, F.C. Grozema and L.D.A. Siebbeles, *manuscript in preparation*.

8. *Anisotropy in Optical and Conductive Properties of Large-Area Liquid Crystalline Monodomains*
W.J. Grzegorczyk, T.J. Savenije, J.J.P. Valeton, <u>S. Fratiloiu</u>, F.C. Grozema D.M. de Leeuw and L.D.A. Siebbeles, *manuscript in preparation*.

9. *Opto-Electronic Properties of Self-Organizing Porphyrin Trimers*
<u>S. Fratiloiu</u>, F.C. Grozema, R. van Hameren, J.A.A.W. Elemans, A.E. Rowan, R.J.M. Nolte and L.D.A. Siebbeles, *manuscript in preparation*.

10. *Optical Absorption Spectra of Charged Oligodiacetylenes Studied by Time-Resolved VIS/NIR Spectroscopy and Time-Dependent Density Functional Theory*
<u>S. Fratiloiu</u>, F.C. Grozema, G.Z. Pilzak, C.C.J. Hendrikx, H. Zuilhof and L.D.A. Siebbeles, *manuscript in preparation*.

Propositions belonging to the thesis:

Opto-Electronic Properties of Charged Conjugated Molecules

1. Addition of oxygen as electron scavenger to conjugated oligomer solutions in benzene does not prevent the formation of radical anions of the oligomer on a short time scale in addition to the well-known oligomer radical cations.

Chapters 6 and 7 of this thesis

2. By means of the choice of the quantum chemical method a large range of results for the degree of charge delocalization on a conjugated chain can be obtained.

Chapter 9 of this thesis

3. The application of quantum mechanics in chemistry is limited by the available computational power, rather than by understanding of the physics behind it.

4. The increased user friendliness of quantum chemical software has a negative effect on the average quality of publications describing quantum chemical studies.

5. Perception, rather than curiosity, is the essence of science.

6. The number of scientific papers published does not necessarily reflect the professional attributes of a PhD student.

7. Scientists generally learn more from unsuccessful experiments than from successful ones.

8. The attitude of most Dutch family doctors towards diagnosis and treatment is: "If there are no complaints, don't fix it!"

9. The balance between the availability of goods and the amount of money that Romanians had to buy these goods has reversed after December 1989.

Silvia Frățiloiu
Delft, February 2007

These propositions are considered opposable and defendable and as such have been approved by the supervisor, prof. dr. L.D.A. Siebbeles.

Stellingen behorende bij het proefschrift:

Opto-Elektronische Eigenschappen van Geladen Geconjugeerde Moleculen

1. Het toevoegen van zuurstof als 'scavenger' van elektronen aan oplossingen van geconjugeerde oligomeren voorkomt niet dat er op korte tijdschaal naast de bekende radicaal kationen ook radicaal anionen van het oligomeer gevormd worden.

Hoofdstukken 6 and 7 van dit proefschrift

2. Door middel van de keuze van de kwantum chemische methode kan een grote variatie worden verkregen in de mate van uitgebreidheid van een lading op een geconjugeerde keten.

Hoofdstuk 9 van dit proefschrift

3. De toepassing van kwantummechanica in de chemie wordt meer beperkt door de beschikbare rekenkracht dan door het begrip van de fysica die erachter zit.

4. De toegenomen gebruikersvriendelijkheid van kwantumchemische software heeft een negatief effect op de gemiddelde kwaliteit van publicaties die kwantumchemische studies beschrijven.

5. Perceptie is, meer dan nieuwsgierigheid, de essentie van de wetenschap.

6. Het aantal gepubliceerde wetenschappelijke artikelen weerspiegelt niet noodzakelijkerwijs de professionele kwaliteiten van een promovendus.

7. Wetenschappers leren in het algemeen meer van onsuccesvolle experimenten dan van succesvolle.

8. De houding van de meeste Nederlandse huisartsen ten opzichte van diagnose en behandeling is: "als er geen klachten zijn, niks doen !".

9. De balans tussen de beschikbaarheid van goederen en de hoeveelheid geld die Roemenen hadden om deze goederen te kopen is omgedraaid na december 1989.

Silvia Frățiloiu
Delft, februari 2007

Deze stellingen worden opponeerbaar en verdedigbaar geacht en zijn als zodanig goedgekeurd door de promotor, prof. dr. L.D.A. Siebbeles.